

**The Mass Spectrometric Characterization of Polychlorinated  
*n*-Alkanes and the Methodology for their Analysis in the  
Environment.**

**By**

**Gregg T. Tomy**

**A Thesis submitted to the  
Faculty of Graduate Studies in Partial  
Fulfillment of the Requirements for the Degree of  
DOCTOR OF PHILOSOPHY**

**Chemistry Department  
University of Manitoba  
Winnipeg, Manitoba  
June 1997.**



**National Library  
of Canada**

**Acquisitions and  
Bibliographic Services**

**395 Wellington Street  
Ottawa ON K1A 0N4  
Canada**

**Bibliothèque nationale  
du Canada**

**Acquisitions et  
services bibliographiques**

**395, rue Wellington  
Ottawa ON K1A 0N4  
Canada**

*Your file Votre référence*

*Our file Notre référence*

**The author has granted a non-exclusive licence allowing the National Library of Canada to reproduce, loan, distribute or sell copies of this thesis in microform, paper or electronic formats.**

**The author retains ownership of the copyright in this thesis. Neither the thesis nor substantial extracts from it may be printed or otherwise reproduced without the author's permission.**

**L'auteur a accordé une licence non exclusive permettant à la Bibliothèque nationale du Canada de reproduire, prêter, distribuer ou vendre des copies de cette thèse sous la forme de microfiche/film, de reproduction sur papier ou sur format électronique.**

**L'auteur conserve la propriété du droit d'auteur qui protège cette thèse. Ni la thèse ni des extraits substantiels de celle-ci ne doivent être imprimés ou autrement reproduits sans son autorisation.**

**0-612-23674-9**

**THE UNIVERSITY OF MANITOBA  
FACULTY OF GRADUATE STUDIES  
\*\*\*\*\*  
COPYRIGHT PERMISSION PAGE**

**THE MASS SPECTROMETRIC CHARACTERIZATION OF POLYCHLORINATED  
n-ALKANES AND THE METHODOLOGY FOR THEIR ANALYSIS  
IN THE ENVIRONMENT**

**BY**

**GREGG T. TOMY**

**A Thesis/Practicum submitted to the Faculty of Graduate Studies of The University  
of Manitoba in partial fulfillment of the requirements of the degree  
of  
DOCTOR OF PHILSOPHY**

**Gregg T. Tomy     1997 (c)**

**Permission has been granted to the Library of The University of Manitoba to lend or sell  
copies of this thesis/practicum, to the National Library of Canada to microfilm this thesis  
and to lend or sell copies of the film, and to Dissertations Abstracts International to publish  
an abstract of this thesis/practicum.**

**The author reserves other publication rights, and neither this thesis/practicum nor  
extensive extracts from it may be printed or otherwise reproduced without the author's  
written permission.**

# **TABLE OF CONTENTS**

	<b>Page</b>
Acknowledgements .....	i-1
Abstract .....	i-4
List of Tables .....	i-6
List of Figures .....	i-9
List of Schemes .....	i-18
Abbreviations and Symbols .....	i-20
1. INTRODUCTION .....	1
1.1 Literature Review of Polychlorinated <i>n</i> -alkanes .....	1
1.1.1 Industrial Synthesis .....	3
1.1.2 Physical and Chemical Properties .....	6
1.1.3 Uses and Applications .....	8
1.1.4 Release of PCAs into the Environment .....	10
1.2 Illustration of the Complexity of Industrial Formulations .....	12
1.3 Review of Recent Analytical Methods for PCA Analysis .....	16
1.4 Objectives of Present Research .....	23
2. MASS SPECTROMETRY .....	27
2.0 Instrumentation .....	27
2.1 Mass Analysers .....	27
2.1.1 Double Focussing Analysers .....	27
2.1.2 Quadrupole Analysers .....	32
2.2 Methods of Ionization .....	32

2.2.1	Electron Ionization	34
2.2.2	Electron Capture Negative Ionization	36
2.2.3	Plasmaspray™ Ionization	37
2.3	Metastable Ions	39
2.3.1	Daughter Ion Scanning	41
2.3.2	Parent Ion Scanning	44
2.3.3	Constant Neutral Loss Scanning	45
2.4	Collisionally Induced Dissociation	48
2.5	Selected Ion Monitoring	49
2.6	Resolving Power	49
3.	EXPERIMENTAL	52
3.	Chromatography	52
3.1	High Pressure Liquid Chromatography	52
3.2	High Resolution Gas Chromatography	52
3.2	Mass Spectrometry	53
3.2.1	Kratos Concept High Resolution Mass Spectrometer	53
3.2.2	Trio 1000 Low Resolution Mass Spectrometer	54
3.3	Chemicals and Synthesis	54
3.3.1	Chemicals	54
3.3.2	Synthesis of Polychlorinated <i>n</i> -alkanes	55
3.3.3	Preparation of an Analytical Reference Standard	57
3.4	Collection Sites of Environmental Samples for PCA analysis	58
3.5	Extraction of PCAs from Environmental Samples	58
3.5.1	Biota Extraction and Clean-Up	58

3.5.2	Sediment Collection and Dating .....	59
3.5.2.1	Sediment extraction and Clean-Up .....	60
3.5.3	Water Collection .....	60
3.5.3.1	Water Extraction and Clean-Up .....	60
3.5.4	Air Collection .....	61
3.5.4.1	Air Extraction and Clean-Up .....	61
3.5.5	Marine Mammal Extraction and Clean-Up .....	62
3.5.6	Human Breast Milk Extraction and Clean-Up .....	62
3.6	Quality Control-Recovery Efficiencies .....	62
3.7	Structural Calculations .....	63
4.	MASS SPECTRAL STUDIES .....	64
4.0	Plasmaspray <sup>TM</sup> Ionization of a Commercial PCA Mixture .....	64
4.1	Synthesized PCA Congeners .....	66
4.1.1	EI and CID Positive Ion Mass Spectrometry .....	68
4.1.1.1	Introduction .....	68
4.1.1.2	General Features .....	72
(A)	1,10-Dichloro- <i>n</i> -decane .....	87
(B)	1,2-Dichloro- <i>n</i> -undecane .....	93
(C)	1,2,9,10-Tetrachloro- <i>n</i> -decane .....	97
(D)	2,3,8,9-Tetrachloro- <i>n</i> -decane .....	101
(E)	1,2,10,11-Tetrachloro- <i>n</i> -undecane .....	102
(F)	2,3,9,10-Tetrachloro- <i>n</i> -undecane .....	107
(G)	1,2,11,12-Tetrachloro- <i>n</i> -dodecane .....	111
(H)	1,2,5,6,9,10-Hexachloro- <i>n</i> -decane .....	115

4.1.2	ECNI Mass Spectrometry .....	119
4.1.2.1	Introduction .....	119
4.1.2.1.1	Ion Source Temperature .....	120
4.1.2.1.2	The [M+Cl] <sup>-</sup> adduct and Sample Concentration	129
5.	THE ANALYTICAL PROTOCOL. QUANTIFYING PCAs IN ENVIRONMENTAL SAMPLES .....	137
5.0	Introduction .....	137
5.1	Determining the Composition of Industrial Mixtures .....	138
5.1.2	Elution Profiles and Retention Time Windows .....	142
5.1.3	Qualitative Analysis-Generating Plots of the Ion Signal Profiles .....	148
5.1.4	Quantitative Procedure .....	153
5.2	Linearity of Response .....	155
5.3	Detection Limits .....	155
5.4	Potential Interference .....	157
5.5	Assessing the Accuracy of the Analytical Protocol .....	158
5.6	Quality Control-Recovery Efficiencies .....	162
6.	ENVIRONMENTAL LEVELS .....	164
6.0	Introduction .....	164
6.1	Detroit River and Lake Erie Samples .....	164
6.2	Egbert Air Samples .....	171
6.3	Water from the Red River near Selkirk, Manitoba .....	176
6.4	Marine Mammals from the Arctic and the St. Lawrence River . . . .	176

6.5	Human Breast Milk .....	190
6.6	PCAs in Standard Reference Materials .....	192
6.7	Occurrence of PCAs in Canadian Mid-Latitude and Arctic Lake Sediments .....	196
6.7.1	Introduction .....	197
6.7.2	Profiles of $\Sigma$ PCAs and other OCs in Sediment Cores .....	209
6.7.3	Flux Calculations .....	211
6.7.4	Variation of Congener Profiles with Sampling Depth .....	211
SUMMARY .....		215
LITERATURE CITED .....		217
APPENDICES		
1a	HRGC-EI/MS total ion chromatogram of 1,10-dichloro- n-decane .....	232
	HRGC-EI/MS total ion chromatogram of reaction products formed by the reaction of molecular chlorine with	
(b)	1-undecene .....	233
(c)	1,9-decadiene .....	234
(d)	2,8-decadiene .....	235
(e)	1,10-undecadiene .....	236
(f)	2,9-undecadiene .....	237
(g)	1,11-dodecadiene .....	238
(h)	1,5,9-decatriene .....	239

2.	Ion fragmentation pathways established by linked-field scanning	
	(a) 1,10-dichloro-n-decane .....	240
	(b) 1,10-dichloro-n-undecane .....	241
	(c) 1,2,9,10-tetrachloro-n-decane .....	242
	(d) 2,3,8,9-tetrachloro-n-decane .....	244
	(e) 1,2,10,11-tetrachloro-n-undecane .....	246
	(f) 2,3,9,10-tetrachloro-n-undecane .....	248
	(g) 1,2,11,12-tetrachloro-n-dodecane .....	250
	(h) 1,2,5,6,9,10-hexachloro-n-decane .....	252
3.	Effect of ion source temperature and concentration of injected PCA on the ECNI mass spectrum of	
	(a) 1,2,9,10- $M_{10,4}$ .....	254
	(b) 1,2,x,9,10- $M_{10,5}$ .....	255
	(c) 1,2,5,6,9,10- $M_{10,6}$ .....	256
	(d) 1,2,5,x,6,9,10- $M_{10,7}$ .....	258
	(e) 1,2,10,11- $M_{11,4}$ .....	259
	(f) 1,2,x,10,11- $M_{11,5}$ .....	260
	(g) 1,2,x,y,10,11- $M_{11,6}$ .....	261
	(h) 1,2,x,y,z,10,11- $M_{11,7}$ .....	262
4.	Derivation of the equation used for estimating analyte PCA concentration .....	263
5.	An example calculation of analyte PCA concentration .....	264

## ***ACKNOWLEDGEMENTS***

The successful completion of this work is due to the efforts of many people. I wish to record publicly my deepest appreciation for their help and encouragement. Professor John Westmore, Chemistry Department at the University of Manitoba, and Derek Muir, Research Scientist at the Freshwater Institute, my co-supervisors, have been wonderful mentors of their respective areas of specialty throughout the course of this project. John's creative and meticulous writing skills, as well as his rich knowledge of mass spectrometry have contributed tremendously to the writing and the research described in this thesis. Derek's seemingly endless knowledge of environmental chemistry together with his high standards and enthusiasm have made this project a wonderful learning experience. He has also done a masterful job of spearheading this project.

My thanks also go to Gary Stern, Research Scientist at the Freshwater Institute. Gary, not only supplied the energy and enthusiasm when needed throughout the years, but also provided a lot of assistance with the development of the analytical protocol described in this thesis. He has shared with me his expertise in running the mass spectrometer, tremendous support and encouragement. Through the course of this project we have also managed to foster a wonderful friendship.

Many other people at the Freshwater Institute contributed in very important ways to this project. Aaron Fisk, graduate student, for engaging in often times provoking discussions; Thea Rawn, graduate student, who kindly provided me with some of the data she has generated; Erin Burns-Flett and Marilyn Henzel, chemists at the Inspection Branch, have been very generous by allowing me ample usage of their mass spectrometer. Erin has also offered a great deal of support and encouragement

through the years.

I am also grateful to the Natural Sciences and Engineering Research Council of Canada (NSERC) and the Canadian Chlorine Coordinating Committee (C4) for their financial support. Phil Ostrowski is also acknowledged for sharing his knowledge and his helpful discussions. I would also like to thank Pierre Beland for providing the St. Lawrence beluga samples, Rune Dietz for the Greenland beluga samples, Erik Born for the walrus samples, and Don Metner for the Hendrickson Island beluga samples.

Kathryn Murison has also been helpful for one summer in the laboratory, but more importantly has provided me with immense support and understanding throughout this endeavour. I greatly appreciate the efforts of Sheryl Tittlemier who has assisted in the laboratory for two summers, and ultimately hastened the completion of this research. Larry Skanderbeg's, Eric Braekvelt's, Errol Hosein's and Jim Baksh's support I much appreciated. Reaz Ali's, Dominic Slack's, Uzor Nwoko's and Colin Tomy's friendship, laughter and encouragement have not gone unnoticed.

To my relatives, in particular, Inez and Bruce Rowson, I am eternally grateful to for their love and support. Nabie Tomy, Sally Slack, Peter and Evelyn Tomy and Nesrine and Hugh Marchan, have all provided unyielding encouragement.

Finally, I wish to express my love and appreciation to my loving family who have made this all possible. To my wonderful parents for their unwavering encouragement throughout the years and to my two wonderful sisters, Shelley and Giselle, for their love and support throughout the years.

*To my loving parents and  
two wonderful sisters*

## **ABSTRACT**

The major objective of the research was to develop a method for sensitive and specific analysis of C<sub>10</sub>-C<sub>13</sub> polychloroalkanes (PCAs) in environmental samples. Our method of choice became high resolution gas chromatography/electron capture negative ion high resolution mass spectrometry (HRGC/ECNI-HRMS) in the selected ion monitoring (SIM) mode. The development of the method involved several steps: (a) Because commercial PCA preparations may contain several thousands of compounds, eight representative compounds of known structure were synthesized in order to examine their chromatographic and mass spectral properties. (b) The electron ionization (EI) positive ion mass spectra, generated with a Kratos Concept (EBE geometry) mass spectrometer, were interpreted with the aid of unimolecular and collision assisted dissociation mass spectra, and enthalpy of formation and force-field estimates of strain energy of ions. (c) ECNI mass spectra were investigated under various ion source conditions to find optimum parameters for sensitivity. (d) Based on these results, a profile of the components of significant abundance in the PCA is determined by an ECNI selected ion monitoring method. The profile can be used not only for quantitative measurements but also for assessment of origin, mode of environmental transport, and biological modification of PCAs. (e) Finally, a quantitative analytical procedure was developed. The protocol has been applied to the quantification of PCAs in a wide variety of environmental samples from Canada and the United States.

Total PCA concentrations ( $\Sigma$ PCAs) in sediment samples from the mouth of the Detroit River (MI) (0.3  $\mu$ g/g) were higher than of  $\Sigma$ DDT (DDT plus metabolites) (0.19  $\mu$ g/g) but lower than of  $\Sigma$ PCBs (1.5  $\mu$ g/g) and  $\Sigma$ PCTs (2.5  $\mu$ g/g).  $\Sigma$ PCA levels in yellow perch (1.0  $\mu$ g/g) were similar to  $\Sigma$ PCB levels in silver bass (0.09-1.2 $\mu$ g/g)

Mean  $\Sigma$ PCA levels ( $n=5$ ) in air samples from Egbert, Ont., ( $44^{\circ} 14' N$ ,  $79^{\circ} 47' W$ ), collected in 1990, were  $543 \pm 318 \text{ pg/m}^3$ , which is similar to  $\Sigma$ PCB levels (74–682  $\text{pg/m}^3$ ) reported earlier. The highest observed  $\Sigma$ PCA concentration of  $924 \text{ pg/m}^3$  was higher than the highest  $\Sigma$ PCB concentration ( $\Sigma = 91$  congeners),  $\sim 682 \text{ pg/m}^3$ .

The mean  $\Sigma$ PCA concentration for water collected over a six month period from Selkirk, MB, of  $30 \pm 14 \text{ ng/L}$  was significantly higher than that of  $\Sigma$ PCBs ( $1.1 \pm 1.2 \text{ ng/L}$ ).

Concentrations of  $\Sigma$ PCAs in beluga whales (*Delphinapterus leucas*) from the St. Lawrence River estuary were higher than in blubber samples from a variety of marine mammals from various regions of the Arctic; the similarity of its PCA composition to that of an industrial formulation suggests local source contamination.  $\Sigma$ PCAs levels were also compared to other organochlorines.

Sediment cores from 4 Canadian lakes ranging from  $49^{\circ}N$  to  $81^{\circ}N$ , were also analyzed for PCAs. Concentrations of total PCAs in surface sediments from Lake Winnipeg ( $50^{\circ}N/96^{\circ}W$ , Manitoba) and Hazen lake ( $81^{\circ}N/71^{\circ}W$ , High Arctic) were 176 and  $4.5 \text{ ng/g}$  (dry wt), respectively; corresponding surficial fluxes were 147 and  $0.9 \text{ } \mu\text{g/m}^2 \text{ yr}$ . The high flux of PCAs to Lake Winnipeg suggests local contamination. The surficial flux of PCAs to Fox lake ( $61^{\circ}N/135^{\circ}W$ ), a sub-arctic lake in the Yukon, was also high,  $34 \text{ } \mu\text{g/m}^2 \text{ yr}$ , but much lower in Lake Nipigon ( $49^{\circ}N/89^{\circ}W$ , N. Ontario),  $3 \text{ } \mu\text{g/m}^2 \text{ yr}$ . PCA concentrations were highest in sediment slices dated from the early 1980s to the 1990s, which is consistent with the usage patterns of PCAs. The change in congener profiles with increasing sediment depth observed in sediments from Fox lake and Lake Winnipeg suggests that biodegradation has occurred. The detection of PCAs in lakes from both populated and remote regions suggests that these organochlorines, are widespread trace contaminants of freshwater environments in Canada.

## ***LIST OF TABLES***

<b>Table</b>	<b>Page</b>
1.1 Physical properties of individual PCA congeners . . . . .	7
1.2 Consumption patterns of PCAs in Canada, U.S.A. and Western Europe . . . . .	9
1.3 The number of positional isomers calculated for $n\text{-C}_n\text{H}_{2n+2-2z}\text{Cl}_z$ by assuming no more than one bound Cl atom on any C atom . . . . .	15
1.4 Published environmental concentrations of $\Sigma$ PCAs . . . . .	17
2.1 Characteristics of scanning modes for observation of metastable ions formed in the IFFR . . . . .	42
3.1 Reaction products of $n$ -alkenes with molecular chlorine . . . . .	56
4.1 Molecular mass and molecular formulas of ions observed in peaks labelled 1 and 2 in figure 1.2(b) . . . . .	67
5.1 Average chlorine number, $z_{\text{avg}}$ , in PCAs of 60-70% chlorine content by mass. . . . .	140
5.2 Calculated $m/z$ values of $[\text{M}-\text{Cl}]^-$ ions monitored and their % natural	

	abundances and experimental % relative responses, for $C_nH_{2n+2-2}Cl_z$ isomers present in PCA-60 and PCA-70 .....	146
5.3	Mean percent recoveries of PCA-60 and chlordane from spiked fish muscle (Arctic Lake Trout) and sodium sulfate .....	163
6.1	Mean percent recovery of $^{13}C_1$ -chlordane from spiked samples and mean PCA concentrations recovered from biota (ng/g wet wt) and sediment (ng/g dry wt) from the Detroit River and Lake Erie (all samples run in duplicate) .....	172
6.2	Sampling dates in 1995 and concentrations of $\Sigma$ PCAs and $\Sigma$ PCBs in water from the Red River, Selkirk, MB .....	179
6.3	Collection location, characteristics and concentrations of $\Sigma$ DDT, $\Sigma$ PCB and $\Sigma$ PCAs in beluga sampled from the St. Lawrence River Estuary .....	185
6.4	Characteristics and concentrations of $\Sigma$ DDT, $\Sigma$ PCB, $\Sigma$ CHB and PCAs in ringed seal blubber from SW Ellesmere Island, Eureka (1994)	186
6.5	Characteristics and concentrations of $\Sigma$ DDT, $\Sigma$ PCB, $\Sigma$ CHB and $\Sigma$ PCAs in marine mammal samples from Arctic waters .....	187
6.6	Concentrations of $\Sigma$ PCB, $\Sigma$ DDT and $\Sigma$ PCA in certified natural biological matrices of SRM standards .....	195

<b>6.7</b>	<b>Focused corrected fluxes of <math>\Sigma</math>PCA (<math>\mu\text{g}/\text{m}^2 \text{ yr}</math>) and characteristics of the lakes investigated in this study .....</b>	<b>208</b>
<b>6.8</b>	<b>Focused corrected fluxes (<math>\text{ng}/\text{m}^2 \text{ yr}</math>) of <math>\Sigma</math>PCA, <math>\Sigma</math>CHB, <math>\Sigma</math>DDT and <math>\Sigma</math>PCB in surface sediments from lakes in the Yukon Territory, Ontario, the Arctic, and Manitoba .....</b>	<b>212</b>

## ***LIST OF FIGURES***

<b>Figure</b>	<b>Page</b>
1.1 Flow diagram of a commercial PCA production process . . . . .	4
1.2 (a) HRGC/ECNI-MS total ion chromatogram ( $m/z$ 65-600) of PCA-60 and (b) HPLC-NPSP-MS total ion chromatogram ( $m/z$ 350-650) of PCA-70 . . . . .	13
2.1 Schematic diagram of a single-focusing magnetic sector instrument . . . . .	28
2.2 Schematic diagram of a double-focusing electric and magnetic sector instrument of Nier-Johnson geometry in which the electrostatic analyzer precedes the magnetic analyzer (EB geometry) . . . . .	31
2.3 Schematic diagram of a quadrupole analyzer . . . . .	33
2.4 Schematic diagram of an electron-ionization ion source . . . . .	35
2.5 Schematic diagram of a combined Thermospray/Plasmaspray™ ion source . . . . .	38
2.6 (A) Two overlapping ion peaks $M_1$ and $M_2$ of equal intensity.	

	(B) Cross-contribution at different resolving powers: (I) Low resolving power—significant cross contribution between ions,	
	(ii) Higher resolving power—no cross-contribution between ions	51
4.1	NPSP mass spectrum of peak labelled • in figure 1.2(b) . . . .	65
4.2	Electron Ionization positive ion mass spectrum of 1,10-dichloro- <i>n</i> -decane . . . . .	73
4.3	Electron Ionization positive ion mass spectrum of 1,11-dichloro- <i>n</i> -undecane . . . . .	74
4.4	Electron Ionization positive ion mass spectrum of 1,2,9,10-tetrachloro- <i>n</i> -decane . . . . .	75
4.5	Electron Ionization positive ion mass spectrum of 2,3,8,9-tetrachloro- <i>n</i> -decane . . . . .	76
4.6	Electron Ionization positive ion mass spectrum of 1,2,10,11-tetrachloro- <i>n</i> -undecane . . . . .	77
4.7	Electron Ionization positive ion mass spectrum of 2,3,9,10-tetrachloro- <i>n</i> -undecane . . . . .	78
4.8	Electron Ionization positive ion mass spectrum of 1,2,11,12-tetrachloro- <i>n</i> -dodecane . . . . .	79

4.9	Electron Ionization positive ion mass spectrum of 1,2,5,6,9,10-hexachloro- <i>n</i> -decane .....	80
4.10	Estimated $\Sigma S$ energies (kcal/mol) for positional isomers of $C_7H_{11}^+$	85
4.11	$\Delta H_f^+$ for ions in the $C_nH_{2n-1}^+$ ion series .....	86
4.12	$\Delta H_f^+$ for ions in the $C_nH_{2n-3}^+$ ion series .....	88
4.13	ECNI mass spectra of 1,2,9,10-tetrachloro- <i>n</i> -decane at ion source temperatures of (a) 220°C, (b) 175°C and (c) 120°C .....	121
4.14	ECNI mass spectra of 1,2,x,9,10-pentachloro- <i>n</i> -decane at ion source temperatures of (a) 220°C, (b) 175°C and (c) 120°C .....	122
4.15	ECNI mass spectra of 1,2,5,6,9,10-hexachloro- <i>n</i> -decane at ion source temperatures of (a) 220°C, (b) 175°C and (c) 120°C ..	123
4.16	ECNI mass spectra of 1,2,x,5,6,9,10-heptachloro- <i>n</i> -decane at ion source temperatures of (a) 220°C, (b) 175°C and (c) 120°C	124
4.17	ECNI mass spectra of 1,2,10,11-tetrachloro- <i>n</i> -undecane at ion source temperatures of (a) 220°C, (b) 175°C and (c) 120°C ..	125
4.18	ECNI mass spectra of 1,2,x,10,11-pentachloro- <i>n</i> -undecane at ion source temperatures of (a) 220°C, (b) 175°C and (c) 120°C	126

4.19	ECNI mass spectra of 1,2,x,y,10,11-hexachloro- <i>n</i> -undecane at ion source temperatures of (a) 220°C, (b) 175°C and (c) 120°C	127
4.20	ECNI mass spectra of 1,2,x,y,z,10,11-heptachloro- <i>n</i> -undecane at ion source temperatures of (a) 220°C, (b) 175°C and (c) 120°C	128
4.21	Effect of ion source temperature and concentration of injected PCA on the formation of the [M-Cl] <sup>-</sup> ion . . . . .	130
4.22	Effect of ion source temperature and concentration of injected PCA on the formation of the [M-Cl] <sup>-</sup> ion . . . . .	131
4.23	Effect of ion source temperature and concentration of injected PCA on the formation of the [M+Cl] <sup>-</sup> adduct ion . . . . .	135
5.1	Elution profiles for the C <sub>10</sub> components found in PCA-60 standard . . . . .	141
5.2	Elution profiles for the C <sub>11</sub> components found in PCA-60 standard . . . . .	143
5.3	Elution profiles for the C <sub>12</sub> components found in PCA-60 standard . . . . .	144
5.4	Elution profiles for the C <sub>13</sub> components found in PCA-60 standard . . . . .	145

5.5	HRGC/ECNI-HRMS elution profiles of monitored ions in PCA-60 aligned to show the seven time windows used . . . . .	147
5.6	Molar "composition" of PCA-60, based on the assumption that the SIM signal of a formula group is proportional (A) to molar concentration, (B) to molar concentration weighted by chlorine number . . . . .	150
5.7	Molar "composition" of PCA-70, based on the assumption that the SIM signal of a formula group is proportional (A) to molar concentration, (B) to molar concentration weighted by chlorine number . . . . .	152
5.8	Calibration curves for (A) PCA-60 and (B) PCA-70 standards determined by integrating the response of the $[M-Cl]^-$ ion for the molecular species $C_{11}H_{18}Cl_6$ and $C_{11}H_{16}Cl_8$ , respectively . . . . .	156
5.9	(A) Molar compositions of the analytical "reference" standard derived by acid-treating the products formed by chlorination of 1,5,9-decatriene (B) Molar composition of PCA-60 standard	161
6.1	Location of sampling sites on the Detroit River and the Western basin of Lake Erie. Sediment, yellow perch, channel catfish and zebra mussels were collected at sampling site #1. Zebra mussels were collected at sampling site #2. Also shown is the CARE ( ● ) sampling station where air samples were collected . . . . .	166
6.2	ECNI selected ion chromatograms for the heptachloro-decane	

	<b>(<i>m/z</i> 346.9275) congener in various samples from the Detroit River and the PCA-60 external standard . . . . .</b>	<b>167</b>
<b>6.3</b>	<b>ECNI selected ion chromatograms for the nonachloro-undecane (<i>m/z</i> 430.8623) congener in various samples from the Detroit River and the PCA-60 external standard . . . . .</b>	<b>168</b>
<b>6.4</b>	<b>ECNI selected ion chromatograms for the octachloro-dodecane (<i>m/z</i> 408.9199) congener in various samples from the Detroit River and the PCA-60 external standard . . . . .</b>	<b>169</b>
<b>6.5</b>	<b>Ion signal profiles of samples collected from the Detroit River and western Lake Erie. The most abundant congener (highlighted in bold), whose [M-Cl]<sup>-</sup> is used as the quantitation ion, is shown for each sample . . . . .</b>	<b>170</b>
<b>6.6</b>	<b>Ion signal profiles for components in (a) Egbert, Ont., air samples and (b) PCA-60 standard. The most abundant congener (highlighted in bold), whose [M-Cl]<sup>-</sup> is used as the quantitation ion, is also shown. (c) PCAs concentrations of air samples collected in 1990. . . . .</b>	<b>174</b>
<b>6.7</b>	<b>Map showing the flow of the Red River into the southern basin of Lake Winnipeg . . . . .</b>	<b>177</b>
<b>6.8</b>	<b>Ion signal profiles for components in (A) Red River water samples from Selkirk, MB., and (B) PCA-60 standard. The most abundant congener (highlighted in bold), whose [M-Cl]<sup>-</sup> is used as the</b>	

	quantitation ion, is also shown .....	178
6.9	Map showing the sampling sites of the marine mammals examined in this study .....	182
6.10	Ion signal profiles for components in (A) Ringed Seal, Eureka (B) Walrus, Greenland and (C) Beluga Whale, Greenland. The most abundant congener (highlighted in bold), whose [M-Cl] <sup>-</sup> ion is used as the quantitation ion, is shown for each species .....	183
6.11	Ion signal profiles for components in beluga whales from (a) St. Lawrence River estuary and (b) Hendrickson Island. The most abundant congener (highlighted in bold), whose [M-Cl] <sup>-</sup> ion is used as the quantitation ion, is shown for both species .....	184
6.12	Ion signal profiles for components in (a) human breast milk from an Inuit woman in Northern Quebec and (B) PCA-60 standard. The most abundant congener (highlighted in bold), whose [M-Cl] <sup>-</sup> ion is used as the quantitation ion, is also shown .....	191
6.13	Ion signal profiles for components in (A) SRM 1588 and (B) SRM 1945. The most abundant congener (highlighted in bold), whose [M-Cl] <sup>-</sup> ion is used as the quantitation ion, is also shown ..	194
6.14	Map of Canada and surrounding region showing the locations of the lakes sampled in this study .....	199

6.15	Concentration profiles of $\Sigma$ PCB, $\Sigma$ DDT, $\Sigma$ CHB and $\Sigma$ PCA in a dated sediment core from Lake Nipigon, Ont. ....	200
6.16	Concentration profiles of $\Sigma$ PCB, $\Sigma$ DDT, $\Sigma$ CHB and $\Sigma$ PCA in a dated sediment core from the southern basin of Lake Winnipeg, MB. ....	201
6.17	Concentration profiles of $\Sigma$ PCB, $\Sigma$ DDT, $\Sigma$ CHB and $\Sigma$ PCA in a dated sediment core from Fox Lake, Yukon ....	202
6.18	Concentration profiles of $\Sigma$ PCB, $\Sigma$ DDT, $\Sigma$ CHB and $\Sigma$ PCA in a dated sediment core from Hazen Lake, high Arctic ....	203
6.19	Variation in the congener ion signal profiles with sampling depth of dated sediment slices from the southern basin of Lake Winnipeg, MB. The most abundant congener (highlighted in bold), whose $[M-Cl]^-$ ion is used as the quantitation ion, is shown for each slice ....	204
6.20	Variation in the congener ion signal profiles with sampling depth of dated sediment slices from Fox Lake, Yukon. The most abundant congener (highlighted in bold), whose $[M-Cl]^-$ ion is used as the quantitation ion, is shown for each slice ....	205
6.21	Variation in the congener ion signal profiles with sampling depth of dated sediment slices from Hazen lake, Arctic. The most abundant congener (highlighted in bold), whose $[M-Cl]^-$ ion is used as the quantitation ion, is shown for each slice ....	206

6.22 Variation in the congener ion signal profiles with sampling depth of dated sediment slices from Lake Nipigon, Ont. The most abundant congener (highlighted in bold), whose  $[M-Cl]^-$  ion is used as the quantitation ion, is shown for each slice ..... 207

## ***LIST OF SCHEMES***

<b>Scheme</b>	<b>Page</b>
4.1 Ion decomposition mechanisms for 1,10-dichloro- <i>n</i> -decane established by linked-field scanning .....	90
4.2 Ion decomposition mechanisms for 1,2-dichloro- <i>n</i> -undecane established by linked-field scanning .....	95
4.3 Ion decomposition mechanisms for 1,2,9,10-tetra-chloro- <i>n</i> -decane established by linked-field scanning .....	99
4.4 Ion decomposition mechanisms for 2,3,8,9-tetra-chloro- <i>n</i> -decane established by linked-field scanning .....	103
4.5 Ion decomposition mechanisms for 1,2,10,11-tetra-chloro- <i>n</i> -undecane established by linked-field scanning .....	105
4.6 Ion decomposition mechanisms for 2,3,9,10-tetra-chloro- <i>n</i> -undecane established by linked-field scanning .....	109
4.7 Ion decomposition mechanisms for 1,2,11,12-tetra-chloro- <i>n</i> -dodecane established by linked-field scanning .....	112
4.8 Ion decomposition mechanisms for 1,2,5,6,9,10-hexachloro- <i>n</i> -decane	

**established by linked-field scanning ..... 116**

# ***ABBREVIATIONS AND SYMBOLS***

## **Abbreviations**

<b>A<sup>+</sup></b>	<b>Fragment or daughter ion</b>
<b>AES</b>	<b>Atmospheric Environment Service</b>
<b>AMM</b>	<b>Average Molar Mass</b>
<b>B</b>	<b>Magnetic field</b>
<b>B/E</b>	<b>Daughter ion scan, linked-field scanning</b>
<b>B<sup>2</sup>/E</b>	<b>Parent ion scan, linked-field scanning</b>
<b>CARE</b>	<b>Center for Atmospheric Research Experiments</b>
<b>CEPA</b>	<b>Canadian Environmental Protection Act</b>
<b>CHBs</b>	<b>Chlorinated Hydrobornanes, or Toxaphene</b>
<b>CID</b>	<b>Collisionally Induced Dissociation</b>
<b>CNL</b>	<b>Constant Neutral Loss linked-field scanning</b>
<b>d.c.</b>	<b>Direct current</b>
<b>DDE</b>	<b>2,2-<i>bis</i> (<i>p</i>-chlorophenyl)-1,1-dichloroethylene</b>
<b>DDT</b>	<b>1,1,1-trichloro-2,2-<i>bis</i> (<i>p</i>-chlorophenyl)ethane</b>
<b>DFO</b>	<b>Department of Fisheries and Oceans</b>
<b>e</b>	<b>Electronic charge</b>
<b>E</b>	<b>Electric field</b>
<b>E<sub>act</sub></b>	<b>Activation energy</b>
<b>ECNI</b>	<b>Electron Capture Negative Ion</b>
<b>EI</b>	<b>Electron Ionization</b>
<b>EPA</b>	<b>Environmental Protection Agency</b>
<b>e<sup>-</sup><sub>th</sub></b>	<b>Thermal electron</b>

FFR	Field free region
FWI	Freshwater Institute
GPC	Gel Permeation Chromatography
HLC	Henry's Law Constant ( $\text{Pa}\cdot\text{m}^3/\text{mol}$ )
HPLC	High Pressure Liquid Chromatography
HRGC	High Resolution Gas Chromatography
HRMS	High Resolution Mass Spectrometry
IADN	Integrated Atmospheric Deposition Network
keV	kilo-electron volts
m	Mass of an ion
$M^+$	Molecular ion
m/z	mass-to-charge ratio of an ion
MMQA	Marine Mammal Quality Assurance
N	Neutral fragment
NCI	Negative Chemical Ionization
NPSP	Negative ion Plasmaspray <sup>TM</sup>
OCs	Organochlorines
PCAs	Polychlorinated <i>n</i> -alkanes
PCA-60	Industrial formulation composed of $C_{10}$ - $C_{13}$ carbon chain length and 60% Cl by mass
PCA-70	Industrial formulation composed of $C_{10}$ - $C_{13}$ carbon chain length and 70% Cl by mass
PCBs	Polychlorinated Biphenyls
PCTs	Polychlorinated Terphenyls
PFK	Perfluorokerosene
PUF	Polyurethane foam
r	Radius of curvature of magnetic sector

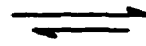
<b>%RA</b>	<b>Relative abundance of an ion as a percentage of the abundance of the base peak</b>
<b>r.f.</b>	<b>Radio frequency</b>
<b>RP</b>	<b>Resolving power (<math>m/\Delta m</math>)</b>
<b>S</b>	<b>Strain energy (kJ/mol)</b>
<b>SIM</b>	<b>Selected Ion Monitoring</b>
<b>SRM</b>	<b>Standard Reference Material</b>
<b>TRI</b>	<b>Toxic Release Inventory</b>
<b>TSP</b>	<b>Thermospray</b>
<b>V</b>	<b>Accelerating voltage</b>
<b>VP</b>	<b>Vapour Pressure (Pa)</b>
<b>WS</b>	<b>Water Solubility (<math>\mu\text{g/L}</math>)</b>
<b>z</b>	<b>Charge number of an ion</b>
<b><math>z_{\text{avg}}</math></b>	<b>Average chlorine number</b>
<b><math>\Sigma</math></b>	<b>Total</b>
<b>1,10-<math>M_{10,2}</math></b>	<b>1,10-dichloro-<i>n</i>-decane</b>
<b>1,2-<math>M_{11,2}</math></b>	<b>1,2-dichloro-<i>n</i>-undecane</b>
<b>1,2,9,10-<math>M_{10,4}</math></b>	<b>1,2,9,10-Tetrachloro-<i>n</i>-decane</b>
<b>2,3,8,9-<math>M_{10,4}</math></b>	<b>2,3,8,9-Tetrachloro-<i>n</i>-decane</b>
<b>1,2,5,6,9,10-<math>M_{10,6}</math></b>	<b>1,2,5,6,9,10-Hexachloro-<i>n</i>-decane</b>
<b>1,2,10,11-<math>M_{11,4}</math></b>	<b>1,2,10,11-Tetrachloro-<i>n</i>-undecane</b>
<b>2,3,9,10-<math>M_{11,4}</math></b>	<b>2,3,9,10-Tetrachloro-<i>n</i>-undecane</b>
<b>1,2,11,12-<math>M_{12,4}</math></b>	<b>1,2,11,12-Tetrachloro-<i>n</i>-dodecane</b>

## Symbols

 Process confirmed by linked-field scanning

 Indication of a two electron shift

 Indication of a one electron shift

 Interconversion of two structures with the conformer on the right predominating

# ***Chapter 1***

## ***INTRODUCTION***

### **1.1 LITERATURE REVIEW OF POLYCHLORINATED *n*-ALKANES.**

Commercially produced polychloroalkanes (PCAs), of the general formula  $C_nH_{2n+2-z}Cl_z$ , have carbon chain lengths from  $C_{10}$  to  $C_{30}$  and chlorine content from 30 to 70% by mass [1-3]. Also known industrially as chlorinated paraffins, they are formed by direct chlorination of *n*-alkane feedstocks with molecular chlorine under forcing conditions (high temperature and/or UV irradiation). These reactions, which have low positional selectivity [4-6], yield complex formulations consisting of mixtures of optical isomers and congeners (*i.e.*, homologues and their isomers) [7]. Based on the principal *n*-alkane feedstocks, which are derived from petroleum fractions, the commercial PCA mixtures fall into different categories:  $C_{10}$ - $C_{13}$  (short),  $C_{14}$ - $C_{17}$  (medium) and  $C_{20}$ - $C_{30}$  (long). These mixtures are further subcategorized into their weight content of chlorine: 40 to 50%, 50 to 60% and 60 to 70% [2].

Owing to varying carbon chain length and chlorine percentages, PCAs provide a range of properties for different applications. The extent and conditions of chlorination used depend ultimately on the desired application [8,9].

PCAs have been produced since 1930, and the first major commercial use was in the preparation of an antiseptic solution, in the form of a chlorocosane (*i.e.*, a  $C_{20}$ -PCA) during World War I [8]. Later they found use as flame retardants and

were applied to canvases and other textiles during World War II [10]. Today PCAs are used in a wide variety of consumer products and industrial processes.

In Canada, PCAs are classified as Priority Toxic Substances under Canadian Environmental Protection Act (CEPA), and in the USA, have been placed on the Environmental Protection Agency (EPA) Toxic Release Inventory (TRI). Presently, PCAs represent the largest group of chlorinated hydrocarbons produced in Western Europe and in North America, and are among the last industrially produced high molecular weight organochlorine compounds in North America [11].

Of particular interest are the  $C_{10}$ - $C_{13}$  PCAs, which have the greatest potential for environmental release [2], appear to exhibit the highest toxicity [1,7,10], and, because of their environmental mobility, persistence and their almost ubiquitous appearance in industrialized countries, could have adverse effects on terrestrial and aquatic organisms and on humans [2,12]. In a recent study, researchers in Sweden have found that the  $C_{10}$ - $C_{13}$  PCAs inhibit intercellular communication in rat liver epithelial cells, a phenomenon which suggests that these chemicals may be acting as tumour promoters [13].

To date, there has been limited information on the behavior of these compounds in the environment. This is due both to a lack of published analytical methods for their analysis, and hence unreliable determination of environmental levels, and to the limited knowledge on their physicochemical properties. The objective of this thesis was to address some of these knowledge gaps.

The sections that follow (1.1.1-1.1.5) introduce the various features of this complex class of compounds, including their synthesis in industry, their physical

and chemical properties, their uses and, finally, the possible sources of release of PCAs into the environment.

### 1.1.1 INDUSTRIAL SYNTHESIS.

PCAs are produced by chlorination, with molecular chlorine, of an *n*-alkane either neat, or in a solvent, typically carbon tetrachloride [14]. Depending upon the *n*-alkane feedstock, the reaction takes place at temperatures between 50 and 150°C, at elevated pressures, and/or in the presence of UV light [3]. Figure 1.1 shows a schematic flow diagram of a typical one stage reactor used in a PCA production process [7].

The desired *n*-alkane feedstocks used in a typical PCA production process are derived from purified fractions collected from an industrial scale distillation process [15-17]. Because this purification process cannot isolate *n*-alkanes of single chain length, or sufficiently remove undesired impurities, the feedstocks used consist of a mixture of homologues, and thus the final preparation would contain a mixture of their chlorinated analogues, and some other chlorinated impurities. The nature and effects of these impurities are addressed later.

The reaction mechanism for the substitution of hydrogen atoms in *n*-alkanes by chlorine atoms is an example of a chain reaction involving free radicals [15]. The first in the series of chain reactions is the *initiation step* (1-1); here energy is absorbed by chlorine molecules, either in the form of heat or light, causing homolysis of the Cl-Cl bond, thereby generating reactive chlorine radicals, Cl•.



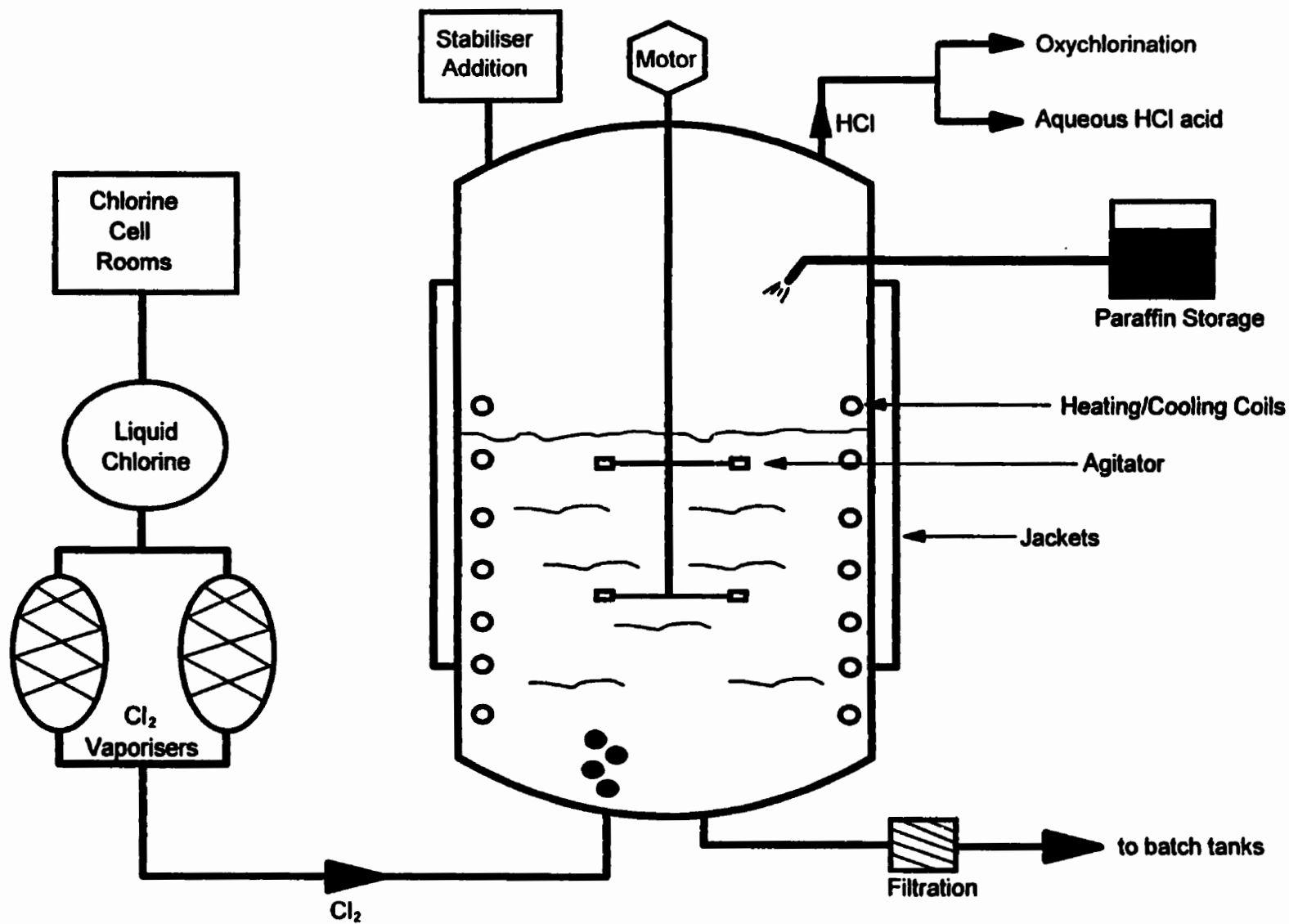
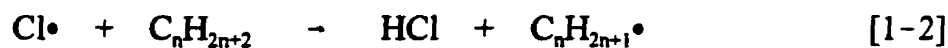
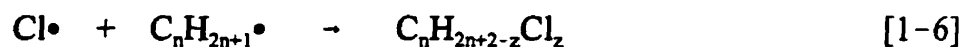


Figure 1.1 Flow diagram of a commercial PCA production process [7]

Second in the chain of reactions are the *propagation steps* (1-2 and 1-3); here free radicals are both generated and consumed. Reactive Cl• atoms once formed, have sufficient energy, viz., activation energy ( $E_{act}$ ), to induce a chemical reaction with the typically unreactive *n*-alkane. This reaction results in the abstraction of a hydrogen atom by a chlorine atom, in turn forming another reactive intermediate,  $C_nH_{2n-1}•$ . These reactive alkyl radicals then react with  $Cl_2$ , to produce  $C_nH_{2n-1}Cl$ , which will be a substrate for further reactions, which eventually generate the PCA.



Last in the series of steps are the *chain termination steps* (1-4 to 1-6); here all the reactive particles are consumed without further generation, either by their union, or by capture of one of them by the walls of the reaction vessel.



As mentioned previously, the presence of impurities in *n*-alkane feedstocks is unavoidable in an industrial PCA preparation. PCA mixtures may be contaminated by isoparaffins (~1%), aromatic compounds (~0.5-1%), by metals and by unreacted *n*-alkanes [3]. In addition, stabilizers are normally added during the chlorination process to inhibit decomposition of the PCA, *via* HCl loss, at elevated temperatures. Common stabilizers include epoxides and organotin compounds. The concentration of these additives, however, is usually below

0.05% [18].

### **1.1.2 PHYSICAL AND CHEMICAL PROPERTIES.**

Industrially prepared PCA mixtures are viscous, colorless or yellowish, dense oils, except for C<sub>20</sub>-C<sub>30</sub> PCAs of high chlorine content (70%) which are solids. To date, reported physicochemical property data, *viz.*, vapour pressure (VP), water solubility (WS) and Henry's Law constant (HLC), on PCAs have been measured by using industrial mixtures because individual PCA congeners have been unavailable.

Recently, more meaningful physicochemical data measurements have been made on individual PCA congeners [19,20]. This is, in part, due to their availability from the syntheses described later in this thesis. The data shown in Table 1.1, which summarizes some of the physicochemical properties for individual PCA congeners, reveal a number of interesting trends.

The WS of the PCA congeners, in contrast to those of PCB congeners, appear to increase with an increase in chlorine content; they appear to be dependent on the positioning of the chlorine atoms on the carbon backbone, and decreases with longer carbon chain lengths. This behaviour suggests that highly chlorinated lower carbon chain length PCAs will become quickly dispersed once they enter the environment *via* the hydrological cycle, and less likely to be associated to sediment and biological phases. Conversely, the lower chlorinated higher carbon chain length PCAs would tend to be found preferentially sorbed onto sediment rather than in the dissolved phase.

In addition, the HLC of the congeners appears to decrease with increasing

**Table 1.1 Physical properties of individual PCA congeners [19,20].**

Compound	WS <sup>a</sup> (µg/L)	HLC <sup>b</sup> (Pa•m <sup>3</sup> /mol)	log Kow <sup>c</sup>	VP <sup>d</sup> (Pa)
1,10-C <sub>10</sub> H <sub>20</sub> Cl <sub>2</sub>	257	499.4	5.13	0.500
1,2,9,10-C <sub>10</sub> H <sub>18</sub> Cl <sub>4</sub>	668	17.67	4.92	0.028
1,2,x,9,10-C <sub>10</sub> H <sub>17</sub> Cl <sub>5</sub>	667	4.92	4.95	0.004
1,2,10,11-C <sub>11</sub> H <sub>20</sub> Cl <sub>4</sub>	575	6.32	4.98	0.010
1,2,x,10,11-C <sub>11</sub> H <sub>19</sub> Cl <sub>5</sub> <sup>e</sup>	546	1.46	5.03	0.001
1,2,x,y,11,12-C <sub>12</sub> H <sub>20</sub> Cl <sub>6</sub> <sup>e</sup>	36.7	1.37	4.69	NA

<sup>a</sup> Water solubility

<sup>b</sup> Henry's Law constant

<sup>c</sup> Log octanol:water partition coefficient

<sup>d</sup> Vapor pressure

<sup>e</sup> x and y denote unknown Cl position

chlorine content with PCAs containing similar carbon chain lengths. This would suggest that lower chlorinated lower carbon chain length PCAs would tend to volatilize from water bodies and disperse through the environment *via* atmospheric transportation.

### **1.1.3 USES AND APPLICATIONS.**

PCAs have been in production since 1930 and world consumption has been growing steadily since that time [7]. In 1961, Hardie *et al.* reported world consumption estimates between 38–50 kt/year, while in 1977, estimates were reported to be about 230 kt/year [21]. Global consumption estimates for 1993 were reported to be 300 kt/year [2]. In Canada and the U.S. consumption estimates are reported to be 3.5–5 kt/year and 44–45 kt/year, respectively. It is believed that the demand for PCAs will likely continue to grow at about 1% per year [2].

PCAs are generally used where the demand for chemical stability is high [22], and common applications include high temperature lubricants, plasticizers, flame retardants, and additives in adhesives, paints, rubber and sealants [3,7]. Table 1.2 shows the consumption patterns of PCAs in Canada, the U.S. and Western Europe.

A major use of PCAs is as extreme temperature additives in metal working fluids (typically short or medium carbon chain length compounds of 50–60% Cl by weight), where they find use in a variety of engineering and metal working operations such as drilling, machining/cutting, drawing and stamping [7,10]. The PCAs are blended with other additives, such as corrosion inhibitors, emulsifiers, biocides and surface active agents. The PCA content of the metal working fluid usually ranges from 2–10%, but can be up to 80% or more for speciality

**Table 1.2. Consumption patterns of PCAs in Canada, U.S.A. and Western Europe.**

Consumption Pattern	Country and % usage		
	U.S. <sup>a</sup>	Canada <sup>b</sup>	Western Europe <sup>c</sup>
Lubricating additives and fire retardants	45	20	70
Plastics	20	65	4
Rubber	13	8	10
Paints	9	3	8
Adhesives and Sealants	6	2	4
Miscellaneous	7	2	4

<sup>a</sup> Ref 14

<sup>b</sup> Ref 2

<sup>c</sup> Ref 10

applications [10].

It is thought that PCAs improve the temperature and pressure- accepting capability of the metal working machinery by releasing HCl during degradation, which reacts with the metal surface to form metal chlorides. The metal chlorides formed have good lubricating and parting effects and so help to prevent the welding together of the metal parts under high pressure and thermal conditions [7,10].

PCAs (typically medium carbon chain length compounds of 50–60% Cl by weight) are also used as secondary plasticizers for polyvinyl chloride (PVC) and can partially replace primary plasticizers such as phthalates and phosphate esters [12]. As a plasticizer, PCAs possess a number of advantages over conventional plasticizers; these include: lower cost, an increase in flexibility of the material as well as an increase in flame retardancy, and low-temperature strength [23]. Their flame-retarding properties result from their ability to inhibit radical reactions that take place during combustion, by halide release at elevated temperatures [10].

PCAs are also used as additives to paints, coatings and sealants to improve resistance to water and chemicals, which is most suitable when used in marine paints, as coatings for industrial flooring, vessels and swimming pools, and as road marking paints [12]. Their flame-retarding properties also make them useful in some of these applications [10].

#### **1.1.4 RELEASE OF PCAs INTO THE ENVIRONMENT.**

The release of PCAs into the environment could occur during (1) production, (2) storage, (3) transportation, or (4) industrial use; leaching (5) from

landfill sites is also possible. Of these, however, the major releases are thought to be from production and from industrial usage [2,11,12,23].

Waterborne releases from production sites could occur either from spills or facility wash-down, in particular, during the cleaning of the reactor vessel [2,23]. There are a few reports regarding the levels of PCAs in the aquatic environment receiving effluents directly from PCA industrial manufacturing sites [24,25]. Metcalfe-Smith *et al.* reported C<sub>14</sub>-C<sub>17</sub> PCA levels from the effluent of Imperial Chemicals Industries Forest Products (ICI) in Canada, on the St. Lawrence River at Cornwall, Ontario, to be 12.7 µg/L [24]. Murray *et al.* reported C<sub>10</sub>-C<sub>13</sub> PCA levels from an impounded drainage ditch containing waters which receive effluent discharge from Dover Chemicals, Dover, Ohio, to be between 0.25-0.57 µg/L [25].

Atmospheric emissions from PCA production sites are also known to occur [7,12]. Emissions measured at a PCA manufacturing plant in the Federal Republic of Germany (FRG) in 1988 were in the order of 30 mg/m<sup>3</sup> [7]. During production in 1990, atmospheric emissions of PCAs in the western states of the FRG, measured as either being sorbed onto dust particulates or as a vapor, were estimated to be ~250 kg for that year [12].

PCAs have also been found as contaminants in common laboratory solvents, *viz.*, dichloromethane, albeit at low levels (~ 0.15 µg/L) [27]. Presumably, PCAs can therefore be present as a by-product during industrial chlorination of many other hydrocarbon feedstocks, and improper disposal of these chemicals could lead to environmental contamination.

The majority of the release of PCAs into the environment, particularly of

$C_{10}$ - $C_{13}$  compounds, is thought to be *via* industrial usage [2,11,12]. Releases can result from improper disposal of used metal-working lubricants and storage drums or carry-off from work pieces. Used drums, which have been sent to drum reconditioning companies where they are washed and refurbished, may be another potential source for entry into the environment [2].

In Sweden, it has been estimated that as much as 55%, *i.e.*, ~227 tons/year, of the  $C_{10}$ - $C_{13}$  PCAs used as high-temperature lubricants in industry may be directly discharged as waste into the air and water [11]. In 1991, the U.S. estimate was ~161 tons [2]. No published data exist regarding discharge levels in Canada.

Disposal of waste containing PCAs may be another potential source of entry of these compounds into the environment. Dumping of products such as PVC, textiles, paint cans and oils containing PCAs may result in slow leaching and/or volatilization from these matrices [2,18]. However, because of their low vapour pressure and water solubility these releases are thought to be low [18].

## **1.2. ILLUSTRATION OF THE COMPLEXITY OF INDUSTRIAL FORMULATIONS.**

Figure 1.2 (a and b) illustrates the complexity of industrially prepared PCA mixtures. The top trace shows the total ion chromatograms (TIC) of a  $C_{10}$ - $C_{13}$  PCA mixture containing 60% (PCA-60) by mass of chlorine, when analyzed by high resolution gas chromatography electron capture negative ion mass spectrometry (HRGC/ECNI-MS) [28]. The bottom trace shows the TIC of  $C_{10}$ - $C_{13}$  PCA mixture containing 70% (PCA-70) by mass of chlorine, when analyzed by high pressure liquid chromatography negative ion plasmaspray mass spectrometry (HPLC-NPSP-MS) [29].

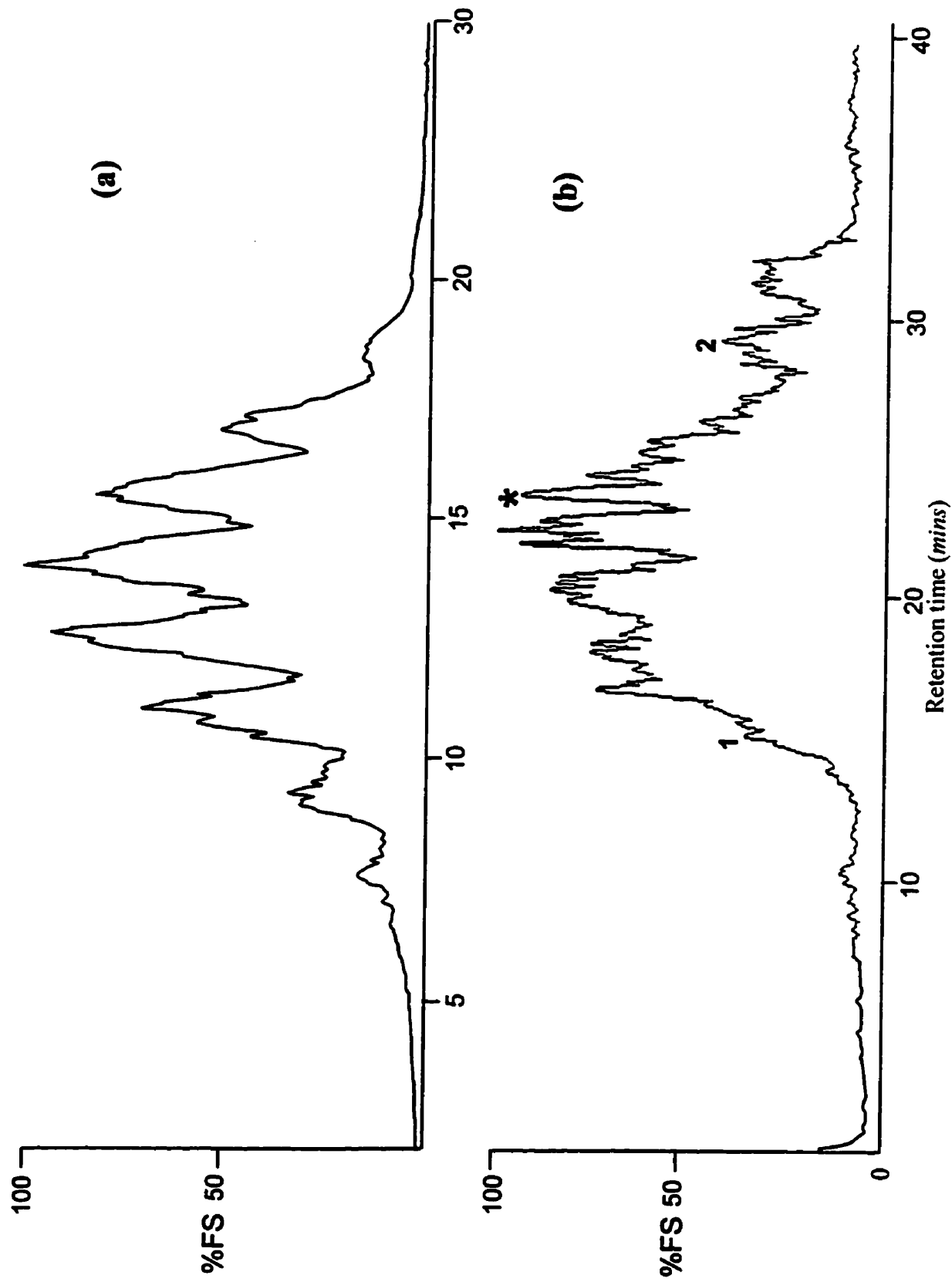


Figure 1.2. (a) HRGC/ECNI-MS total ion chromatogram ( $m/z$  65-600) of PCA-60 and (b) HPLC-NPSP-MS total ion chromatogram ( $m/z$  350-650) of PCA-70 [28,29].

The general appearance of these mixtures is typical of results previously reported in other laboratories [24-26,30-32]. These *multi*-congeneric mixtures generally elute over a wide retention time range, and components are not resolved to baseline even with high resolution GC or LC columns [28,29]. The underlying broad hill results from the large number of congeners present in low concentrations, while congeners present at higher concentrations give rise to the broad unresolved peaks because of co-elution [29].

To further illustrate the complexity of industrial PCA formulations we have calculated the theoretical number of positional isomers (*see* Table 1.3) possible for C<sub>10</sub>-C<sub>13</sub> PCAs having no more than one chlorine atom bound to any carbon atom. The restriction of no more than one chlorine atom bound to any carbon atom was imposed because, although free-radical chlorination has low positional selectivity, a second chlorine atom does not readily substitute for hydrogen at a carbon already bound to chlorine [4-6]. Although chlorine for hydrogen substitution at adjacent carbons is discriminated against we have included this possibility in the calculations because the discrimination is not severe, as confirmed by our ability to make PCAs with high chlorine contents in which vicinal chlorines *must* be present.

The complexity of PCA formulations would actually be an order of magnitude greater than that indicated in Table 1.3 because chlorine substitution at a secondary carbon atom usually produces a chiral carbon atom so that enantiomers and diastereomers will be generated. For example, 2,4,6,8-tetrachloro-*n*-decane has four chiral carbon atoms; thus 16 stereoisomers, as 8 diastereomeric pairs of enantiomers, will be generated.

Additionally, even though the hydrocarbon feedstocks used to prepare the PCAs are primarily *n*-alkanes, as noted earlier they do contain impurities which,

Table 1.3. The number of positional isomers calculated for  $n\text{-C}_n\text{H}_{2n+2-z}\text{Cl}_z$  by assuming no more than one bound Cl atom on any C atom<sup>a</sup>.

$n-z$	10	11	12	13
1	5	6	6	7
2	25	30	36	42
3	60	85	110	146
4	110	170	255	365
5	126	236	396	651
6	110	236	472	868
7	60	170	396	868
8	25	85	255	651
9	5	30	110	365
10	1	6	36	146
11		1	6	42
12			1	7
13				1

<sup>a</sup> Given by  $N = \frac{1}{2} [\{n! / z!(n-z)!\} + s]$ , where  $s$  = number of symmetrical isomers.

Four different cases arise.

(a)  $n$  even,  $z$  even:  $s = \{\frac{1}{2} n\}! / \{\frac{1}{2} z\}! \{\frac{1}{2} n - \frac{1}{2} z\}!$

(b)  $n$  even,  $z$  odd:  $s = 0$

(c)  $n$  odd,  $z$  even:  $s = \{\frac{1}{2} (n-1)\}! / \{\frac{1}{2} z\}! \{\frac{1}{2} (n-1) - \frac{1}{2} z\}!$

(d)  $n$  odd,  $z$  odd:  $s = \{\frac{1}{2} (n-1)\}! / \{\frac{1}{2} (z-1)\}! \{\frac{1}{2} (n-1) - \frac{1}{2} (z-1)\}!$

undoubtedly, would add to the complexity of the mixture. Even if only small percentages of the theoretically possible number of chloro-*n*-alkanes are readily formed, the data in Table 3 demonstrate that even the short chain length C<sub>10</sub>-C<sub>13</sub> commercial PCA mixtures contain many thousands of compounds.

### **1.3 REVIEW OF RECENT ANALYTICAL METHODS FOR PCA ANALYSIS.**

In this section a comprehensive review of the more recent analytical methods for PCA analysis, 1980- to date, will be addressed, but no attempt will be made to review methods prior to this date, *viz.*, thin-layer chromatography (TLC) or neutron activation methods [33,34]. In addition, the drawbacks and problems associated with each of the methods will be discussed in the section to follow. The environmental concentrations of PCAs reported in the literature are shown in Table 1.4.

Gjøes and Gustavsen, in 1982, were the first to report the use of negative ion chemical ionization mass spectrometry (NCI-MS) and its applicability to PCA analysis [35]. In their study, an industrial C<sub>10</sub>-C<sub>13</sub> formulation, containing 70% Cl by weight, was introduced into the ion source of the mass spectrometer *via* a direct insertion probe, and the resulting mass spectra were recorded under full scan conditions. With methane as the moderating gas, their NCI mass spectra were dominated by ions at odd mass; the major fragment ions were assigned as [M-H]<sup>-•</sup>, but contributions from [M-Cl]<sup>-</sup> and [M-HCl-Cl]<sup>-</sup> were also present.

Müller and Schmid (1984) extended the earlier work of Gjøes and Gustavsen by introducing a PCA mixture *via* a gas chromatograph fitted with a 15m capillary column into the ion source of the MS [30]. The total ion chromatograms generated for the three commercial mixtures studied resemble those shown in Figures 1.2 (a

Table 1.4. Published Environmental Concentrations of ΣPCAs.

<b>Environmental Medium</b>	<b>PCA measured</b>	<b>Location</b>	<b>Country</b>	<b>Year</b>	<b>Conc (µg/L)</b>	<b>Reference</b>
	C <sub>10</sub> -C <sub>20</sub> , 45-52% Cl	<i>Irish Sea<sup>a</sup></i>	UK	1980	1.0	Campbell & McConnell [19]
	C <sub>10</sub> -C <sub>20</sub> , 45-52% Cl	<i>Barmouth Harbour<sup>a</sup></i>	UK	1980	0.5	"
	C <sub>10</sub> -C <sub>20</sub> , 45-52% Cl	<i>Sound of Taransay<sup>a</sup></i>	UK	1980	4.0	"
	C <sub>10</sub> -C <sub>30</sub> , 45-52% Cl	<i>North Sea<sup>a</sup></i>	UK	1980	ND	"
	C <sub>10</sub> -C <sub>20</sub> , 45-52% Cl	<i>River Trent, Newark<sup>b</sup></i>	UK	1980	4.0	"
	C <sub>10</sub> -C <sub>20</sub> , 45-52% Cl	<i>River Thames, Oxford<sup>b</sup></i>	UK	1980	2.0	"
	C <sub>10</sub> -C <sub>20</sub>	<i>River Trent, Burton<sup>a</sup></i>	UK	1986	1.45	Willis <i>et al.</i> [10]
<b>Water</b>	C <sub>20</sub> -C <sub>30</sub>	<i>River Trent, Humber<sup>b</sup></i>	UK	1986	3.75	"
	C <sub>10</sub> -C <sub>13</sub> , 62% Cl	<i>Sewage plant run-off<sup>a</sup></i>	FRG	1995	0.115	Rieger & Ballschmiter [26]
	C <sub>10</sub> -C <sub>13</sub> , 62% Cl	<i>Upstream Sewage plant<sup>a</sup></i>	FRG	1995	0.08	"
	C <sub>14</sub> -C <sub>17</sub> , 52% Cl	<i>St. Lawrence River<sup>b</sup></i>	Canada	1995	12.7	Metcalfe-Smith <i>et al.</i> [24]
	C <sub>10</sub> -C <sub>13</sub> , 60% Cl	<i>Impound drainage ditch<sup>b</sup></i>	USA	1988	0.25-0.57	Murray <i>et al.</i> [25]
	C <sub>10</sub> -C <sub>13</sub> , 60% Cl	<i>Sugar Creek, Ohio<sup>b</sup></i>	USA	1988	0.20-0.30	"
	C <sub>14</sub> -C <sub>17</sub> , 52% Cl	<i>Sugar Creek, Ohio<sup>b</sup></i>	USA	1988	0.16-0.24	"

... cont'd

Table 1.4. Published Environmental Concentrations of  $\Sigma$ PCAs

Environmental Medium	PCA measured	Location	Country	Year	Conc ( $\mu\text{g}/\text{kg}$ )	Reference
	$C_{10}-C_{20}$ , 45-52% Cl	<i>Irish Sea<sup>a</sup></i>	UK	1980	100	Campbell & McConnell [19]
	$C_{10}-C_{20}$ , 45-52% Cl	<i>Barmouth Harbour<sup>a</sup></i>	UK	1980	500	"
	$C_{10}-C_{30}$ , 45-52% Cl	<i>North Sea<sup>a</sup></i>	UK	1980	50	"
	$C_{10}-C_{20}$ , 45-52% Cl	<i>River Aire, Leeds<sup>b</sup></i>	UK	1980	10000	"
	$C_{10}-C_{30}$ , 45-52% Cl	<i>River Tees, Middlesborough<sup>b</sup></i>	UK	1980	15000	"
	$C_{20}-C_{30}$ , 45-52% Cl	<i>River Tees, Middlesborough<sup>b</sup></i>	UK	1980	3000	"
<b>Sediment</b>	$C_{20}-C_{30}$ , 42% Cl	<i>Impound drainage ditch<sup>b</sup></i>	USA	1988	170000	Murray <i>et al.</i> [25]
	$C_{10}-C_{13}$ , 60% Cl	<i>Impound drainage ditch<sup>b</sup></i>	USA	1988	40000	"
	$C_{14}-C_{17}$ , 52% Cl	<i>Impound drainage ditch<sup>b</sup></i>	USA	1988	50000	"
	$C_{10}-C_{13}$ , 60% Cl	<i>Sewage sludge<sup>b</sup></i>	FRG	1993	47000	Rieger & Ballschmiter [26]
	$C_{10}-C_{13}$ , 60% Cl	<i>Sewage sludge<sup>b</sup></i>	FRG	1991	65000	"
	$C_{14}-C_{17}$ , 52% Cl	<i>St. Lawrence River<sup>b</sup></i>	Canada	1995	ND	Metcalf-Smith <i>et al.</i> [24]
	$C_{14}-C_{18}$ , 52% Cl	<i>Lake Zürich<sup>a</sup></i>	SWZ	1985	5	Schmid & Müller [31]
	$C_{14}-C_{18}$ , 52% Cl	<i>Sewage sludge<sup>b</sup></i>	SWZ	1985	30000	"

... cont'd

Table 1.4. Published Environmental Concentrations of ΣPCAs.

Environmental Medium	PCA measured	Species	Country	Year	Conc (µg/kg)	Reference
	C <sub>10</sub> -C <sub>20</sub> , 45-52% CI	<i>Grey Seal</i>	UK	1980	75 <sup>c</sup>	Campbell & McConnell [19]
	C <sub>10</sub> -C <sub>20</sub> , 45-52% CI	<i>Mussels</i>	UK	1980	3250 <sup>c</sup>	"
	C <sub>10</sub> -C <sub>30</sub> 45-52% CI	<i>Heron (seabird) eggs</i>	UK	1980	1500	"
	C <sub>10</sub> -C <sub>20</sub> , 45-52% CI	<i>Human tissue</i>	UK	1980	300	"
	C <sub>10</sub> -C <sub>13</sub> , 60% CI	<i>Rabbit</i>	SWD	1993	4400	Jansson <i>et al.</i> [36]
	C <sub>10</sub> -C <sub>13</sub> , 60% CI	<i>Moose</i>	SWD	1993	140	"
	C <sub>10</sub> -C <sub>13</sub> , 60% CI	<i>Reindeer</i>	SWD	1993	1000	"
	C <sub>10</sub> -C <sub>13</sub> , 60% CI	<i>Whitefish</i>	SWD	1993	570	"
	C <sub>10</sub> -C <sub>13</sub> , 60% CI	<i>Arctic Char</i>	SWD	1993	1500 <sup>c</sup>	"
	C <sub>10</sub> -C <sub>13</sub> , 60% CI	<i>Herring</i>	SWD	1993	205 <sup>c</sup>	"
	C <sub>14</sub> -C <sub>18</sub> , 52% CI	<i>Human Tissue</i>	SWZ	1985	200	Schmid & Müller [31]
	C <sub>14</sub> -C <sub>17</sub> , 52% CI	<i>Zebra Mussels<sup>b</sup></i>	Canada	1995	ND	Metcalfe-Smith <i>et al.</i> [24]
	C <sub>14</sub> -C <sub>17</sub> , 52% CI	<i>Yellow Perch<sup>b</sup></i>	Canada	1995	ND	"
	C <sub>20</sub> -C <sub>30</sub> , 42% CI	<i>White Sucker<sup>b</sup></i>	Canada	1995	ND	"

... cont'd

Table 1.4. Published Environmental Concentrations of  $\Sigma$ PCAs.

<b>Environmental Medium</b>	<b>PCA measured</b>	<b>Location</b>	<b>Country</b>	<b>Year</b>	<b>Conc.</b>	<b>Reference</b>
<b><i>Air</i></b>	$C_{10}-C_{30}$	<i>Manufacturing plant<sup>b</sup></i>	FRG	1988	30 mg/m <sup>3</sup>	Mukherjee [7]
	$C_{10}-C_{30}$	<i>Western states</i>	FRG	1990	250 kg	Willis <i>et al.</i> [10]
<b><i>Paving Stones</i></b>	$C_{10}-C_{13}$ , 56% Cl	<i>Metal-working industrial plant<sup>b</sup></i>	FRG	1993	582 mg/kg	Junk & Meisch [38]

<sup>a</sup> sampling site remote from industrialized area

<sup>b</sup> sampling site near industrialized area

<sup>c</sup> mean value

and b) in that little separation of components present in the mixture was observed. Subsequent to their initial work, Schmid and Müller (1985) extended their method to the analyses of real world samples [31]. Quantitation of environmental samples was achieved by first preselecting six prominent ions from an external standard on which the quantitation was based. The integrated areas of these six ions, monitored under selected ion monitoring (SIM) conditions and at nominal resolution, determined from an injection of a known amount of standard, was then compared to the integrated areas of a sample which had been calculated in the same manner. By this method, PCA levels were determined in a variety of environmental matrices (*see* Table 1.4).

In a refinement of the Schmid and Müller technique, Murray *et al.* (1988) quantified PCAs in a variety of environmental matrices by preselecting characteristic cumulative mass ranges, based on the chain length of the PCA to be determined [25]. For example, to quantify C<sub>10</sub>-C<sub>13</sub> PCAs the following mass ranges were selected: 324-329, 359-364, 367-372 and 393-401, during which time the MS would scan, at nominal resolution, the masses within each range. Quantitation was then achieved by comparing the integrated areas of the ions monitored from an injection of a known amount of an external standard, to that of a sample, whose integrated response, had been calculated in the same manner. The efficiency of their method was further improved by dividing the total recording time into a number of preselected retention time windows, during which a small fraction of the ions were monitored. PCA levels (C<sub>10</sub>-C<sub>30</sub>) were determined in a number of environmental samples from two creeks receiving effluent discharge from a manufacturing plant in Dover, Ohio (*see* Table 1.4).

Jansson *et al.* (1991) developed a low resolution method for PCA analyses,

based on GC-ECNI-MS in the SIM mode [36]. PCAs were selectively removed from other common environmental contaminants by gel permeation chromatography (GPC) [37], and quantitation was performed by integrating the response of the  $\text{Cl}_2^-$  ( $m/z$  70) ion [36], an ion that predominates in the mass spectra of individual PCA congeners at high ion source temperatures (this is discussed later). By this method they were able to determine levels of PCAs in a variety of terrestrial animals (*see* Table 1.4).

Junk and Meisch (1993) developed a low resolution method for PCA analyses based on GC/electron ionization (EI) MS in the SIM mode [38]. By introducing a commercial formulation directly into the ion source of the MS *via* a direct insertion probe, and under full scan conditions, they selected the  $\text{C}_5\text{H}_{10}^{35}\text{Cl}^+$  ( $m/z$  105) ion to be the characteristic ion, *i.e.*, the quantitation ion, of the standard. By using the integrated area of this ion, determined from an injection of a known amount of an external standard, and by comparing the ratios of the signal for samples to that of the standard, which were calculated in the same manner, they were able to determine PCA levels in paving stones taken from a German metal-working industrial plant (*see* Table 1.4).

Rieger and Ballschmiter (1995) developed a low resolution method for PCA analyses, based on GC/ECNIMS in the SIM mode [26]. Their method of quantifying PCAs in environmental samples is based on a *triangulation method* previously developed in their laboratory for the analysis of toxaphene [39]. For PCAs, typically four ions, known to be prominent in the external standard, are monitored in separate injections of a known amount of standard and in the sample, and the areas of the broad PCA 'lump', taken to be the area of a triangle drawn from the start of the PCA elution to its end, are then compared. The choice of

external standard used is based on *pattern matching*, *i.e.*, visually comparing the elution time and signal structure of the sample to those of a number of 'in-house' standards [40]. This method of standard selection is similar to the methodology that was employed for polychlorinated biphenyls (PCBs) analyses in environmental samples prior to the synthesis of individual chlorinated biphenyl (CB) congeners in 1984 [41,40]. PCA levels in sewage sludge samples from industrial and residential areas in Germany are shown in Table 1.4.

Finally, Metcalfe-Smith *et al.* (1995) employed a low resolution method for PCA analyses based on GC/ECNIMS in the full scan mode [24]. They reported that, although the environmental samples taken from the St. Lawrence River, Ont., contained interferences, *viz.*, PCBs and dioxins, their presence was not a problem, because their full scanning technique could distinguish them from the PCAs. They analyzed a number of different sample matrices, but were only able to detect PCAs in the effluent from a PCA manufacturing plant in Cornwall, Ontario (*see* Table 1.4).

#### **1.4 OBJECTIVES OF PRESENT RESEARCH.**

It is clear from the discussions above that there are a number of analytical methods in use for determining the levels of PCAs in environmental matrices. Unfortunately, all the methods published to date rely on low resolution MS, and, as we will show, the inherent problem associated with this technique is that it lacks *specificity*. In addition, many of these methods also lack the *sensitivity* often required to measure trace amounts of PCAs [24,25,38].

Procedures based on monitoring the uncharacteristic  $m/z$  70-73 ions, *i.e.*,  $\text{Cl}_2^-$  and  $\text{HCl}_2^-$  [36], present the problem that many other persistent

chlorohydrocarbon contaminants fragment to yield such ions, *e.g.*, *p,p'*-DDT, *p,p'*-DDE, lindane, dieldrin, aldrin and endrin, to name a few [42-44]. So that if these contaminants are not *selectively* removed from the sample matrix during the extraction or clean-up procedures, they would ultimately contribute to the response of the quantitation ion,  $\text{Cl}_2^-$  ( $m/z$  70), and lead to an overestimation in the level of PCAs in samples.

Methods that monitor ions at nominal mass [24-26,31,35,38] present the problem that interferences from higher PCBs, toxaphene and chlordane-related compounds, all of which have similar GC-retention times to PCAs and similar molecular masses to PCAs (*i.e.*, 350-500 u), as we will show, are detected [28]. Reiger and Ballschmiter have applied a simple subtraction technique to circumvent the effects of these interferences, but it is unclear, at the moment, how this procedure compromises the accuracy of their quantitation method [26].

Even with rigorous clean-up procedures, selective isolation of PCAs from other environmental contaminants have not been possible in our laboratory. Although Jansson *et al.* reported to have successfully separated PCAs from other environmental contaminants in their laboratory by GPC [36], attempts to duplicate their results in our laboratory were not met with success. Chromatography on Florisil (60-100 mesh size) columns did, however, separate PCAs from many other contaminants, *viz.*, PCBs, DDT and DDE, but other chlorohydrocarbons, including chlordane, toxaphene, dieldrin and heptachlor epoxide still co-eluted with our collected PCAs fractions [28].

Clearly there is a need for a more selective, sensitive and accurate method for the analysis of these very complicated compounds in environmental matrices. The primary objective of this research, therefore, was to formulate such an

analytical protocol.

Our journey toward this goal began by synthesizing simpler PCA analogues. This was a necessary first step because industrial mixtures provided us with little information regarding the behavior of these compounds in the ion source of the MS. The compounds we investigated were synthesized by simple chlorine additions to *n*-alkenes, using molecular chlorine, which results in the formation of PCA congeners containing known numbers of carbon and chlorine atoms, and also, chlorine atoms residing in known positions. We used these synthesized congeners as *surrogates* for the industrial formulations, and were able to gain a much better understanding of their behavior in the ion source.

Very little information exists in the literature on the EI behavior of the compounds we synthesized. EI mass spectra of only a few polychloro C<sub>3</sub> to C<sub>9</sub> alkanes have been published [45] but, in general, the mass spectra have not been evaluated; in fact, only a limited number of spectra of PCAs are available in the NIST mass spectral database [46]. We therefore investigated, in detail, the fragmentation behavior of these compounds by examining the metastable and collisionally induced dissociation (CID) processes as determined by daughter ion scans (B/E), parent ion scans (B<sup>2</sup>/E) and constant neutral loss (CNL) linked-field scanning.

This thesis will describe the synthesis of individual PCA congeners, their mass spectrometric behavior under both ECNI and EI conditions (*Chapter 4*), and unveil the steps that were taken in developing our specific, sensitive and accurate analytical method for the analysis of PCAs in environmental samples by high resolution gas chromatography electron capture negative ion high resolution mass spectrometry (HRGC/ECNI/HRMS) (*Chapter 5*). By this method we determined

the levels of PCAs, from samples in Canada and the U.S., in fish, sediment, air, water, marine mammals and in human breast milk (*Chapter 6*).

# Chapter 2

## MASS SPECTROMETRY

### 2. INSTRUMENTATION

#### 2.1 MASS ANALYZERS

Several forms of mass analyzers, which separate ions according to their mass-to-charge ( $m/z$ ) ratio, exist, *e.g.*, double focusing analyzers, quadrupole mass filters, ion traps, time-of-flight analyzers, and ion cyclotron resonance instruments [47-49]. The first two types have been used extensively throughout the course of this research, and will be discussed in more detail.

##### 2.1.1 DOUBLE FOCUSING ANALYZERS

The principle of the single-focusing magnetic deflection mass spectrometer is illustrated in Figure 2.1 [48]. After a substance is ionized, ions are accelerated through a potential difference of 2 to 10 keV away from the ion source and toward the source slit, which is maintained at earth potential [47-51]. The fall in potential energy for the ions is equal to their gain in kinetic energy, and is given by

$$zeV = \frac{mv^2}{2} \quad [2-1]$$

where  $e$  is the electronic charge,  $z$  is the number of such charges on the ion,  $m$  is the mass and  $v$  is the velocity of the ion and  $V$  is the accelerating voltage.

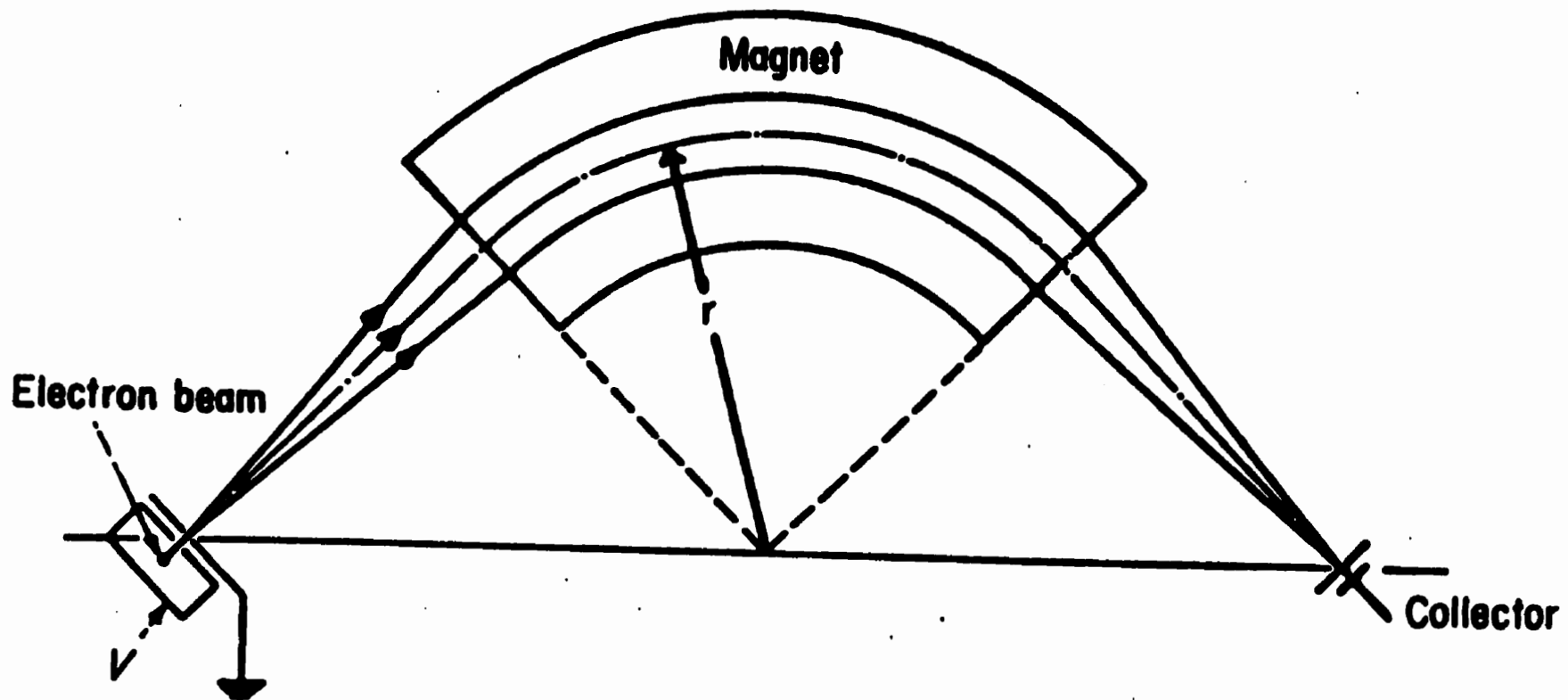


Figure 2.1 Schematic diagram of a single-focussing magnetic sector instrument [48]

For an ion to reach the collector slit and be recorded, it must traverse a path of radius of curvature  $r$  through the magnetic field of strength  $B$ . The equation of motion of the ion is

$$\frac{mv}{r} = Bze \quad [2-2]$$

Rearrangement of equation 2-2 in the form  $mv = Bzer$ , demonstrates that a magnetic sector is a momentum analyzer, rather than a mass analyzer as is commonly assumed [48,49].

Combining equations 2-1 and 2-2 gives the basic mass spectrometer equation governing the path of an ion through the magnetic sector

$$\frac{m}{z} = \frac{B^2 r^2 e}{2V} \quad [2-3]$$

Equation 2-3 shows that by varying either  $B$  or  $V$ , ions of different  $m/z$  ratio, separated by the magnetic field, can be made to reach the collector, thereby yielding a mass spectrum. The most common form of the mass scan is the exponential magnet scan, *i.e.*, changing  $B$ , downwards in mass [48]. Scanning of the accelerating voltage,  $V$ , would, at first sight, appear to be advantageous because of the ease of rapid scanning and the ease of scan control. Change of  $V$ , however, causes defocusing and loss of sensitivity, and is consequently seldom used as a method of scanning [48].

Since a magnetic sector is a momentum rather than a mass analyser, ions of the same mass but of differing translational energy are not brought to focus in a

single-focusing magnetic deflection instrument [47-49,52]. The translational energy spread of the ions formed in the ion source, will cause a broadening of the mass spectral peaks and therefore limit the instrument resolution [52].

The inability of a single magnetic sector instrument to provide more than a limited resolution under practical conditions can be overcome by the addition of an electrostatic sector (see Figure 2.2). Coupling the two sectors now reduces the translational energy spread by introducing the velocity focusing properties of the electrostatic sector. As shown in Figure 2.2, if the outer plate of the electric sector is made positive with respect to the inner plate and a beam of positive ions, varying slightly in kinetic energy, enters the radial electric field, only those ions with a kinetic energy such that the electrostatic force,  $Eze$ , on the ions causes them to follow the correct path of radius,  $R_e$ , will pass through the electric sector

$$Eze = \frac{mv^2}{R_e} \quad [2-4]$$

By combining equations 2-1 and 2-4 we obtain the relation for the path of an ion through the electric sector

$$R_e = \frac{2V}{E} \quad [2-5]$$

The electric sector, when its voltage is kept constant ( $E$  is proportional to the electric sector voltage), focuses ions according to their kinetic energy only (independent of  $m/z$ ) and is therefore referred to as an energy or velocity focussing device. The combined use, and the geometry, of the electric and magnetic sectors shown in Figure 2.2 gives a double-focussing mass spectrometer of Nier-Johnson

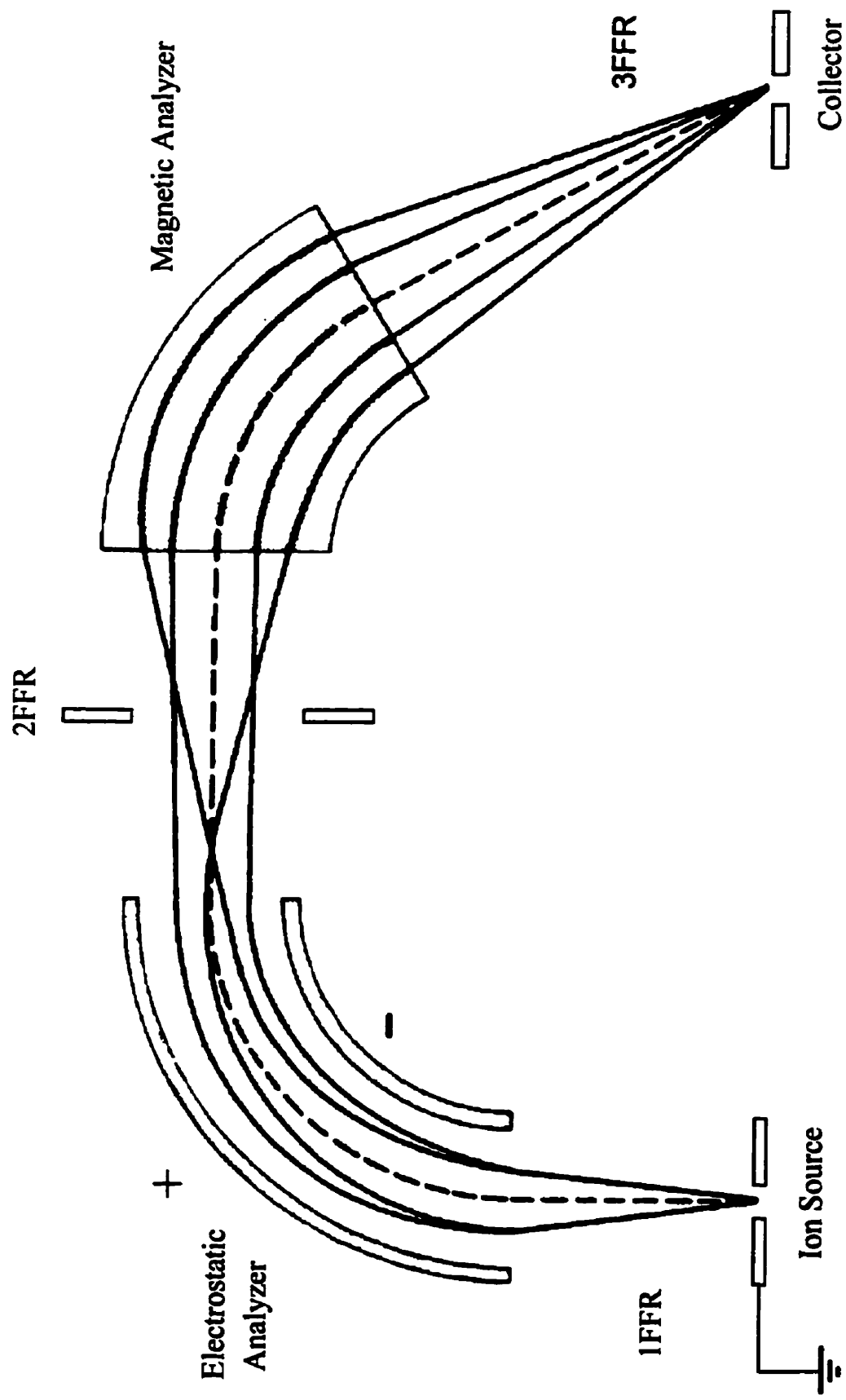


Figure 2.2. Schematic diagram of a double-focussing magnetic sector instrument of Nier-Johnson geometry, in which the electrostatic analyzer precedes the magnetic analyzer (EB geometry) [46].

geometry.

### **2.1.2 QUADRUPOLE ANALYZER**

The quadrupole mass analyser consists of four parallel rods of hyperbolic or circular cross-section that are symmetrically arranged with respect to the z-axis as shown in Figure 2.3 [48,49]. A voltage made up of a d.c. component,  $U$ , and a radio-frequency (r.f.) component,  $V_0 \cos \omega t$ , is applied between adjacent rods ( $\omega$  is the frequency of the r.f. voltage). Ions injected into the filter with a small accelerating voltage, typically 10–20 V, are made to oscillate in the  $x$  and  $y$  directions, *i.e.*, in the planes normal to the rod length, by the applied electric fields [48,49,53]. Provided its oscillations in these planes are stable, an ion of a particular  $m/z$  will drift along the z-axis, on its oscillatory path, within the bounds of the rod assembly, and reach the collector. Stable oscillations are achieved by ions of a given  $m/z$ , oscillation frequency, r.f. and d.c. voltages [49,53]. Mass scanning is achieved by varying the d.c. and r.f. voltages, while maintaining the ratio,  $U/V_0$ , constant. A combination of  $U$  and  $V_0$  in this manner, ensures that only ions of a particular  $m/z$  have stable trajectories and are thus allowed to pass through the system, at any one point in the scan, with all other ions being excluded [52].

### **2.2 METHODS OF IONIZATION**

Three different methods of ion formation were utilized in this research; electron ionization (EI), electron capture negative ionization (ECNI) and plasm spray<sup>TM</sup> ionization (PSP), all of which will be described briefly.

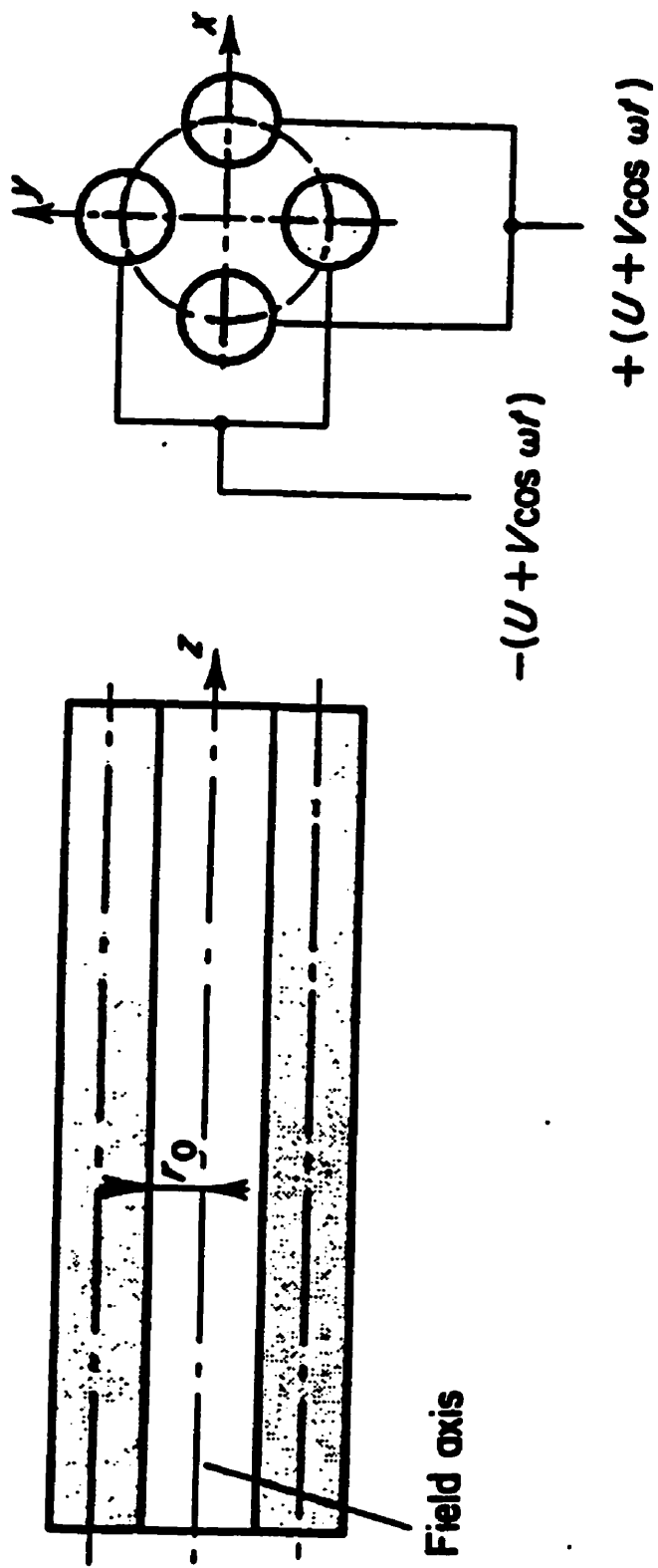


Figure 2.3 Schematic diagram of a quadrupole analyzer [48]

### 2.2.1 ELECTRON IONIZATION

In the EI ion source, first described by Dempster in 1921 [54], and subsequently developed commercially by Nier [55], sample vapour at a reduced pressure flows through a region traversed by an electron beam (*see* Figure 2.4) [48,49]. Electrons, obtained by heating a tungsten or rhenium filament, are accelerated by a voltage (5 to 100V) towards the wall of the ionization chamber, A. The ionizing beam passes through a narrow slit, aided by a pair of collimating magnets to provide a field of a few hundred gauss, which confines the electron beam to a narrow helical path. The ionizing beam current may be controlled by monitoring the total filament emission, or, more commonly, by feedback control from the current reaching the trap plate, *i.e.*, trap stabilization [50].

Volatilized analyte molecules (M) entering the ionizing region, will be ionized by an electron which impinges upon it only if the electron energy is greater than the ionization energy (IE) of M. Ionization occurs when the electron imparts sufficient energy to the neutral M, to bring about ionization (equation 2-6). It is estimated that only 1 in 100 molecules in the ion source are ionized [47-52].



This *electron-molecule* interaction results in the formation of a positively charged species,  $M^{+\bullet}$ , referred to as the molecular ion. Now, if the electron colliding with M imparts more energy than that necessary to ionize M, the energy becomes stored as internal energy, which is subsequently released by the formation of fragment ions (equation 2-7). This fragmentation would, of course, be characteristic of the molecule being ionized.

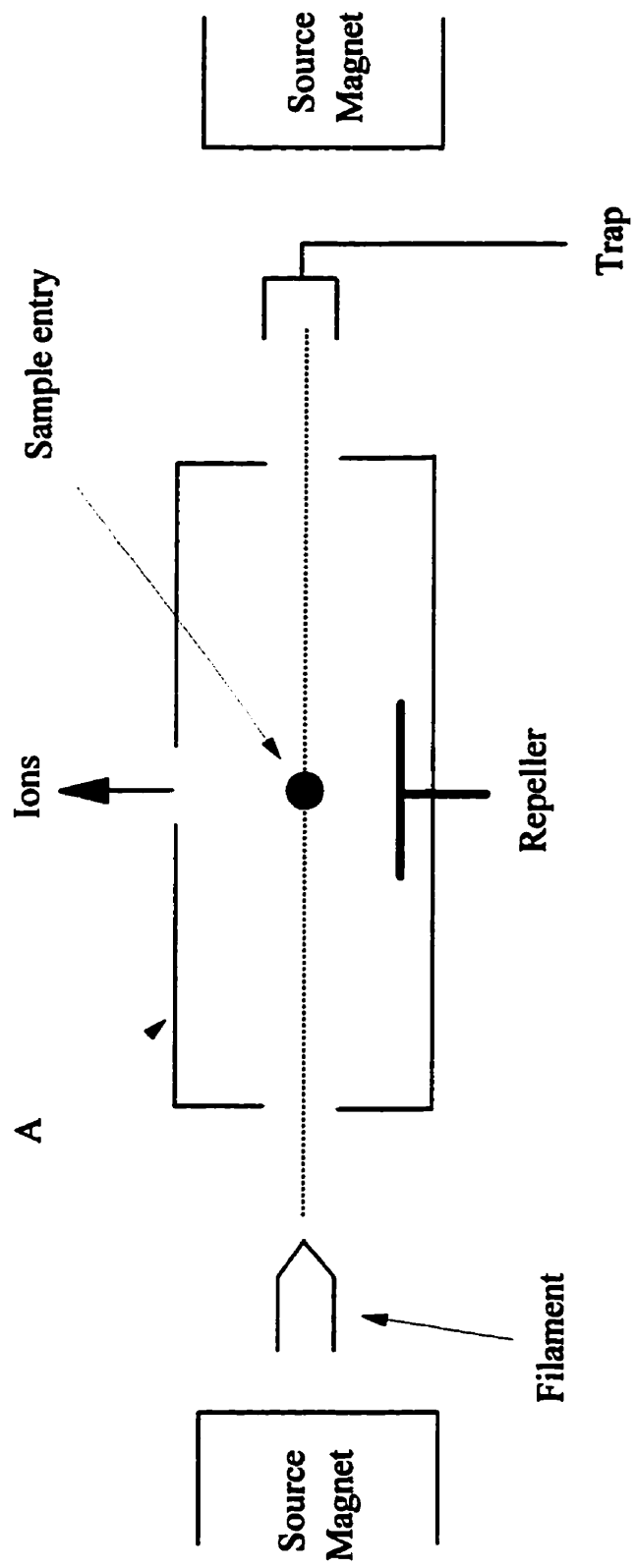


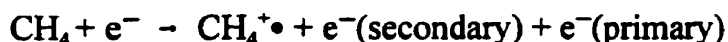
Figure 2.4. Schematic diagram of an electron-ionization ion source.



### 2.2.2 ELECTRON CAPTURE NEGATIVE IONIZATION.

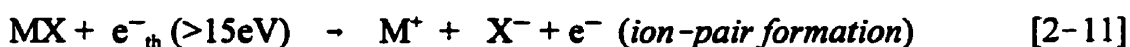
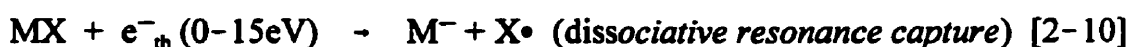
Electron capture negative ionization (ECNI), a derivative of the classical chemical ionization (CI) technique developed by Munson and Field (1966), produces negative ions that are characteristic of analyte molecules by the interaction of thermal electrons ( $e^-_{th}$ ), *i.e.*, electrons of low energy, with neutral analyte molecules (M) [44,49,56,57]. It is important to emphasize that, unlike the classical CI technique the basis of which is *ion-molecule* reactions, ECNI mass spectrometry generates negative ions by *electron-molecule* reactions [44].

Monoenergetic electrons of near thermal energies can be generated by colliding high energy electrons, which are emitted from a filament, with an enhancement or moderating gas (typically methane or argon) present in the ion source of the MS at a pressure of  $\sim 1$  torr [44,58]. Bombardment of the moderating gas with high energy electrons produces a mixture of ions, electrons and radicals; the secondary electrons produced have near thermal energies (equation 2-8) [44].



The energies of the electrons are further reduced by collisions with neutral molecules of the moderating gas. At an ion source pressure of 1 Torr, it has been estimated that approximately 55% of the electrons in the source have energies close to 0.0 eV, and another 6% have energies of  $\sim 0.2$  eV [58,59].

Neutral analyte molecules entering the MS are now exposed to a high pressure ion source having a small cross-sectional area, saturated with  $e^-_{th}$ . Providing the analyte molecules contain atoms of high electrophilicity (X), negative ions can be generated by one of three mechanisms, depending upon the energy of the  $e^-_{th}$  [44].



### 2.2.3 PLASMASPRAY IONIZATION

Plasmaspray<sup>TM</sup> ionization (PSP) is a derivative of the classical thermospray ionization (TSP) technique developed by Vestal and co-workers (1980) for on-line liquid-chromatography MS (LC-MS) coupling [60-62]. Commonly referred to as discharge assisted thermospray, PSP is a gas phase ionization technique similar in concept to CI wherein the mobile phase vapor is used as the reagent gas [63].

Effluent from an LC-column is interfaced directly to the MS *via* a heated capillary (0.15 mm i.d. x 1.5 mm o.d) vaporizer (*see* Figure 2.5) [63]. The capillary is heated sufficiently so that the mobile phase is partially vaporized, producing a high velocity jet that propels the analyte and the remainder of the solvent into the ion source as a beam of droplets or particles [60]. Prior to the injection of effluent into the ion source, an electrical discharge struck from a discharge electrode inserted through the walls of the ion source causes ionization of the solvent vapor ( $S^-$ ). The ionized solvent vapor forms a CI reagent gas

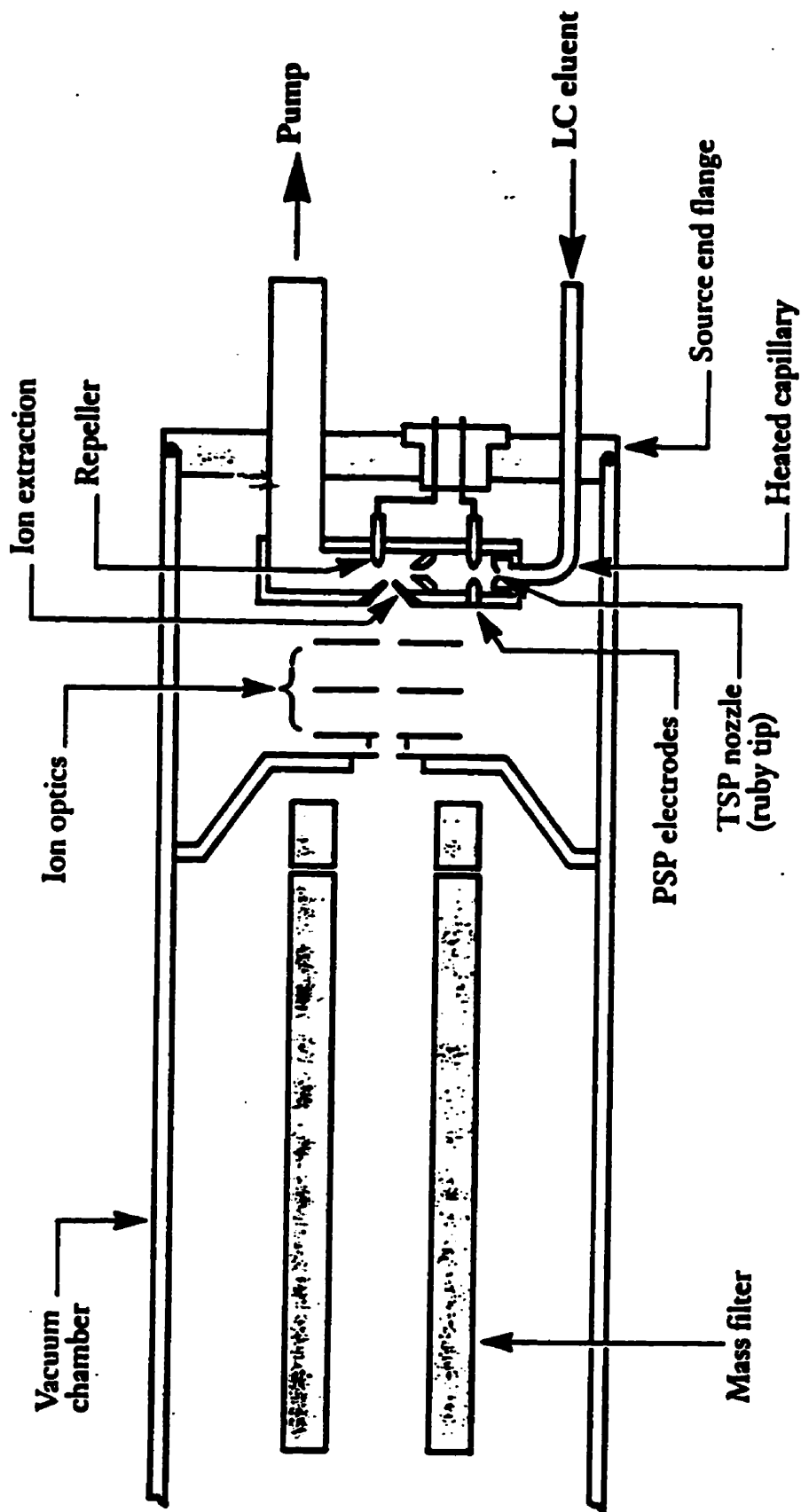


Figure 2.5 Schematic diagram of a combined Thermospray/Plasmaspray™ ion source [63]

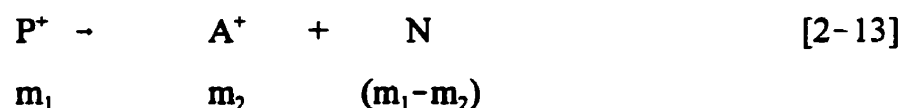
plasma, which in turn ionizes neutral analyte molecules (equation 2-12) [63]. Negative analyte ions are formed by proton abstraction by the negative solvent vapor ions ( $S^-$ ), and ionization efficiencies are governed by the relative proton affinities of the solvent vapor and the analyte [63].



### 2.3 METASTABLE IONS.

The ionization of neutral analyte molecules in the ion source of a MS results in the formation of three types of ions: (i) stable ions, *i.e.*, ions which travel to the detector without decomposition (rate constant for decomposition  $< 10^4 \text{ s}^{-1}$ ) and are recorded as  $M^{+\bullet}$ , (ii) unstable ions, *i.e.*, ions which decompose immediately in the ion source (rate constant for decomposition  $> 10^6 \text{ s}^{-1}$ ) so that only fragment ions travel to the detector and are recorded as part of the normal mass spectrum, and (iii) metastable ions, *i.e.*, ions that leave the ion source but have sufficient excess internal energy so that they decompose (rate constant for decomposition  $10^4 - 10^6 \text{ s}^{-1}$ ) before they reach the detector [48,52,64].

Consider a decomposition in which a parent ion,  $P^+$ , of mass  $m_1$ , yields a fragment ion  $A^+$ , of mass  $m_2$ , and a neutral fragment N (equation 2-13).



As shown earlier, ions  $P^+$  and  $A^+$  present *in the ion source* will, after acceleration, possess kinetic energy equal to  $zeV$  [equation 2-1]. By suitable adjustment of the magnet current, B, ions  $P^+$  and  $A^+$  are collected at the detector according to equation 2-3,  $m/z = B^2 r^2 e / 2V$ ; these are called *normal* ions.

Consider now, the reaction shown in equation 2-13, occurring *outside the ion source*. The kinetic energy in  $P^+$ , viz., zeV, now must be shared between  $A^+$  and  $N$  in accordance with the law of conservation of momentum [52]. Thus,  $A^+$ , referred to as a *metastable product ions*, will have only a part of the original energy imparted to  $P^+$ , zeV, and will not be allowed to pass through the electrostatic analyzer because, as shown earlier, it is an energy focussing device. Although product  $A^+$  ions, have the same mass as normal  $A^+$  ions, they are collected differently because they do not possess the same kinetic energy [52].

The actual place in the mass spectrometer where fragmentation occurs (equation 2-13) determines how the metastable decompositions may be detected. In a double focusing mass spectrometer of EB geometry (Figure. 2.2), there are three distinct regions where metastable ions may decompose and these are referred to as the first (between the ion source and electrostatic analyzer, 1FFR), second (between the electrostatic and magnet analyzers, 2FFR) and third (between the magnet and collector, 3FFR) field free regions (*see* Figure 2.2).

Decompositions occurring in the 2FFR, give rise to diffuse peaks at an apparent mass  $m^*$  given by  $m_2^2/m_1$ , in the normal mass spectrum [50,52]. The broadness and relatively low abundance usually associated with these peaks, as well as the fact that there may be no unique solution for  $m^*$  (two unknown variables  $m_1$  and  $m_2$ ), make it difficult, in some cases, to assign unambiguous values to  $m_1$  and  $m_2$  [51].

Decompositions occurring in the 1FFR, however, can give one a direct indication of the parent-daughter relationship between ions in a mass spectrum, because the position and kinetic energy of the ions can now be defined accurately, and because simple computer controlled scanning techniques can be used to detect

metastable product ions without interference from normal ions. These techniques, collectively referred to as *linked scanning*, involve varying the electric sector voltage simultaneously with either the accelerating voltage or the magnetic field so as to maintain a specified relationship throughout the scan [49,50,52,65-67].

Table 2.1 illustrates some of the characteristics of the three types of linked scanning techniques, viz., B/E, B<sup>2</sup>/E and (B/E)(E<sub>0</sub>-E)<sup>1/2</sup>, used extensively throughout the course of this research. The following sections illustrate the derivations of these B-E scans.

### 2.3.1 DAUGHTER ION SCANNING

The aforementioned B/E linked scan, commonly referred to as daughter ion linked scanning, enables the daughter ions, A<sup>+</sup>, formed from a particular parent ion, P<sup>+</sup>, to be identified [51,52,65]. After acceleration, the kinetic energies of P<sup>+</sup> and A<sup>+</sup> ions formed in 1FFR are  $zeV = m_1 v_1^2 / 2$  and  $zeV(m_2/m_1) = m_2 v_2^2 / 2$ , respectively. Thus A<sup>+</sup> ions formed in 1FFR will have a velocity  $v_2 = v_1 = v = (2zeV/m_1)^{1/2}$ . If B<sub>0</sub> and B are the respective magnetic fields required to transmit P<sup>+</sup> and A<sup>+</sup> ions formed in 1FFR, through the magnetic sector, then from equation 2.2 we obtain:

$$B_0 = \frac{m_1 v}{ze r} ; \quad B = \frac{m_2 v}{ze r}$$

and therefore:

$$\frac{B}{B_0} = \frac{m_2}{m_1} , \quad \text{or} \quad B = \left(\frac{m_2}{m_1}\right) B_0 \quad [2-14]$$

**Table 2.1 Characteristics of scanning modes for observation of metastable ions formed in the IFFR.**

<b>Type of Scan</b>	<b>Description of Mode</b>	<b>Metastable ions determined</b>
<b>B/E</b>	Accelerating voltage constant, the electric sector voltage and magnetic field scanned, such that the ratio B/E is kept constant.	Parent ion is examined, and the daughter(s) ion formed during fragmentation determined.
<b>B<sup>2</sup>/E</b>	Accelerating voltage constant, the electric sector voltage and the magnetic field scanned such that the ratio B <sup>2</sup> /E is kept constant.	Daughter ion is examined, and the parent(s) ion giving rise to them are determined.
<b>(B/E)(E<sub>0</sub> - E)<sup>1/2</sup></b>	Accelerating voltage constant, the electric sector voltage and the magnetic field scanned such that the ratio (B/E)(E <sub>0</sub> - E) <sup>1/2</sup> is kept constant.	Daughter ions arising from the loss of a neutral species of constant mass from various parent ions are determined.

The magnetic field, initially set to focus only P<sup>+</sup> ions, must therefore be decreased by a factor of m<sub>2</sub>/m<sub>1</sub> so as to allow A<sup>+</sup> ions to pass through the magnetic sector.

If E<sub>0</sub> and E are the respective electric sector fields needed to transmit P<sup>+</sup> and A<sup>+</sup> ions formed in the 1FFR through the electric sector then, from equation 2-4, we have

$$E_0 = \frac{m_1 v^2}{R_0 z e} ; \quad E = \frac{m_2 v^2}{R_0 z e}$$

and therefore:

$$\frac{E}{E_0} = \frac{m_2}{m_1} , \quad \text{or} \quad E = \left(\frac{m_2}{m_1}\right) E_0 \quad [2-15]$$

The electric sector voltage, initially set to focus those ions with the full kinetic energy imparted to them in the ion source must, like B, be decreased by a factor of m<sub>2</sub>/m<sub>1</sub> so as to allow A<sup>+</sup> ions formed in the 1FFR to pass through the electric sector. On combining equations 2-14 and 2-15 we have:

$$\frac{B}{B_0} = \frac{E}{E_0} = \frac{m_2}{m_1}$$

$$\frac{B_0}{E_0} = \frac{B}{E} = \text{constant} \quad [2-16]$$

Since B and E are changed by the same factor, m<sub>2</sub>/m<sub>1</sub>, then scanning the magnetic and electric fields simultaneously such that B/E remains constant will reveal all the

product ions resulting from dissociation of selected 1FFR metastable parent ions [51].

### 2.3.2 PARENT ION SCANNING

In a  $B^2/E$  linked scan, commonly referred to as parent ion linked scanning, the electric sector voltage and the magnetic field are initially set to transmit normal  $A^+$  ions formed in the ion source [48,51,52,65]. After acceleration, their velocity is  $v = (2zeV/m_2)^{1/2}$ . The velocity of  $A^+$  ions formed in the 1FFR from metastable  $P^+$  ions, however, is  $v_0 = (2zeV/m_1)^{1/2}$ . Therefore, if  $B_0$  and  $B$  are the respective magnetic fields needed to transmit normal  $A^+$  ions and  $A^+$  ions formed in the 1FFR through the magnetic field then from equation 2-2, we have:

$$B = m_2 \frac{(2zeV/m_1)^{1/2}}{r z e}$$

$$B_0 = m_2 \frac{(2zeV/m_2)^{1/2}}{r z e}$$

and therefore:

$$B = \left(\frac{m_2}{m_1}\right)^{1/2} B_0 \quad [2-17]$$

As in the  $B/E$  linked scan, the electric sector voltage in this linked scan must be decreased by a factor of  $m_2/m_1$  so as to allow the transmission of daughter ions through the electric sector, *i.e.*,  $E = (m_2/m_1)E_0$ . On combining equations 2-15 and 2-17 we obtain:

$$\frac{B^2}{B_0^2} = \frac{E}{E_0} = \frac{m_2}{m_1}$$

$$\frac{B_0^2}{E_0} = \frac{B^2}{E} = \text{constant} \quad [2-18]$$

So that, to observe parent ions of a chosen daughter ion,  $A^+$ , requires scanning such that  $B^2/E$  remains constant [51].

### 2.3.3 CONSTANT NEUTRAL LOSS SCANNING

In a  $(B/E)(E_0 - E)^{1/2}$  linked scan, commonly referred to as constant neutral loss (CNL) linked scanning, the electric sector and magnetic field are set to detect all metastable ions which result from fragmentations involving elimination of a neutral species of a chosen mass [48,52,66,67].

Consider the 1FFR decompositions:

$$(a) \ m_{a1}^+ \rightarrow m_{a2}^+ + n \quad v_{\text{parent}} = v_{\text{daughter}} = v_a \quad [2-19]$$

$$(b) \ m_{b1}^+ \rightarrow m_{b2}^+ + n \quad v_{\text{parent}} = v_{\text{daughter}} = v_b \quad [2-20]$$

If  $E_0$  is electric sector field needed to transmit the parent ions  $m_{a1}^+$  and  $m_{b1}^+$ , which decompose in the 1FFR, then

$$E_0 = \frac{m_{a1} v_a^2}{e r_e} = \frac{m_{b1} v_b^2}{e r_e} \quad [2-21]$$

and thus

$$\frac{V_a}{V_b} = \left(\frac{m_{b1}}{m_{a1}}\right)^{1/2} \quad [2-22]$$

Similarly, if  $E_a$  and  $E_b$  are the electric sector energies needed to transmit the daughter ions  $m_{a2}$  and  $m_{b2}$  formed in the IFFR, then

$$E_a = \frac{m_{a2}V_a^2}{e r_e} \quad [2-23]$$

and

$$E_b = \frac{m_{b2}V_b^2}{e r_e} \quad [2-24]$$

Combining equations 2-21 with 2-23 and 2-24 we obtain

$$\frac{E_a}{E_o} = \frac{m_{a2}}{m_{a1}} \quad ; \quad \frac{E_b}{E_o} = \frac{m_{b2}}{m_{b1}}$$

Now if  $B_a$  and  $B_b$  are the respective magnetic sector fields required to transmit the daughter ions  $m_{a2}$  and  $m_{b2}$ , then

$$B_a = \frac{m_{a2}V_a}{e r} \quad ; \quad B_b = \frac{m_{b2}V_b}{e r}$$

therefore:

$$\frac{B_a}{B_b} = \frac{m_{a2}v_a}{m_{b2}v_b} = \frac{m_{a2}}{m_{b2}} \left(\frac{m_{b1}}{m_{a1}}\right)^{1/2} \quad [2-25]$$

Combining equations 2-23 and 2-24 with 2-25 we obtain

$$\frac{B_a}{B_b} = \frac{E_a}{E_b} \left(\frac{m_{a1}}{m_{b1}}\right) \left(\frac{m_{b1}}{m_{a1}}\right)^{1/2} = \frac{E_a}{E_b} \left(\frac{m_{a1}}{m_{b1}}\right)^{1/2}$$

Now from equation 2-19

$$\frac{m_{a2}}{m_{a1}} = \frac{m_{a1} - n}{m_{a1}} = 1 - \frac{n}{m_{a1}} = \frac{E_a}{E_o}$$

and

$$\frac{n}{m_{a1}} = 1 - \frac{E_a}{E_o} = \frac{E_o - E_a}{E_o}$$

therefore

$$\frac{m_{a1}}{n} = \frac{E_o}{E_o - E_a}$$

Similarly,

$$\frac{m_{b1}}{n} = \frac{E_o}{E_o - E_b}$$

Therefore

$$\frac{B_a}{B_b} = \frac{E_a}{E_b} \left( \frac{E_0 - E_b}{E_0 - E_a} \right)^{1/2}$$

$$\frac{B_a}{E_a} (E_0 - E_a)^{1/2} = \frac{B_b}{E_b} (E_0 - E_b)^{1/2} \quad [2-26]$$

So that, to observe daughter ions which arise from the loss of a neutral species of constant mass from various parents ions requires scanning such that the ratio  $(B/E)(E_0 - E)^{1/2}$  is kept constant.

## 2.4 COLLISIONALLY INDUCED DISSOCIATION

Metastable ions decompose spontaneously because of their internal energy and, as we have shown, are easily detected if the decomposition occurs within a field free region. This decomposition is often termed unimolecular because the decomposition involves no second body interaction. Stable ions, however, can also be made to decompose if enough internal energy is imparted to them. One way to achieve this is to cause the ions to collide with a neutral gas, thus producing a bimolecular interaction, resulting ultimately in decompositions of the ion [64].

In practice, an inert gas (usually argon or helium) is introduced into the IFFR. The gas is normally leaked into a small collision cell, which is maintained at a relatively high pressure, while the regions around it are still at very low pressures. Stable ions, passing through the collision region, that collide inelastically with the collision gas have a small fraction of their translational energy converted into internal energy ( $\sim 10\text{eV}$ ) and this can result in subsequent

fragmentation [50,52,64]. These collisionally induced decompositions (CID) give rise to CID spectra which can be measured in the same way as metastable ion spectra.

## **2.5 SELECTED ION MONITORING**

In selected ion monitoring (SIM), the mass spectrometer is tuned only to a few *pre-selected* ions (usually 6 to 10); complete mass spectra are, therefore, not taken during the GC-MS analysis. SIM can be used for the detection of very low ion abundances, and the gain in sensitivity over scanning the complete mass spectrum for a specific ion is proportional to the ratio of the time the mass spectrometer is tuned to that ion, to the time the mass spectrometer spends on the same ion when scanning to obtain a complete mass spectrum [68].

Consider a mass spectrum covering a 500 u range that has been scanned in 2 sec. The mass spectrometer would therefore, only be tuned to each specific  $m/z$  for  $\sim 2/500$  sec. If the mass spectrometer was tuned to only one ion for the entire 2 sec, this would represent an increased sensitivity factor of 500 for that ion [68].

In practice, SIM is achieved by keeping the magnetic field constant and by rapidly switching the accelerating voltage so that ions of a particular  $m/z$  can be focused. Apart from the increase in sensitivity, selectivity is also increased, since ions other than the few *pre-selected* ions will not be detected. Sensitivity can be increased further by dividing the total recording time into a number of retention time windows, during which a smaller number of ions is monitored.

## **2.6 RESOLVING POWER**

The resolving power (RP) of a MS is a measure of its ability to separate two

ions of any defined mass difference [52]. The resolving power necessary to separate two ions of mass  $m$  and  $(m+\Delta m)$  respectively is given by:

$$RP = m/\Delta m \quad [2-27]$$

Magnetic sector instruments use the classical 10% valley definition of peak separation (Figure 2.6(a)). For two overlapping peaks,  $m_1$  and  $m_2$ , the RP may be defined in terms of the mass difference ( $\Delta m$ ) between them such that the peaks are said to be resolved if  $(h/H) \times 100 \leq 10$ , where  $H$  is the height of the peaks and  $h$  measures the depth of the valley between them. The RP is then the value of  $m_1/\Delta m$  when  $(h/H) \times 100$  is equal to 10 [52].

The RP of a mass spectrometer is often increased so that the cross-contribution between one mass and another is reduced, and so that the interferences from background or other sample components, which are close to the mass being monitored, can be discriminated against (see Figure 2.6(b)) [48]. The operation of the mass spectrometer at increased RP, however, decreases the absolute sensitivity of the instrument.

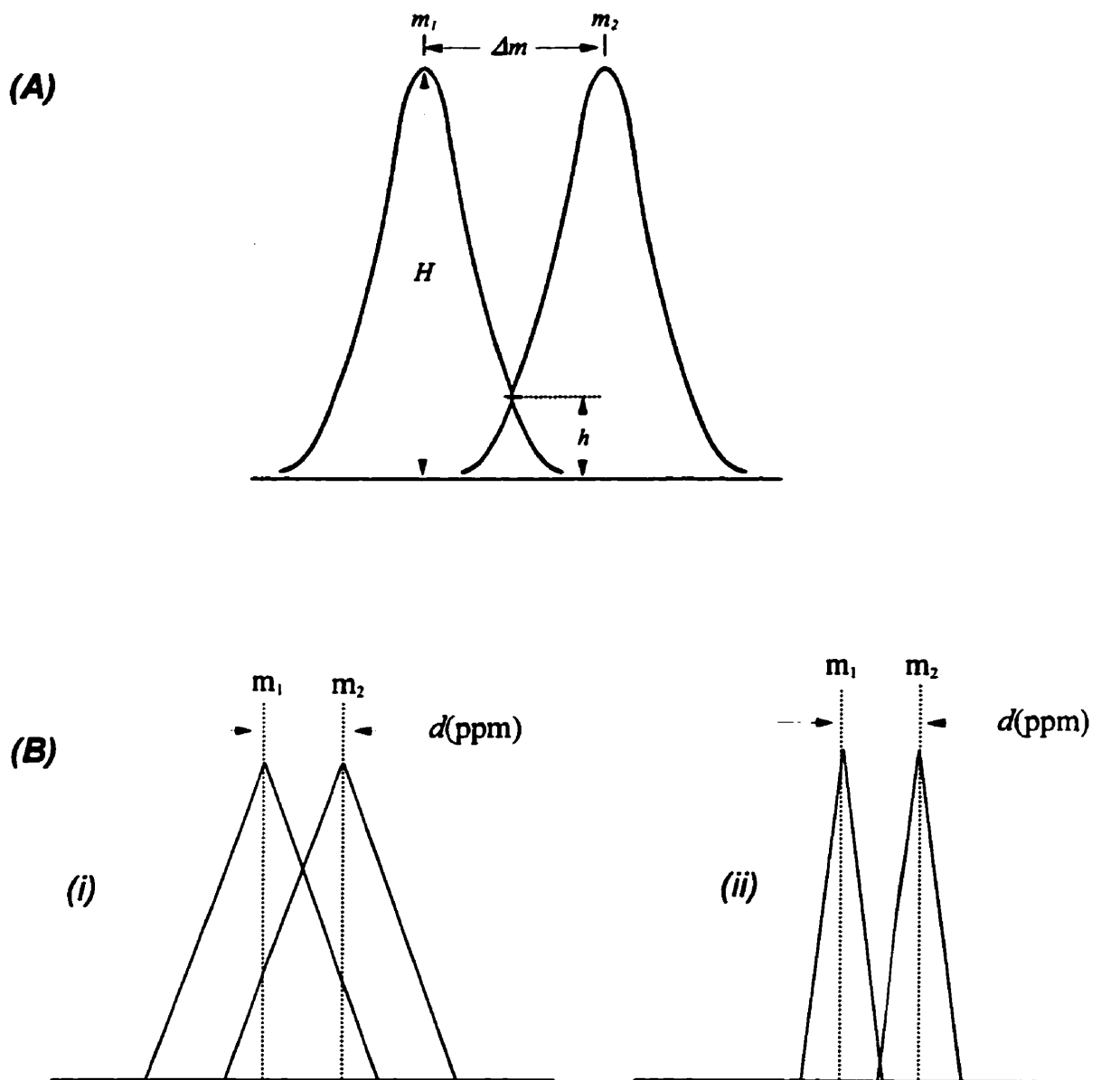


Figure 2.6. (A) Two overlapping ion peaks  $M_1$  and  $M_2$  of equal intensity.  
 (B) Cross-contribution at different resolving powers:  
 (i) Low resolving power - significant cross-contribution between ions,  
 (ii) Higher resolving power - no cross-contribution between ions.

## ***Chapter 3***

### ***EXPERIMENTAL***

#### **3. CHROMATOGRAPHY**

##### **3.1 HIGH PRESSURE LIQUID CHROMATOGRAPHY**

HPLC separations were performed on a Waters Novapak™ 150 mm x 3.9 mm C<sub>18</sub> column with 3 μm packings, maintained at a temperature of 30°C. Solvent delivery was provided by a Waters 600-MS system controller (Waters Chromatography Division, Millipore Corp., Massachusetts), and a model U6K injection valve. A gradient elution was performed using HPLC grade tetrahydrofuran (Caledon Laboratories Ltd., Canada) (A) and Milli-Q water (B). The solvents were filtered through a 0.45 μm filter and sonicated in a water bath to remove dissolved air prior to use. The initial condition 50%A:50%B was held for 3 minutes, ramped linearly to 51%A:49%B over 5 minutes, held there for 15 minutes, and then ramped linearly to 52%A:48%B over 5 minutes, and held there 15 minutes. A constant flow rate of 0.75 mL/min was used throughout the gradient. Injections were performed with a Hamilton 25 μL syringe (Hamilton Company, Nevada).

##### **3.2 HIGH RESOLUTION GAS CHROMATOGRAPHY.**

Analyses were performed on a Hewlett-Packard (HP) 5890 Series II gas chromatograph, fitted with a high resolution 5% phenyl-substituted methylpolysiloxane stationary phase (DB-5MS) fused silica column (30 m x 0.25

mm i.d., 0.25  $\mu\text{m}$  film thickness; Chromatographic Specialities, Brockville, Ontario), connected to the mass spectrometer through a heated transfer line maintained at 280°C. All sample injections, as solutions in either hexane or isooctane, were made by a CTC A200SE autosampler under data system control. The injector port temperature was 220°C and helium carrier gas flow rate of 0.75 mL/min was maintained by an electronic pressure program. For the environmental analyses the column temperature program was: initial 150°C; hold for 1 min; ramp to 260°C at 7°C min<sup>-1</sup>; hold for 8:18 min; ramp to 280°C at 10°C min<sup>-1</sup>; hold for 13 min. For the mass spectral analyses (EI and ECNI) of individually synthesized PCAs, the column temperature program was: initial 100°C; hold 0 mins; ramp to 280°C at 10°C min<sup>-1</sup>; hold for 20 mins.

## **3.2 MASS SPECTROMETRY**

### **3.2.1 KRATOS CONCEPT HIGH RESOLUTION MASS SPECTROMETER**

Electron ionization mass spectra of GC effluents were obtained in the positive ion mode with a Kratos Concept (Kratos Analytical, Manchester, England) high resolution double focussing mass spectrometer (EBE geometry) controlled by a Mach 3 data system. Operating conditions were as follows: electron beam energy adjusted for maximum sensitivity (~55eV), electron beam current 500  $\mu\text{A}$ , ion acceleration voltage 8 kV and an ion source temperature of 220°C, measured by a thermocouple located in the ion source body. The scan range used was dependent on the molecule being examined, but was usually  $m/z$  400 to  $m/z$  40, at a fixed rate of 0.7 sec per decade. Perfluorokerosene (PFK) was used as the mass calibrant. Collisional activation was implemented, when necessary, to enhance ion decomposition by introducing argon gas into the

collision cell in 1FFR at a pressure sufficient to attenuate the  $m/z$  231 ion of PFK by *ca.* 50%.

Electron capture negative ion mass spectra, at nominal resolution, were scanned at 1 sec per decade over the mass range  $m/z$  600 to  $m/z$  65, with methane initially, but later changed to argon, as the moderating gas, at an ambient gas pressure of  $\sim 2 \times 10^{-4}$  torr, as recorded by the source ion gauge located adjacent to the source. The electron emission current was 100  $\mu\text{A}$ , the initial electron beam energy was  $\sim 180$  eV, and the ion accelerating voltage was 5.3 kV. Mass spectra were recorded at different ion source temperatures ranging from 120°C to 220°C. In the SIM mode, performed at a resolving power of  $\sim 12\,000$ , the cycle time for each window was 1 sec, with equal dwell times for each ion monitored.

### **3.2.2 TRIO 1000 LOW RESOLUTION MASS SPECTROMETER**

Negative ion plasm spray ionization (NPSP) mass spectra of HPLC effluents was performed with a Trio 1000 (Fisons Analytical Ltd., Canada) quadrupole mass spectrometer. Mass spectra were recorded in the negative ion mode with a plasm spray current of 150  $\mu\text{A}$ , a source temperature of 200°C, a nozzle temperature of 170°C, a repeller voltage of 225 V and an ion source pressure of  $1 \times 10^{-4}$  mbar. NPSP mass spectra were scanned from  $m/z$  350 to  $m/z$  650 in 0.5 sec, under control of a Lab-Base 2.13 data system.

## **3.3 CHEMICALS AND SYNTHESIS**

### **3.3.1 CHEMICALS**

Two commercial PCA products, used as analytical standards, one of  $\text{C}_{10}$ - $\text{C}_{13}$  chain length and  $\sim 60\%$  chlorine by mass (PCA-60) and the other of

$C_{10}$ - $C_{13}$  carbon chain length and ~70% chlorine by mass (PCA-70) were graciously provided by the manufacturers (Dover Chemical Corp., Dover, OH, and Occidental Chemical Corp., Niagara Falls, NY, respectively). Isotopically labelled  $^{13}C_1$ -chlordane (99%  $^{13}C$ ) and  $^{13}C_8$ -mirex (99%  $^{13}C$ ) were purchased from Cambridge Isotope Laboratories Inc. (CIL) (Burlington, ON). Sources of pesticide test mixtures were: toxaphene (CIL), technical chlordane (CIL), a mixture of 87 PCB congeners (Ultra Scientific, North Kingstown, RI), SRM 2261 (concentrated PCB congeners in isooctane) (NIST, Gaithersburg, MD) and MMQA (Marine Mammal Quality Assurance, an "in house" test mixture of persistent organochlorine compounds).

Reagents used for synthesizing individual PCA congeners are outlined below.

### 3.3.2 SYNTHESIS OF POLYCHLORINATED ALKANES

Individual PCA congeners were synthesized by bubbling chlorine gas, at room temperature, into neat solutions of the respective *n*-alkenes, contained in a flask wrapped in aluminum foil to exclude light. In the absence of light, these conditions were expected to lead, predominantly, to addition at the double bond(s). Clean-up of reaction mixtures was done by shaking with NaOH (0.05M). The aqueous phase was then removed and the organic phase was dried with  $MgSO_4$ . The drying agent was removed by filtration, and the residual solution diluted with hexane to give a final concentration of ~ 0.2% (v/v) prior to GC/MS analysis.

The *n*-alkene reagents that were chlorinated, the products formed from the reactions, and the reagent suppliers are shown in Table 3.1. The notation a,b- $M_{x,y}$ , which is used hereafter, denotes the number of carbon (x) and chlorine atoms (y)

Table 3.1 Reaction products of *n*-alkenes with molecular chlorine.

Starting Reagent	Supplier	Products Formed
1,9-Decadiene	Aldrich <sup>a</sup>	(a) 1,2,9,10-M <sub>10,4</sub> <sup>*</sup> (b) 1,2,x,9,10-M <sub>10,5</sub> (c) 1,2,x,y,9,10-M <sub>10,6</sub>
2,8-Decadiene	Wiley-Organics <sup>b</sup>	(a) 2,3,8,9-M <sub>10,4</sub> <sup>*</sup>
1,5,9-Decatriene	Aldrich	(a) 1,2,5,6,9,10-M <sub>10,6</sub> <sup>*</sup> (b) 1,2,5,6,x,9,10-M <sub>10,7</sub>
1-Undecene	Aldrich	(a) 1,2-M <sub>11,2</sub> <sup>*</sup>
1,10-Undecadiene	Wiley-Organics	(a) 1,2,10,11-M <sub>11,4</sub> <sup>*</sup> (b) 1,2,x,10,11-M <sub>11,5</sub> (c) 1,2,x,y,10,11-M <sub>11,6</sub>
2,9-Undecadiene	Wiley-organics	(a) 2,3,9,10-M <sub>11,4</sub> <sup>*</sup> (b) 2,3,x,9,10-M <sub>11,5</sub>
1,11-Dodecadiene	Wiley-Organics	(a) 1,2,11,12-M <sub>12,4</sub> <sup>*</sup> (b) 1,2,x,11,12-M <sub>12,5</sub>

<sup>a</sup> Aldrich Chemical Co.

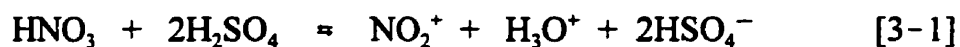
<sup>b</sup> Wiley-Organics

<sup>\*</sup> Compounds investigated by linked scanning mass spectrometry.

present in the PCA molecule; in addition, the numerical prefixes indicate the known positions of the chlorine atoms. When necessary we will indicate the position of a chlorine atom residing in an unknown position with the prefix *x*; this arises from the substitution of hydrogen atoms by chlorine atom *via* free radical chlorination, and is addressed later.

### 3.3.3 PREPARATION OF AN ANALYTICAL REFERENCE STANDARD.

In an attempt to prepare an analytical standard, to be used to determine the accuracy of our analytical protocol, we purified the products derived from the chlorination of 1,5,9-decatriene (0.25 mL) with H<sub>2</sub>SO<sub>4</sub>:HNO<sub>3</sub> (1:1) (2 mL) at 70°C for 20 mins, then cooled them in an ice-bath. The acid-base reaction of the two strong acids (equation 1), generates a nitronium ion, NO<sub>2</sub><sup>+</sup>, which reacts with any residual sites of unsaturation, to form a water soluble product that can be easily removed [69].



After distilled water (5 mL) had been added the mixture was extracted with hexane (F3 x 3 mL). The combined extracts were concentrated to 1mL for clean-up on Florisil. Fractionation on 8 g of reagent grade 60-100 mesh deactivated Florisil (1.2% w/w water) was achieved with the solvent sequence 38 mL of hexane (F1), 42 mL of 15:85 dichloromethane (DCM):hexane (F2), and 52 mL of 1:1 DCM:hexane (F3). Fractions F2 and F3 contained the PCAs and were combined.

Analysis of the cleaned-up extract by full scan GC/EIMS, *i.e.*, in the positive ion mode, showed the major products to be C<sub>10</sub>H<sub>16</sub>Cl<sub>6</sub>, C<sub>10</sub>H<sub>15</sub>Cl<sub>7</sub>,

$C_{10}H_{14}Cl_8$ ,  $C_{10}H_{13}Cl_9$ . Additional peaks in the chromatogram accounted for  $7 \pm 2\%$  of the TIC.

### **3.4 COLLECTION SITES OF ENVIRONMENTAL SAMPLES FOR PCA ANALYSIS**

PCAs were determined in a variety of samples from many different regions in Canada and in the U.S. For clarity, we will reserve the description of the collection sites for *Chapter 6*, where environmental levels of PCA are discussed.

### **3.5 EXTRACTION OF PCAs FROM ENVIRONMENTAL SAMPLES**

A review of procedures used for extraction and isolation of PCAs from environmental matrices revealed that methods for determination of persistent organochlorines should be suitable for recovery of PCAs [70,71]. PCA levels were determined in a variety of environmental matrices; the extraction and clean-up of each are described in separate sections. Extraction and isolation of PCAs from sediments and fish were performed by standard procedures used at the analytical laboratory of the Freshwater Institute (FWI) for determining organochlorine compounds in sediments and biota, with small modifications [70,71]. Extractions of air and water samples were done according to procedures outlined by Hoff *et al.* and Rawn *et al.*, respectively [72,73].

#### **3.5.1 BIOTA EXTRACTION AND CLEAN-UP.**

Biota, which were frozen upon collection, were ground cryogenically (dry ice). Samples (~10 g wet weight) were mixed with anhydrous  $Na_2SO_4$  to yield a flowable powder, spiked with a recovery standard, namely  $^{13}C_1$ -chlordane, and then Soxhlet extracted (glass thimble) with 350 mL of 1:1 (DCM):hexane for 4 h. Ten percent of the extract was used to determine lipid levels gravimetrically; the

remaining extract was used for PCA determination. Lipids were first removed from the samples by gel permeation chromatography (GPC) [37]. The GPC columns (29.5 mm i.d. x 400 mm) were packed with 60 g (dry weight) of 200–400 mesh SX-3 Bio-Beads (Bio-Rad Laboratories, Hercules, CA) that had been soaked in DCM:hexane (1:1) overnight. The column was eluted with 325 mL of DCM:hexane; the first 150 mL contained lipids and was discarded. The remainder was evaporated to 1 mL for clean-up on Florisil. Fractionation on 8 g of reagent grade 60-100 mesh deactivated Florisil (1.2% w/w water) was achieved with the solvent sequence 38 mL of hexane (F1), 42 mL of 15:85 DCM:hexane (F2), and 52 mL of 1:1 DCM:hexane (F3). Fraction F1 contained all the PCBs, chlorinated benzenes, DDT and its metabolites, and other chlorinated aromatics, but no PCAs. Fractions F2 and F3 contained PCAs, along with the  $^{13}\text{C}_1$ -chlordanes, while F3 contained more polar organochlorines such as heptachlor epoxide and dieldrin. For PCA analysis, F2 and F3 were combined, diluted with hexane, and then the solvent volume was reduced to 0.5 mL by a gentle stream of nitrogen prior to GC/MS analysis. A known amount of  $^{13}\text{C}_8$ -mirex, to be used as an internal standard for SIM, was added to the residual solutions at this stage.

### **3.5.2 SEDIMENT COLLECTION AND DATING**

Lakes were sampled by Brian Billeck, Bob Danell and Paul Wilkinson (FWI), from the ice surface with a specially designed box corer (30 x 30 cm) or a 10 cm KB corer [70]. In general, duplicate box and KB cores were collected from the lake, and cores were extruded on site. Cores were then sliced at 1 cm intervals, and the sediment put into plastic bags, sealed at ambient temperature and frozen immediately after collection. After transport to the laboratory, they were stored at 5°C until analysis. The  $^{210}\text{Pb}$  dating technique, previously described by Robbins

(1978), used to determine the sedimentation rates and to assign median ages to the core slices, was performed by Paul Wilkinson (FWI) [74].

### **3.5.2.1 SEDIMENT EXTRACTION AND CLEAN-UP**

Collected sediment samples were freeze dried and sub-samples (~10 g dry weight) were spiked with the same recovery standards as the biota samples, and then Soxhlet extracted with 250 mL of 1:1 DCM:hexane for 24 hr. After removal of sulfur-containing compounds by treatment of the extracts with copper powder (nitric acid washed) for 15 min at room temperature the extracts were fractionated on Florisil, as described above for fish samples. The combined extract (F2 and F3) was diluted with hexane and reduced to a volume sufficient to give a satisfactory response by GC/MS (this varied appreciably, and depended on the sampling site, and ultimately on the level of PCAs present in the sample). A known amount of  $^{13}\text{C}_8$ -mirex, used as the internal standard, was then added.

### **3.5.3 WATER COLLECTION**

Procedures were essentially those described by Rawn *et al.* [73]. In brief, water was collected by Thea Rawn and Thor Halldorson (FWI) using a submersible pump which was placed in the center of the lake, with pumping continued until 18 L had been collected in stainless steel containers. Samples were filtered under pressure through precleaned 1  $\mu\text{m}$  GFC glass fibre filters prior to extraction and clean-up.

#### **3.5.3.1 WATER EXTRACTION AND CLEAN-UP**

Water was adjusted to pH 2 to enable extraction of acid herbicides and phenol derivatives, and then taken to pH 10 to recover hydrophobic organics [73].

Extraction was then performed using DCM. Extracts were evaporated to ~1 mL for clean-up on Florisil. Fractionation on deactivated Florisil (5% w/w water) was achieved with the solvent sequence 20 mL of hexane (F1) followed by 85 mL of 18% ethyl acetate in hexane (F2). For PCA analysis, F1 and F2 were combined, diluted with hexane, and then the solvent volume was reduced to 100  $\mu$ L by a gentle stream of nitrogen prior to GC/MS analysis. A known amount of  $^{13}\text{C}_8$ -mirex was added to the residual solutions as an internal standard.

### **3.5.4 AIR COLLECTION**

Air sample extracts from the Center for Atmospheric Research Experiments (CARE) station at Egbert, ON, were obtained from Ken Brice. Procedures for sample collection were previously outlined by Hoff *et al.* [72]. In brief, collection (~300m<sup>3</sup>) was achieved by using a Sierra Andersen PS-1 PUF sampler. The sample head contained a 10.2 cm diameter Whatman GF/A glass fiber filter (for collection of airborne particulates) followed by a 7.2 cm diameter by 7.5 cm long PUF plug (for collection of organic vapours) of density 0.022 g/cm. Prior to their usage, however, the foam plugs were precleaned by a large-volume Soxhlet extraction with distilled-in-glass grade DCM for at least 12 h. Each foam plug was then dried in air and placed in 250 mL glass sample jars. After sampling, the foam plugs were replaced in the original sample jars, and refrigerated at 4°C, and shipped to the FWI for analysis.

#### **3.5.4.1 AIR EXTRACTION AND CLEAN-UP**

PUF plugs and filters were Soxhlet extracted by Bovar- Concord Environmental (Toronto, ON), with hexane for 4 h. Extracts were then reduced to ~1 mL with a gentle stream of N<sub>2</sub>, and fractionated on Florisil, as described above.

The combined fractions (F2 and F3) were diluted with hexane, and the solvent volume was reduced to 50  $\mu\text{L}$ . A known amount of  $^{13}\text{C}_8$ -mirex was then added prior to GC/MS analysis.

### **3.5.5 MARINE MAMMAL EXTRACTIONS AND CLEAN-UP**

Procedures for extraction and clean-up of blubber tissues were previously described by Muir *et al.* [75]. In brief, samples of blubber (2.2 g) were mixed with anhydrous sodium sulfate (pretreated by heating at 600°C for 6 h) and ball-milled (30 min) with hexane. The extract was centrifuged and a portion (1/11) removed for lipid determination. Extracts were then evaporated to ~ 0.5 mL for clean-up on deactivated Florisil (1.2% v/w) as described above for biota. For PCA analysis, F2 and F3 were combined, diluted with hexane, and then the solvent volume was reduced to 25  $\mu\text{L}$  by a gentle stream of nitrogen prior to GC/MS analysis. A known amount of  $^{13}\text{C}_8$ -mirex was added to the residual solutions at this stage.

### **3.5.6 HUMAN BREAST MILK EXTRACTION AND CLEAN-UP**

Human breast milk samples, voluntarily donated by Inuit women in Northern Québec, were provided by Eric Dewailly of the Community Health Department, Québec. The extraction and clean-up on the samples were reported previously [76]. In brief, the milk sample was hydrolyzed with an alkaline solution to eliminate fats, and was extracted using a hexane-ether mixture. The extract was then purified on Florisil. F2 and F3 were combined, diluted with hexane, and then the solvent volume was reduced to 25  $\mu\text{L}$  by a gentle stream of nitrogen prior to GC/MS analysis. A known amount of  $^{13}\text{C}_8$ -mirex was added to the residual solutions at this stage.

### **3.6 QUALITY CONTROL - RECOVERY EFFICIENCIES**

Analytical recovery efficiencies were assessed by duplicate analyses of multiple samples of sediments and biota with high and low contaminant concentrations [28]. Recovery studies on biota were done by spiking samples of fish from a lake in the Canadian Arctic, which was assumed to have low levels of PCAs. Lake trout muscle tissue homogenates (each ~10 g), collected from Maguse Lake, NWT, Canada, were spiked with 1 µg and 10 µg doses of PCA-60 (six samples at low dose, six at high dose). Another, non-spiked sample, was used as a blank. <sup>13</sup>C<sub>1</sub>-chlordane (8 ng) was also added to each sample. Extraction, work-up, and analytical procedures were identical to those described above.

PCA recovery efficiencies from sediments were estimated by spiking twelve 10 g samples of Na<sub>2</sub>SO<sub>4</sub> with 1 µg and 10 µg doses of PCA-60 (six samples at low dose, six at high dose). Another non-spiked sample of Na<sub>2</sub>SO<sub>4</sub> was used as a blank. <sup>13</sup>C<sub>1</sub>-chlordane (8 ng) was also added to each sample. Extraction, work-up, and analytical procedures were identical to those described above.

### **3.7 STRUCTURAL CALCULATIONS**

Interatomic distances and strain energies of ionized PCAs were estimated with the Molecular Modeling Pro program (WindowChem Software Inc., Fairfield, CA, Version 1.4) and enthalpies of formation with HyperChem (Hypercube Inc., Gainesville, FL, Version 4.5).

## Chapter 4

### MASS SPECTRAL STUDIES

#### 4.0 PLASMASPRAY IONIZATION OF A COMMERCIAL PCA MIXTURE

In 1992 we explored the use of HPLC-NPSP-MS for the analysis of PCA mixtures, with the intent of formulating an alternative approach for quantifying PCAs in environmental matrices [29]. We were prompted to take this approach because a review of the literature, at that time, showed that PCAs would undergo thermal decompositions at elevated temperatures and have low volatilities, two properties that would make them unamenable to GC analysis [1,12,16,18] (we have shown in collaboration with Barrie Webster and Len Sarna, Soil Science, University of Manitoba, that this, in fact, is not the case).

Figure 1.2 (b) showed the HPLC-NPSP-MS total ion chromatogram of a commercial mixture, *viz.*, PCA-70 ( $C_{10}$ - $C_{13}$ , 70% Cl), that was 'separated' into 'peaks' superimposed on a broad hill-like shape, on a reverse phase LC-column [29]. The NPSP mass spectrum of the peak labelled \* in Figure 1.2(b) is shown in Figure 4.1. The high mass ion group of peaks starting at  $m/z$  510 (the  $^{35}\text{Cl}$  isotopic combination), corresponds to ten chlorine atoms, indicating the molecular formula  $C_{12}H_{16}Cl_{10}^{-}$ . The odd-mass peaks in this group correspond, mainly, to loss of a hydrogen atom from the molecular ion. The ion group starting at  $m/z$  496 corresponds to the ion formula  $C_{11}H_{14}Cl_{10}^{-}$ , upon which is superimposed  $C_{11}H_{13}Cl_{10}^{-}$ . Similarly, the groups starting at  $m/z$  476 and  $m/z$  462 correspond to

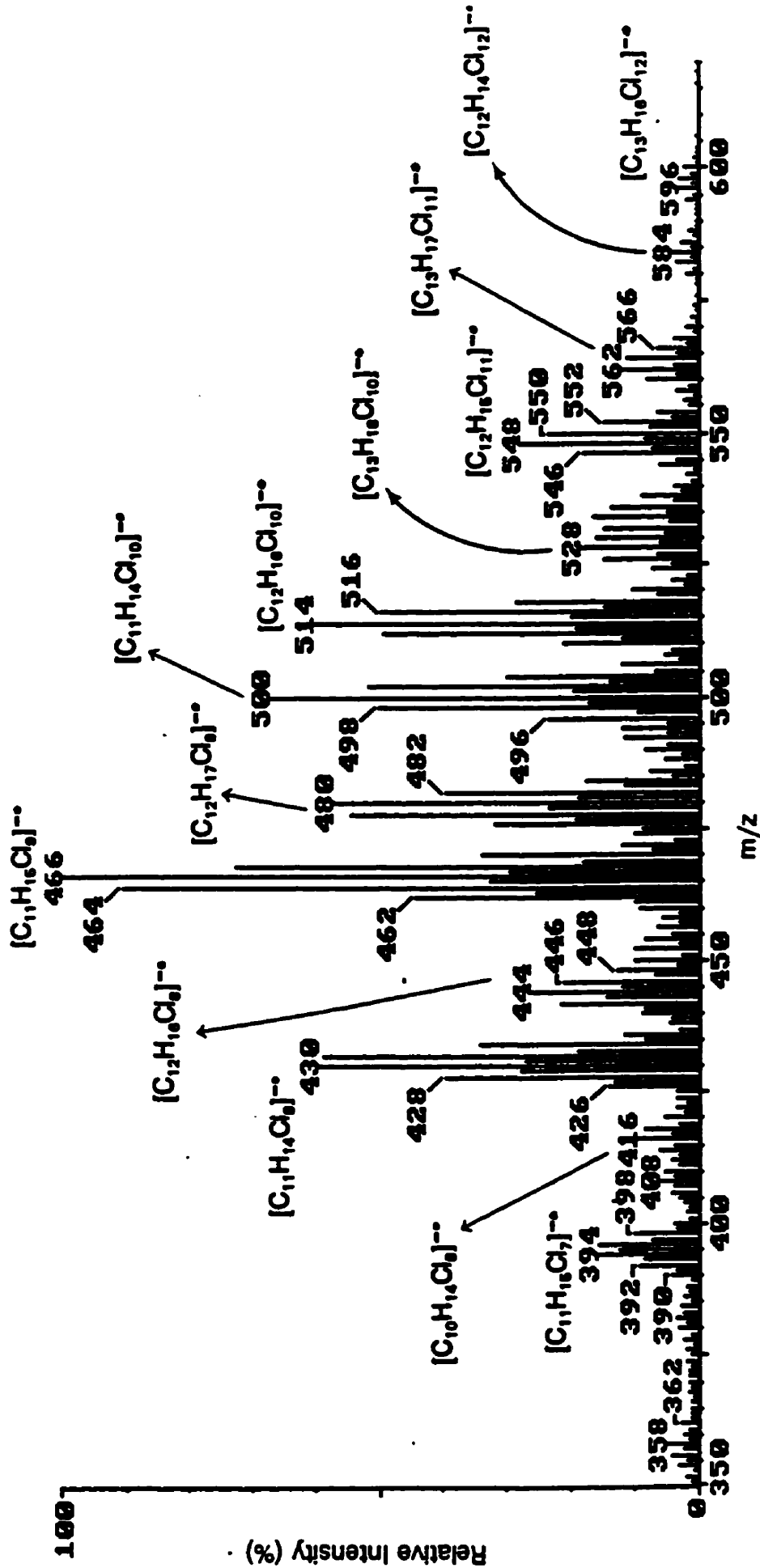


Figure 4.1 NPS mass spectrum of peak labelled \* in figure 1.2 (b).

the molecular ions  $C_{12}H_{17}Cl_9^-$  and  $C_{11}H_{15}Cl_9^-$ , respectively.

The two isotopic patterns of low abundance are probably fragment ions. The ion group starting at  $m/z$  440 corresponds to the formula  $C_{12}H_{16}Cl_8^-$  and could be derived by a losses of HCl or  $Cl_2$  from the molecular ions  $C_{12}H_{17}Cl_9^-$   $C_{12}H_{16}Cl_{10}^-$ , respectively. The ion group starting at  $m/z$  441 corresponds to the formula  $C_{12}H_{17}Cl_8^-$  and is derived by a loss of  $Cl\cdot$  from the molecular ion  $C_{12}H_{17}Cl_9^-$ .

The isotopic pattern starting at  $m/z$  426 corresponds to eight chlorine atoms and is derived from dehydrochlorination of the molecular ion  $C_{11}H_{15}Cl_9^-$ .

The mass spectra of peaks labelled 1 and 2 in Figure 1.2(b) were also examined. Table 4.1 shows the molecular mass and molecular formulas of the ions observed in these peaks, and shows that different molecular formulas are contained within a single peak.

Further development of this method was curtailed once individual PCA congeners were synthesized because we learnt, contrary to statements in the literature, that these compounds do in fact have sufficient volatilities and do not appear to undergo thermal degradation at normal GC operating temperatures. The next sections, therefore, discuss the EI and ECNI mass spectrometry performed on the individually synthesized PCA congeners.

#### **4.1 SYNTHESIZED PCA CONGENERS**

As we mentioned earlier, the synthesis of individual PCA congeners was an essential step toward developing our analytical protocol for quantifying PCAs in environmental matrices by GC/MS because it provided us with an understanding of the behavior of these compounds in the ion source of the mass spectrometer.

Table 4.1. Molecular mass and molecular formulas of ions observed in peaks labelled 1 and 2 of figure 1.2 (b).

Peak No.	Ion Cluster m/z	Molecular formula of ions	Neutral Species
1	391/393/395/397/399	$C_{11}H_{14}Cl_7^- [M_{11,9}-Cl-HCl]^-$	$C_{11}H_{15}Cl_9$ ( $M_{11,9}$ )
	392/394/396/398/400	$C_{11}H_{15}Cl_7^- \bullet [M_{11,9}-Cl_2]^- \bullet$	
	426/428/430/432/434	$C_{11}H_{14}Cl_8^- \bullet [M_{11,9}-HCl]^- \bullet$	
	427/429/431/433/435	$C_{11}H_{15}Cl_8^- [M_{11,9}-Cl]^-$	
	462/464/466/468/470	$C_{11}H_{15}Cl_9^- \bullet [M_{11,9}]^- \bullet$	
2	461/463/465/467/469	$C_{11}H_{14}Cl_9^- [M_{11,9}-H]^-$	$C_{11}H_{15}Cl_9$ ( $M_{11,9}$ )
	462/464/466/468/470	$C_{11}H_{15}Cl_9^- \bullet [M_{11,9}]^- \bullet$	
	475/477/479/481/483	$C_{12}H_{16}Cl_9^- [M_{12,9}-H]^-$	$C_{12}H_{17}Cl_9$ ( $M_{12,9}$ )
	476/478/480/482/484	$C_{12}H_{17}Cl_9^- \bullet [M_{12,9}]^- \bullet$	
	495/497/499/501/503	$C_{11}H_{13}Cl_{10}^- [M_{11,10}-H]^-$	$C_{11}H_{14}Cl_{10}$ ( $M_{11,10}$ )
	496/498/500/502/504	$C_{11}H_{14}Cl_{10}^- \bullet [M_{11,10}]^- \bullet$	
	509/511/513/515/517	$C_{12}H_{15}Cl_{10}^- [M_{12,10}-H]^-$	$C_{12}H_{16}Cl_{10}$ ( $M_{12,10}$ )
	510/512/514/516/518	$C_{12}H_{16}Cl_{10}^- \bullet [M_{12,10}]^- \bullet$	
	543/545/547/549/551	$C_{12}H_{14}Cl_{11}^- [M_{12,11}-H]^-$	$C_{12}H_{15}Cl_{11}$ ( $M_{12,11}$ )
	544/546/548/550/552	$C_{12}H_{15}Cl_{11}^- \bullet [M_{12,11}]^- \bullet$	

*Appendix 1(a-h)* shows the HRGC-EI/MS total ion chromatograms of the reaction products formed by the reaction of molecular chlorine with the seven alkenes listed in Table 3.1, and also of 1,10- $M_{10,2}$  (which was purchased from Aldrich). In the next section we will discuss the EI positive ion mass spectra of individual PCA congeners of unequivocal structure, namely 1,10-dichloro-*n*-decane (1,10- $M_{10,2}$ ); 1,2,9,10-tetrachloro-*n*-decane (1,2,9,10- $M_{10,4}$ ); 2,3,8,9-tetrachloro-*n*-decane (2,3,8,9- $M_{10,4}$ ); 1,2,5,6,9,10-hexachloro-*n*-decane (1,2,5,6,9,10- $M_{10,6}$ ); 1,2-dichloro-*n*-undecane (1,2- $M_{11,2}$ ); 1,2,10,11-tetrachloro-*n*-undecane (1,2,10,11- $M_{11,4}$ ); 2,3,9,10-tetrachloro-*n*-undecane (2,3,9,10- $M_{11,4}$ ) and 1,2,11,12-tetrachloro-*n*-dodecane (1,2,11,12- $M_{12,4}$ ).

#### **4.1.1 EI AND CID POSITIVE ION MASS SPECTROMETRY.**

##### **4.1.1.1 INTRODUCTION**

Our interpretation of the EI positive ion mass spectra of PCAs is aided by the following observations from the literature.

Two major fragmentations of the molecular ion, in addition to loss of a chlorine atom, have been identified in the EI positive ion mass spectra of monochloroalkanes. The simplest of these, observed from hexyl- through to octadecyl-chloride, is the formation of a five-membered cyclic  $C_4H_8Cl^+$  ( $m/z$  91) ion as described by McLafferty (1962), with concomitant elimination of an alkyl radical, which gives rise to major or base peaks [78]. McLafferty also suggested the formation of six- and four-membered cyclic ions, *viz*,  $C_5H_{10}Cl^+$  ( $m/z$  105) and  $C_3H_6Cl^+$  ( $m/z$  77), the latter of which is scarcely detectable. The formation of the five-membered cyclic ion, therefore, was thought to be a useful structural indicator for molecules with a sufficiently long alkyl chain [78].

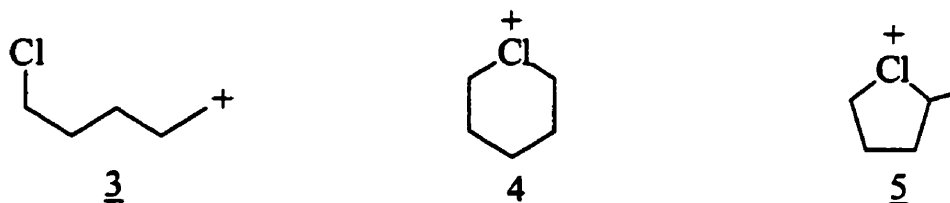
We have used a force-field modeling program (Molecular Modeling Pro) and a semi-empirical quantum mechanical model (AM1, HyperChem) to estimate the relative stabilities of a few of the cyclic structures postulated by McLafferty [78]. The approach used compared the energy estimated for the total strain ( $\Sigma S$ ) of a given ion after minimization and refinement using the modeling programs and the enthalpies of formation ( $\Delta H_f^+$ ) for all the possible structures. The rationale for this approach is that the most likely conformation, *i.e.*, the most stable, would correspond to the smallest  $\Sigma S$  and  $\Delta H_f^+$  energies.

Using the model we estimated a  $\Sigma S$  energy of  $146 \pm 12$  kJ/mol for the cyclic conformer (2) of the  $C_4H_8Cl^+$  ion, while for the acyclic analogue (1)  $\Sigma S$  was estimated to be  $13.8 \pm 0.1$  kJ/mol; corresponding  $\Delta H_f^+$  values are 820.6 and 709.7 kJ/mol, respectively. The difference in  $\Sigma S$  energy is undoubtedly much less than the interaction between chlorine lone pair electrons and the positive charge so that the cyclic structure is more stable, as confirmed by the  $\Delta H_f^+$  values, consistent with the proposal of McLafferty [78].



The  $\Sigma S$  energy for the six-membered ring structure (4) of the  $C_5H_{10}Cl^+$  ion of  $10.0 \pm 0.1$  kJ/mol was slightly lower than for the acyclic analogue (3),  $14.6 \pm 0.1$  kJ/mol, suggesting that the cyclic structure would be sterically favored. The  $\Sigma S$  energy for the five-membered ring 5 of  $121.4 \pm 12$  kJ/mol is higher than both structures 3 and 4. Similar conclusions can be made based on the  $\Delta H_f^+$  values;

for structures 3, 4 and 5,  $\Delta H_f^+$  values of 784.4, 672.8 and 688.9 kJ/mol, respectively, were determined. In addition, formation of a six-membered ring is favored energetically over formation of a five-membered ring so that kinetic factors must control the favored formation of five-membered rings.



The cyclic form of the  $C_3H_6Cl^+$  (7) ion was found to have a  $\Sigma S$  energy of  $347 \pm 8$  kJ/mol, while the acyclic conformer (6) was, as expected, significantly lower,  $13.8 \pm 0.1$  kJ/mol. Respective  $\Delta H_f^+$  values for 6 and 7 were 858.61 and 819.6 kJ/mol. The relatively high values are likely to be a significant factor in the low abundance of such ions.



The second decomposition, elimination of HCl, is more complicated, and the mechanism involved has been the focus of considerable discussion [79–86]. In the case of 1-chlorobutane, deuterium labelling experiments showed that elimination of HCl is predominantly (93%) a 1,3 process, while even in 1-chloropentane the 1,3 process still contributes 72% of the total HCl loss, with the 1,4-elimination making up the bulk of the remainder [79]. The increase in 1,4-elimination in 1-chloropentane, relative to 1-chlorobutane, is consistent with

the observation that abstraction of a secondary hydrogen atom is generally easier than abstraction of a primary hydrogen atom; 1,4-elimination in 1-chlorobutane would, of course, require primary hydrogen abstraction [79]. Elimination of HCl is also a 1,3 process in the case of 1-chloropropane and a number of small branched chain chloroalkanes [80,81]. For 1,3-elimination, formation of ionized cyclopropane ( $\Sigma S = 904 \pm 17$  kJ/mol) or a substituted cyclopropane was proposed [80,81]. However, 1,2-elimination is also known; it occurs in the cases of chloroethane and 2-chloropropane, and competes with the 1,3-elimination in the case of 2-chlorobutane [80,81,83].

The site selectivity of the hydrogen-abstracting elimination reactions has been discussed in terms of the closest approach of the chlorine and various hydrogen atoms in the ionized chloroalkanes; these distances, estimated from molecular models, were 2.4, 1.8 and 0.8 Å for Cl and H atoms separated by 2, 3 and 4 carbon atoms, respectively [83]. The closest approaches we found by a force-field calculation using our modeling program were slightly larger, namely 2.6, 2.1 and 0.9 Å, respectively. From the latter estimates, and from the observation that 1,3-elimination is strongly favored over 1,2-elimination, the critical H—Cl distance for HCl elimination therefore lies between 2.1 and 2.6 Å.

Experiments on energy partitioning by ion kinetic energy mass spectrometry led to the following generalizations concerning HCl elimination: (i) secondary hydrogens are more readily abstracted than primary hydrogens but the nature of the chlorine (primary or secondary) appears to be much less important, and (ii) the ring size in the transition state favors 1,3-elimination compared to 1,2-elimination [85]. Charge-stripping mass spectra and appearance energy measurements suggested that loss of HCl from ionized 1-chloropentane produces

ethylcyclopropane by a 1,3-elimination [86]. Even for the less probable 1,4-elimination a subsequent energetically favorable 1,2-hydrogen shift also leads to ionized ethylcyclopropane.

Collisional activation mass spectra are also consistent with the formation of a methylcyclopropane radical ion by 1,3-elimination of HCl from 1-chlorobutane [83]. In contrast, ionized propene, rather than ionized cyclopropane is produced by charge stripping of ionized 1-chloropropane, in keeping with its greater thermochemical stability (by 45 kJ/mol) [86,87]. Part of the apparent conflict in these results could arise from different internal energies of the cyclic ions in each study. When formed with little internal energy, cyclopropane radical ions can be stable for milliseconds but with higher internal energies they isomerize readily to the more stable propene radical ion [88,89].

Detailed information, supported by labelling experiments, on the mechanism of HCl elimination from the molecular ion of molecules larger than 1-chlorobutane is lacking. Even less is known on the relationship between the mass spectra and structure of PCAs. Mass spectra of a few polychlorinated C<sub>3</sub> to C<sub>9</sub> compounds have been published but, in general, the mass spectra of these compounds have not been evaluated; in fact, only a limited number of spectra of PCAs are available in the NIST mass spectral database [4,46].

#### **4.1.1.2 GENERAL FEATURES.**

The EI positive ion mass spectra of the PCA congeners examined in this study are shown in Figures 4.2-4.9. Inspection of the spectra reveals a number of even-electron odd-mass ions of low *m/z* common to all of the congeners investigated and which belong to a number of distinct ion series. In this section we

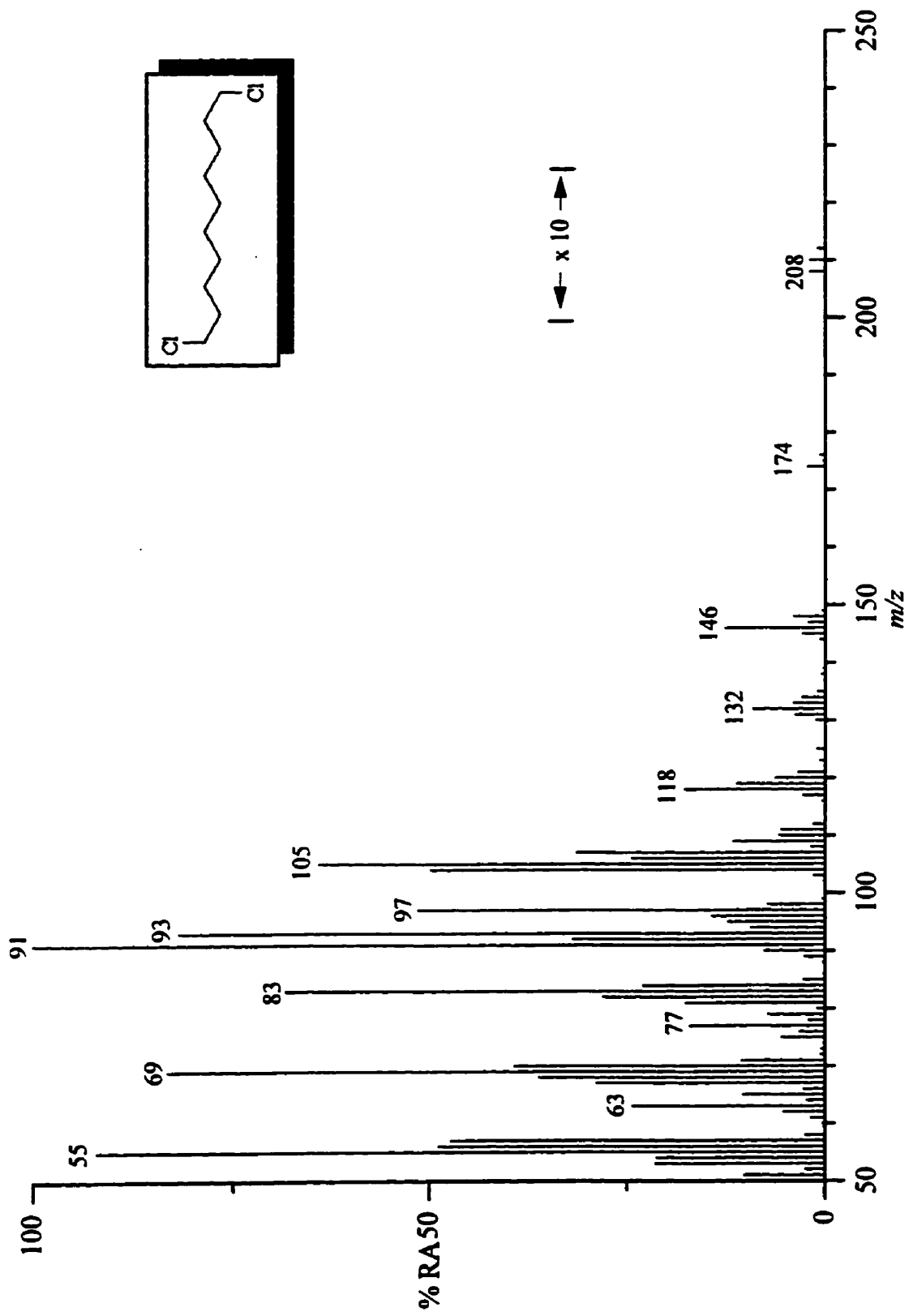


Figure 4.2. Electron ionization positive ion mass spectrum of 1,10-dichloro-*n*-decane.

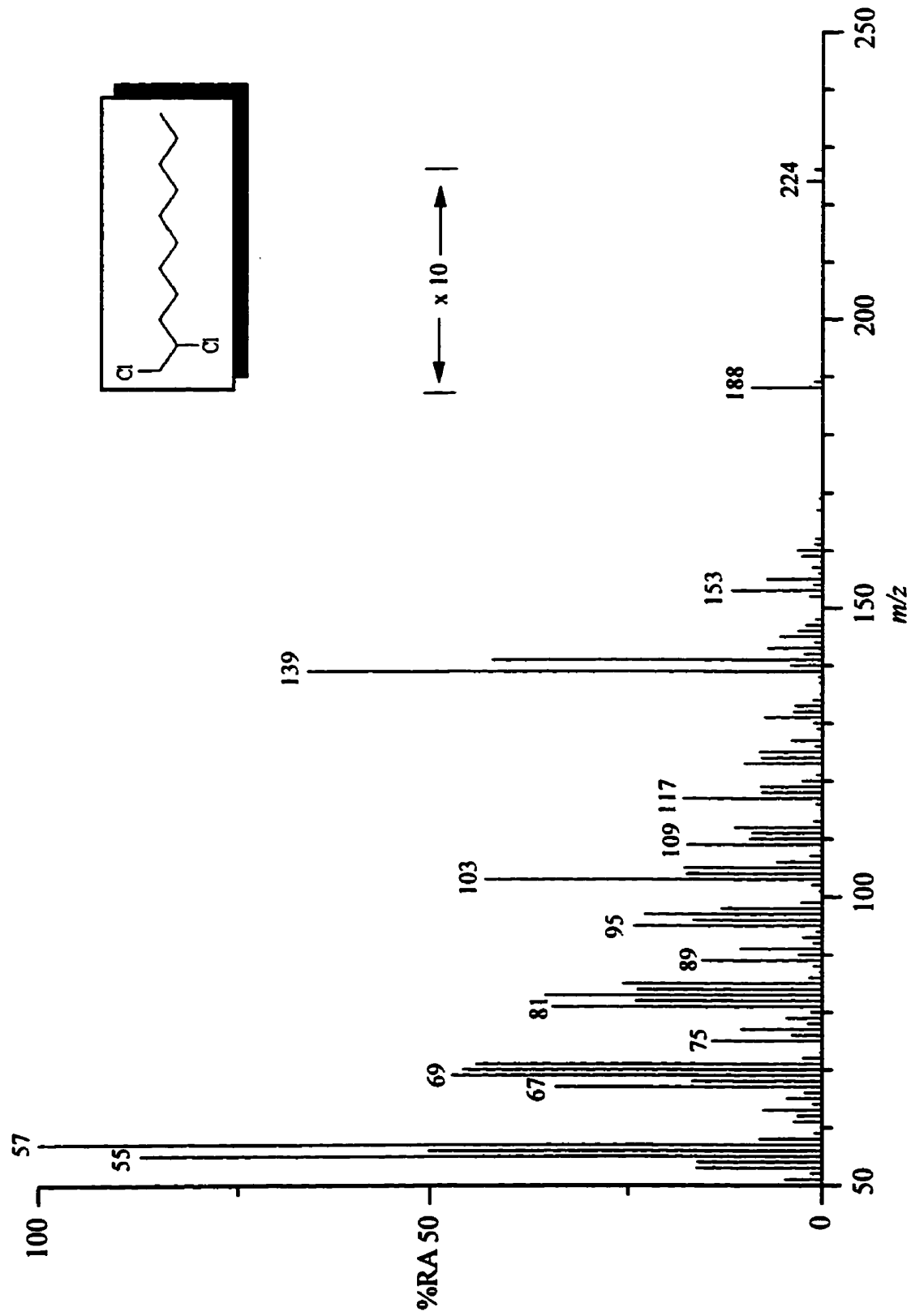


Figure 4.3. Electron ionization positive ion mass spectrum of 1,2-dichloro-*n*-undecane.

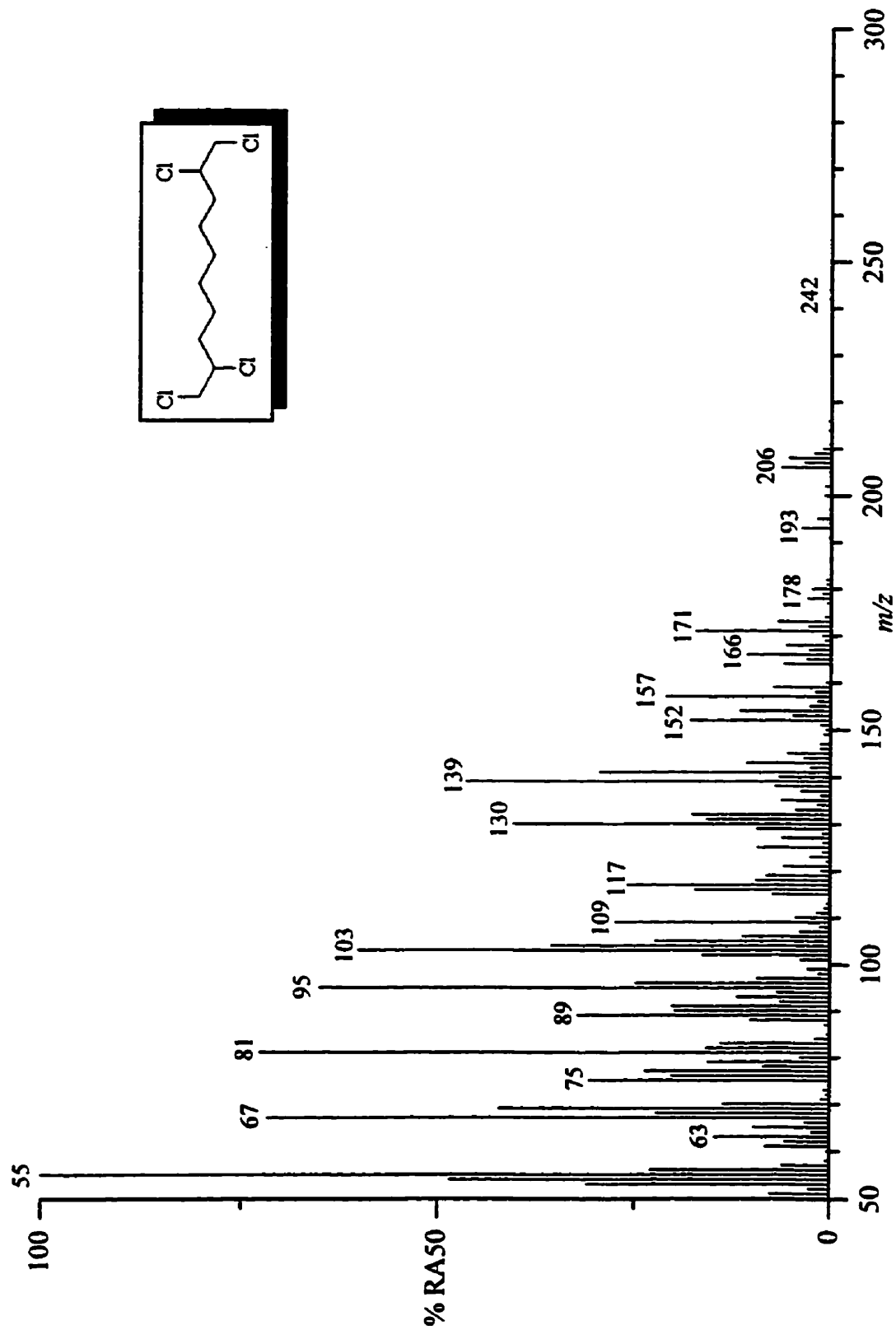


Figure 4.4. Electron ionization positive ion mass spectrum of 1,2,9,10-tetrachloro-*n*-decane.

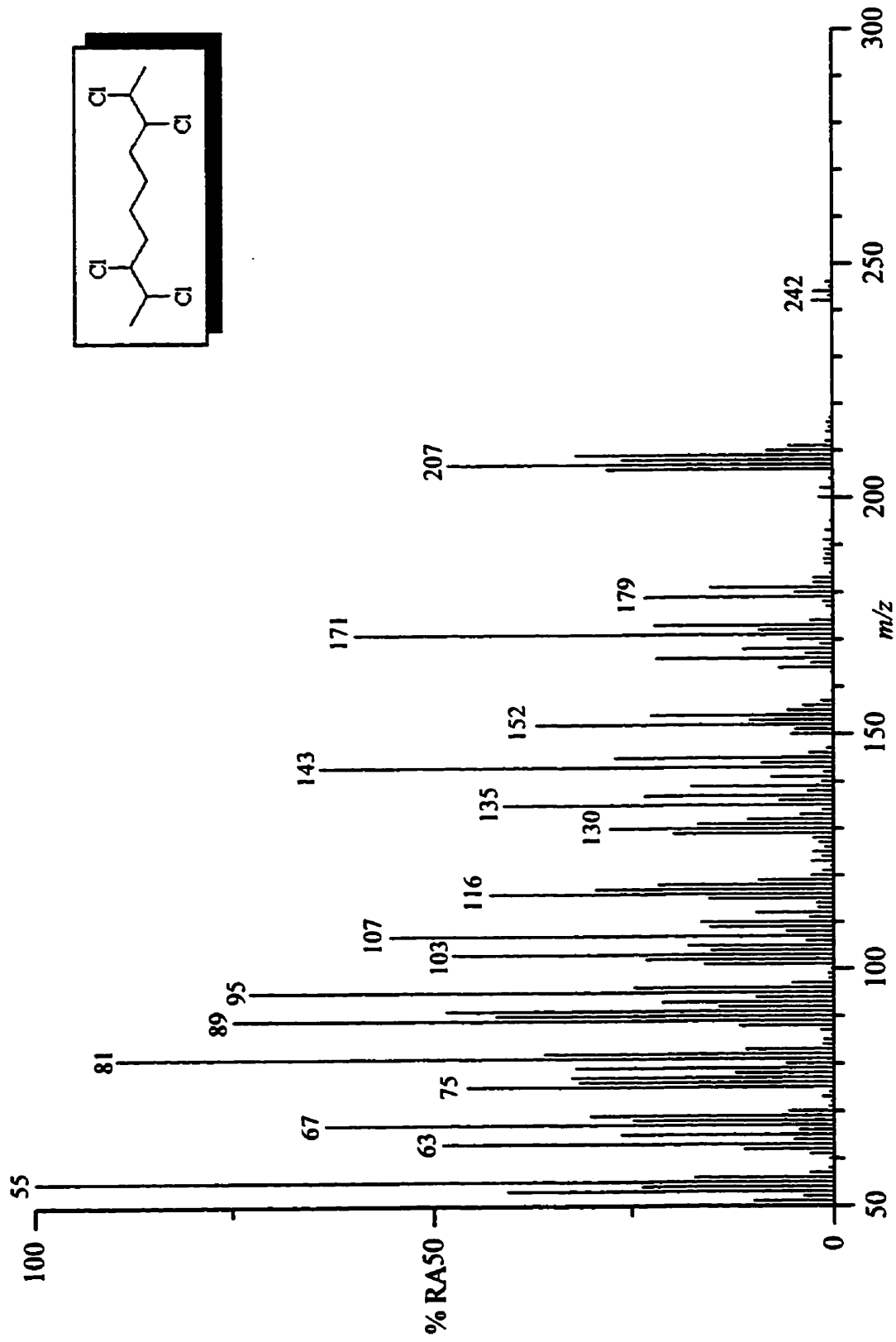


Figure 4.5. Electron ionization positive ion mass spectrum of 2,3,8,9-tetrachloro-*n*-decane.

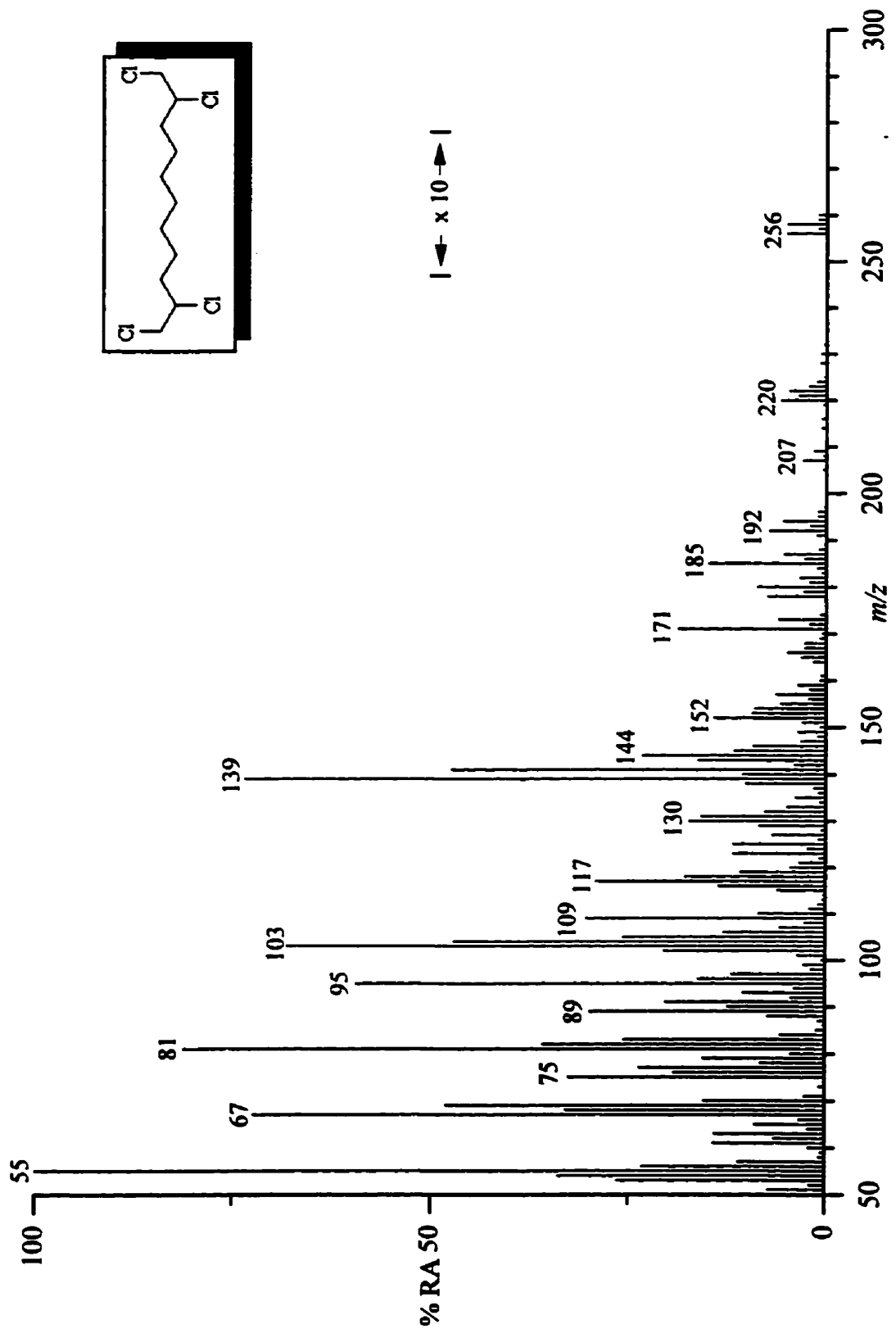


Figure 4.6. Electron ionization positive ion mass spectrum of 1,2,10,11-tetrachloro-*n*-undecane.

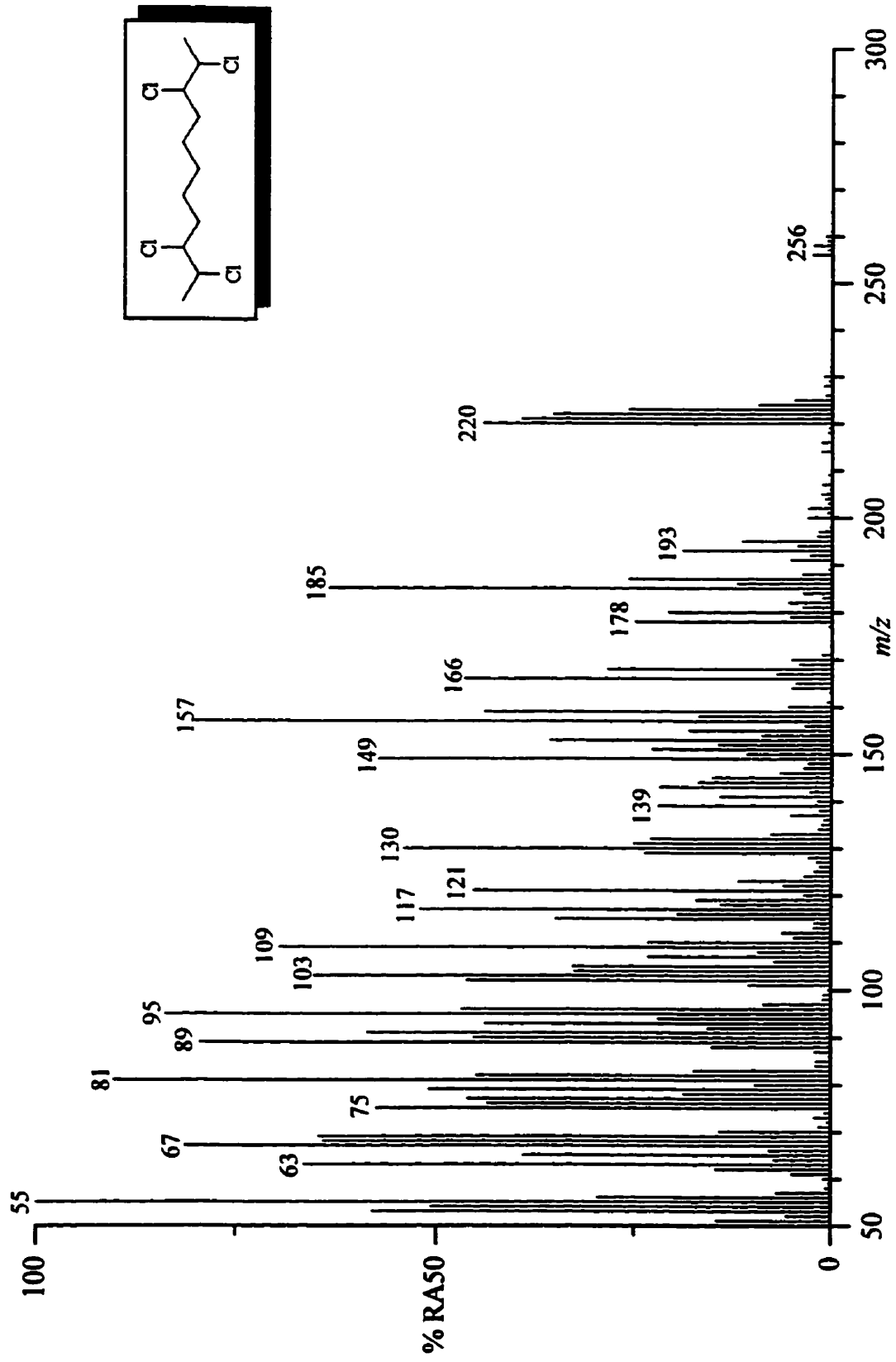


Figure 4.7. Electron ionization positive ion mass spectrum of 2,3,9,10-tetrachloro-*n*-undecane.

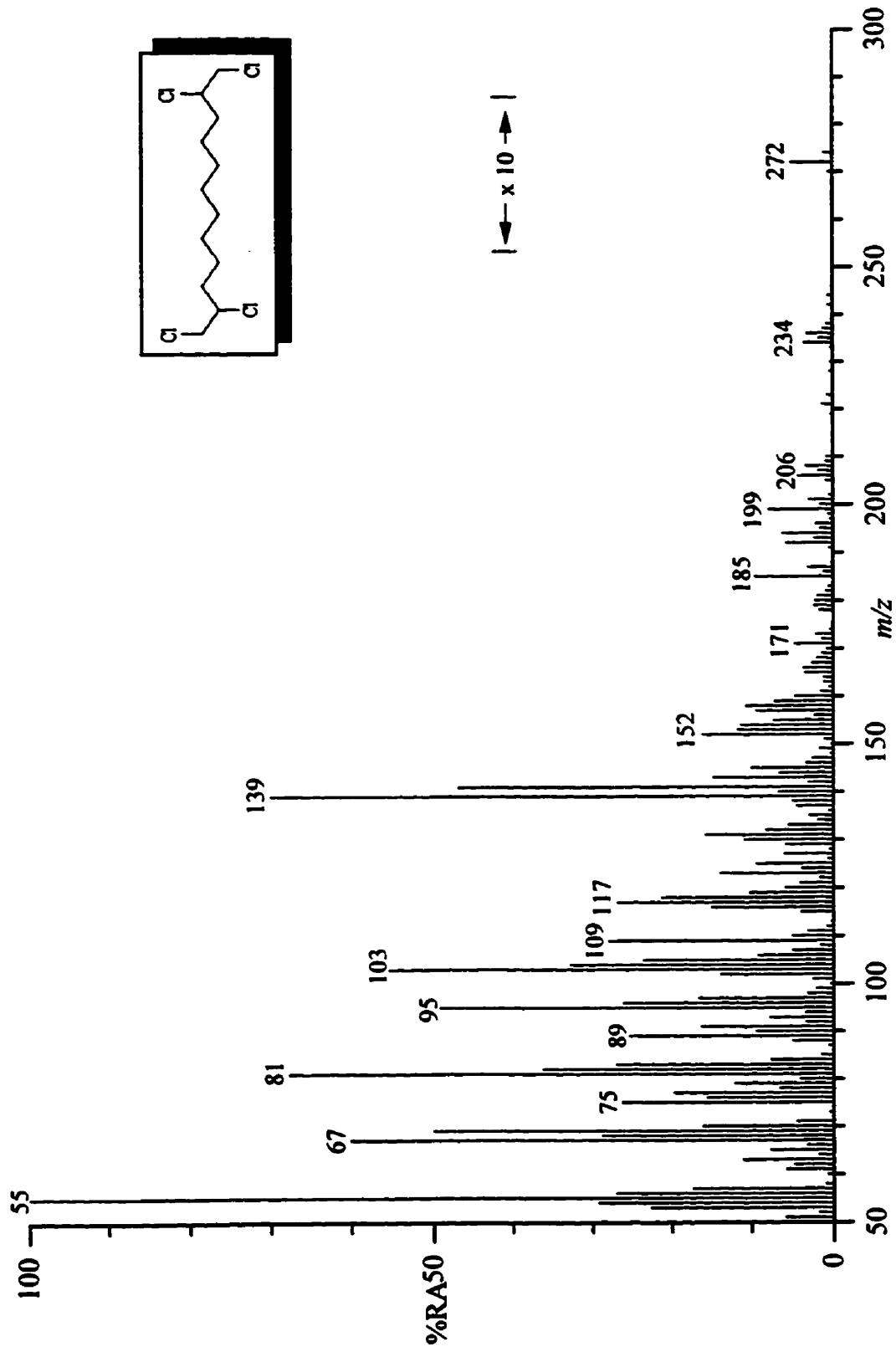


Figure 4.8. Electron ionization positive ion mass spectrum of 1,2,11,12-tetrachloro-*n*-dodecane.

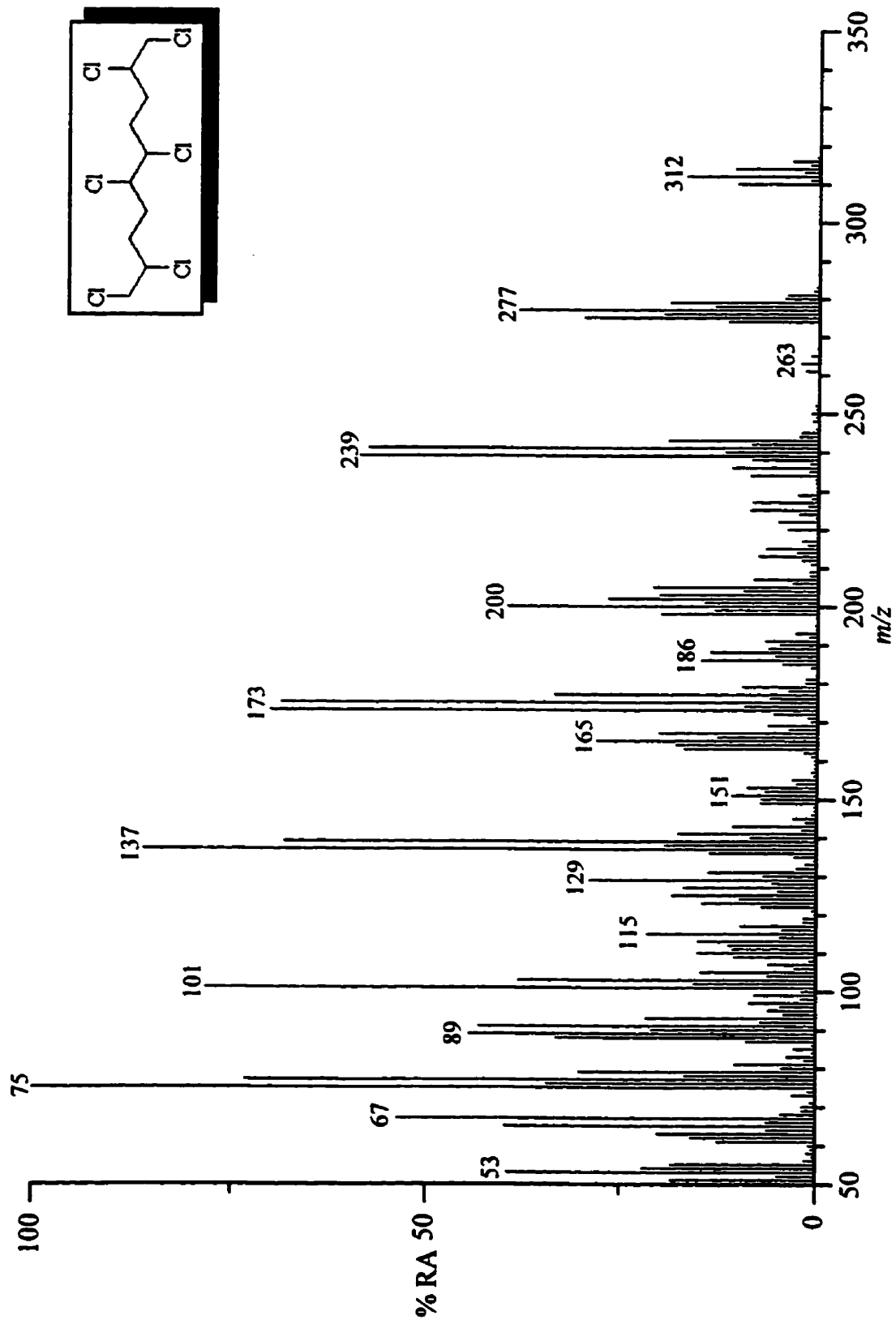
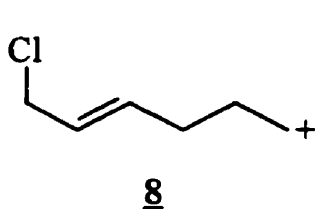


Figure 4.9. Electron ionization positive ion mass spectrum of 1,2,5,6,9,10-hexachloro-*n*-decane.

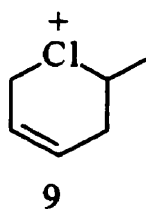
will identify these ions, and discuss the most likely conformation they will adopt by results obtained with the modeling programs.

The chloroalkane ions  $C_5H_{10}Cl^+$  ( $m/z$  105),  $C_4H_8Cl^+$  ( $m/z$  91),  $C_3H_6Cl^+$  ( $m/z$  77) and  $C_2H_4Cl^+$  ( $m/z$  63), were observed in the mass spectra of all the PCA congeners. The structures of  $m/z$  105, 91 and 77 were discussed in the preceding section. Based on the arguments described earlier, we can assume that the  $C_2H_4Cl^+$  ion exists predominantly in the acyclic form.

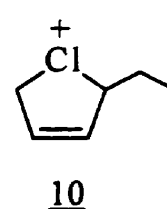
The chloroalkene ions at  $m/z$  117, 103, 89 and 75 belong to the ion series  $C_nH_{2n-2}Cl^+$ . For the  $C_6H_{10}Cl^+$  ion,  $m/z$  117, the three most probable structures, 8-10, and the estimated  $\Sigma S$  energies are shown below. These  $\Sigma S$  values would suggest that the six-membered cyclic structure, 9, which is significantly strained, would not be favored relative to 8 or 10.



$$\Sigma S = 42.3 \pm 0.4 \text{ kJ/mol}$$



$$\Sigma S = 332 \pm 3 \text{ kJ/mol}$$

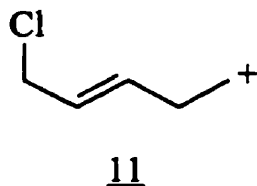


$$\Sigma S = 197 \pm 4 \text{ kJ/mol}$$

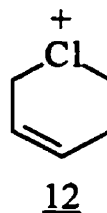
Interestingly, the substituted cyclopentenyl ion, 10, has about half the strain of the substituted cyclohexenyl ion. (We confirmed this result by comparing the estimated  $\Sigma S$  energies of the unsubstituted cyclopentene ( $178 \pm 1$  kJ/mol) with that of the unsubstituted cyclohexene ( $264 \pm 4$  kJ/mol). However, the  $\Sigma S$  energy of cyclohexane,  $10.0 \pm 0.1$  kJ/mol, is as expected, significantly lower than that of cyclopentane,  $115 \pm 4$  kJ/mol.)

Our calculated  $\Delta H_f^+$  values for 8, 9 and 10 of 872.1, 767.5 and 774.5 kJ/mol, respectively, would suggest, however, that structures 9 and 10, which have almost identical  $\Delta H_f^+$  values, would both be favored relative to 8.

For the  $C_5H_8Cl^+$  ion,  $m/z$  103, the  $\Sigma S$  energy of the acyclic structure (11) is 270 kJ/mol lower than its cyclic analogue (12); this difference is expected to be of the order of the chloride-carbocation interaction energy (probably in the range 200–300 kJ/mol) so both structures are plausible. The corresponding  $\Sigma S$  energy differences between the cyclic and acyclic isomers of the  $C_4H_6Cl^+$  ( $m/z$  89) and  $C_3H_4Cl^+$  ( $m/z$  75) ions are 173 kJ/mol and 306 kJ/mol, respectively; thus, the cyclic form would be favored for the former, and the acyclic form for the latter.



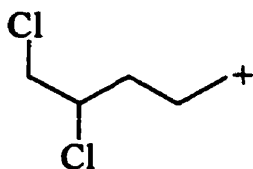
$$\Sigma S = 44 \pm 1 \text{ kJ/mol}$$



$$\Sigma S = 314 \pm 8 \text{ kJ/mol}$$

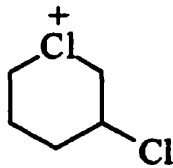
A prominent peak observed at  $m/z$  139, in the mass spectra of all the congeners except for that of 1,10- $M_{10,2}$  corresponds to the  $C_3H_9Cl_2^+$  ion. A prerequisite for the formation of this ion is the presence of vicinal chlorine atoms; 1,10- $M_{10,2}$ , obviously, does not fill this requirement. For congeners with chlorine atoms that are vicinal and with one of the two chlorines residing in a terminal position, *i.e.*, at positions 1,2 along the carbon backbone, the relative abundance of this ion is very high (> 50%). For cases where two chlorine atoms are vicinal,

neither one occupying a terminal position, this ion is not as abundant, but is still observed. We can rationalise this disparity by examining the  $\Sigma S$  energies for the three likely structures of this ion, 13-15.



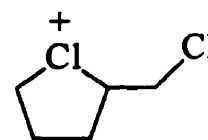
13

$$\Sigma S = 14.0 \pm 0.1 \text{ kJ/mol}$$



14

$$\Sigma S = 9.2 \pm 0.1 \text{ kJ/mol}$$



15

$$\Sigma S = 142 \pm 8 \text{ kJ/mol}$$

For the instance where one of chlorine atoms resides in the terminal position, as depicted in the acyclic conformer (13), our estimated  $\Sigma S$  energies suggests that the cyclized analogue (14) would be the likely structure. The five-membered cyclic structure, 15, is more strained than both 13 or 14, and so would not be energetically favored, although the earlier discussion indicates that it will be formed more rapidly. For the case where the chlorine atoms are positioned on carbons 2,3 of the acyclic conformer, cyclization to the favored six-membered analogue is sterically inhibited, and thus, the less favored acyclic conformer would be the only possible structure. Based on these arguments, then, we can expect the 1,2 positional isomer of the  $C_5H_9Cl_2^+$  ion to be more stable than the 2,3 isomer, and thus have a longer life-time in the ion source before subsequent decompositions.

Many ions observed in the spectra are hydrocarbon ions, in particular, unsaturated ones. It should be noted here that the positions of double bonds that are created because of either (i) HCl elimination from an even electron ion, or (ii)  $Cl\cdot$  elimination from an odd electron ion, in some cases, are widely distributed. This seems to be inconsistent with the trend in the stability associated with

positionally isomeric acyclic dienes. For example, Figure 4.10 shows the  $\Sigma S$  energies of a number of positional isomers of a diene molecule. Although any straight chain diene can be used for the illustration, we will use  $C_7H_{11}^+$ .

As expected the lowest  $\Sigma S$  energy observed is for the conjugated molecules (17 and 22), while the highest is for the allene molecules (16, 21 and 24). The  $\Sigma S$  for the remaining structures are similar, except for the molecule with the double bonds located at the terminal positions, (20), which is slightly lower. We expect then, where formed, the conjugated systems to be the likely decomposition structures. Similar analogies can be made for positional isomers of acyclic trienes.

The results obtained from our linked-field scanning, however, suggests that some decompositions, which we will allude to later, must proceed *via* less sterically favored molecules. This would imply, therefore, that these molecules have a finite life-time in the ion source. We shall address these structures when they occur. In addition, eliminations invoking HCl loss will be treated in terms of the formation of a single structure.

In the  $C_nH_{2n-1}^+$  ion series, the ions at  $m/z$  97, 83, 69 and 55 correspond to  $C_7H_{13}^+$ ,  $C_6H_{11}^+$ ,  $C_5H_9^+$  and  $C_4H_7^+$ , respectively. Three likely structures for the  $C_7H_{13}^+$  ion are depicted as 25-27. The estimated  $\Sigma S$  energies for the acyclic and six-membered cyclic structures, 25 and 26, respectively, are similar, and the net bond energies are similar, and so we can assume that the energy difference between them is small. This view is supported by available  $\Delta H_f^+$  values for several ions, as shown in Figures 4.11 [87]. Except for 1,2-hydride shifts the activation energy barrier for interconversion between structures is high enough to prevent interconversion between them.

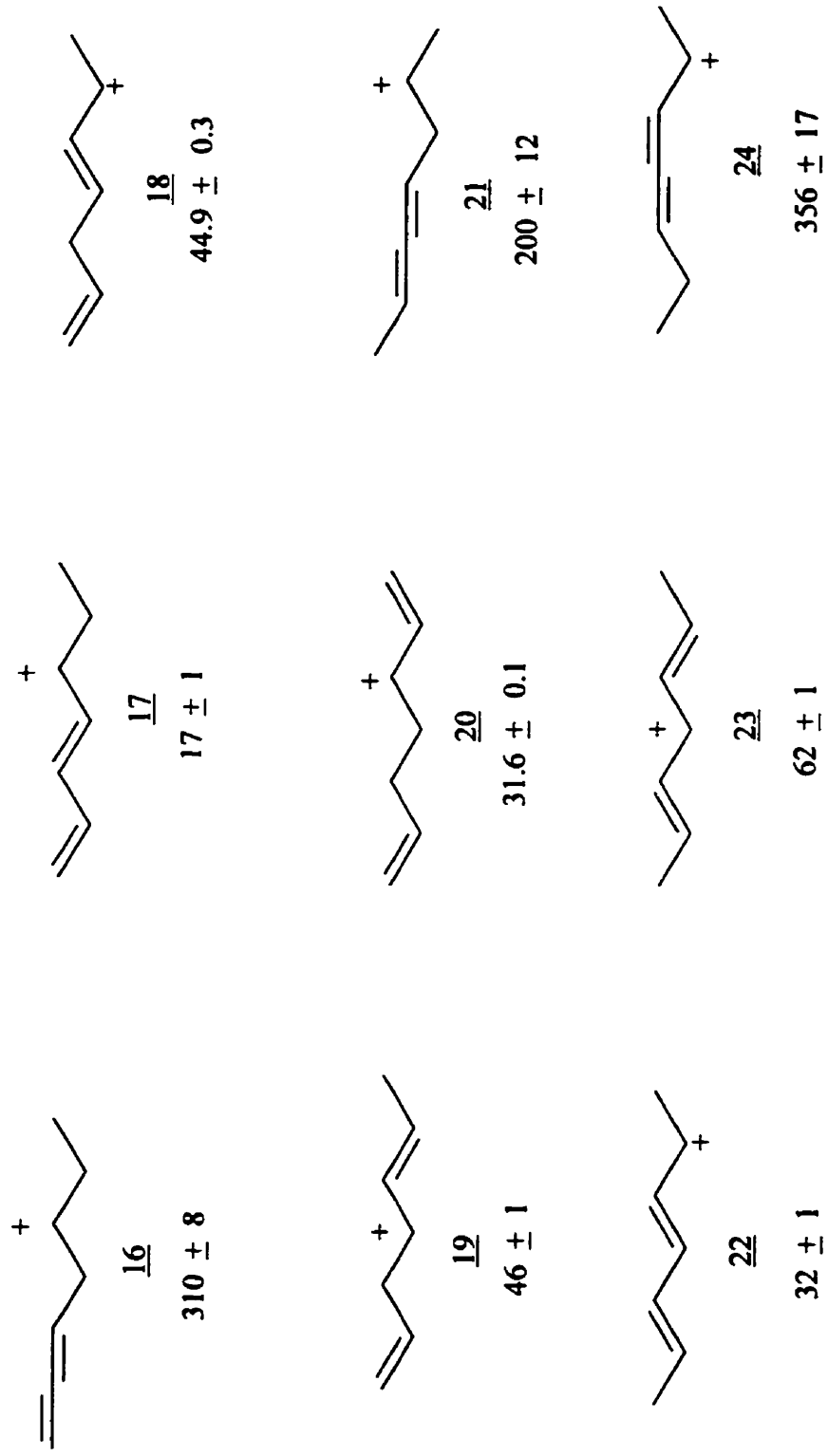


Figure 4.10. Estimated  $\Sigma S$  energies (kJ/mol) for positional isomers of  $C_7H_{11}^+$ .

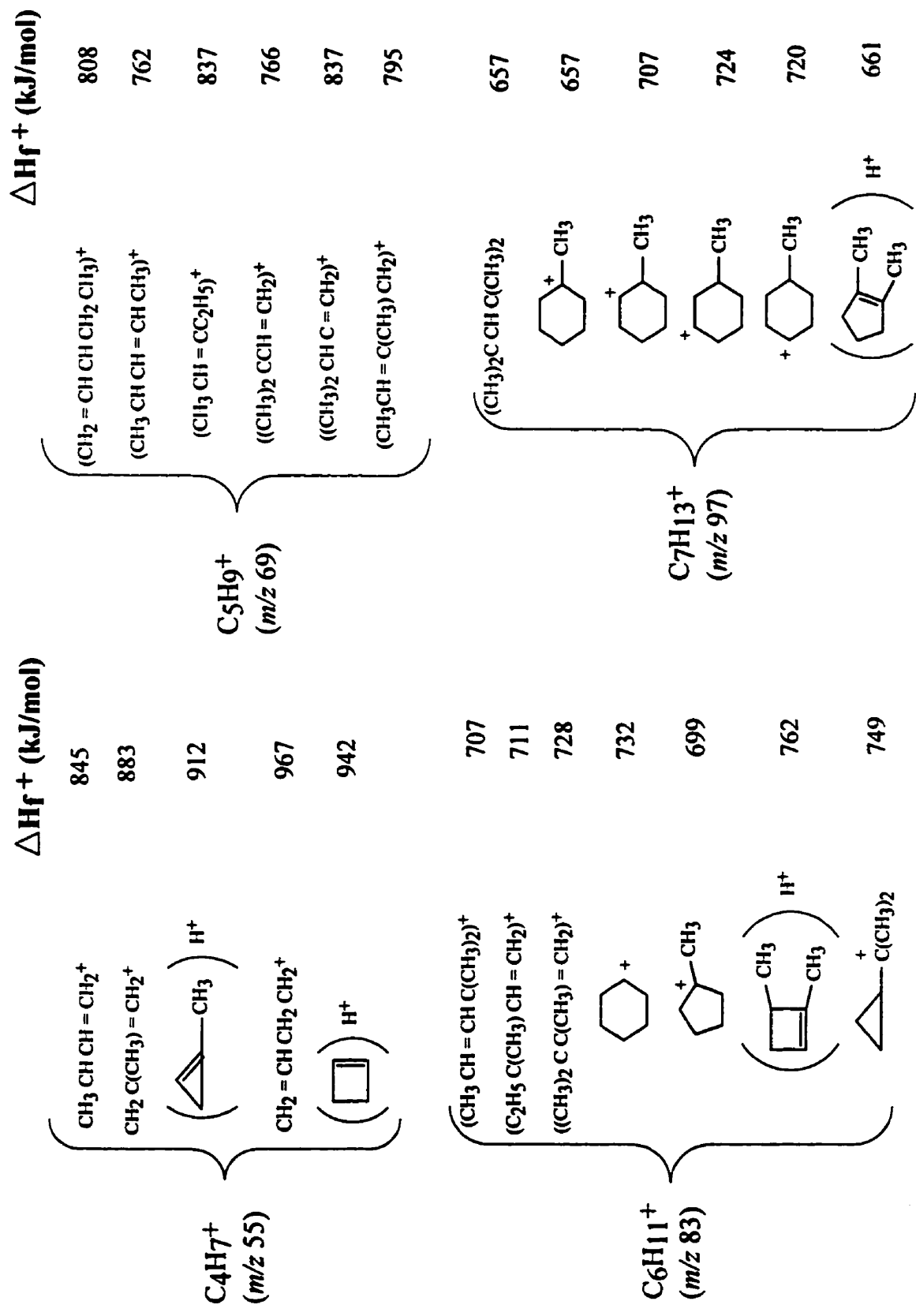
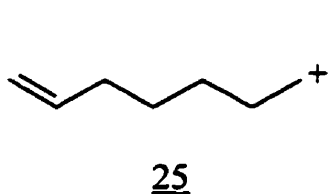
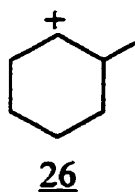


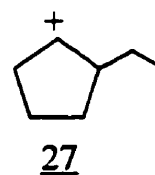
Figure 4.11  $\Delta H_f^+$  for ions in the  $\text{C}_n\text{H}_{2n-1}^+$  ion series.



$$\Sigma S = 29.7 \pm 0.4 \text{ kJ/mol}$$



$$\Sigma S = 37 \pm 1 \text{ kJ/mol}$$



$$\Sigma S = 131 \pm 3 \text{ kJ/mol}$$

The ions  $C_8H_{13}^+$  ( $m/z$  109),  $C_7H_{11}^+$  ( $m/z$  95),  $C_6H_9^+$  ( $m/z$  81),  $C_5H_7^+$  ( $m/z$  67) and  $C_4H_5^+$  ( $m/z$  53) belong to the diene  $C_nH_{2n-3}^+$  ion series. Based on their  $\Sigma S$  energies (not shown), none of these ions are favored in their respective cyclic forms. Because  $\Delta H_f^+$  values are available for only a few of these ions it is unclear whether larger ring sizes, *viz.*,  $C_8H_{13}^+$  and  $C_7H_{11}^+$ , would be favored (*see* Figure 4.12) [87]. (The size of the ring, undoubtedly, would have an effect on the stability of the ion formed.) We will, therefore, represent these ions in their respective acyclic forms.

#### (A) 1,10-Dichloro-*n*-decane.

Figure 4.2 shows the EI positive ion mass spectrum of 1,10- $M_{10,2}$ . Ion fragmentation pathways established by linked-field scanning for this species are shown in *Appendix 2a*. The  $[M_{10,2}-HCl]^+$ ,  $m/z$  174, decomposes by losses of  $C_2H_4$ ,  $C_3H_6$ ,  $C_4H_8$ ,  $C_5H_{10}$ ,  $C_3H_6Cl^\bullet$ ,  $C_6H_{11}^\bullet$ ,  $C_4H_8Cl^\bullet$ , and  $C_7H_{13}^\bullet$  to give the ions  $C_8H_{15}Cl^+$  ( $m/z$  146),  $C_7H_{13}Cl^+$  ( $m/z$  132),  $C_6H_{11}Cl^+$  ( $m/z$  118),  $C_5H_9Cl^+$  ( $m/z$  104),  $C_7H_{13}^+$  ( $m/z$  97),  $C_4H_8Cl^+$  ( $m/z$  91),  $C_6H_{11}^+$  ( $m/z$  83) and  $C_3H_6Cl^+$  ( $m/z$  77), respectively. The  $C_4H_8Cl^+$  ion further decomposes by loss of HCl to  $C_4H_7^+$  ( $m/z$  55).

The  $C_8H_{15}Cl^+$  ion further decomposes by losses of  $C_2H_4$ ,  $C_3H_6$ ,  $CH_2Cl^\bullet$ ,

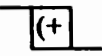
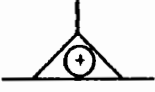
		$\Delta H_f^+$ (kJ/mol)			$\Delta H_f^+$ (kJ/mol)	
$C_4H_5^+$ ( <i>m/z</i> 53)	{	$CH_2 = CH C = CH_2^+$	1030	{	$CH_2 = CH \overset{+}{CH} CH = CH_2$	921
		$CH \equiv C CH CH_3^+$	1076		$HC \equiv C C(CH_3)_2^+$	979
		$CH_3C \equiv CCH_2^+$	1055			833
			992			
$C_6H_9^+$ ( <i>m/z</i> 81)	{	$CH_3 \equiv C C(CH_3)_2^+$	904			
			800			
			795			
			845			
			833			

Figure 4.12.  $\Delta H_f^+$  for ions in the  $C_nH_{2n-3}^+$  ion series.

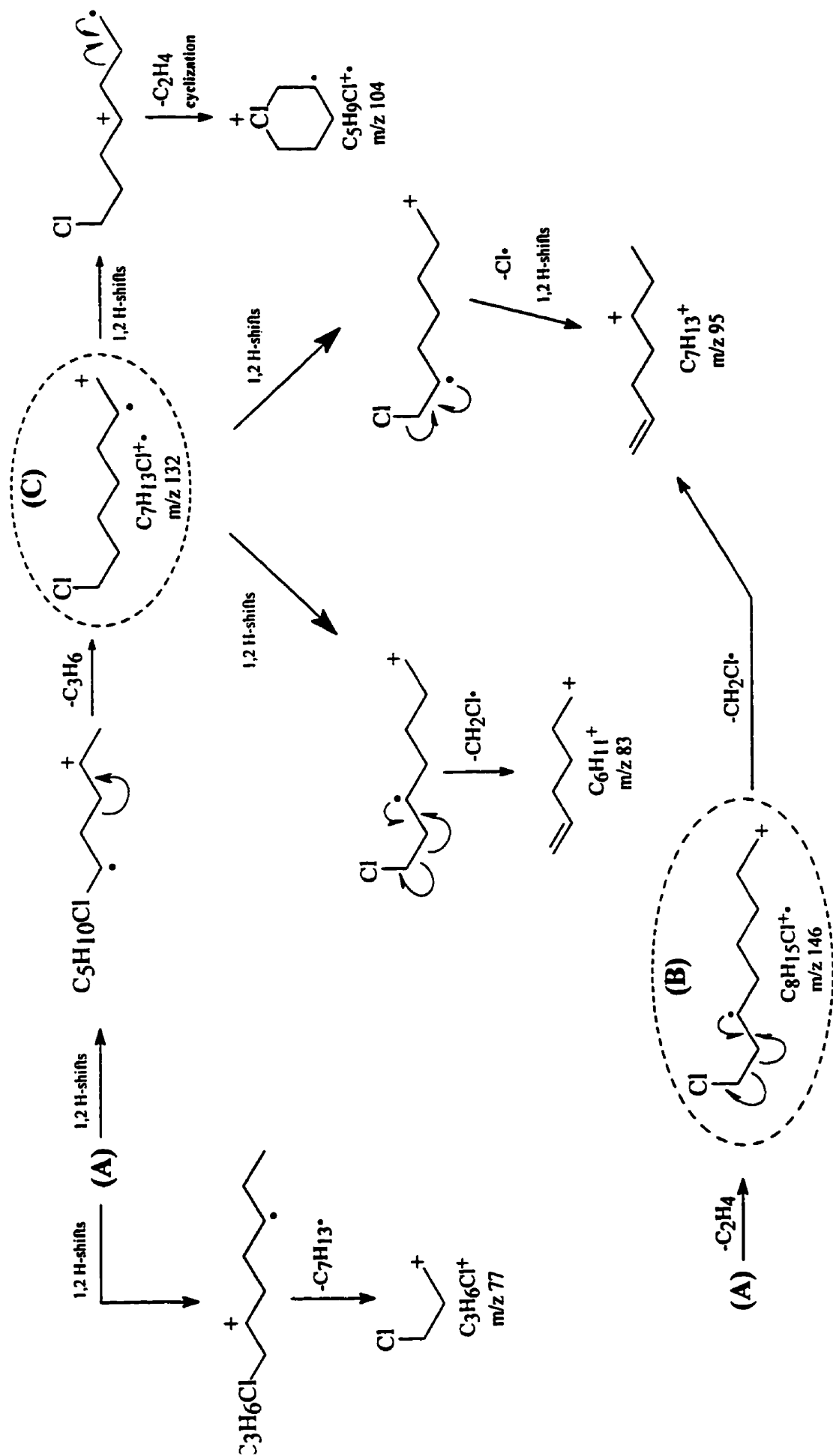
$C_4H_7\cdot$  and  $C_2H_4Cl\cdot$  to yield the ions  $C_6H_{11}Cl^+$  ( $m/z$  118),  $C_5H_9Cl^+$  ( $m/z$  104),  $C_7H_{13}^+$  ( $m/z$  97),  $C_4H_8Cl^+$  ( $m/z$  91) and  $C_6H_{11}^+$  ( $m/z$  83), respectively. Subsequent decomposition of the  $C_6H_{11}Cl^+$  ion, proceeds by losses of  $CH_2$ ,  $Cl\cdot$ ,  $C_3H_5\cdot$  and  $CH_2Cl\cdot$ , to yield the ions  $C_5H_9Cl^+$  ( $m/z$  104),  $C_6H_{11}^+$  ( $m/z$  83),  $C_3H_6Cl^+$  ( $m/z$  77) and  $C_5H_9^+$  ( $m/z$  69), respectively. The  $C_7H_{13}Cl^+$  ( $m/z$  132), decomposes by losses of  $C_2H_4$ ,  $Cl\cdot$ ,  $CH_2Cl\cdot$  and  $C_4H_7\cdot$  yielding  $C_5H_9Cl^+$  ( $m/z$  104),  $C_7H_{13}^+$  ( $m/z$  97),  $C_6H_{11}^+$  ( $m/z$  83) and  $C_3H_6Cl^+$  ( $m/z$  77), respectively.

Mechanisms proposed for some of the decompositions are illustrated in *Scheme 4.1*. A prominent ion,  $m/z$  105,  $C_5H_{10}Cl^+$ , had no identifiable precursor, so is assumed to be formed by rapid decomposition of  $M^+$  in the ion source. As shown earlier, the most stable structure of this ion is the six-membered (4) ring.

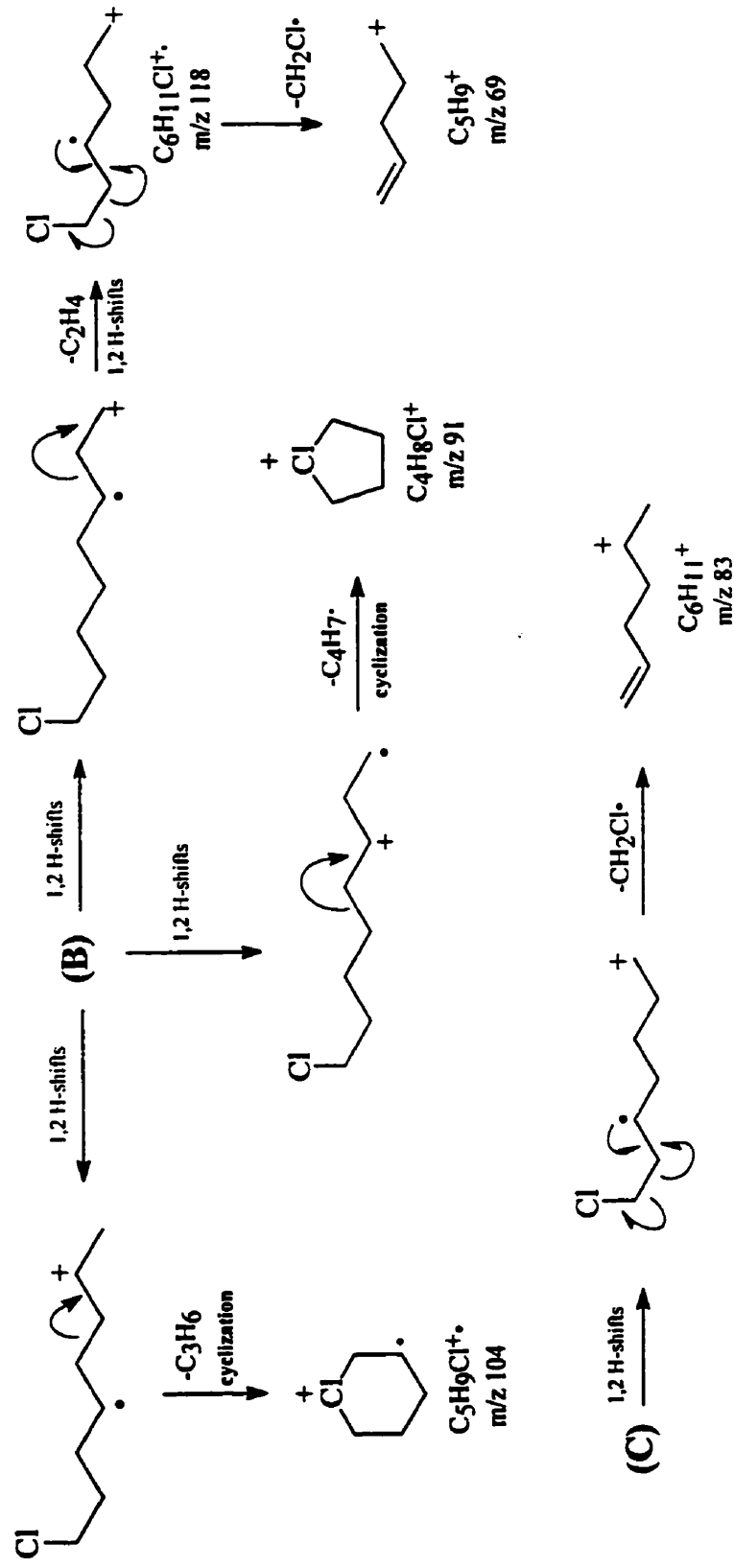
From the introductory discussion we anticipate that a major decomposition of  $M^+$  will result in formation of the cyclic (1)  $C_4H_8Cl^+$ ,  $m/z$  91. As expected, this ion is prominent in the spectrum; because its formation from  $M^+$  could not be confirmed by linked-field scanning we assume that it is formed rapidly, in the ion source. Support for this proposal is given by the high prominence of the cyclic  $C_5H_{10}Cl^+$  ion. The decompositions leading to the formation of  $m/z$  91 from  $m/z$  174 and  $m/z$  146, although supported by linked-field scanning, are probably less important pathways.

The  $[M_{10,2}-HCl]^+$  ion is the ultimated precursor of the majority of the ions in the mass spectrum. The introductory discussion implies that it is initially formed as a cyclopropane radical ion. The  $\Sigma S$  energy estimated for the substituted cyclopropane radical (depicted as **A** in *Scheme 4.1*) was  $1172 \pm 42$  kJ/mol. Subsequent collisional activation and sufficient time before analysis provide ample opportunity for rearrangement to the more stable acyclic structure to occur;  $\Sigma S$  for





Scheme 4.1. (cont'd) Ion decomposition mechanisms for 1,10-dichloro-*n*-decane established by linked-field scanning.

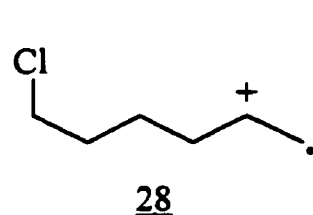


**Scheme 4.1 (cont'd)** Ion decomposition mechanisms for 1,10-dichloro-*n*-decane established by linked-field scanning.

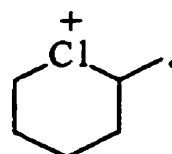
the acyclic analogue of the substituted cyclopropane radical is  $14 \pm 6$  kJ/mol. While  $C_3H_6$  could be lost as cyclopropane or propene, many of the other neutral hydrocarbons could be lost as alkenes following a sequence of rapid 1,2-hydrogen shifts, process for which activation energies are very small.

A prominent ion in the EI mass spectrum of 1,10- $M_{10,2}$  is  $m/z$  104,  $C_5H_9Cl^+$ . The estimated  $\Sigma S$  energies for the possible structures of this ion were found to be very similar to those of  $C_5H_{10}Cl^+$  ( $m/z$  105), and, thus, similar analogies can be made.

The  $\Sigma S$  energies were also determined for the  $C_6H_{11}Cl^+$  ( $m/z$  188) ion. 1,10- $M_{10,2}$ . The structures and estimated  $\Sigma S$  energies of the possible isomers of  $C_6H_{11}Cl^+$  are shown below. The  $\Sigma S$  energies imply that the cyclic structure (29) would be more stable owing to the stability imparted by C-Cl bond formation.



$$\Sigma S = 14 \pm 1 \text{ kJ/mol}$$



$$\Sigma S = 10.6 \pm 0.1 \text{ kJ/mol}$$

### (B) 1,2-Dichloro-*n*-undecane

Figure 4.3 shows the EI positive ion mass spectrum of 1,2- $M_{11,2}$ . The ion fragmentation pathways established by linked-field scanning for this species are shown in *Appendix 2b*. Losses of HCl,  $C_5H_{11}^\bullet$  and  $C_6H_{13}^\bullet$  from  $M_{11,2}^+$ ,  $m/z$  224, are observed. The  $[M_{11,2}-HCl]^+$  ion,  $m/z$  188, decomposes by losses of  $C_4H_9^\bullet$ ,  $C_5H_{11}^\bullet$ ,  $C_6H_{11}^\bullet$  and  $C_7H_{13}^\bullet$  to yield  $C_7H_{12}Cl^+$  ( $m/z$  131),  $C_6H_{10}Cl^+$  ( $m/z$  117),

$C_5H_{10}Cl^+$  ( $m/z$  105) and  $C_4H_8Cl^+$  ( $m/z$  91), respectively. The  $C_7H_{12}Cl^+$  ion,  $m/z$  131, then decomposes by a loss of HCl to yield  $C_7H_{11}^+$  ( $m/z$  95). This ion further decomposes to  $C_5H_7^+$ ,  $m/z$  67, and  $C_6H_9^+$ ,  $m/z$  81 by loss of  $C_2H_4$  and  $:CH_2$ , respectively.

The  $[M_{11,2}-C_5H_{11}]^+$  ion,  $m/z$  153, decomposes by losses of HCl,  $C_4H_8$  and 2HCl to yield  $C_6H_{10}Cl^+$  ( $m/z$  117),  $C_2H_3Cl_2^+$  ( $m/z$  97) and  $C_6H_9^+$  ( $m/z$  81), respectively. The first ion (depicted as **C** in *Scheme 4.2*), decomposes by losses of  $:CH_2$ ,  $C_2H_4$ , HCl,  $C_3H_6$  and  $C_2H_3Cl$  to yield  $C_5H_8Cl^+$  ( $m/z$  103),  $C_4H_6Cl^+$  ( $m/z$  89),  $C_6H_9^+$  ( $m/z$  81),  $C_3H_4Cl^+$  ( $m/z$  75) and  $C_4H_7^+$  ( $m/z$  55), respectively.

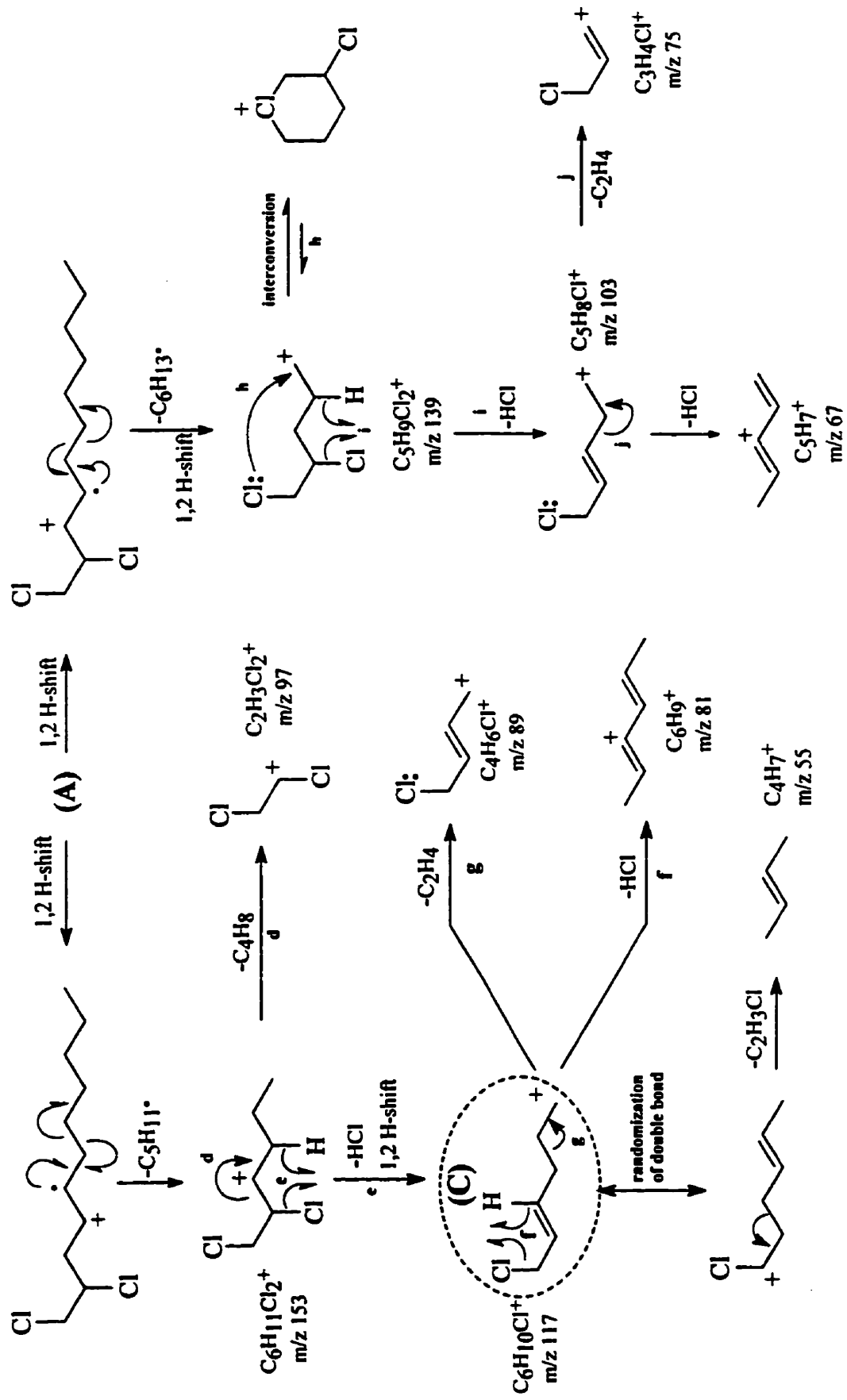
The  $[M_{11,2}-C_6H_{13}]^+$  ion,  $m/z$  139, decomposes by losses of HCl and  $C_3H_6$  to yield  $C_5H_8Cl^+$  ( $m/z$  103) and  $C_2H_3Cl^+$  ( $m/z$  97), respectively. The former ion decomposes further to yield  $C_4H_6Cl^+$  ( $m/z$  89),  $C_3H_4Cl^+$  ( $m/z$  75) and  $C_5H_7^+$  ( $m/z$  67), by losses of  $:CH_2$ ,  $C_2H_4$  and HCl, respectively.

Mechanisms proposed for some of the decompositions are shown in *Scheme 4.2*. The  $\Sigma S$  energy for the highly strained substituted cyclopropane radical (depicted as **B** in *Scheme 4.2*) was estimated to be  $1240 \pm 60$  kJ/mol, while its acyclic analogue was  $23 \pm 4$  kJ/mol; rapid ring opening to the acyclic analogue is to be expected.

*Scheme 4.2* illustrates that decompositions of the  $C_6H_{10}Cl^+$  ion, depicted as **C**, must proceed *via* more than a single positional isomer. Although there are other structures that are possible for this ion, we have identified two; the process by which they are formed is by a random positioning of the double bond.

A prominent ion in the EI mass spectrum of 1,2- $M_{11,2}$  is  $m/z$  139,  $C_5H_9Cl_2^+$ ,





Scheme 4.2. (cont'd) Ion decomposition mechanisms for 1,2-dichloro-*n*-undecane established by linked field-scanning.

which is formed by a loss of  $C_6H_{13}^\bullet$  from  $M_{11,2}^{+\bullet}$ . The structure which is thought to dominate (14) was discussed earlier. The  $C_5H_9Cl_2^+$  ion, in addition, was identified as the parent of the cyclic  $C_5H_8Cl^+$  ion ( $m/z$  103), which further decomposes to  $C_4H_7^+$  ( $m/z$  55), the base peak, *via* a loss of  $:CHCl$ .

### (C) 1,2,9,10-Tetrachloro-*n*-decane

Figure 4.4 shows the EI positive ion mass spectrum of 1,2,9,10- $M_{10,4}$ . Ion fragmentation pathways established by linked-field scanning for this species are shown in *Appendix 2c*. The  $m/z$  243 and 242 ions correspond to  $[M_{10,4}-Cl]^+$  and  $[M_{10,4}-HCl]^+$ , respectively. The  $[M_{10,4}-HCl]^+$  ion is the immediate precursor of  $C_{10}H_{17}Cl_2^+$  ( $m/z$  207),  $C_{10}H_{16}Cl_2^{+\bullet}$  ( $m/z$  206),  $C_9H_{14}Cl^+$  ( $m/z$  157) and  $C_6H_{10}Cl^+$  ( $m/z$  117), which are formed by losses of  $Cl^\bullet$ ,  $HCl$ ,  $(HCl+CH_2Cl^\bullet)$ , and  $(HCl+C_4H_6Cl^\bullet)$ , respectively. The  $C_{10}H_{17}Cl_2^+$  ion further decomposes to  $C_{10}H_{16}Cl^+$  ( $m/z$  171),  $C_7H_{11}Cl^+$  ( $m/z$  130),  $C_6H_{10}Cl^+$  ( $m/z$  117),  $C_5H_8Cl^+$  ( $m/z$  103) and  $C_4H_8Cl^+$  ( $m/z$  91) by losses of  $HCl$ ,  $C_3H_6Cl^\bullet$ ,  $C_4H_7Cl$ ,  $C_5H_9Cl$  and  $C_6H_9Cl$ , respectively.

The  $C_{10}H_{16}Cl_2^{+\bullet}$  ion decomposes to  $C_{10}H_{16}Cl^+$  ( $m/z$  171),  $C_9H_{14}Cl^+$  ( $m/z$  157),  $C_7H_{11}Cl^+$  ( $m/z$  130),  $C_5H_{10}Cl^+$  ( $m/z$  117),  $C_5H_8Cl^+$  ( $m/z$  103) and  $C_4H_8Cl^+$  ( $m/z$  91) by losses of  $Cl^\bullet$ ,  $CH_2Cl^\bullet$ ,  $C_3H_5Cl$ ,  $C_3H_6Cl^\bullet$ ,  $C_5H_8Cl^\bullet$  and  $C_6H_8Cl^\bullet$ , respectively. Subsequent decompositions of  $C_9H_{14}Cl^+$  by losses of  $C_3H_4$ ,  $:CHCl$ ,  $C_4H_6$ ,  $C_5H_8$ ,  $C_6H_{10}$  and  $C_4H_7Cl$  yield the ions  $C_6H_{10}Cl^+$  ( $m/z$  117),  $C_8H_{13}^+$  ( $m/z$  109),  $C_5H_8Cl^+$  ( $m/z$  103),  $C_4H_6Cl^+$  ( $m/z$  89),  $C_3H_4Cl^+$  ( $m/z$  75) and  $C_5H_7^+$  ( $m/z$  67), respectively.

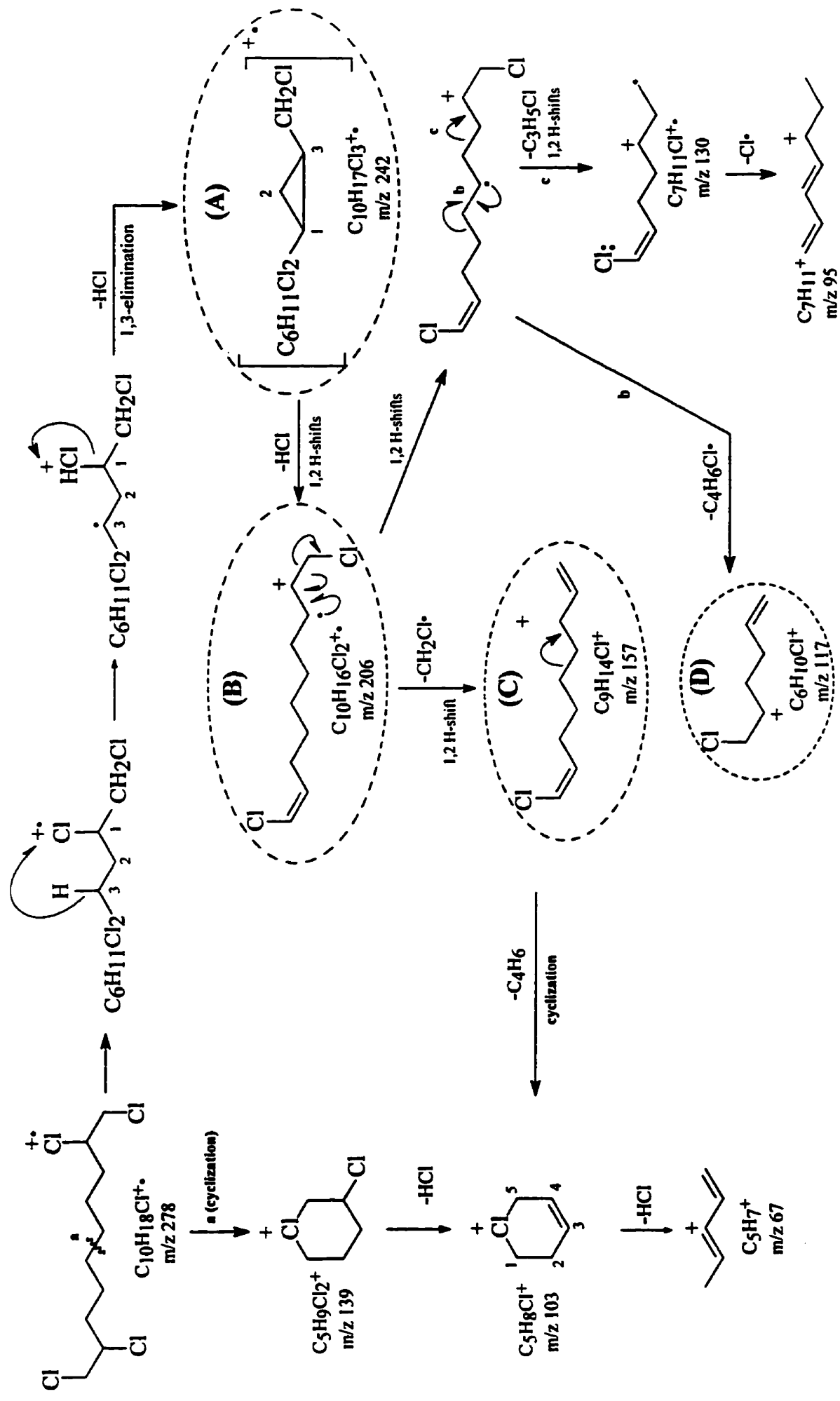
The  $C_7H_{11}Cl^+$  ion decomposes further to  $C_7H_{11}^+$  ( $m/z$  95),  $C_4H_8Cl^+$  ( $m/z$  91),  $C_4H_6Cl^+$  ( $m/z$  89),  $C_6H_9^+$  ( $m/z$  81) and  $C_4H_7^+$  ( $m/z$  55) by losses of  $Cl^\bullet$ ,  $C_3H_3^\bullet$ ,  $C_3H_5^\bullet$ ,  $CH_2Cl^\bullet$  and  $C_3H_4Cl^\bullet$ , respectively. In addition, the  $C_6H_{10}Cl^+$  ion,

decomposes by losses of  $\text{:CH}_2$ ,  $\text{C}_2\text{H}_2$ ,  $\text{C}_2\text{H}_4$ ,  $\text{HCl}$ ,  $\text{C}_3\text{H}_6$  and  $\text{C}_2\text{H}_3\text{Cl}$  to yield  $\text{C}_5\text{H}_8\text{Cl}^+$  ( $m/z$  103),  $\text{C}_4\text{H}_8\text{Cl}^+$  ( $m/z$  91),  $\text{C}_4\text{H}_6\text{Cl}^+$  ( $m/z$  89),  $\text{C}_6\text{H}_9^+$  ( $m/z$  81),  $\text{C}_3\text{H}_4\text{Cl}^+$  ( $m/z$  75) and  $\text{C}_4\text{H}_7^+$  ( $m/z$  55), respectively. By losses of  $\text{:CH}_2$  and  $\text{HCl}$  from  $\text{C}_5\text{H}_8\text{Cl}^+$  ( $m/z$  103) decomposes to yield  $\text{C}_4\text{H}_6\text{Cl}^+$  ( $m/z$  89) and  $\text{C}_5\text{H}_7^+$  ( $m/z$  67), respectively.

A prominent ion in the EI mass spectrum of 1,2,9,10- $\text{M}_{10,4}$  at  $m/z$  139,  $\text{C}_5\text{H}_9\text{Cl}_2^+$ , was found to have no identifiable precursors, so is assumed to be formed rapidly from  $\text{M}_{10,4}^+$  in the ion source. The structure of this ion was depicted earlier (see 14).

Mechanisms proposed for some of the decompositions are illustrated in *Scheme 4.3*. The  $\Sigma\text{S}$  energy of the highly strained substituted cyclopropane radical (depicted as **A** in *Scheme 4.3*) estimated as  $1180 \pm 60$  kJ/mol, is  $\sim 1150$  kJ/mol higher than for its acyclic analogue ( $25 \pm 4$  kJ/mol) and, thus, rapid ring opening is expected.

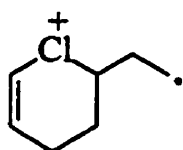
Closer examination of *Scheme 4.3*, reveals that there exist a number of positional isomers of the  $\text{C}_9\text{H}_{14}\text{Cl}^+$  ion,  $m/z$  157 (depicted as **C**). For example, the formation of  $\text{C}_5\text{H}_8\text{Cl}^+$  ion ( $m/z$  103) *via* a loss of  $\text{C}_4\text{H}_6$ , must proceed with one double bond at the terminal position; the position of the second double bond cannot be known, but is probably at the other terminal position. Similarly, the formation of the  $\text{C}_4\text{H}_6\text{Cl}^+$  ion ( $m/z$  89) can arise only with the double bonds at non-conjugated positions. Based on the energy argument described earlier, the conjugated form of this ion would, undoubtedly, be the most stable, however, plausible mechanisms for the formation of  $\text{C}_5\text{H}_8\text{Cl}^+$  and  $\text{C}_4\text{H}_6\text{Cl}^+$  ions from  $\text{C}_9\text{H}_{14}\text{Cl}^+$  ion can only be explained with decompositions *via* these less stable structures.



Scheme 4.3 Ion decomposition mechanisms for 1,2,9,10-tetrachloro-*n*-decane established by linked-field scanning.

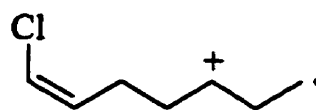


Two likely structures of the  $C_7H_{11}Cl^+$  ( $m/z$  130) ion, a precursor to many low mass even electron ions, are depicted below as 30 and 31. The six-membered cyclohexene derivative (30) was found to have a  $\Sigma S$  200 kJ/mol higher than the acyclic analogue (31), rather less than the expected interaction between the Cl and C+ centres, so the former is the preferred structure.



30

$$\Sigma S = 250 \pm 8 \text{ kJ/mol}$$



31

$$\Sigma S = 50 \pm 4 \text{ kJ/mol}$$

#### (D) 2,3,8,9-Tetrachloro-*n*-decane.

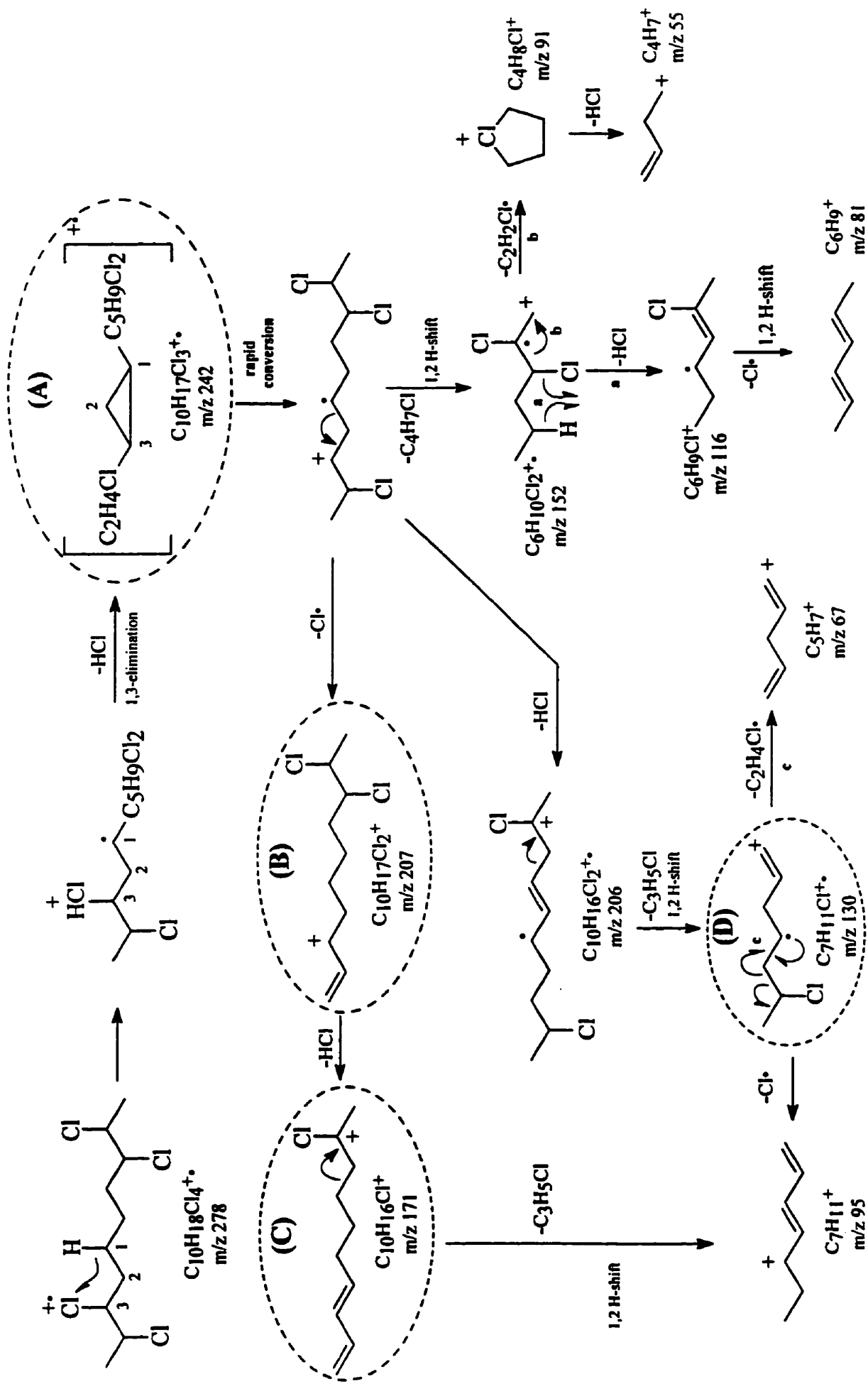
Figure 4.5 shows the EI positive ion mass spectrum of 2,3,8,9- $M_{10,4}$ . Ion fragmentation pathways established by linked-field scanning for this species are shown in *Appendix 2d*. In general, the appearance of its mass spectrum is similar to that of its positional isomer, 1,2,9,10- $M_{10,4}$ , with a few differences. The abundances of the  $m/z$  206 and 207 ions for the 2,3,8,9- $M_{10,4}$  are significantly higher than those for 1,2,9,10- $M_{10,4}$ . The prominent  $m/z$  139 ion,  $C_5H_9Cl_2^+$ , in the spectrum 1,2,9,10- $M_{10,4}$  is not observed in the mass spectrum of 2,3,8,9- $M_{10,4}$ ; a terminal Cl atom is a prerequisite for formation of  $C_5H_9Cl_2^+$ , instead we observe an intense ion at  $m/z$  143,  $C_8H_{12}Cl^+$ , arising from losses of  $C_2H_4Cl\cdot$  and  $C_2H_4$  from the  $[M_{10,4}-2HCl]^+$  ( $m/z$  206) and  $C_{10}H_{16}Cl^+$  ( $m/z$  171) ions, respectively. Another prominent ion observed in the mass spectrum of the 2,3,8,9- $M_{10,4}$  congener is  $C_8H_{11}^+$ ,  $m/z$  107, an octatrienyl ion, which arises from loss of HCl from  $C_8H_{12}Cl^+$ .

Mechanisms proposed for some of the decompositions are illustrated in *Scheme 4.4*. The  $\Sigma S$  energy of the highly strained substituted cyclopropane radical intermediate (depicted as **A** in *Scheme 4.4*), estimated as  $1060 \pm 25$  kJ/mol, is  $\sim 1030$  kJ/mol higher than for its acyclic analogue ( $27 \pm 1$  kJ/mol), so rapid ring opening is expected.

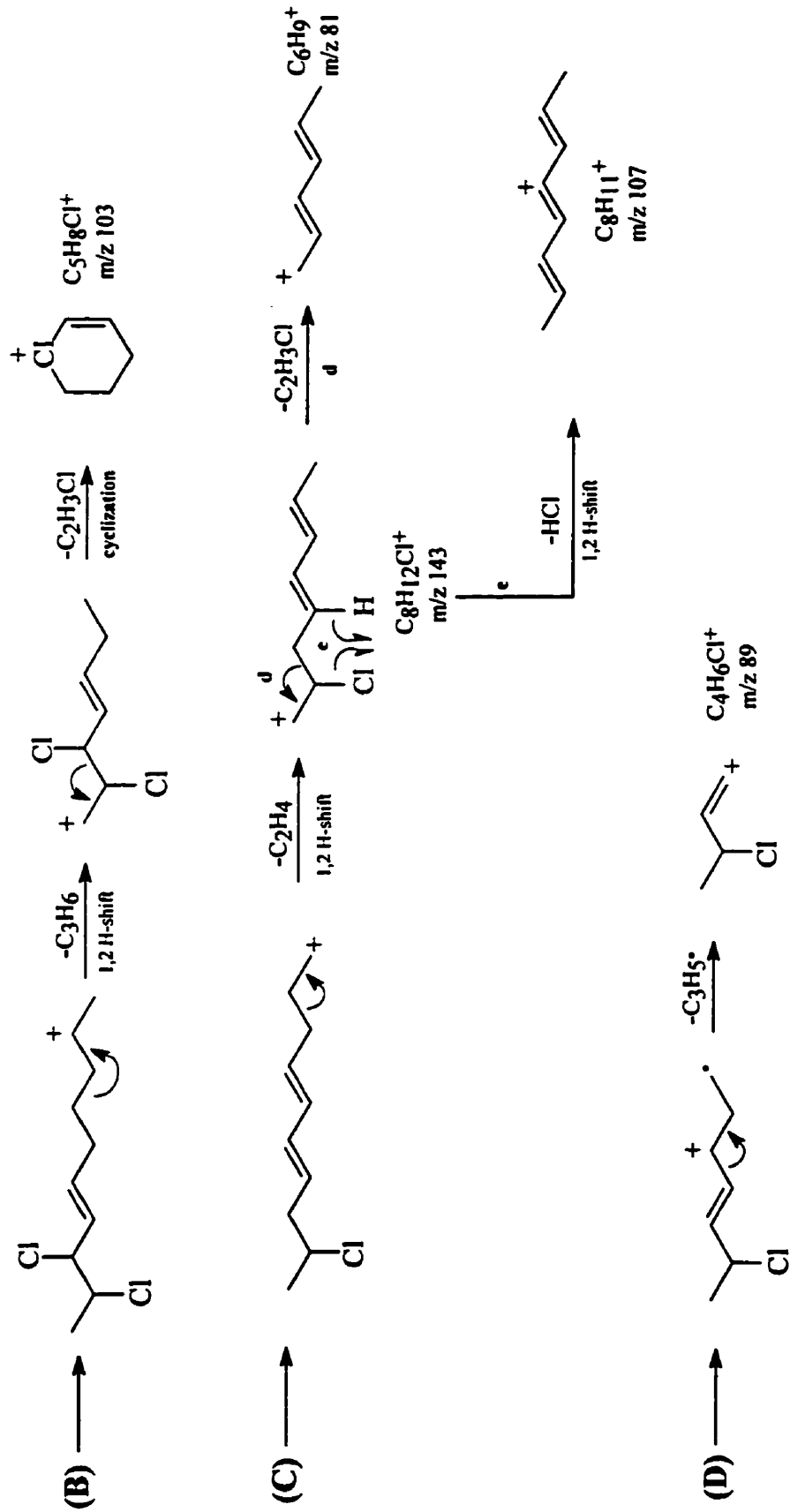
### (E) 1,2,10,11-Tetrachloro-*n*-undecane.

Figure 4.6 shows the EI positive ion mass spectrum of 1,2,10,11- $M_{11,4}$ . Ion fragmentation pathways established by linked-field scanning for this species are shown in *Appendix 2e*. The  $m/z$  256 ion, corresponding to  $[M_{11,4}-HCl]^{\bullet+}$  initially formed as a cyclopropane radical ion (depicted as **A** in *Scheme 4.5*,  $\Sigma S = 1280 \pm 17$  kJ/mol) - which then rearranges to the more stable acyclic conformer ( $\Sigma S = 28.5 \pm 0.4$  kJ/mol), is the immediate precursor of  $C_{11}H_{19}Cl_2^+$  ( $m/z$  221),  $C_{11}H_{18}Cl_2^{\bullet+}$  ( $m/z$  220),  $C_{11}H_{19}Cl_2^+$  ( $m/z$  221),  $C_{11}H_{18}Cl^+$  ( $m/z$  185) and  $C_5H_9Cl_2^+$  ( $m/z$  139); the structure (14) and prominence of this latter ion was discussed earlier. The  $C_{11}H_{18}Cl_2^{\bullet+}$  ion then decomposes to  $C_9H_{14}Cl_2^{\bullet+}$  ( $m/z$  192),  $C_{11}H_{18}Cl^+$  ( $m/z$  185),  $C_{10}H_{16}Cl^+$  ( $m/z$  171),  $C_8H_{13}Cl^{\bullet+}$  ( $m/z$  144),  $C_7H_{11}Cl^{\bullet+}$  ( $m/z$  130),  $C_4H_5Cl_2^+$  ( $m/z$  123) and  $C_8H_{13}^+$  ( $m/z$  109) by losses of  $C_2H_4$ ,  $Cl^{\bullet}$ ,  $CH_2Cl^{\bullet}$ ,  $C_3H_5Cl$ ,  $C_4H_7Cl$ ,  $C_7H_{13}^{\bullet}$  and  $C_3H_5Cl_2^{\bullet}$ , respectively. The  $C_9H_{14}Cl_2^{\bullet+}$  and  $C_{11}H_{18}Cl^+$  ions further decompose by loss of  $Cl^{\bullet}$  to yield  $C_9H_{14}Cl^+$  ( $m/z$  157) and  $C_7H_{11}Cl^{\bullet+}$  ( $m/z$  130), respectively.

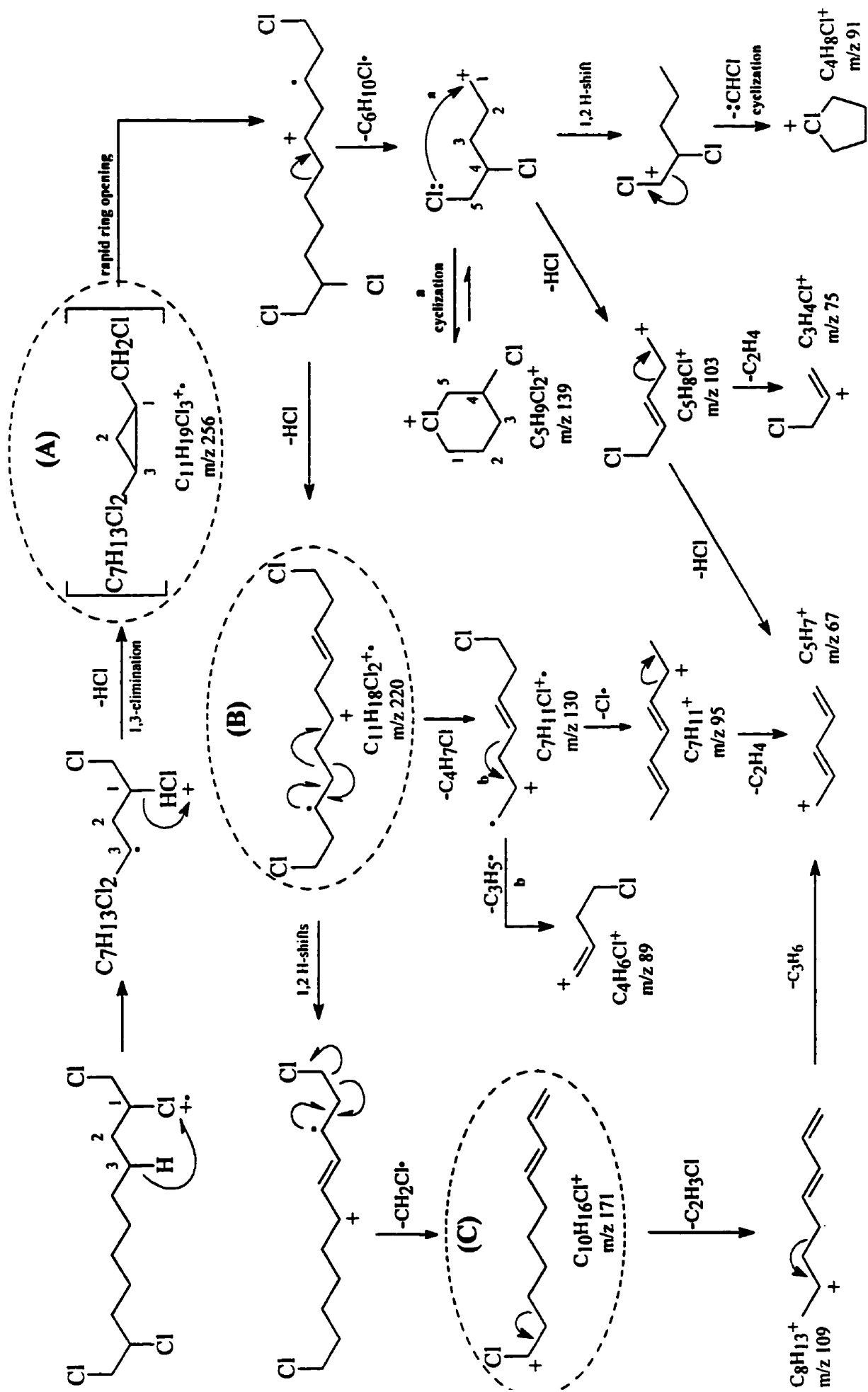
The  $C_{10}H_{16}Cl^+$  ion,  $m/z$  171, identified as the daughter of  $C_{11}H_{18}Cl_2^{\bullet+}$ , decomposes by losses of  $C_3H_6$ ,  $C_4H_6$ ,  $C_4H_8$ ,  $C_2H_3Cl$ ,  $C_6H_8$  and  $C_4H_7Cl$  to yield  $C_7H_{10}Cl^+$  ( $m/z$  129),  $C_6H_{10}Cl^+$  ( $m/z$  117),  $C_6H_8Cl^+$  ( $m/z$  115),  $C_8H_{13}^+$  ( $m/z$  109),  $C_4H_8Cl^+$  ( $m/z$  91) and  $C_6H_9^+$  ( $m/z$  81), respectively.



Scheme 4.4. Ion decomposition mechanisms for 2,3,8,9-tetrachloro-*n*-decane established by linked-field scanning



Scheme 4.4. (cont'd) Ion decomposition mechanisms for 2,3,8,9-tetrachloro-*n*-decane established by linked-field scanning.



Scheme 4.5. Ion decomposition mechanisms for 1,2,10,11-tetrachloro-n-undecane established by linked-field scanning.



The  $[M_{11,4}-C_2H_6Cl_3]^+$ ,  $m/z$  157, decomposes further to  $C_6H_{10}Cl^+$  ( $m/z$  117),  $C_8H_{13}^+$  ( $m/z$  109),  $C_5H_8Cl^+$  ( $m/z$  103),  $C_7H_{11}^+$  ( $m/z$  95),  $C_6H_9^+$  ( $m/z$  81),  $C_3H_4Cl^+$  ( $m/z$  75) and  $C_5H_7^+$  ( $m/z$  67) by losses of  $C_3H_4$ ,  $:CHCl$ ,  $C_4H_6$ ,  $C_2H_3Cl$ ,  $C_3H_5Cl$ ,  $C_6H_{10}$  and  $C_4H_7Cl$ , respectively.

The  $C_8H_{13}Cl^{\bullet}$  ion at  $m/z$  144, identified as the daughter of  $C_{11}H_{18}Cl_2^{\bullet}$ , by losses of  $:CH_2$ ,  $Cl^{\bullet}$ ,  $CH_2Cl^{\bullet}$ ,  $C_4H_7^{\bullet}$ ,  $C_5H_7^{\bullet}$  and  $C_3H_6Cl^{\bullet}$  yields  $C_7H_{11}Cl^{\bullet}$  ( $m/z$  130),  $C_8H_{13}^+$  ( $m/z$  109),  $C_7H_{11}^+$  ( $m/z$  95),  $C_4H_6Cl^+$  ( $m/z$  89),  $C_3H_6Cl^+$  ( $m/z$  77) and  $C_5H_7^+$  ( $m/z$  67), respectively.

Inspection of *Scheme 4.5* reveals the existence of a number of positional isomers of  $C_{11}H_{18}Cl_2^{\bullet}$ ,  $m/z$  220 (depicted as **B**), and of  $C_{10}H_{16}Cl^+$ ,  $m/z$  171 (depicted as **C**). The formation of  $C_4H_7^+$ ,  $m/z$  55, from **B** is likely to proceed with both double bonds at terminal positions, which we have shown earlier is a favorable conformation for a diene (*see* Figure 4.10). The formation of  $C_6H_9^+$ ,  $m/z$  81 from **B**, however, is thought to proceed with the double bonds in the conjugated positions. Similarly, the formation of  $C_7H_{10}Cl^+$ ,  $m/z$  129, from **C** is likely to proceed with the double in the conjugated positions, while  $C_6H_{10}Cl^+$ ,  $m/z$  117, from **C** must proceed with one double bond at the terminal position; the position of the second double bond cannot be known, but is probably at the other terminal position.

#### **(F) 2,3,9,10-Tetrachloro-*n*-undecane.**

Figure 4.7 shows the EI positive ion mass spectrum of 2,3,9,10- $M_{11,4}$ . Ion fragmentation pathways established by linked-field scanning for this species are shown in *Appendix 2f*. The appearance of the mass spectrum of 2,3,9,10- $M_{11,4}$  is quite different from that of its positional isomer, 1,2,10,11- $M_{11,4}$ . The

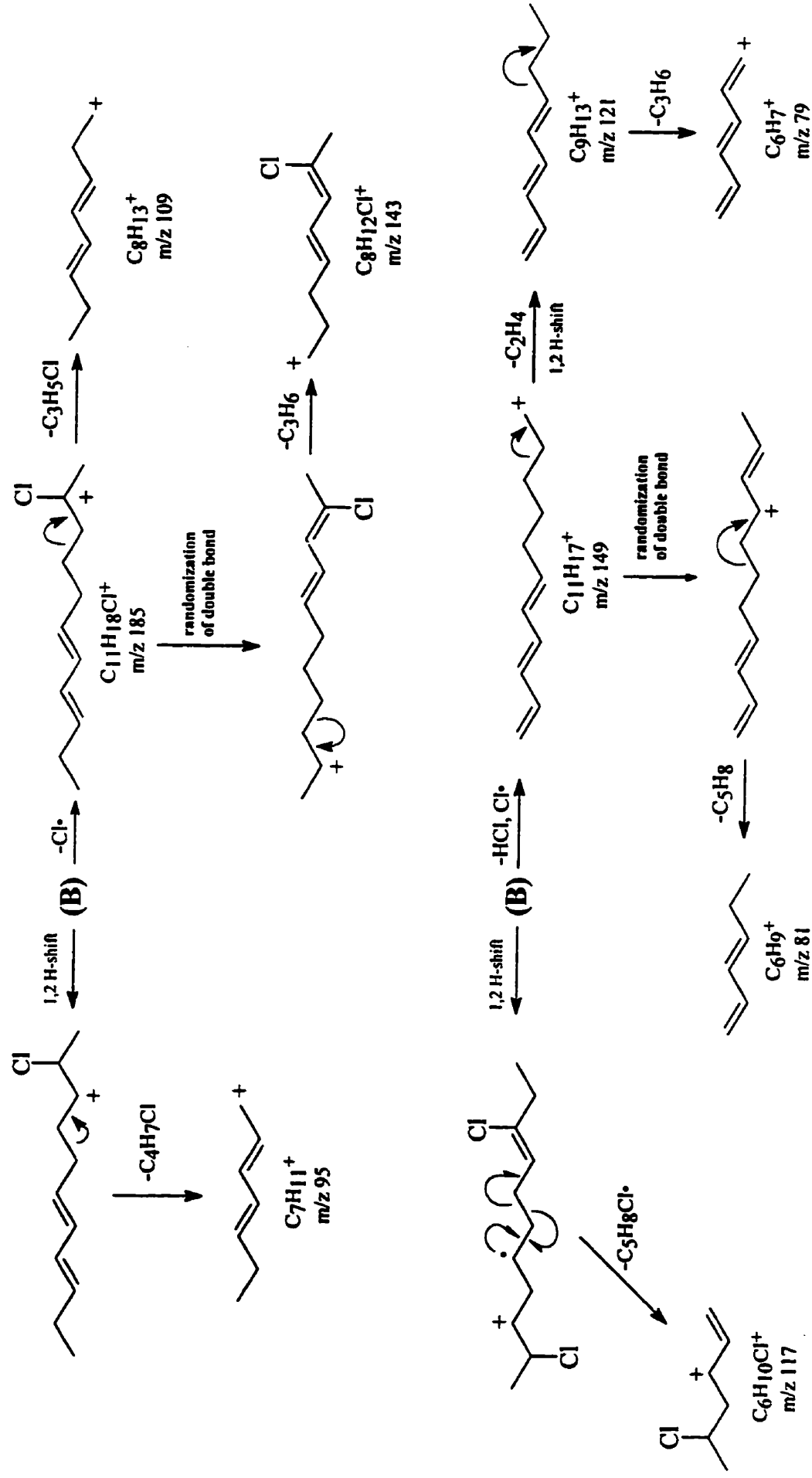
abundances of  $m/z$  220 and 221 ions, corresponding to  $[M_{11,4}-2HCl]^+$  and  $[M-HCl-Cl]^+$ , respectively, in the mass spectrum of 2,3,9,10- $M_{11,4}$  are significantly higher than those for 1,2,10,11- $M_{11,4}$ . A similar observation was made for the intensities of the  $[M_{10,4}-HCl-Cl]^+$  and  $[M_{10,4}-2HCl]^+$  ions in the mass spectra of the positional isomers 1,2,9,10- and 2,3,8,9- $M_{10,4}$ .

These results suggest that the ions formed by multiple losses of Cl• and HCl from the molecular ion is less likely to fragment than those having chlorine atoms residing at non-terminal positions. We can rationalize this as follows: non-terminal chlorine atoms would promote the release of electrons by non-substituted terminal methyl groups, either by induction or hyperconjugation, *i.e.*, the overlap of  $\sigma$ -bonds with the empty  $p$ -orbitals of the electron deficient carbon, thus stabilizing the alkyl halide carbocation and increasing its life-time in the ion source [15].

A prominent ion observed in the spectrum of 2,3,9,10- $M_{11,4}$  is at  $m/z$  157,  $C_9H_{14}Cl^+$ , a chloro-diene, and is derived by a loss of  $C_2H_4Cl$ • from the  $[M_{11,4}-2HCl]^+$  ion,  $m/z$  220. This ion, a precursor of many ions, has a low abundance in the 1,2,10,11- $M_{11,4}$  spectrum. Similarly, the abundant  $m/z$  139 ion,  $C_5H_9Cl_2^+$ , (14), observed in the spectrum of 1,2,10,11- $M_{11,4}$ , is of low abundance in the spectrum of its positional isomer. Finally, the intense ion at  $m/z$  149, corresponding to  $C_{11}H_{17}^+$ , an acyclic triene, is observed in the spectrum of 2,3,9,10- $M_{11,4}$ , decomposes to  $C_9H_{13}^+$  ( $m/z$  121),  $C_6H_9^+$  ( $m/z$  81) and  $C_5H_7^+$  ( $m/z$  67) by respective losses of  $C_2H_4$ ,  $C_5H_8$  and  $C_6H_{10}$ ; it is not detected in the spectrum of 1,2,10,11- $M_{11,4}$ .

*Scheme 4.6* shows the mechanisms for some of the decompositions of 2,3,9,10- $M_{11,4}$ . The highly strained substituted cyclopropane radical intermediate





Scheme 4.6. (cont'd) Ion decomposition mechanisms for 2,3,9,10-Tetrachloro-n-undecane established by linked-field scanning.

(depicted as **A** in *Scheme 4.6*,  $\Sigma S = 1520 \pm 40$  kJ/mol) can be expected to rapidly convert to its acyclic analogue ( $\Sigma S = 27.6 \pm 0.4$  kJ/mol).

Closer examination of *Scheme 4.6* also illustrates that random positioning of the double bonds occurs for the following ions:  $C_{11}H_{18}Cl^+$  ( $m/z$  185),  $C_9H_{14}Cl^+$ , ( $m/z$  157)  $C_{11}H_{17}^+$  ( $m/z$  149) and  $C_7H_{11}Cl^+$  ( $m/z$  130).

### **(G) 1,2,11,12-Tetrachloro-*n*-dodecane.**

Figure 4.8 shows the EI positive ion mass spectrum of 1,2,11,12- $M_{12,4}$ . Ion fragmentation pathways established by linked-field scanning for this species are shown in *Appendix 2g*. The  $m/z$  270 ion corresponds to  $[M_{12,4}-HCl]^+$ , initially formed as a cyclopropane radical ion (depicted as **A** in *Scheme 4.7*,  $\Sigma S = 1240 \pm 25$  kJ/mol) which then rearranges to the more stable acyclic conformer ( $\Sigma S = 27.2 \pm 0.4$  kJ/mol), is the immediate precursor of  $C_{12}H_{20}Cl_2^+$  ( $m/z$  234) and  $C_5H_9Cl_2^+$  ( $m/z$  139). The former ion subsequently decomposes to  $C_{10}H_{16}Cl_2^+$  ( $m/z$  206),  $C_{12}H_{20}Cl^+$  ( $m/z$  199),  $C_{11}H_{18}Cl^+$  ( $m/z$  185),  $C_5H_9Cl_2^+$  ( $m/z$  139),  $C_7H_{12}Cl^+$  ( $m/z$  131) and  $C_6H_{10}Cl^+$  ( $m/z$  117) by losses of  $C_2H_4$ ,  $Cl^+$ ,  $CH_2Cl^+$ ,  $C_7H_{11}^+$ ,  $C_5H_8Cl^+$  and  $C_6H_{10}Cl^+$ , respectively. The  $C_{10}H_{16}Cl_2^+$  ion further decomposes to  $C_{10}H_{16}Cl^+$  ( $m/z$  171),  $C_6H_{10}Cl_2^+$  ( $m/z$  152) and  $C_5H_9Cl_2^+$  ( $m/z$  139) by respective losses of  $Cl^+$ ,  $C_4H_6$  and  $C_5H_7^+$ . Subsequent decompositions of  $C_{10}H_{16}Cl^+$  by losses of  $C_2H_4$ ,  $C_3H_4$ ,  $:CHCl$ ,  $C_2H_3Cl$ ,  $C_5H_8$ ,  $C_3H_5Cl$  and  $C_4H_7Cl$  yields  $C_8H_{12}Cl^+$  ( $m/z$  143),  $C_7H_{12}Cl^+$  ( $m/z$  131),  $C_9H_{15}^+$  ( $m/z$  123),  $C_8H_{13}^+$  ( $m/z$  109),  $C_5H_8Cl^+$  ( $m/z$  103),  $C_7H_{11}^+$  ( $m/z$  95) and  $C_6H_9^+$  ( $m/z$  81), respectively.

Through a series of double bond randomizations the  $C_{12}H_{20}Cl^+$  ion,  $m/z$  199, (see *Scheme 4.7* structure **C**) decomposes to  $C_9H_{14}Cl^+$  ( $m/z$  157),  $C_6H_{10}Cl^+$  ( $m/z$  117),  $C_5H_8Cl^+$  ( $m/z$  103) and  $C_7H_{11}^+$  ( $m/z$  95) by losses of  $C_3H_6$ ,  $C_6H_{10}$ ,  $C_7H_{12}$





and  $C_5H_9Cl$ , respectively. Subsequent decomposition of  $C_9H_{14}Cl^+$  ( $m/z$  157) by losses of  $C_3H_4Cl$ ,  $C_2H_3Cl$ ,  $C_5H_6$  and  $C_3H_5Cl$  yields  $C_6H_{10}Cl^+$  ( $m/z$  117),  $C_7H_{11}^+$  ( $m/z$  95),  $C_4H_8Cl^+$  ( $m/z$  91) and  $C_6H_9^+$  ( $m/z$  81), respectively.

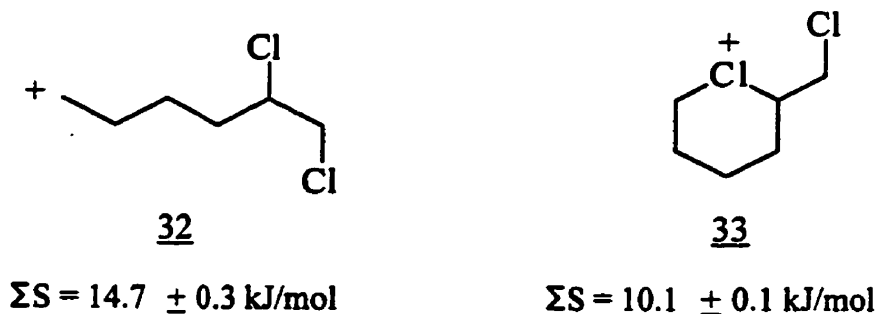
The  $C_6H_{10}Cl_2^+$  ion,  $m/z$  152, identified as the daughter of  $C_{10}H_{16}Cl_2^+$  decomposes further to  $C_6H_{10}Cl^+$  ( $m/z$  117) and  $C_5H_8Cl^+$  ( $m/z$  103) by losses of  $Cl$  and  $CH_2Cl$ , respectively. The former ion,  $C_6H_{10}Cl^+$ , further decomposes by losses of  $:CH_2$ ,  $C_2H_4$ ,  $HCl$  and  $C_3H_6$  to yield  $C_5H_8Cl^+$  ( $m/z$  103),  $C_4H_6Cl^+$  ( $m/z$  89),  $C_6H_9^+$  ( $m/z$  81) and  $C_3H_4Cl^+$  ( $m/z$  75), respectively.

The  $m/z$  143 ion,  $C_8H_{12}Cl^+$ , of low intensity, is a precursor to many low mass even electron ions. Decompositions to  $C_5H_8Cl^+$  ( $m/z$  103),  $C_7H_{11}^+$  ( $m/z$  95),  $C_4H_8Cl^+$  ( $m/z$  91),  $C_6H_9^+$  ( $m/z$  81) and  $C_5H_7^+$  ( $m/z$  67) are achieved by respective losses of  $C_3H_4$ ,  $:CHCl$ ,  $C_4H_4$ ,  $C_2H_3Cl$  and  $C_3H_5Cl$ .

Mechanisms proposed for some of the decompositions are illustrated in *Scheme 4.7*. The ions at  $m/z$  199, 171 and 157 corresponding to  $C_{12}H_{20}Cl^+$  (**C**),  $C_{10}H_{16}Cl^+$  (**E**) and  $C_9H_{14}Cl^+$  (**D**) all contain positional isomers which are formed by the randomization of the double bonds. In addition, two isomeric structures for the  $C_{12}H_{20}Cl_2^+$  ion ( $m/z$  234), depicted as **B** and **B<sub>1</sub>** are shown in *Scheme 4.7*. The former isomer is shown with the two chlorine atoms at terminal positions; decomposition to  $C_7H_{12}Cl^+$ ,  $m/z$  131, can only be explained *via* this structure. However, the decomposition of  $C_{12}H_{20}Cl_2^+$  to  $C_{10}H_{16}Cl_2^+$ ,  $m/z$  206, must proceed *via* isomer, **B<sub>1</sub>**, which depicts the molecule with the two chlorine atoms residing in vicinal positions.

The  $\Sigma S$  energies were also determined for the  $C_6H_{10}Cl_2^+$  ion,  $m/z$  152. The two likely structures for this ion are depicted below as **32** and **33**. The  $\Sigma S$

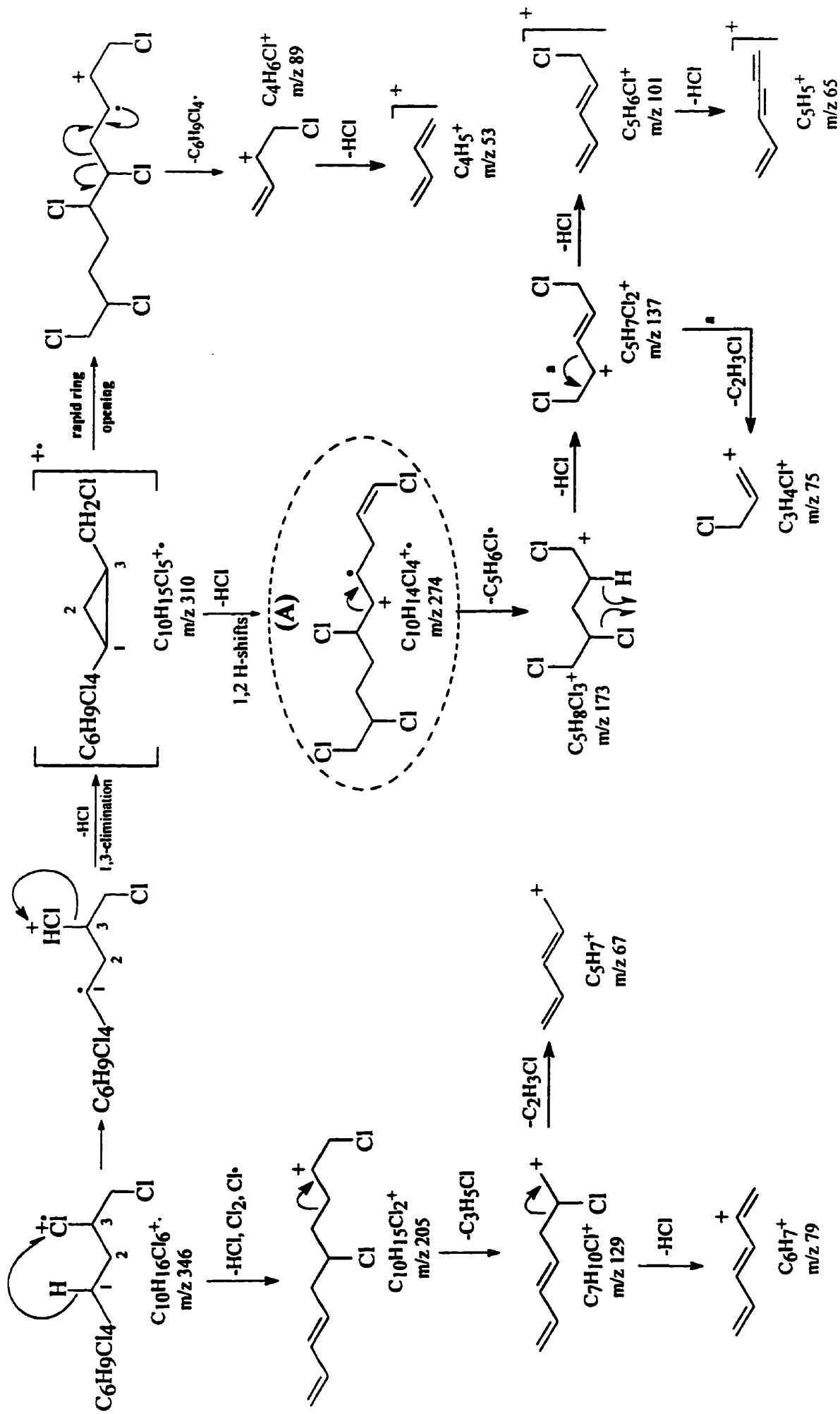
energy of the acyclic structure (33) of  $10.1 \pm 0.2$  kJ/mol is slightly lower than that of its acyclic conformer (32),  $14.7 \pm 0.3$  kJ/mol, and so we can assume that this structure would dominate.



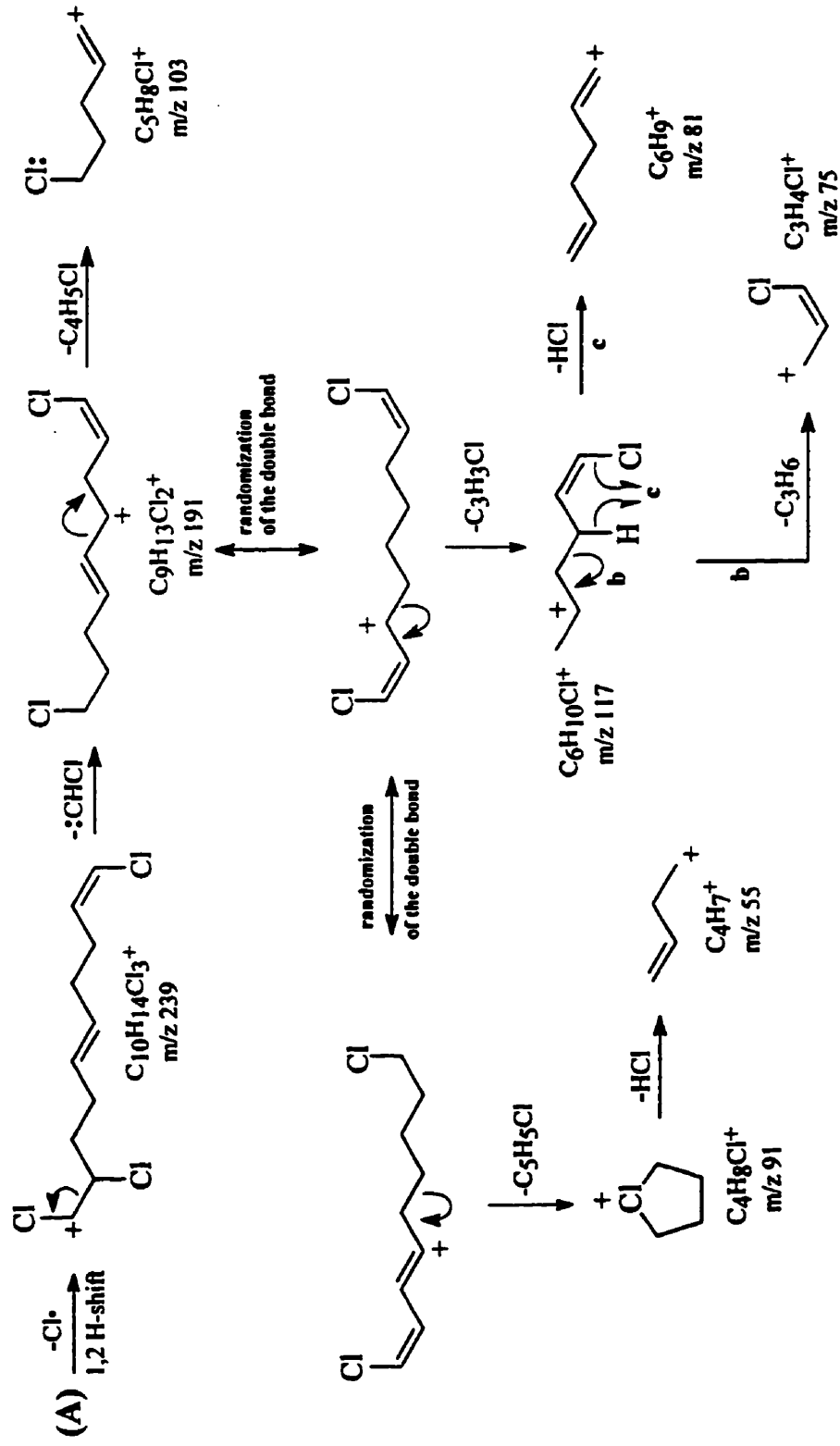
#### (H) 1,2,5,6,9,10-Hexachloro-*n*-decane.

Figure 4.9 shows the EI positive ion mass spectrum of 1,2,5,6,9,10- $M_{10,6}$ . Ion fragmentation pathways established by linked-field scanning for this species are shown in *Appendix 2h*. The  $[M-HCl]^+$  ion,  $m/z$  310, initially formed as a cyclopropane radical ion (depicted as A in *Scheme 4.8*,  $\Sigma S = 1335 \pm 25$  kJ/mol) which then rearranges to the more stable acyclic conformer ( $\Sigma S = 28.1 \pm 0.4$  kJ/mol), by losses of  $Cl^\bullet$ , HCl, ( $Cl^\bullet + HCl$ ),  $C_5H_7Cl_2$  ( $C_3H_5Cl^\bullet + Cl_2$ ) and  $C_6H_9Cl_4^\bullet$ , yields the ions  $C_{10}H_{15}Cl_4^+$  ( $m/z$  275),  $C_{10}H_{14}Cl_4^+$  ( $m/z$  274),  $C_{10}H_{14}Cl_3^+$  ( $m/z$  239),  $C_5H_8Cl_3^+$  ( $m/z$  173),  $C_7H_{10}Cl^+$  ( $m/z$  129) and  $C_4H_6Cl^+$  ( $m/z$  89), respectively. The  $C_{10}H_{15}Cl_4^+$  ion also decomposes by loss of  $Cl_2$  (not directly confirmed, but implied by the observed  $m/z$  346 to  $m/z$  205 pathway) to  $C_{10}H_{15}Cl_2^+$ ,  $m/z$  205.

The  $C_{10}H_{15}Cl_4^+$  ion,  $m/z$  275, decomposes further to  $C_{10}H_{14}Cl_3^+$  ( $m/z$  239),  $C_{10}H_{15}Cl_2^+$  ( $m/z$  205),  $C_{10}H_{13}Cl_2^+$  ( $m/z$  203),  $C_5H_7Cl_2^+$  and ( $m/z$  137), by losses of HCl,  $Cl_2$ , 2HCl and  $C_5H_8Cl_2$ , respectively. The  $C_{10}H_{15}Cl_4^+$  ion also decomposes



Scheme 4.8. Ion decomposition mechanisms for 1,2,5,6,9,10-hexachloro-n-decane established by linked-field scanning.



Scheme 4.8. (cont'd) Ion decomposition mechanism for 1,2,5,6,9,10-hexachloro-n-decane established by linked-field scanning.

by concomitant losses of (a)  $C_3H_5Cl^\bullet$  and  $Cl_2$  and (b)  $C_4H_7Cl_2$  and  $Cl^\bullet$  to yield  $C_7H_{10}Cl^+$  ( $m/z$  129) and  $C_6H_8Cl^+$  ( $m/z$  115), respectively.

The  $C_{10}H_{14}Cl_4^{+\bullet}$  ion,  $m/z$  274, decomposes to  $C_{10}H_{14}Cl_3^+$  ( $m/z$  239) and  $C_5H_8Cl_3^+$  ( $m/z$  173) by losses of  $Cl^\bullet$  and  $C_5H_6Cl^\bullet$ . It also decomposes by concomitant losses of (a)  $HCl$  and  $Cl^\bullet$ , (b)  $:CHCl$  and  $Cl^\bullet$ , (c)  $C_3H_4Cl_2^\bullet$  and  $Cl^\bullet$  to yield  $C_{10}H_{13}Cl_2^{+\bullet}$  ( $m/z$  203),  $C_9H_{13}Cl_2^+$  ( $m/z$  191) and  $C_7H_{10}Cl^+$  ( $m/z$  129), respectively.

The  $C_{10}H_{14}Cl_3^+$  ion,  $m/z$  239, identified as daughters of  $C_{10}H_{15}Cl_5^{+\bullet}$ ,  $C_{10}H_{15}Cl_4^+$  and  $C_{10}H_{14}Cl_4^{+\bullet}$ , by losses of  $:CHCl$  and  $C_5H_7Cl$  yields  $C_9H_{13}Cl_2^+$  ( $m/z$  191) and  $C_5H_7Cl_2^+$  ( $m/z$  137), respectively. Also, concomitant losses of  $C_3H_4Cl^\bullet$  and  $Cl^\bullet$  from  $C_{10}H_{14}Cl_3^+$  yield the ion  $C_7H_{10}Cl^+$ ,  $m/z$  129.

The  $m/z$  205 ion,  $C_{10}H_{15}Cl_2^+$ , further decomposes by losses of  $C_3H_4$ ,  $C_5H_8$ ,  $C_3H_5Cl$  and  $C_4H_5Cl$  to yield  $C_7H_{11}Cl_2^+$  ( $m/z$  165),  $C_5H_7Cl_2^+$  ( $m/z$  137),  $C_7H_{10}Cl^+$  ( $m/z$  129) and  $C_6H_{10}Cl^+$  ( $m/z$  117), respectively. In turn, the  $C_5H_7Cl_2^+$  ion decomposes further to  $C_3H_4Cl^+$ ,  $m/z$  75, by loss of  $C_2H_3Cl$ , and  $C_6H_{10}Cl^+$  decomposes by losses of  $:CH_2$ ,  $C_2H_2$ ,  $C_2H_4$ ,  $HCl$ ,  $C_3H_6$  and  $C_2H_3Cl$  to yield  $C_5H_8Cl^+$  ( $m/z$  103),  $C_4H_8Cl^+$  ( $m/z$  91),  $C_4H_6Cl^+$  ( $m/z$  89),  $C_6H_9^+$  ( $m/z$  81)  $C_3H_4Cl^+$  ( $m/z$  75) and  $C_4H_7^+$  ( $m/z$  55), respectively.

The  $m/z$  173 ion,  $C_5H_8Cl_3^+$ , identified as a daughter of  $C_{10}H_{14}Cl_4^{+\bullet}$  ( $m/z$  274), decomposes by loss of  $HCl$  to  $C_5H_7Cl_2^+$  ( $m/z$  137) and concomitant loss of  $2HCl$  to yield  $C_5H_6Cl^+$  ( $m/z$  101). This latter ion decomposes further to  $C_5H_5^+$  ( $m/z$  65) by loss of  $HCl$ .

Mechanisms proposed for some of the decompositions are illustrated in

*Scheme 4.8.* The  $m/z$  191 ion,  $C_9H_{13}Cl_2^+$ , is depicted in the scheme in three isomeric forms. Decomposition to the ion at  $C_6H_{10}Cl^+$ ,  $m/z$  117, can only proceed with a double bond residing in both the neutral fragment lost and the daughter ion formed; the positions of the double bonds cannot be known, but we assume, based on earlier arguments, they are in the terminal positions. The structure of the isomer leading to the chloroalkane daughter ion at  $m/z$  91,  $C_4H_8Cl^+$ , must proceed via a conjugated double bond arrangement for the  $C_9H_{13}Cl_2^+$  ion; the neutral fragment that is lost carries with it both double bonds. Finally, the structure of the isomer leading to the formation of  $C_5H_8Cl^+$ ,  $m/z$  103, cannot be known with any degree of certainty; however, one of the likely structures is shown in *Scheme 4.8*.

## 4.1.2 ECNI MASS SPECTROMETRY

### 4.1.2.1 Introduction

In *Section 2.2.2* of this thesis we addressed some of the theoretical aspects used to elucidate the generation of ECNI mass spectra. It was shown that the formation of thermalized electrons ( $e^-_{th}$ ) in the ion source of a mass spectrometer, which are necessary for generating negative ions, could be promoted by the addition of an enhancement gas, such as methane or argon. In addition to the type of enhancement gas used, there are a number of other instrumental parameters that affect the propensity of  $e^-_{th}$  formation, and which ultimately influence the relative ion abundance in an ECNI mass spectrum, these include: (a) ion source temperature, (b) ion source pressure, (c) sample concentration, (d) electron beam energy and (e) electron emission current [28,44,90-100].

In the studies described below, the effect of ion source temperature and

sample concentration upon the appearance of the ECNI mass spectra, *i.e.*, the relative ion abundances, of a number of our synthesized congeners were investigated. The impetus for this study was twofold: (1) to obtain optimum ion source conditions, *viz*, maximum sensitivity and selectivity, criteria which are necessary for our analytical protocol, and (2) to aid in our understanding of conditions that are necessary to promote the formation of chloride adduct ions, *i.e.*,  $[M + Cl]^-$ , in the ion source of the mass spectrometer.

#### 4.1.2.1.1 Ion Source Temperature.

Variations in the relative abundance of negative ions that occur because of changes in the temperature of the ion source are well documented [90-96]. In general, a lower ion source temperature enhances the abundance of molecular anions since resonance electron capture becomes more efficient [90]. As well, a decrease in internal energy of the ionized molecule and subsequently lowers the propensity for dissociative reactions (*Section 2.2.1*, equation 2-10 and 2-11) [44,90].

The appearance of the ECNI mass spectra at varying ion source temperatures for *tetra-*, *penta-*, *hexa-* and *hepta-* decane and undecane are shown in Figures 4.13-4.20. (*Appendix 3(a-h)* shows the corrected ion abundances at varying ion source temperatures in tabular form.) In general, at 220°C, spectra are dominated by low mass fragment ions corresponding to  $Cl_2^-$  ( $m/z$  70/72/74) and  $HCl_2^-$  ( $m/z$  71/73/75). As the temperature in the ion source is lowered, the relative abundance of the  $[M - Cl]^-$  ions increases; there are also groups of smaller peaks, in some cases, which arise from further losses of HCl and/or  $Cl^\bullet$ . Also observed, in some cases, in particular at lower source temperatures, are ions corresponding to the addition of a chloride ion to the

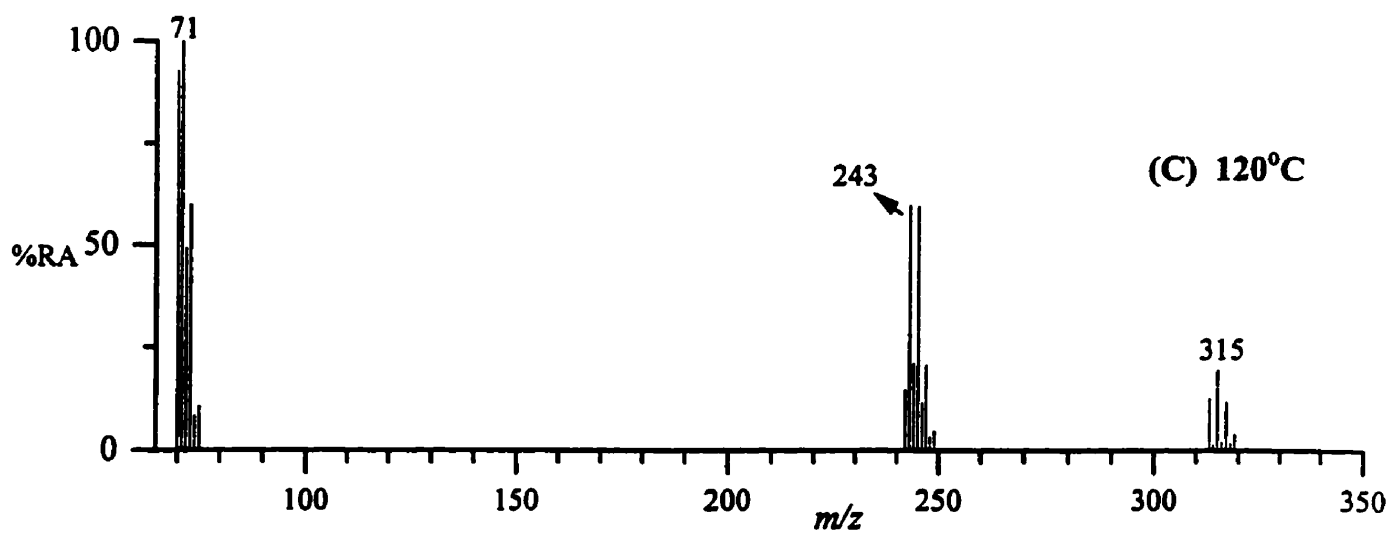
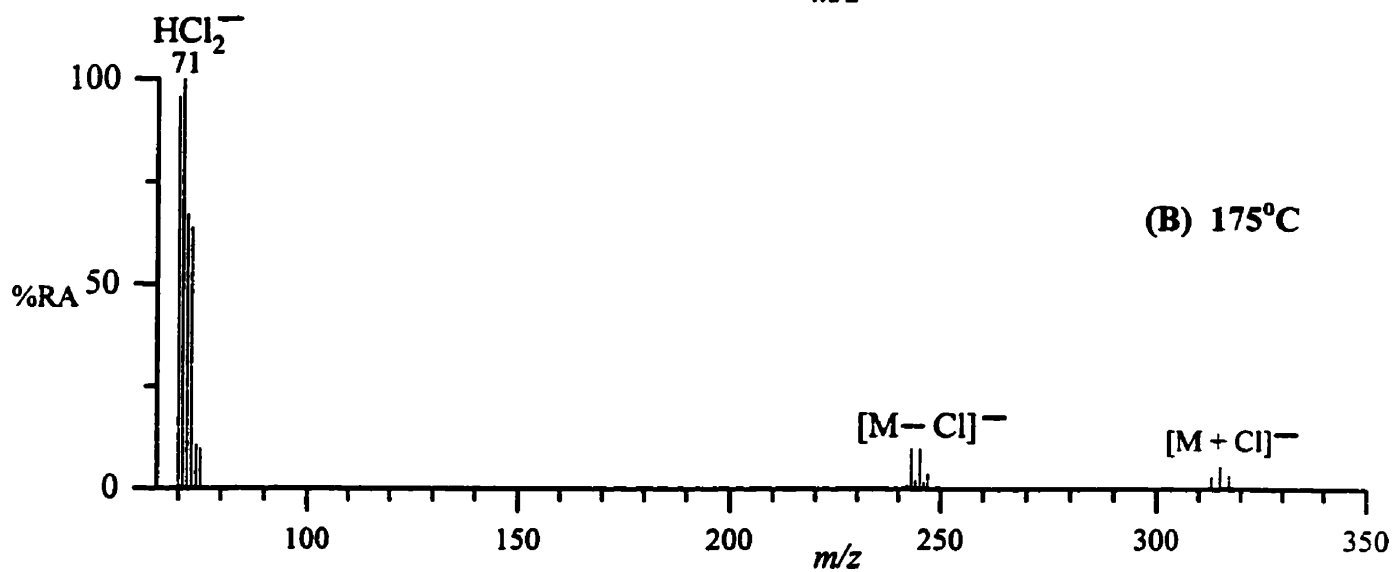
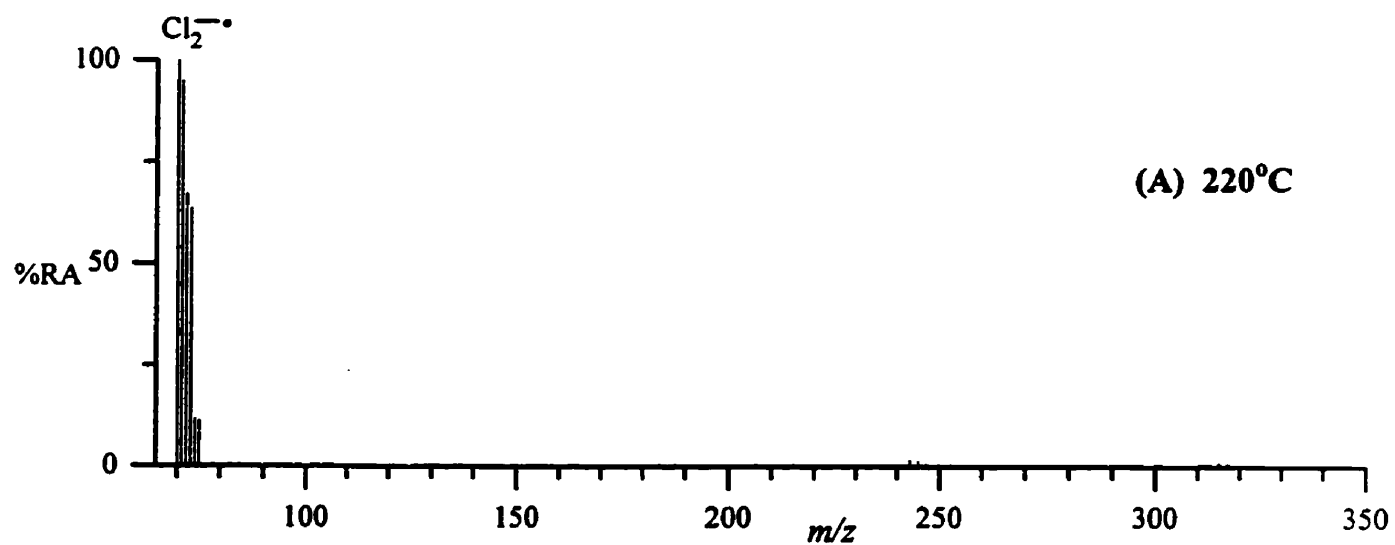


Figure 4.13. ECNI mass spectra of 1,2,9,10-tetrachloro-*n*-decane at ion source temperatures of (a) 220°C, (b) 175°C and (c) 120°C.

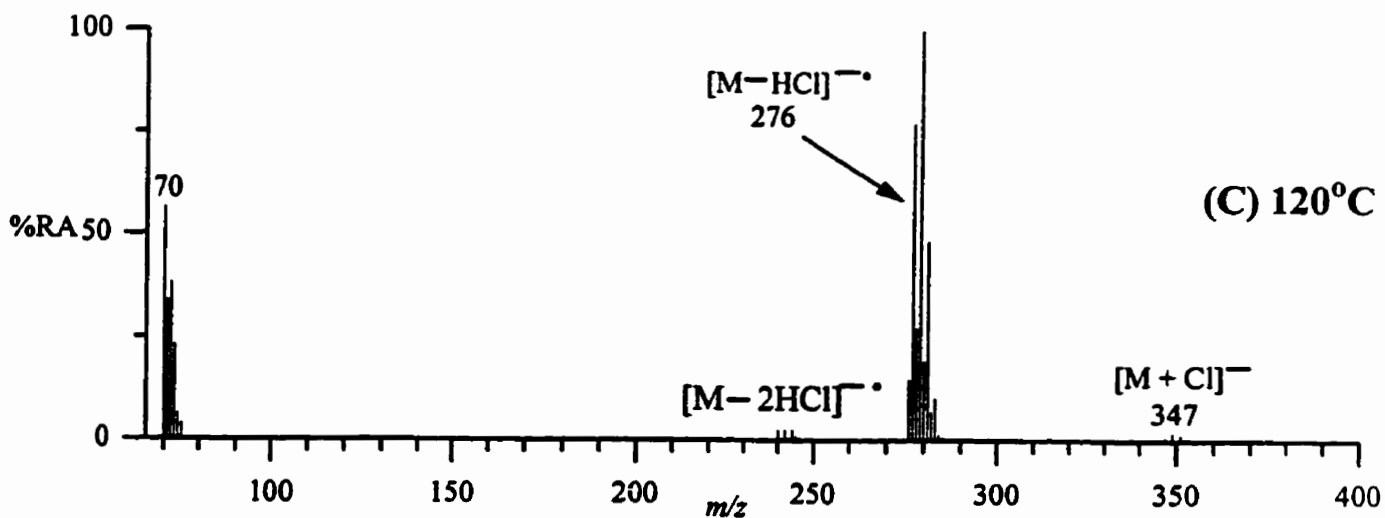
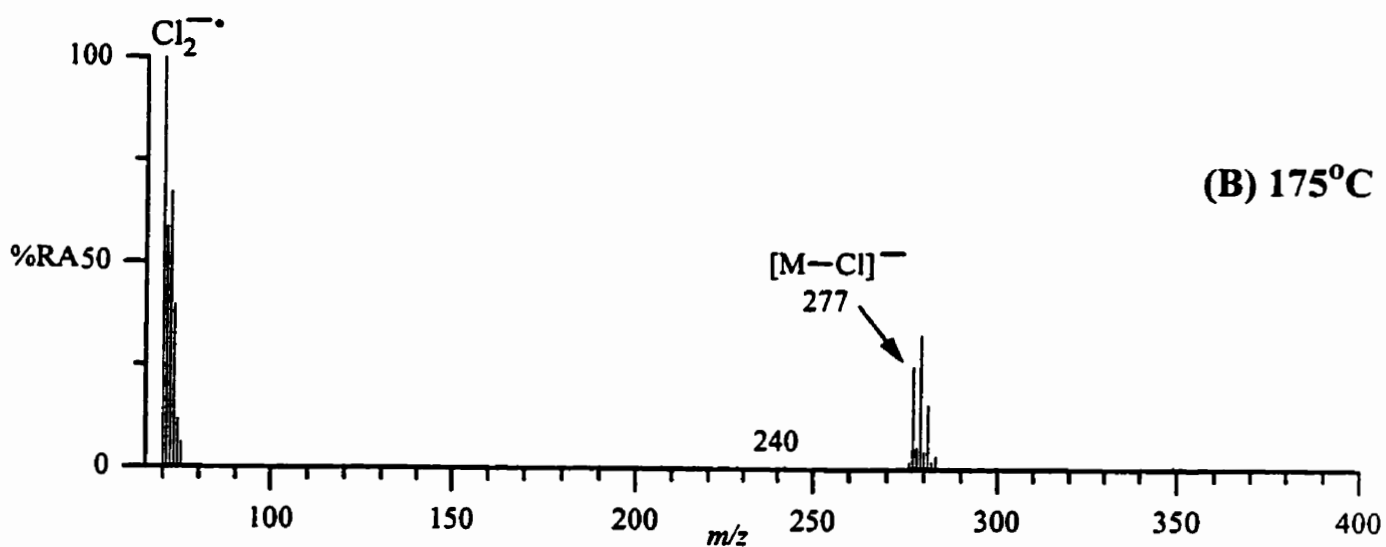
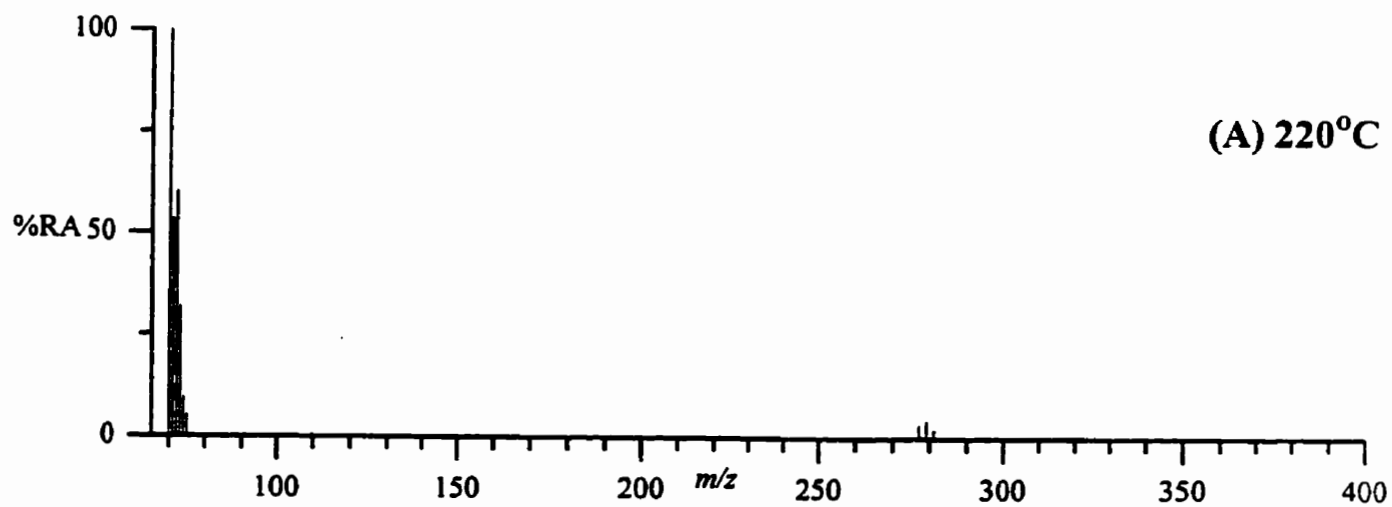


Figure 4.14. ECNI mass spectra of 1,2,x,9,10-pentachloro-*n*-decane at ion source temperatures of (a) 220°C, (b) 175°C and (c) 120°C.

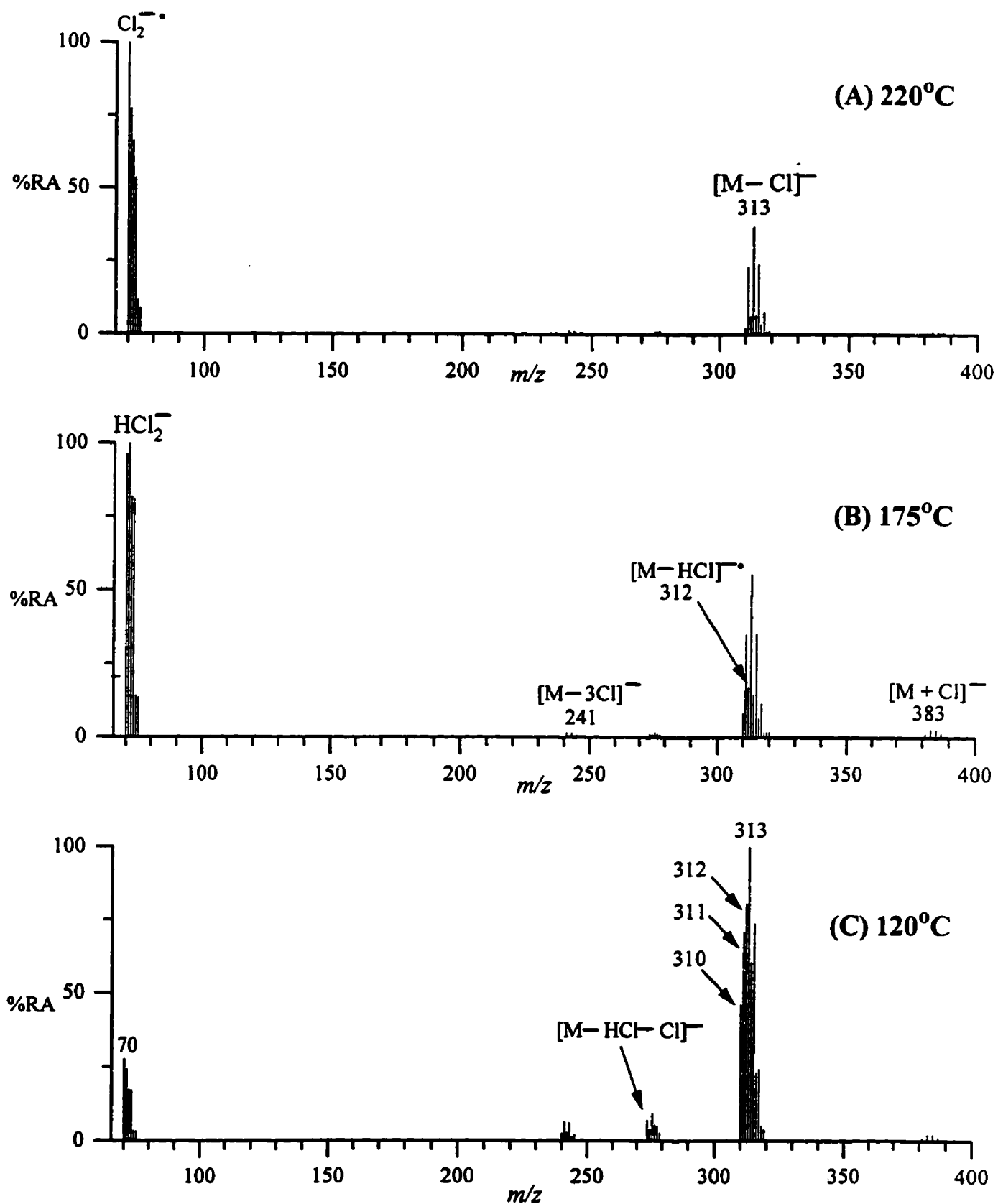


Figure 4.15. ECNI mass spectra of 1,2,5,6,9,10-hexachloro-*n*-decane at ion source temperatures of (a) 220°C, (b) 175°C and (c) 120°C.

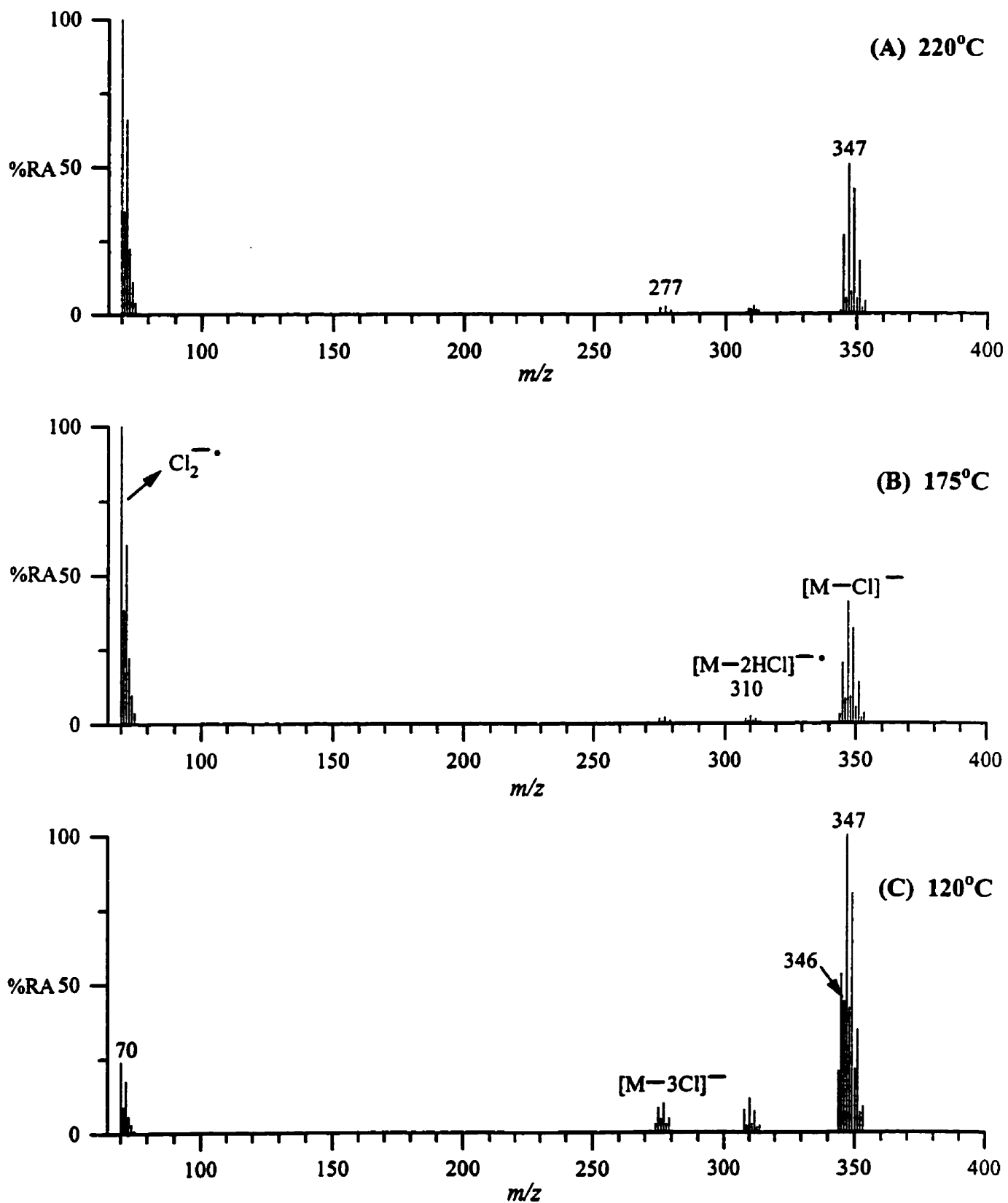


Figure 4.16 ECNI mass spectra of 1,2,x,5,6,9,10-heptachloro-*n*-decane at ion source temperatures of (a) 220°C, (b) 175°C and (c) 120°C.

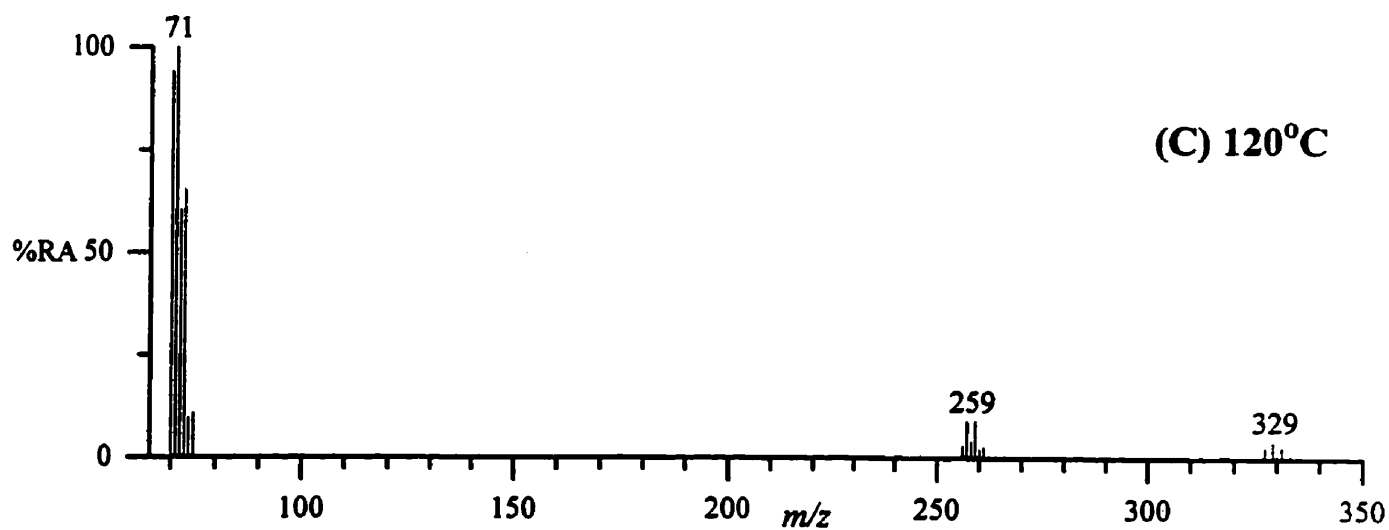
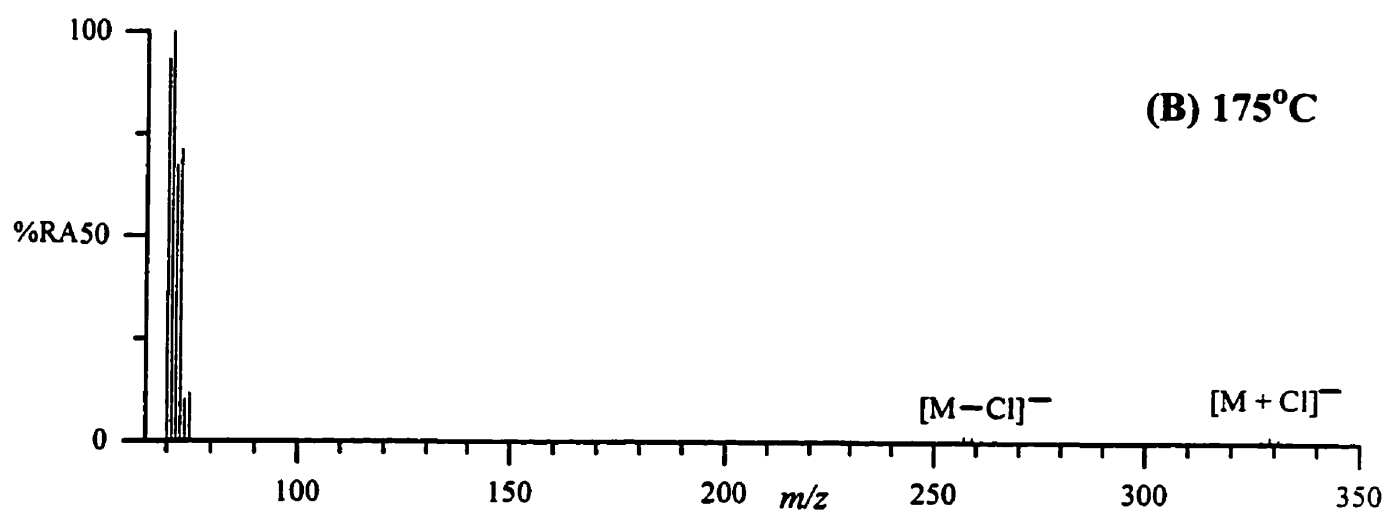
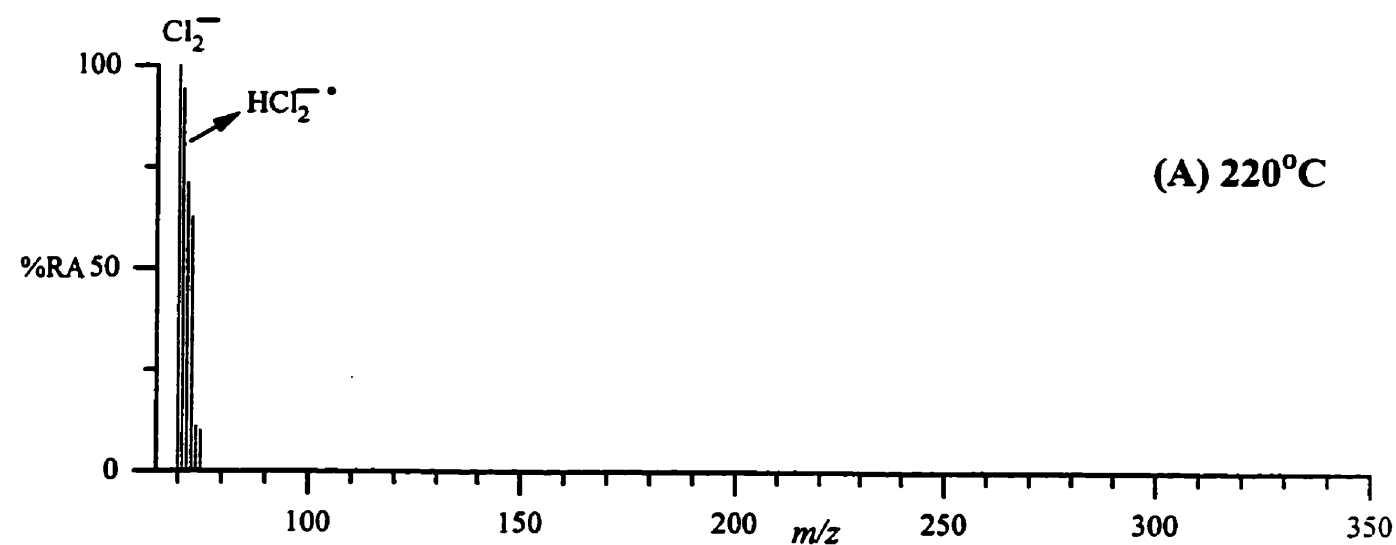


Figure 4.17. ECNI mass spectra of 1,2,10,11-tetrachloro-*n*-undecane at ion source temperatures of (a) 220°C, (b) 175°C and (c) 120°C.

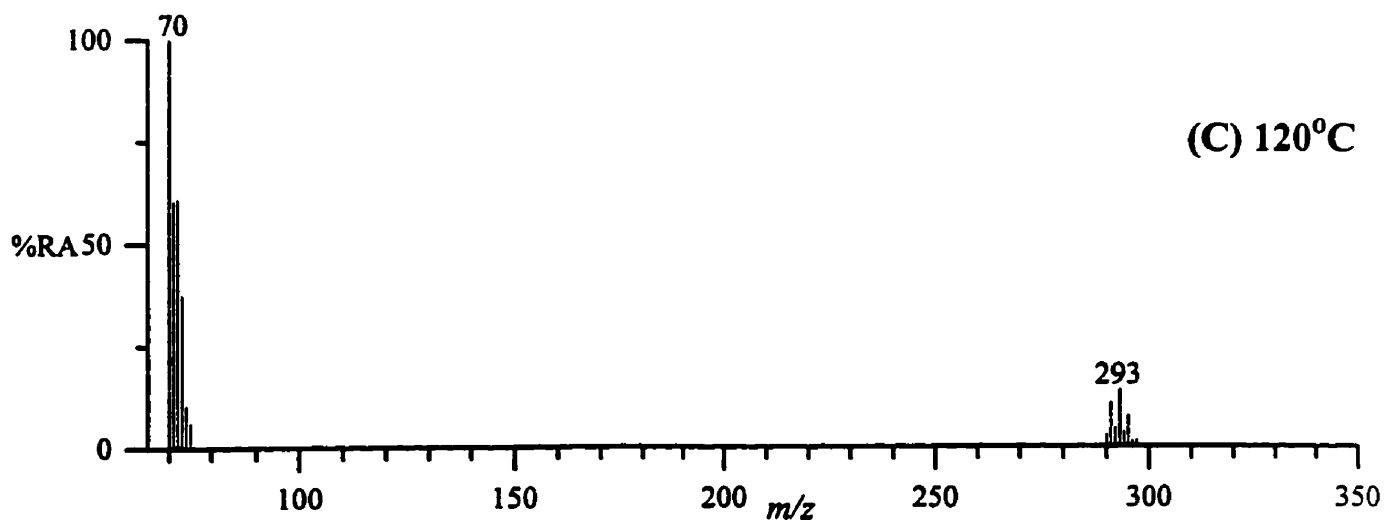
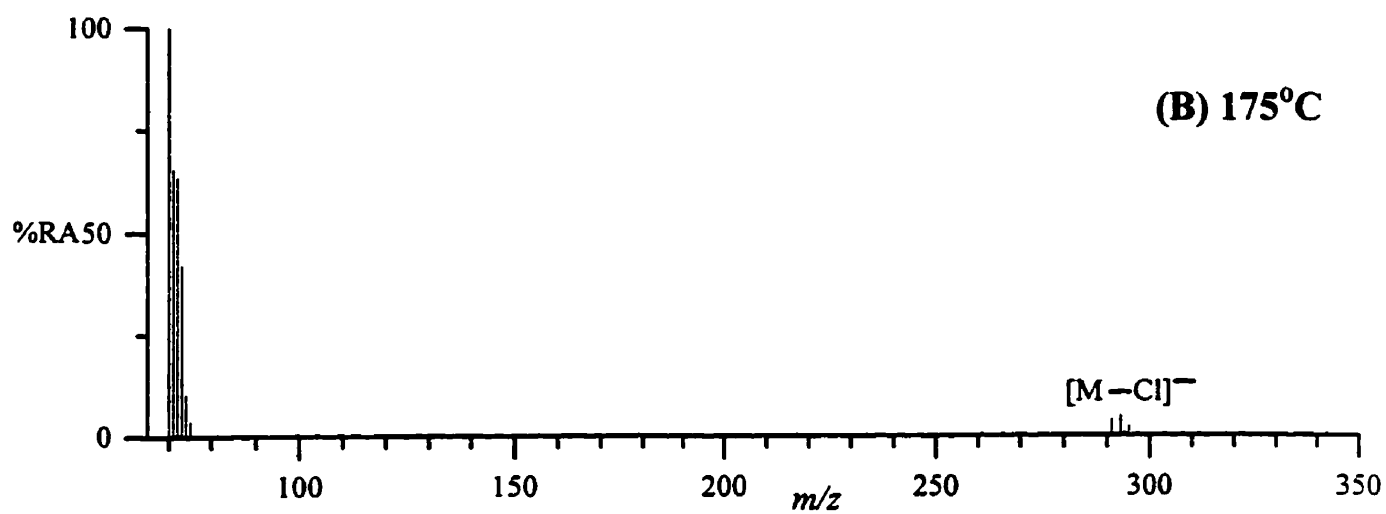
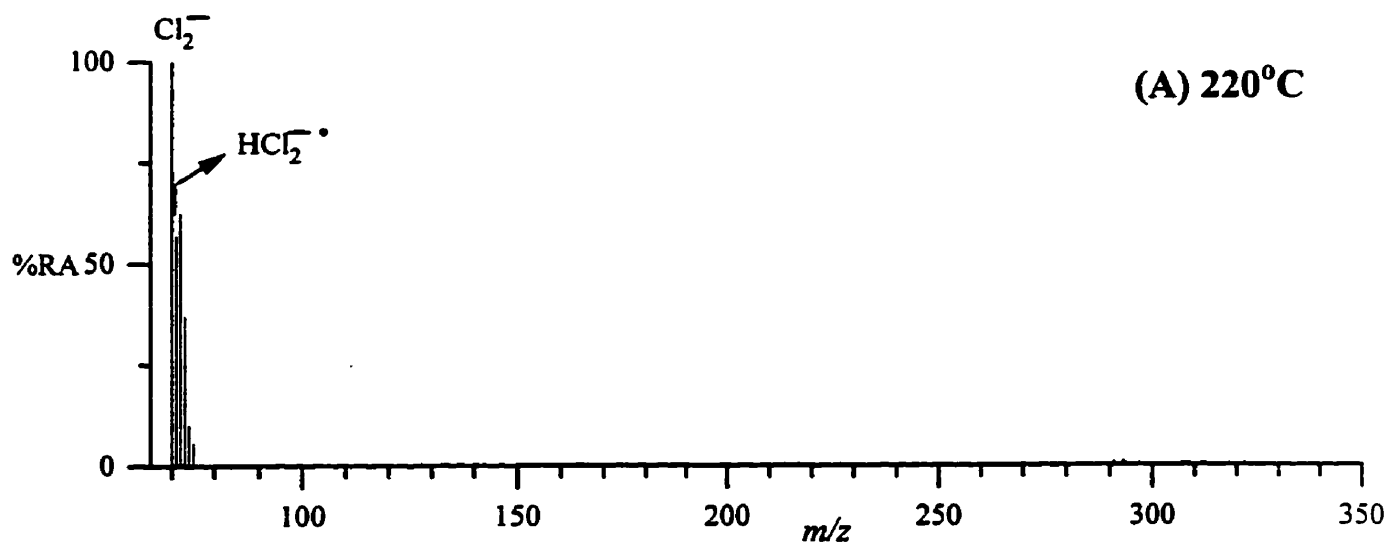


Figure 4.18. ECNI mass spectra of 1,2,x,10,11-pentachloro-*n*-undecane at ion source temperatures of (a) 220°C, (b) 175°C and (c) 120°C.

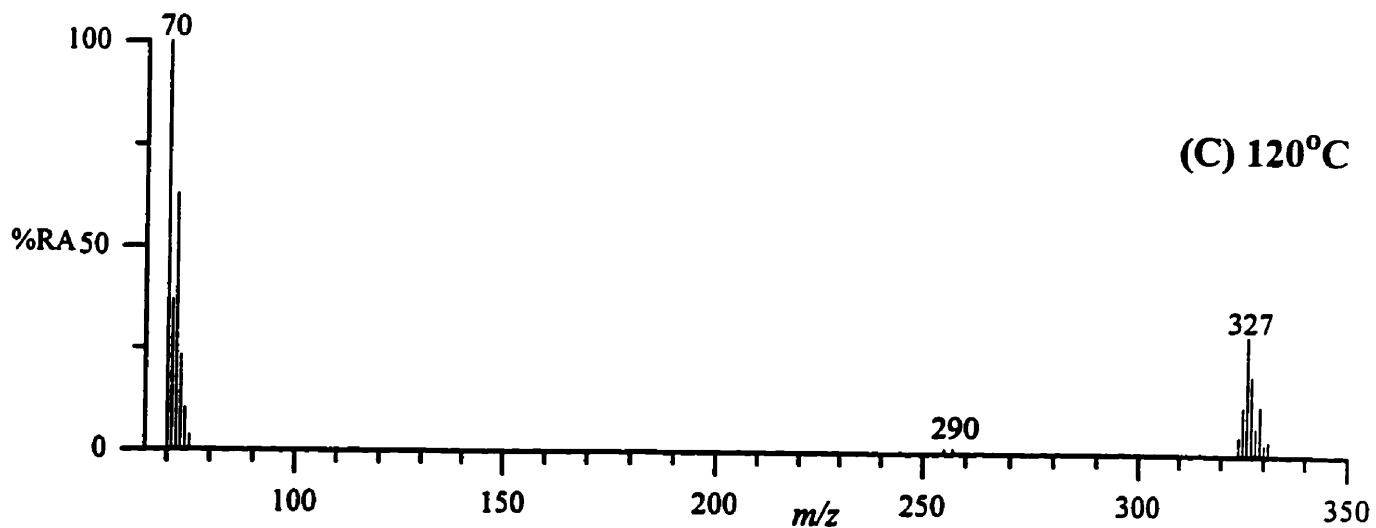
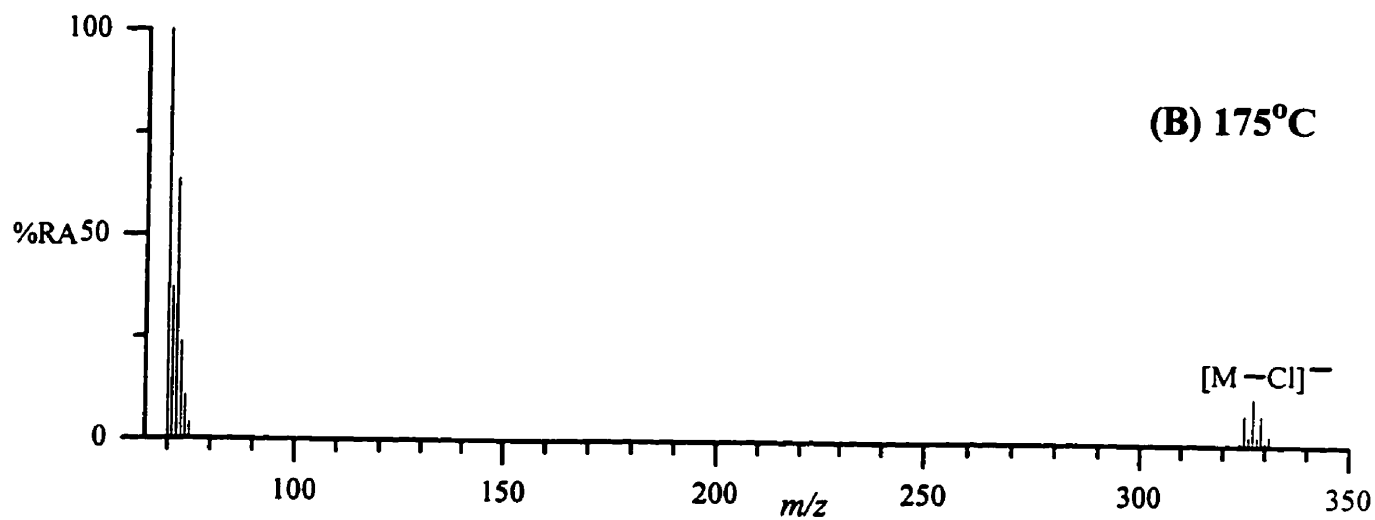
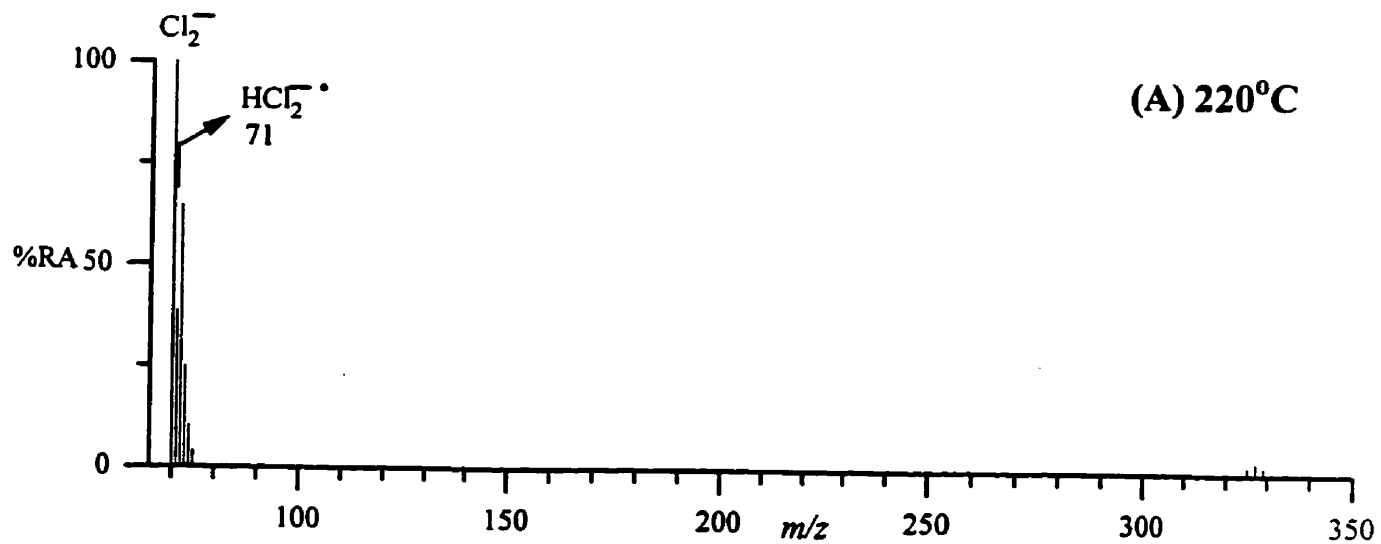


Figure 4.19. ECNI mass spectra of 1,2,x,y,10,11-hexachloro-*n*-undecane at ion source temperatures of (a) 220°C, (b) 175°C and (c) 120°C.

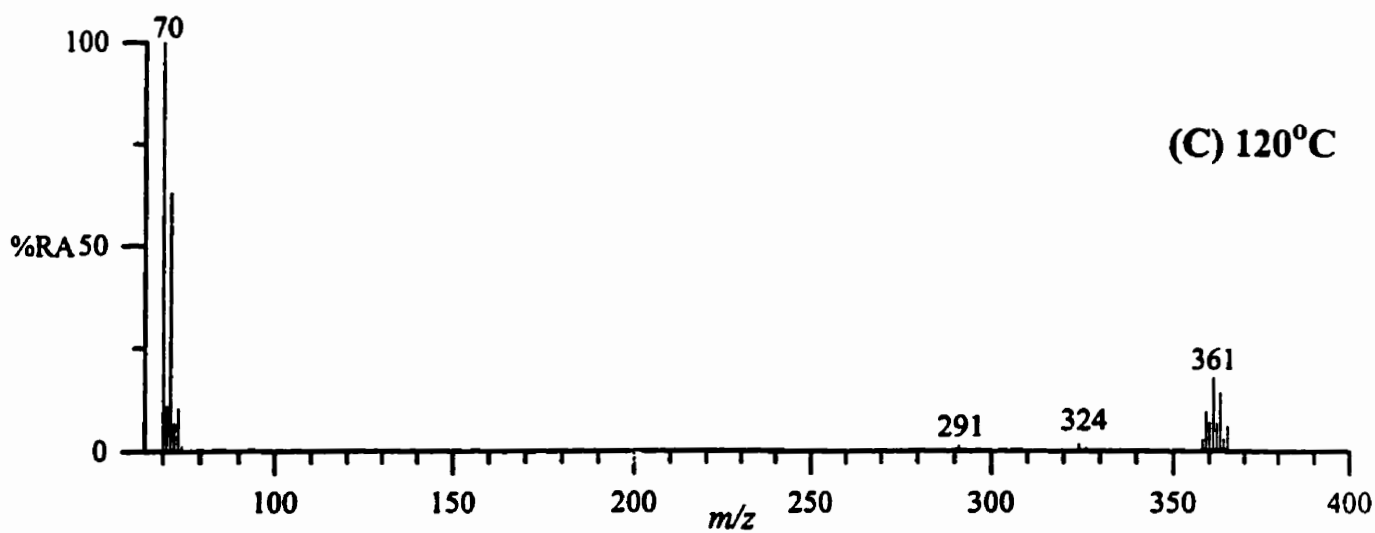
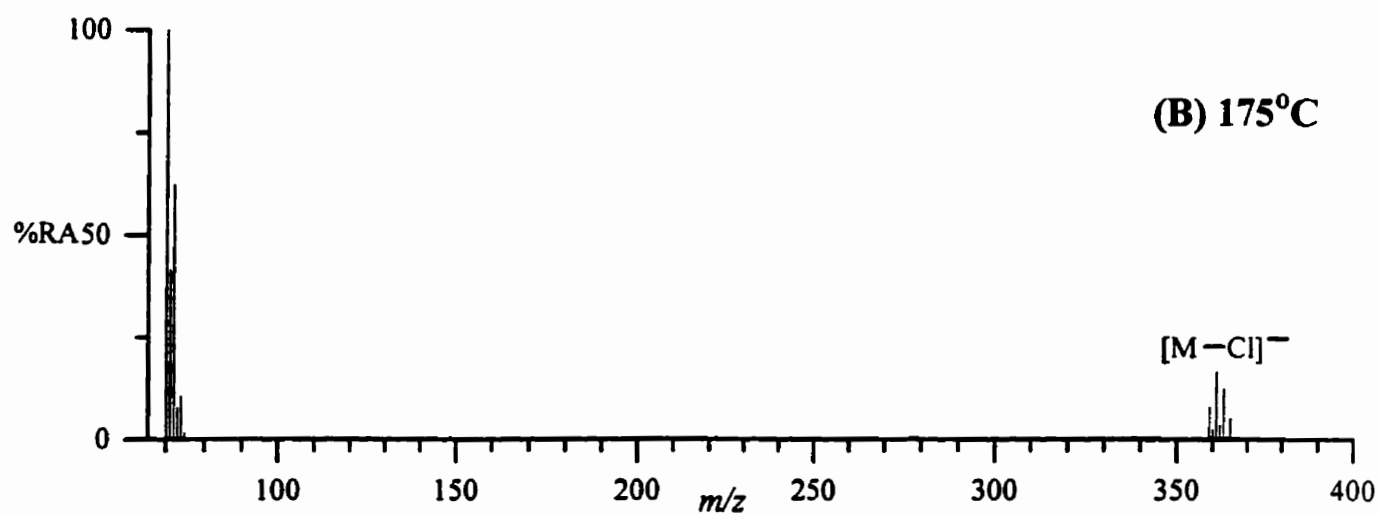
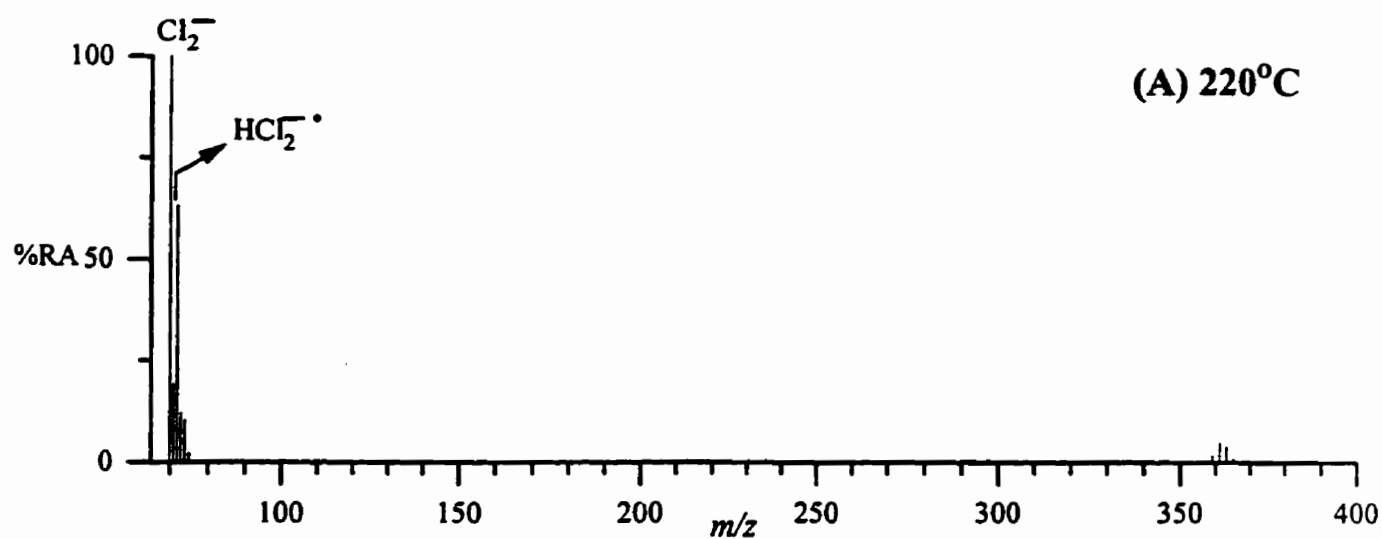


Figure 4.20. ECNI mass spectra of 1,2,x,y,z,10,11-heptachloro-*n*-undecane at ion source temperatures of (a) 220°C, (b) 175°C and (c) 120°C.

neutral analyte molecule. These resulting chloride adduct ions,  $[M + Cl]^-$ , arise because of gas phase ion chemistry in the ion source; this is addressed further in the section to follow [91,99-101].

The domination by  $Cl_2^-$  and  $HCl_2^-$  ions in the spectra of our synthesized PCA congeners at an ion source temperature of 220°C, for analytical purposes, is problematic for two reasons. First, they are not characteristic of any one PCA congener and, second, other persistent chlorohydrocarbon contaminants fragment to yield such ions, *e.g.*, *p,p'*-DDT, *p,p'*-DDE, lindane, dieldrin, aldrin and endrin, to name a few [42-44].

Our objective, therefore, was to attempt to *selectively maximize* the abundance of the structurally specific  $[M - Cl]^-$  ions, relative to the abundance of the  $Cl_2^-$  and  $HCl_2^-$  ions, for all of our synthesized PCA congeners. What we found was that by decreasing the ion source temperature to 120°C, we were able, in most cases, to achieve this goal, *i.e.*, maximize the intensity of the  $[M - Cl]^-$  ions (*see* Figures 4.21 and 4.22). This completed our first step toward the development of our analytical protocol; for measurements made to determine the levels of PCAs in environmental matrices, the lowest practical ion source temperature of 120°C is employed.

#### **4.1.2.1.2 The $[M + Cl]^-$ adduct and Sample Concentration.**

The appearance of adduct ions,  $[M + Cl]^-$ , at low ion source temperatures, in the mass spectra of a few chlorohydrocarbons has been observed in other laboratories [90,91,99-101]. The generation of  $[M + Cl]^-$  ions is thought to occur via the two step reaction shown below.

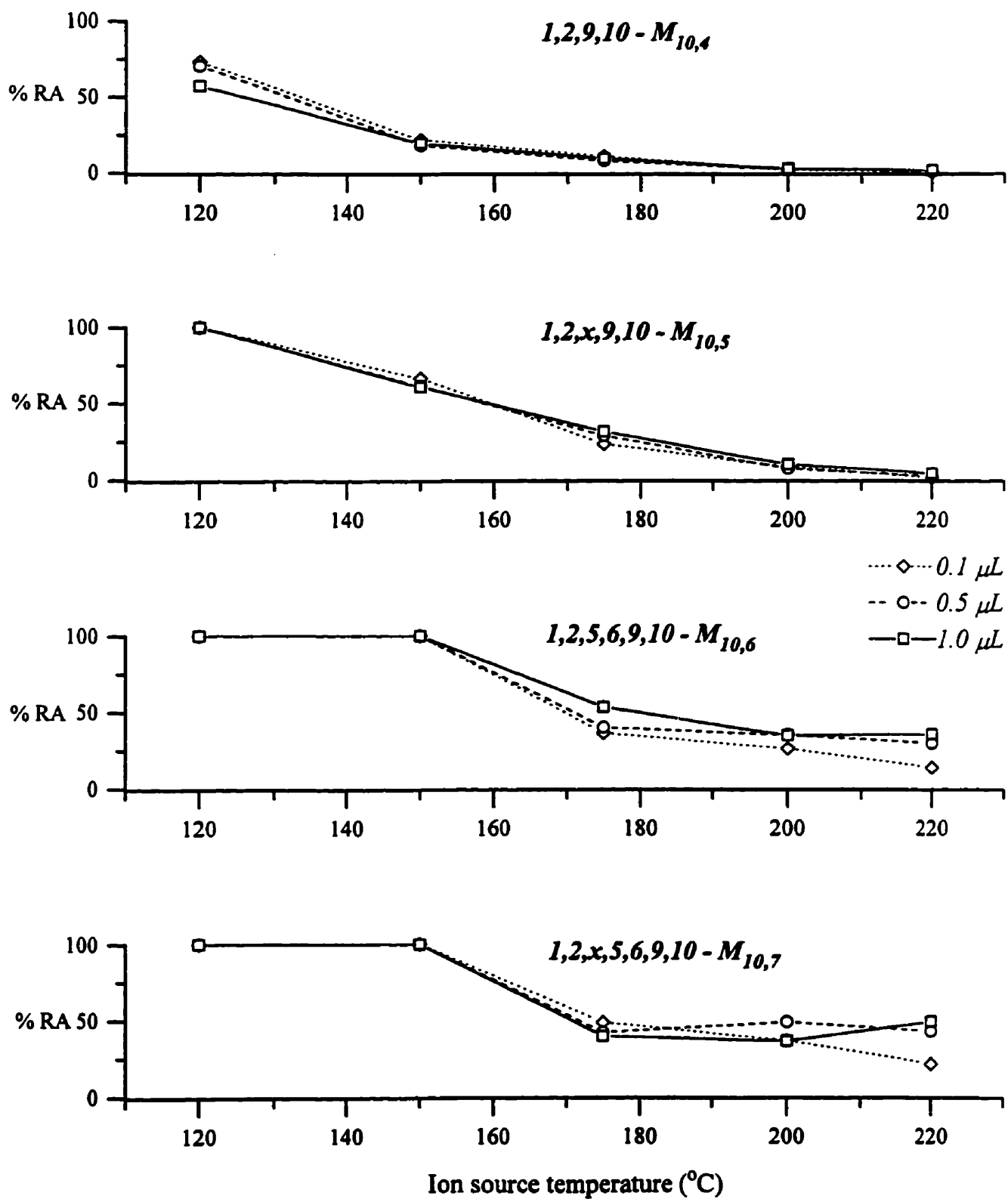


Figure 4.21. Effect of ion source temperature and concentration of injected PCA on the formation of the  $[M - Cl]^+$  ion.

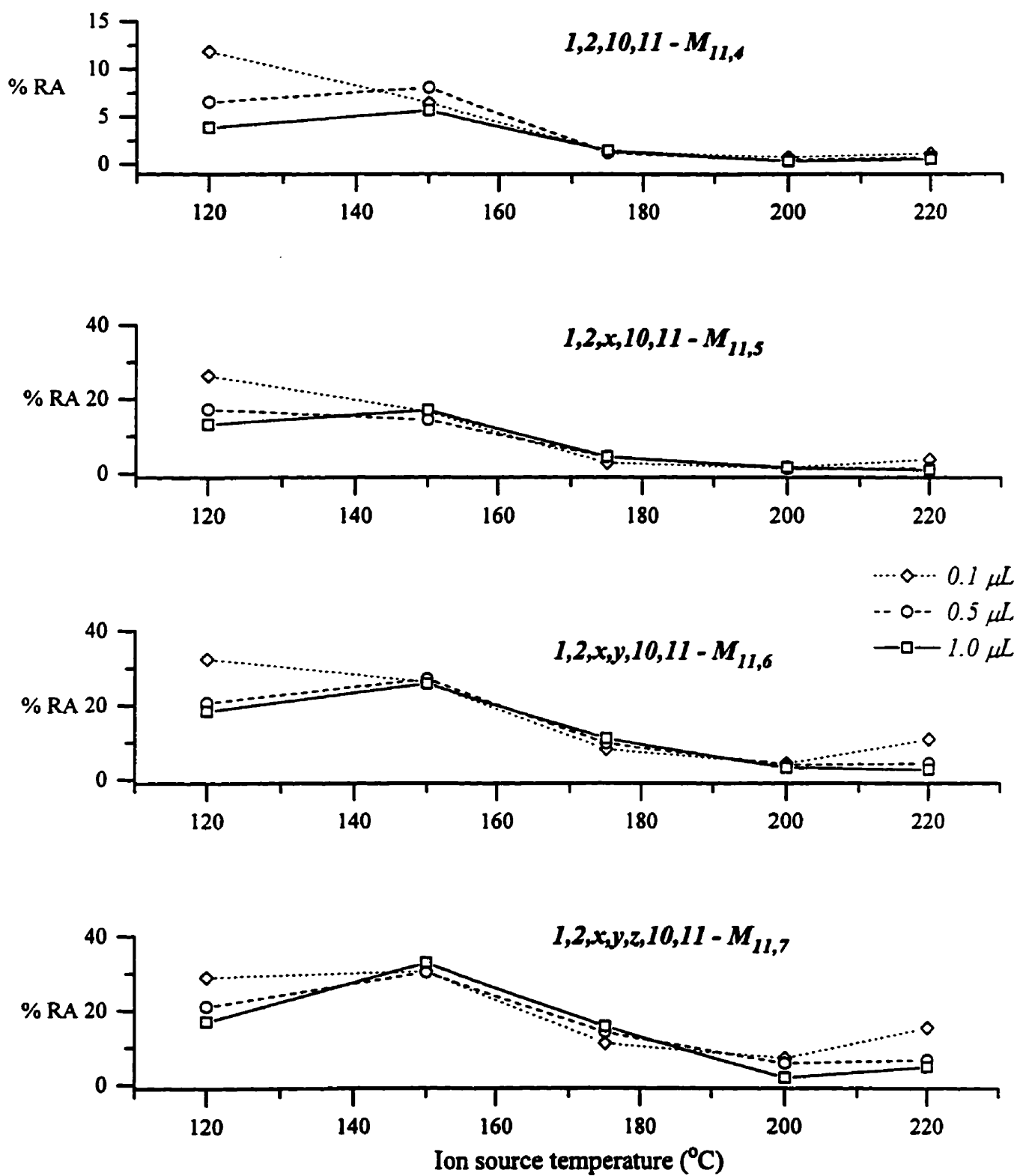
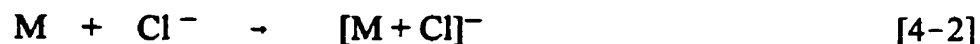
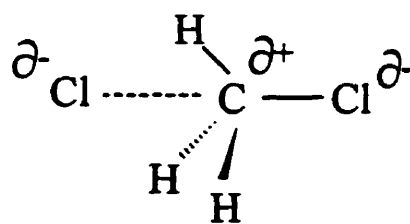


Figure 4.22. Effect of ion source temperature and concentration of injected PCA on the formation of the  $[M - Cl]^+$  ion.

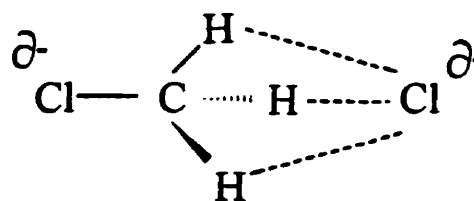


In our case, neutral analyte PCA molecules entering the ion source are an ample source of chloride ions, and are produced under ECNI conditions by dissociative electron capture (equation 4-1). Generation of chloride ions in this manner facilitates their attachment, and thus ionization, to neutral PCA molecules. Ionization of neutral PCA molecules in this way is thought to occur by one of the two mechanisms: by (i) *carbon bonding* (i.e., the association of a nucleophile with a Lewis acid center on a carbon; in this case, the attachment of the  $Cl^{-}$  to the carbon center is *via* a  $S_n2$  transition state) [100], or (ii) *hydrogen bonding* [102] (see below). The structure of the intermediate formed (either A or B), however, has a sufficiently long enough life-time in the ion source to be detected.



(A)

*carbon bonding*



(B)

*hydrogen bonding*

Factors which may influence the abundance of chloride adduct ions include, (i) ion source temperature, (ii) ion source pressure, (iii) concentration of sample molecules, (iv) number and position of chlorine atoms already on the molecule, (v) reagent gas, (vi) the rate of electron capture vs. the rate of chloride attachment, (vii) instrumentation and (viii) the concentration of electrons and their

energy distribution [91].

In the previous section it was shown that lower source temperatures favors the formation of  $[M + Cl]^-$  adduct ions. Tannenbaum *et al.* (1975) have shown that the formation of chloride adduct ions can be enhanced by using methylene chloride as the reagent gas [100]. The chloride ion in this case is generated by dissociative resonance capture of the reagent gas:



Variations in the abundances of  $[M + Cl]^-$  ion because of sample concentration, and ultimately chloride anions, however, has received little attention [91]. Even less is known about the positions of the chlorine atoms already present on the molecule and its relation to the abundance of the  $[M + Cl]^-$  ion. We attempted therefore to address these two issues.

Stemmler and Hites (1985) have studied the effects of sample concentration on the appearance of the ECNI mass spectrum of  $\alpha$ -chlordane [91]. When low quantities (10 ng or less) of the sample were introduced, *via* a GC-column,  $M^{\bullet-}$  and a few fragment ions were produced. However, when microgram quantities of the sample were introduced, *via* a direct insertion probe,  $[M + Cl]^-$  ions dominated the mass spectrum [91].

For our study, because we are dealing with mixtures, introduction of large quantities of analytes into the ion source *via* the direct insertion probe was not feasible. Instead, we prepared three solutions from the products derived from the chlorination of 1,9-decadiene, 1,5,9-decatriene and 1,10-undecadiene, of approximately 0.5% concentration (v/v) in hexane, and injected 0.1, 0.5 and 1.0  $\mu$ L's, separately, onto a GC-column *via* an autosampler.

In addition to addressing the effect of sample concentration upon the abundance of the  $[M + Cl]^-$  ion, we also felt that we could discern the effects of chlorine substitution on the carbon moiety. Figure 4.23 shows the effect of sample concentration on the abundance of the  $[M + Cl]^-$  ion for a number of synthesized PCA congeners. (*Appendix 3(a-h)* shows the corrected ion abundances at varying sample concentrations in tabular form.)

As expected, the relative abundance of the  $[M + Cl]^-$  ion is highest for the 1,2,9,10- $M_{10,4}$  and the 1,2,10,11- $M_{11,4}$  molecules. The terminal positioning of the chlorine atoms already present on the  $C_{10}$  and the  $C_{11}$  backbone, provides a number of unhindered, sterically accessible electrophilic  $sp^3$  carbon centers, which a chloride ion can attack. The effect of the concentration of injected analyte upon the intensity of the  $[M + Cl]^-$  ion is visibly less pronounced.

Conversely, the relative abundances of the  $[M + Cl]^-$  ions are low for the 1,2,x,9,10- $M_{10,5}$  and the 1,2,5,6,9,10- $M_{10,6}$  molecules. Subtle changes are observed, however, for the abundances of the  $[M + Cl]^-$  ions because of sample concentration. In all but one instance, the abundance of the  $[M + Cl]^-$  ion is highest when 1.0  $\mu$ L of sample was injected, as to be expected.

The variability we observe in the ion intensities of the  $[M + Cl]^-$  in the ECNI mass spectra of the PCA congeners examined, which arise because of (1) a change in the ion source temperature, and (2) change in sample concentration and also the dependence of its intensity on the positions of the chlorine atoms initially present on the molecule, illustrates clearly that this ion is not suited for analytical purposes. Although the abundances of the  $[M - Cl]^-$  ion were shown to be dependent on source temperature, very little change was observed when the sample concentration was varied and, thus, this ion was chosen as the quantitation

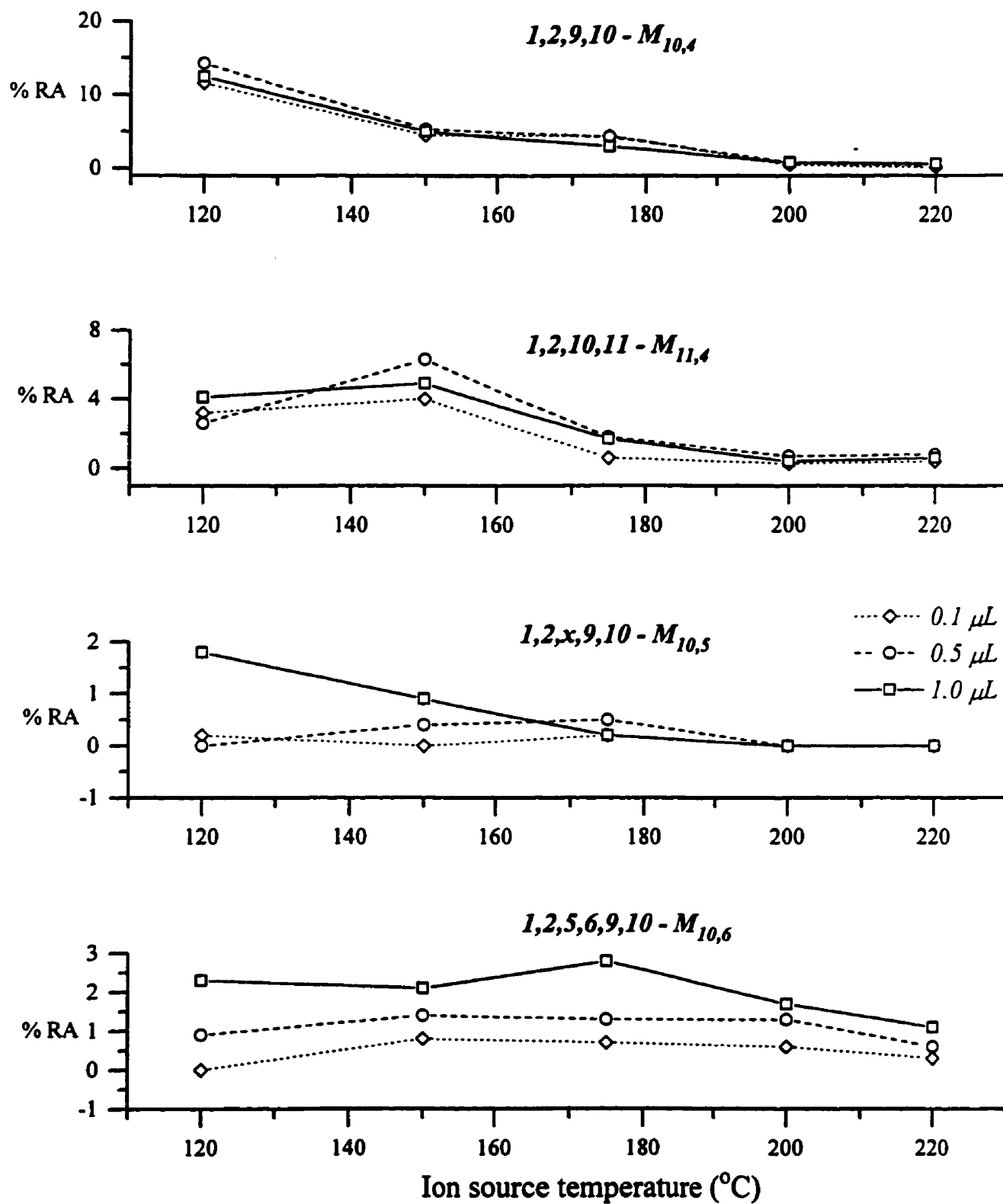


Figure 4.23. Effect of ion source temperature and concentration of injected PCA on the formation of the  $[M + Cl]^+$  adduct ion.

ion in our analytical protocol.

# ***Chapter 5***

## ***THE ANALYTICAL PROTOCOL QUANTIFYING PCAs IN ENVIRONMENTAL SAMPLES***

### **5.0 INTRODUCTION**

In *Chapter 1*, section 1.3 of this thesis a review of the analytical methods used for quantifying PCAs in environmental matrices was discussed, and the limitations inherent to each method was addressed in section 1.4. Presented in the sections to follow are the steps taken in developing our analytical protocol used for measuring the levels of these contaminants in environmental samples.

In brief, the quantitation of PCAs in samples is done relative to an industrial formulation which is used as an external standard. The choice of external standard used is reminiscent of the technique that was employed for quantifying PCBs in environmental samples prior to the synthesis of individual chlorinated biphenyl (CB) congeners in 1984, *viz*, pattern matching [39,40]. Prior to this, however, the composition of industrial mixtures has to be established; the synthesis of individual PCA congeners greatly facilitated this endeavour. Once the elution times of all the components in the external standards are discerned, the efficiency of SIM is improved by dividing the total recording time into a number of windows, during which a few ion types are monitored [28,48]. Elution profiles of characteristic ions in the ECNI mass spectra of the environmental extracts are generated in the same way. The extensive information obtained from these profiles were

invaluable for developing a simplified procedure for quantifying PCAs in environmental samples. Further details of these steps are now described.

## 5.1 DETERMINING THE COMPOSITION OF INDUSTRIAL MIXTURES

Manufacturers of PCA mixtures provide their consumers with two pieces of information: (1) the range of carbon atoms, and (2) the % Cl by mass of their formulation. A guideline for discerning the component make-up of these supplied mixtures, *i.e.*, determining the formulae of the molecules present, can be formulated from first principles [30]. The general formula of a PCA molecule is given by:



For a saturated chlorinated *n*-alkane, the relationship between the number of hydrogen atoms to chlorine and carbon atoms can be expressed as :

$$y = 2n + 2 - z \quad [5-2]$$

Now the % Cl by mass, *i.e.*, its mass fraction,  $m_f$ , can be expressed as:

$$m_f = \frac{35.5z_{avg}}{12n + y + 35.5z_{avg}} \quad [5-3]$$

where  $z_{avg}$  is the average number of chlorine atoms. Substituting equation [5-2] into [5-3] we obtain:

$$= \frac{35.5z_{avg}}{12n + (2n + 2 - z_{avg}) + 35.5z_{avg}} \quad [5-4]$$

Rearranging and solving for  $z_{avg}$ , we obtain:

$$z_{avg} = m_f \left[ \frac{(14n + 2)}{(35.5 - 34.5 m_f)} \right] \quad [5-5]$$

Table 5.1 illustrates the calculated  $z_{avg}$  values for the two short chain PCA analytical standards that are available in our laboratory, viz, PCA-60 ( $C_{10}$ - $C_{13}$ , 60% Cl by mass) and PCA-70 ( $C_{10}$ - $C_{13}$ , 70% Cl by mass). (The values of  $z_{avg}$  are calculated by assuming that for congeners with a specific carbon number the chlorine mass fraction is the same as the overall, or bulk, mass fraction.)

For the PCA-60 standard, the  $C_{10}$  homologue group, for example, contains an average of 5.8 Cl atoms. Because this number represents an average, it provides only a rough estimate and/or a starting point, from which we can begin a more thorough 'search' of the mixture to determine the actual molecular formulas present.

Mixtures are 'searched' by presetting the mass spectrometer to monitor the  $[M - Cl]^-$  ion, for molecular formulas *bracketing* the calculated  $z_{avg}$  values. The  $[M - Cl]^-$  ion is chosen because, as we have shown previously, it represents in most cases, the most dominant, structurally characteristic, ion in the mass spectra of individual PCA congeners at an ion source temperature of 120°C. As an example, for the  $C_{10}$  homologue group of the PCA-60 standard, which contains an average of 5.8 Cl atoms, the MS would be preset to search for the following molecular species:  $C_{10}H_{18}Cl_4$ ,  $C_{10}H_{17}Cl_5$ ,  $C_{10}H_{16}Cl_6$ ,  $C_{10}H_{15}Cl_7$ ,  $C_{10}H_{14}Cl_8$  and  $C_{10}H_{13}Cl_9$ . In this case, the supplied mixture was found to contain between 5 and 9 Cl atoms, inclusive, on the  $C_{10}$  moiety. Figure 5.1 shows the elution profiles for all of the  $C_{10}$ -components found in the PCA-60 standard.

**Table 5.1. Average chlorine number,  $z_{avg}$ , in PCAs of 60–70% chlorine content, by mass.**

<b>n</b>	<b>PCA-60</b>	<b>PCA-70</b>
	<b><math>z_{avg}</math></b>	<b><math>z_{avg}</math></b>
10	5.8	8.8
11	6.3	9.6
12	6.9	10.5
13	7.5	11.4

**For each carbon number, n, the chlorine content is assumed to be the same as the overall chlorine content.**

$C_{10}H_{13}Cl_9$



$C_{10}H_{14}Cl_8$



$C_{10}H_{15}Cl_7$



$C_{10}H_{16}Cl_6$



$C_{10}H_{17}Cl_5$



10:00 15:00 20:00 25:00 30:00 (mins.)

Figure 5.1. Elution profiles for the  $C_{10}$  components found in PCA-60 standard.

This procedure is repeated for all homologue groups of the two standards (Figure 5.1–5.4 shows the formula groups in PCA-60). In Table 5.2 the relative abundance of the molecular formulae found to be present in both the PCA-60 and PCA-70 standards, as determined by monitoring the  $[M - Cl]^-$  ion for each congener is shown. In each case, the highest percent natural abundance  $m/z$  value, *i.e.*, the most abundant isotopic combination, is used as the quantitation ion for SIM and the second highest as a confirmation ion. The resolving power, 12 000, used for these measurements was as high as practical in order to keep the monitored mass acceptance window as small as possible in order to avoid, or to minimize, contributions from interfering ions (at 12 000 resolving power the peaks are 33 mmu wide at  $m/z$  400). The possibility of interfering ions, and their influence on the analysis, is addressed later.

### 5.1.2 ELUTION PROFILES AND RETENTION TIME WINDOWS

As previously noted (*Section 1.2*), any specific molecular formula for a PCA corresponds to a very complex mixture of compounds containing both positional and stereo isomers and, as a result, the compounds present elute over a very broad retention time range. Since elution time ranges can extend over approximately 3 to 6 minutes, co-elution of components becomes an issue and can make establishment of the SIM retention time windows more complicated. Thus, for PCA-60 the characteristic ions of compounds corresponding to significant molecular formulae (*i.e.*, ion signals  $> \sim 0.5\%$  relative to the largest ion signal) were monitored to establish the elution profiles shown in Figure 5.5. Under our conditions we found seven windows, as indicated in Figure 5.5 and Table 5.2, to be convenient and practical for determining these profiles but with different resources and circumstances other choices of windows might be preferred. The

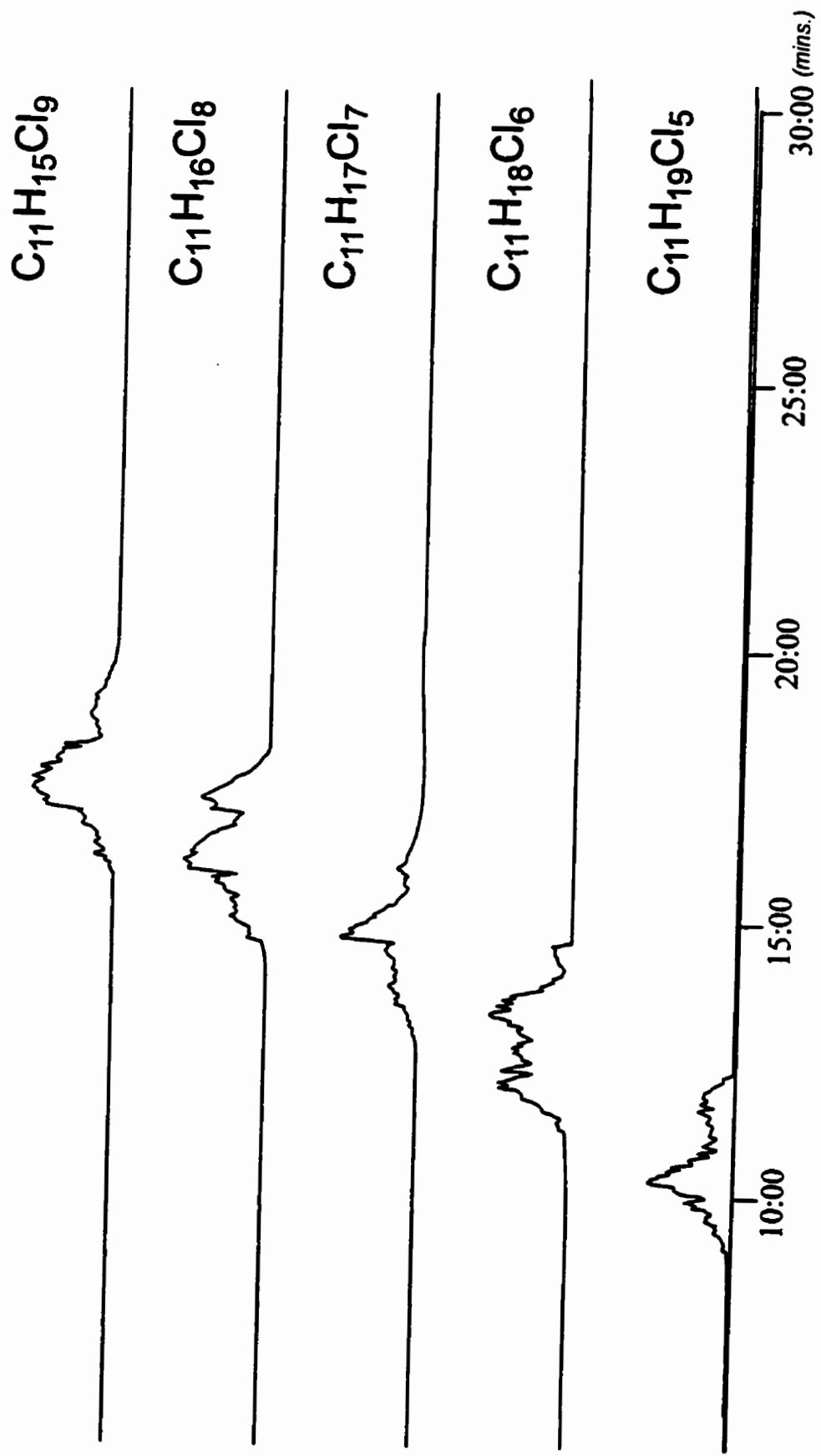


Figure 5.2. Elution profiles for the C<sub>11</sub> components found in PCA-60 standard.

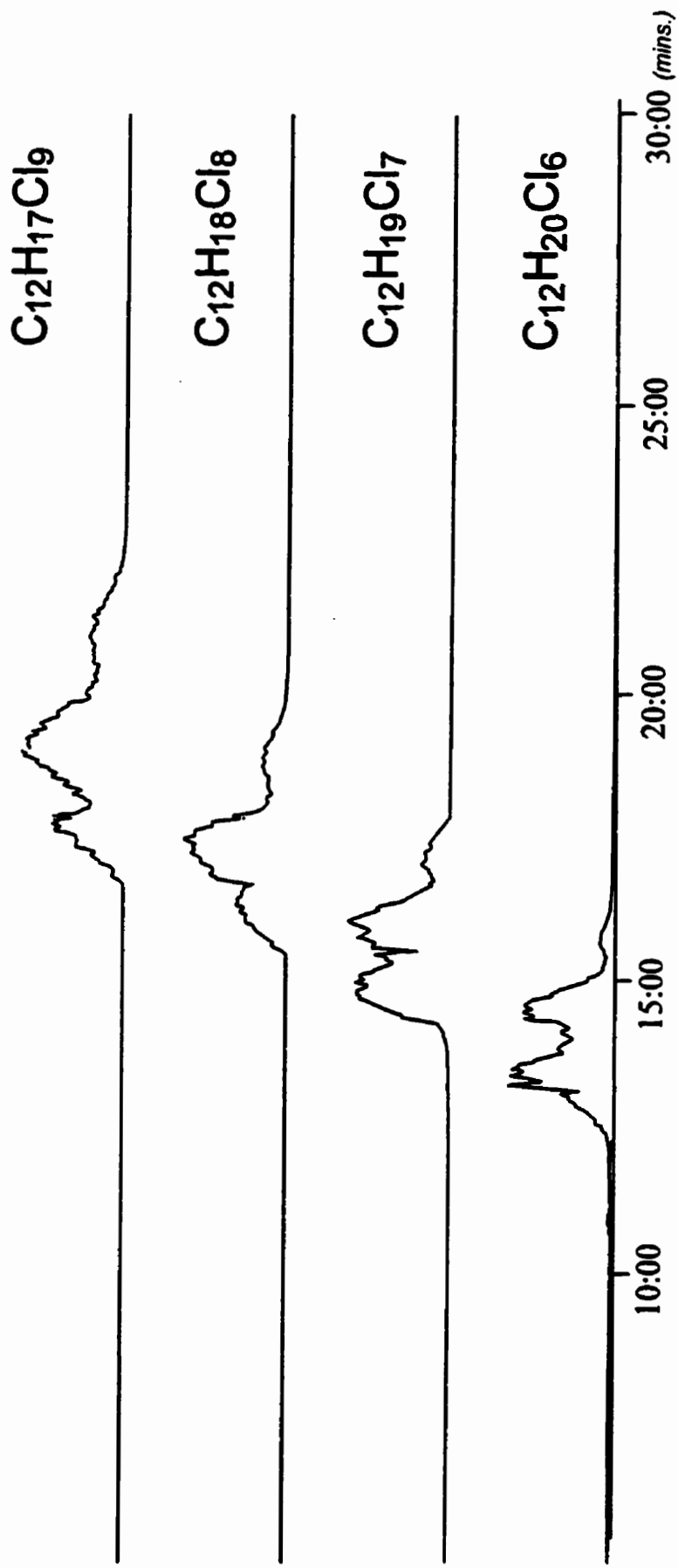


Figure 5.3. Elution profiles for the C<sub>12</sub> components found in PCA-60 standard.

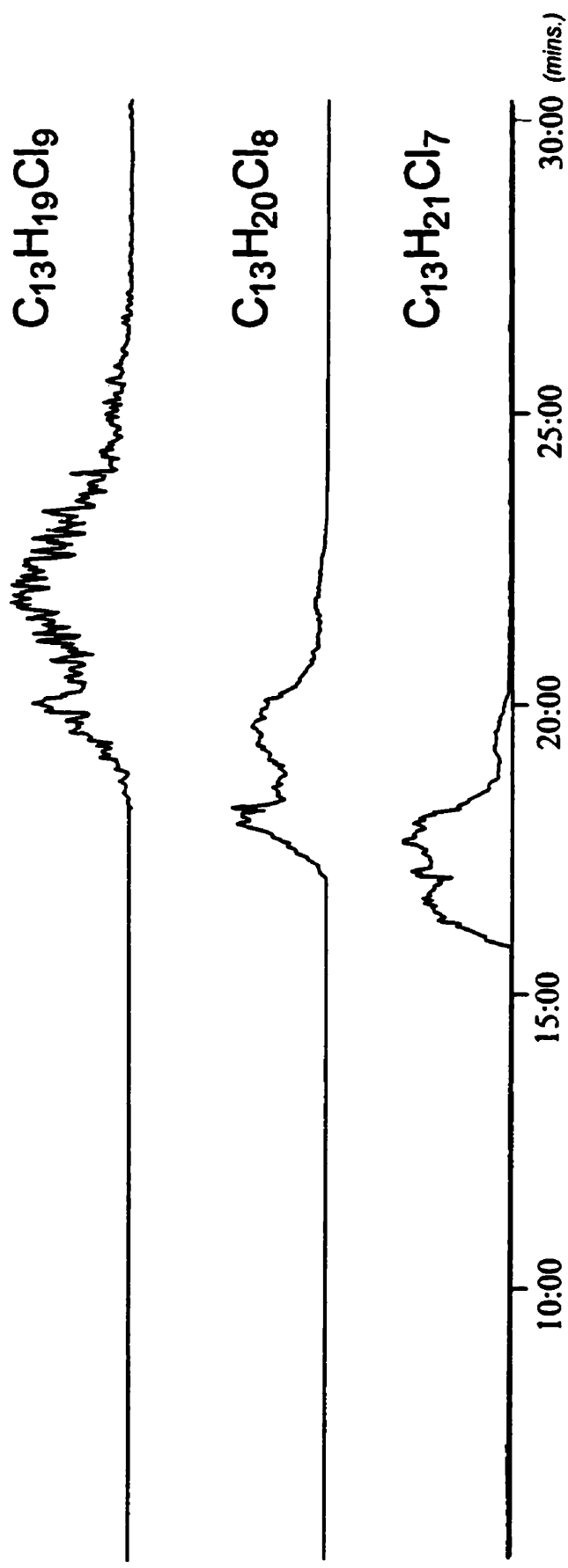


Figure 5.4. Elution profiles for the  $C_{13}$  components found in PCA-60 standard.

Table 5.2. Calculated  $m/z$  values of  $[M - Cl]^-$  ions monitored and their % natural abundances, and experimental % relative responses, for  $C_nH_{m-2}Cl_x$  isomers present in PCA-60 and PCA-70.

Isomer formula (n,z)	$m/z$ value <sup>a</sup> (% natural abundance)		% relative response <sup>b</sup>		Window No. <sup>c</sup>
	Quantitation	Confirmation	PCA-60	PCA-70	
10,5	279.0055 (37.8)(ocm)	277.0084 (29.0)(ocm)	7.6	-	1
10,6	312.9665 (35.7)	314.9636 (23.2)	57	5.3	1,2
10,7	346.9275 (32.3)(ch, tox)	348.9246 (26.3)(ch, tox)	23	14	1-4
10,8	380.8886 (28.5)	382.8856 (27.8)	5.2	24	2-5
10,9	416.8467 (27.9)(tox)	414.8496 (24.6)(tox)	0.9	7	4-6
10,10	450.8077 (27.1)	448.8106 (20.9)	-	0.43	5-7
11,5	293.0211 (37.4)	291.0241 (28,7)	21	-	1
11,6	326.9822 (35.3)	328.9792 (23.0)	100	2.8	1-3
11,7	360.9432 (32.0)(pcb)	362.9402 (26.0)(pcb)	76	49	2-5
11,8	394.9042 (28.1)(pcb)	396.9013 (27.5)(pcb)	38	100	3-6
11,9	430.8623 (27.6)(pcb)	428.8656 (24.3)(pcb)	5.2	57	5-7
11,10	464.8233 (26.8)	462.8263 (20.6)	-	8	6,7
12,6	340.9978 (34.9)	342.9949 (22.8)	32	-	2-5
12,7	374.9588 (31.6)	376.9559 (25.8)(tox)	62	15	3-6
12,8	408.9199 (27.8)	410.9169 (27.2)	33	47	5-7
12,9	444.8779 (27.4)	442.8809 (24.0)	3.3	52	6,7
12,10	478.8390 (26.6)	476.8491 (20.4)	-	11.3	6,7
13,7	388.9745 (31.3)	390.9715 (25.5)	6.2	-	5-7
13,8	422.9355 (27.5)	424.9326 (26.9)	3.3	4.9	6,7
13,9	458.8936 (27.1)	456.8966 (23.8)	0.5	6.6	6,7
<sup>13</sup> C <sub>8</sub> -mirex <sup>d</sup>	409.7747	411.7718	-	-	6

<sup>a</sup> The peak in the  $[M - Cl]^-$  ion group corresponding to the most probable Cl isotopic combination was used for quantitation; the next most probable combination was also monitored to confirm that the relative response of the quantitation ion was not spurious. Interferences detected at a resolving power of 1000, but not at 12 000 (see text), are noted in parentheses: (ocm) organochlorine mixture; (ch) chlordane; (tox) toxaphene; (pcb) PCBs.

<sup>b</sup> As % of greatest response. A missing entry indicates that the response was not detectably above the level of noise. Also not detected were species with carbon or chlorine numbers outside the listed ranges.

<sup>c</sup> Retention time windows, in min (Figure 5.5) : 1; 5:00-12:45; 2; 12:46-14:00; 3; 14:01-15:12; 4; 15:13-16:28; 5; 16:29-17:40; 6; 17:41-18:52; 7; 18:53-30:00.

<sup>d</sup> <sup>13</sup>C<sub>8</sub>-mirex is included in window number 6.



intensity scales of these profiles have been normalized by the data system and hence do not reflect the relative amounts of the respective congeners corresponding to a particular formula in the sample.

Because of the shift to higher chlorine content, somewhat different species were monitored for PCA-70. Table 5.2 illustrates the time windows that are used to generate the elution profiles for this standard.

### **5.1.3 QUALITATIVE ANALYSIS – GENERATING PLOTS OF THE ION SIGNAL PROFILES**

An important step in our analytical protocol involves generating bar graph plots of the ion signal profiles for the standards and samples. Visual inspection of these graphs, which are created by plotting the measured SIM signals for each congener in the standard(s) and analytes, allows us to: (1) select the more suitable external standard for quantification, and (2) apply correction factors which account for variations in the abundances of the congeners in the standard and analyte.

The first step involves electronically integrating the ion signal profiles such as those shown in Figures 5.1–5.4. In Table 5.2 these integrated signals, for ions generated from the PCA-60 and PCA-70, are listed as a percentage of the largest signal for each compound. Since these are based on specific  $m/z$  values monitored, they were converted to the true relative integrated signal for each ion formula by dividing these signals by the fractional natural abundance of the specific  $m/z$  value monitored, and then renormalizing, to give relative adjusted ion signals (not tabulated).

The dependence of the adjusted ion signals upon concentrations is certain to

be complicated and cannot be known; at a minimum the factors which are involved include the relative probabilities of negative ion formation and, also, the relative extents to which losses of  $\text{Cl}^\bullet$  occur. However, because hydrocarbons do not readily form negative ions it is apparent that negative ion formation is dominated by the chlorine content of the molecule. Therefore, we ignored the hydrocarbon part and made two alternative assumptions regarding the influence of the chlorine atoms in the molecules. It will be shown that the resulting quantitative measurements are remarkably insensitive to the difference between the assumptions.

In the first assumption, the relative adjusted ion signals are taken to depend directly on the molar (because the contribution of hydrocarbon part is ignored) concentrations of species present, irrespective of their chlorine content, *i.e.*, the responses of all chlorine-containing molecules are equal. This assumption undoubtedly progressively underestimates the relative concentrations of species as the chlorine content decreases.

In the second assumption, which is probably more realistic, the adjusted ion signals are taken to be proportional to the number of chlorine atoms in the parent molecule, as well as to its molar concentration, *i.e.*, the relative concentrations are calculated from the adjusted ion signals divided by the number of chlorine atoms in the molecule.

The relative molar concentrations of the various significant formula groups present in PCA-60 are plotted in bar graph form in Figure 5.6(a), based upon the first assumption, such that the total relative concentration of all species equals 100%. A similar plot is shown in Figure 5.6(b), based on the second assumption. In Figure 5.6(b), therefore, relative to Figure 5.6(a), the apparent relative

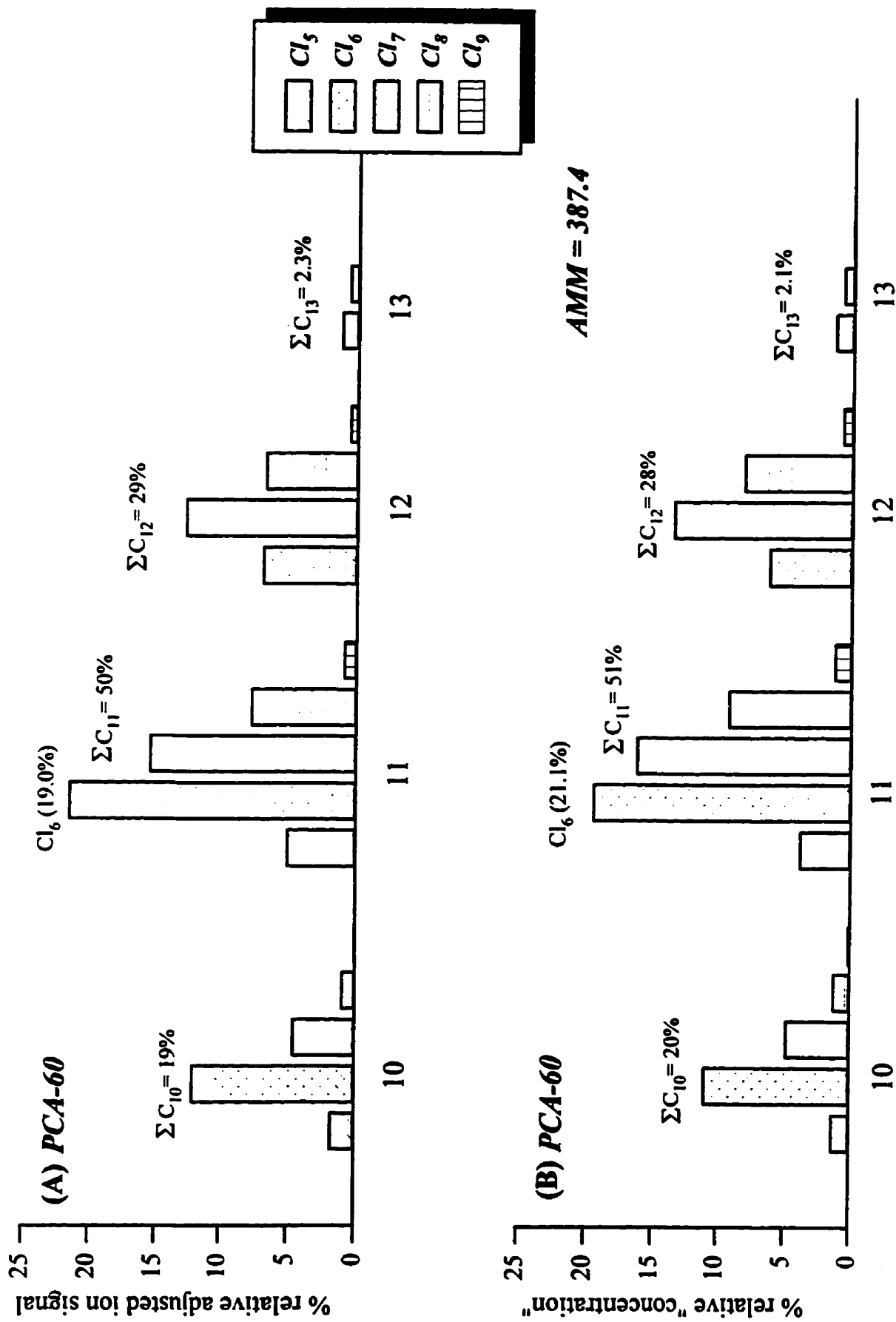


Figure 5.6. Molar "composition" of PCA-60, based on the assumption that the SIM signal of a formula group is proportional (A) to molar concentration, (B) to molar concentration weighted by chlorine number.

concentration of molecules with lower chlorine content is enhanced with respect to those with higher chlorine content, reflecting the underestimation of these species in Figure 5.6(a). However, the change in the apparent relative concentration of the most abundant species,  $C_{11}H_{18}Cl_6$ , is small, *i.e.*, 19.0% – 21.1%, from the first to the second assumption. For each carbon number the relative concentrations, have been totalled and expressed as a percentage of the overall total; Figure 5.6 shows that these values are also insensitive to differences between our assumptions.

For a reason to be stated later, the average molar mass (AMM) of the PCA is needed. (The  $AMM = \sum M_i A_i$ , where  $M_i$  and  $A_i$  are the molar mass and sum of abundances of compounds of formula  $i$ .) It has therefore been calculated for the compositions in Figure 5.6(b) and included in this, and other, figures.

The elution profile signals for PCA-70 have been treated in a similar way (Figure 5.7) and similar conclusions can be drawn. Because of the higher overall chlorine content (*i.e.*, smaller relative percentage changes in chlorine content between molecular formulae) the difference between the two assumptions is even smaller. The change in the apparent relative concentration of the most abundant species,  $C_{11}H_{16}Cl_8$ , is 25.1% – 25.5%, from the first to the second assumption. The dependence of the relative concentrations upon carbon numbers is quite similar to that of PCA-60 indicating, probably, the use of a similar hydrocarbon feedstock for the manufacture of both commercial products.

The similarity of the results based on the two assumptions gives confidence to our method of quantification of the signals, and suggests that errors associated with either assumption will be small. In the remaining discussion we have used the second assumption, *i.e.*, the SIM signals are proportional to molar concentration weighted by chlorine number, because it is intuitively more

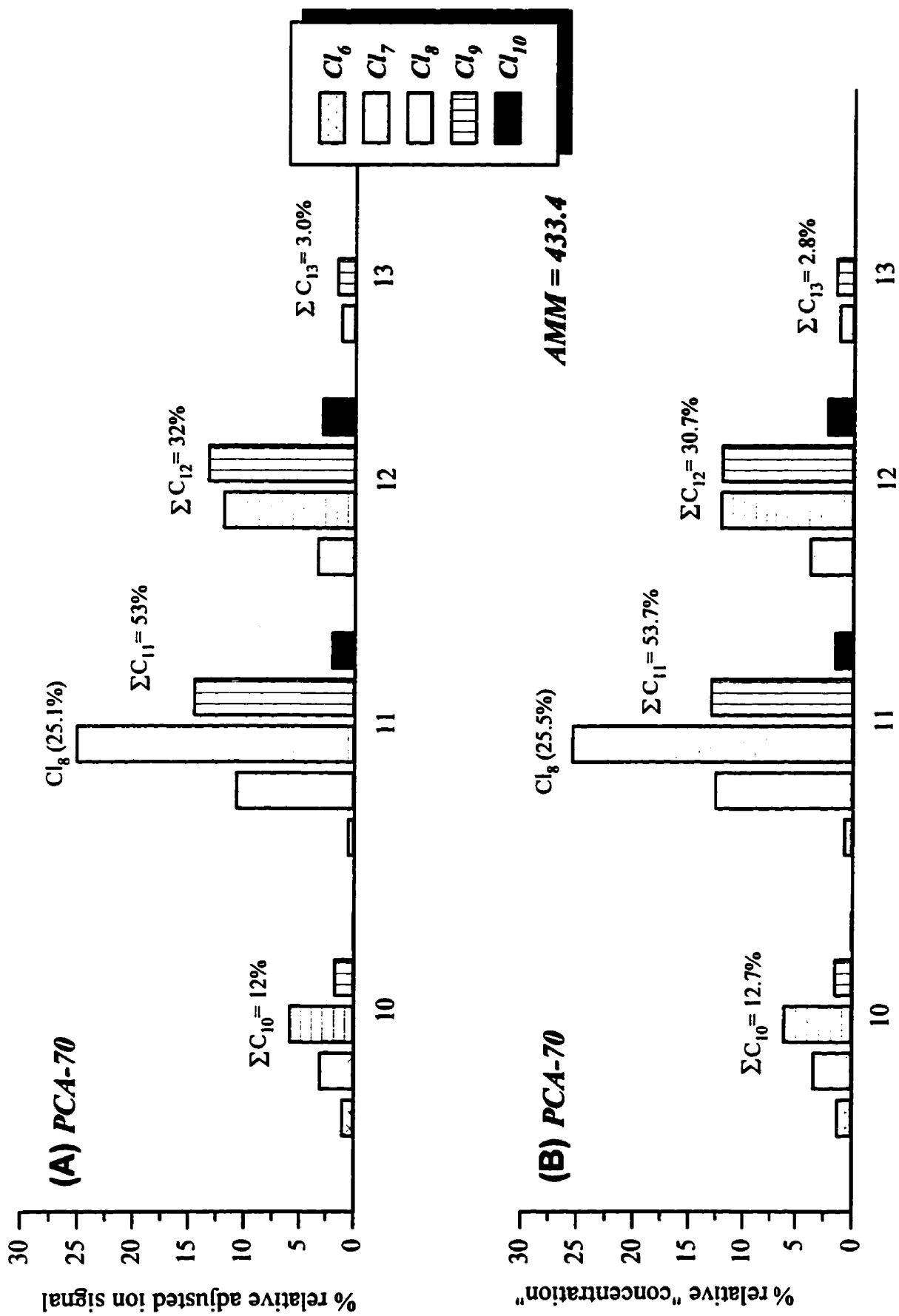


Figure 5.7. Molar "composition" of PCA-70, based on the assumption that the SIM signal of a formula group is proportional (A) to molar concentration, (B) to molar concentration weighted by chlorine number.

satisfying.

#### 5.1.4 QUANTITATIVE PROCEDURE

After the compositions of the external standards and environmental samples have been established, and plots of the ion signal profiles generated, it now becomes possible to recommend a simplified, less time-consuming, analytical procedure based on monitoring a prominent ion of the environmental sample and comparing this to that of a suitable integrated ion signal from the PCA-60 or PCA-70, acting as primary quantitative standards. However, because these products can only be used as external standards, an internal (or secondary) standard is needed in both standard and analyte solutions to relate the relative SIM responses of the GC/MS system for these two injections to each other.

The internal standard used in an analysis should be a compound closely related to the analyte, but which does not give ions that will interfere with their monitored ions. Instead,  $^{13}\text{C}_8$ -mirex,  $^{13}\text{C}_8^{12}\text{C}_2\text{Cl}_{12}$ , which has been used in our laboratory in analysis of another complex organochlorine mixture, viz, toxaphene, was selected, and the  $^{13}\text{C}_8^{12}\text{C}_2^{37}\text{Cl}^{35}\text{Cl}_7^-$  and  $^{13}\text{C}_8^{12}\text{C}_2^{37}\text{Cl}_2^{35}\text{Cl}_6^-$  isotopic species, of  $m/z$  409.7747 and 411.7718, respectively, of the prominent  $[\text{M} - \text{Cl}]^-$  ion were monitored.

Thus, standard solutions of PCA-60 or PCA-70, together with the internal  $^{13}\text{C}_8$ -mirex standard, in hexane were prepared. An aliquot of this solution, sufficient to give acceptable ion signals for the sample and internal standard, was then injected and the appropriate ion signals were monitored.

Recalling that the SIM response is taken to be proportional to the molar (or

weighted molar) concentration then

$$\text{Inj. mols PCA} = C \times \frac{\text{SIM}}{(\text{m/z ab}) (\text{form ab})} \quad [5-6]$$

where C is a constant, SIM is the integrated ion signal of the monitored *m/z* peak, *m/z ab* is the fractional relative abundance of the monitored *m/z* species in the ion formula (Table 5.2), and *form ab* is the fractional relative abundance of the molecular formula in the PCA (as obtained from the bar graphs).

Similarly, an aliquot of a solution of the PCA extract from an environmental sample, containing the internal standard (in a known concentration *ratio* to that in the primary standard solution) is analyzed in the same way. By assuming that the ion source conditions do not change over the short time interval between injections, the ratio of the number of moles of injected PCA in the analyte and primary standard is given by:

$$\frac{\text{Inj. mols PCA}(\text{anal})}{\text{Inj. mols PCA}(\text{std})} = \frac{\text{SIM}(\text{anal})}{\text{SIM}(\text{std})} \times \frac{\text{m/z ab}(\text{std})}{\text{m/z ab}(\text{anal})} \times \frac{\text{form ab}(\text{std})}{\text{form ab}(\text{anal})} \quad [5-7]$$

To determine the injected mass of PCA in a sample we now multiply the injected moles by the average molar mass of the PCAs present. (This value will be included on each bar graph plot of the environmental samples examined in this thesis). Finally, the concentration of PCAs in the injected analyte solution can be calculated from the relative volumes of injected analyte and primary standard solutions by multiplying by R, *i.e.*, the ratio of the integrated SIM signal of the monitored ion of the internal standard in the primary standard solution to its integrated SIM signal in the analyte solution (*see* Appendix 4):

$$\frac{PCA(anal)(ng/\mu L)}{PCA(std)(ng/\mu L)} = \frac{inj. mols PCA(anal)}{inj. mols PCA(std)} \times \frac{AMM(anal)}{AMM(std)} \times R \quad [5-8]$$

## 5.2 LINEARITY OF RESPONSE

Tests for linear dependence of the SIM response upon the amount of PCA injected were carried out for PCA-60 and PCA-70. Two series of solutions were prepared (one series for each PCA), each series containing 0.5 to 500 ng/ $\mu$ L of PCA and a constant amount of the mirex secondary standard. For each injection 1  $\mu$ L of solution was used and the integrated SIM signals were measured for the [M - Cl]<sup>-</sup> ion (of the C<sub>11</sub>H<sub>18</sub>Cl<sub>6</sub> species for PCA-60 and of the C<sub>11</sub>H<sub>16</sub>Cl<sub>8</sub> species for PCA-70), while the SIM signal of the monitored ion of mirex gave precise volume determination.

Figure 5.8(a,b) shows the calibration graphs obtained for the two standards. Very good linear plots, passing through the origin, with correlation coefficients ( $r^2$ ) of 0.997 and 0.998, for PCA-60 and PCA-70, respectively, were obtained.

## 5.3 DETECTION LIMITS

The analytical detection limit (ADL) for both PCAs was estimated to be ~ 60 pg, at a signal-to-noise ratio of 4:1. Method detection limit (MDL), defined as the lowest concentration of an analyte that an analytical process can reliably detect, was determined by measuring the mean of the analyte signals from extracted sodium sulfate (~10g) samples, and are reported as this mean plus 3 times the standard deviation [103,104]. The limit of quantitation (LOQ), defined as the minimum concentration for which an analyte can be reliably quantified, was determined by measuring the mean of the analyte signals as above, plus 10 times

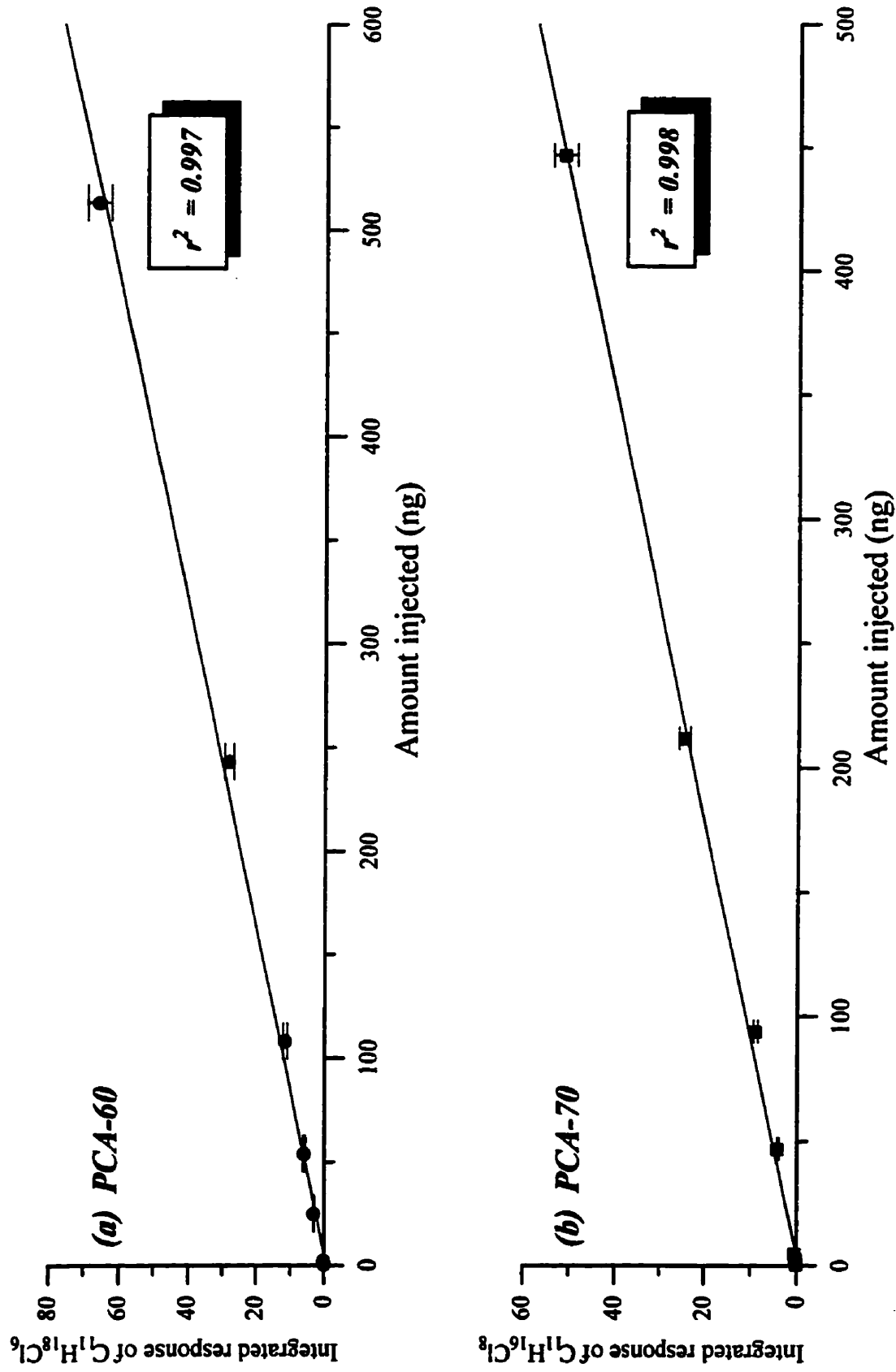


Figure 5.8. Calibration curves for (a) PCA-60 and (b) PCA-70 standards determined by integrating the response of the  $[M - Cl]^-$  ion for the molecular species  $C_{11}H_{18}Cl_6$  and  $C_{11}H_{16}Cl_8$ , respectively.

the standard deviation [104]. The MDL and LOQ were found to be 23 ng/g and 44 ng/g (n = 5 samples), respectively.

#### 5.4 POTENTIAL INTERFERENCES

The most obvious sources of interference are the PCAs themselves because the work-up procedures, HRGC, and ECNI together discriminate strongly against other compounds. The  $[M - HCl]^-$  ion will interfere with the  $[M - Cl]^-$  ion of the same formula group monitored, as could  $[M - Cl]^-$  and  $[M - HCl]^-$  ions of other formula groups that elute at some time during the SIM period of the selected ion. The effects of these interferences can be assessed.

The  $[M - HCl]^-$  ion will interfere with the  $[M - Cl]^-$  ion owing to its natural  $^{13}C$  content; the mass of  $^{13}C$  is 4.5 mmu less than that of  $^{12}CH$ . At 400 u, at a resolving power of 12 000, the mass spectral peaks are 33 mmu wide at 5% of their height; therefore, most of the  $[M - HCl]^-$  peak area will be included in the area recorded for the  $[M - Cl]^-$  isotopic combination of the same nominal mass. By assuming, in the worst case, that 100% of the peak area of  $[M - HCl]^-$  is included, and that the relative abundance of the  $[M - HCl]^-$  ion is 60% of that of the  $[M - Cl]^-$  ion (as in *Section 4.1.2.1.1*, Figure 4.15) then the maximum contribution to the signal for the monitored ion of a  $C_{11}$  PCA is  $60 \times 11 \times 0.011 = 7.3\%$ , where the natural  $^{13}C/^{12}C$  ratio is taken as 1.1%. Of course, similar contributions will apply to the signals for all other  $[M - Cl]^-$  ions monitored and the small errors arising for this reason tend to be self-correcting; therefore it is not worthwhile to attempt to apply factors to correct for the formation of the  $[M - HCl]^-$  ion.

It is possible for the  $[M - Cl]^-$  ions of other formula groups to interfere with

the monitored ion. For example, when monitoring the  $C_{11}H_{16}^{37}Cl^{35}Cl_6^-$  ion of the  $C_{11}H_{16}Cl_8$  formula group a potential interference is the  $C_{13}H_{21}^{37}Cl_4^{35}Cl_2^-$  ion of the  $C_{13}H_{21}Cl_7$  formula group. Since the mass difference is 61 mmu these ions are well separated at a resolving power of 12 000, but would superimpose at a resolving power of 1000; this example, which is typical for these species, illustrates why high resolution mass spectrometry is beneficial for making reliable quantitative measurements.

We also checked to see whether a number of common environmental contaminants, including toxaphene, chlordane, PCBs and mirex, would interfere with the analytical method; although they are discriminated against by the work-up procedure, co-elution during gas chromatography remains a problem if residual interferences escape the clean-up procedures. Thus, separate injections of toxaphene, a technical chlordane mixture, a mixture of 87 PCB congeners, and a mixture of organochlorine pesticides (SRM 2261 and MMQA, see *Section 3.3.1*) were made. The ions listed in Table 5.2 were monitored in the same way as for the PCA mixtures. At a resolving power of 12 000 no interferences were detected above the signal baseline noise but the interferences noted in Table 5.2 occurred at a resolving power of 1000.

## **5.5 ASSESSING THE ACCURACY OF THE ANALYTICAL PROTOCOL.**

Ideally, for analytical data to be reliable, *i.e.*, accurate, standards used in the quantitative analysis should be identical, if not, closely related to the analyte. In quantitative environmental measurements, however, this condition is not often met; the large range of physical, chemical and biological transport, transformation and degradation processes in the environment, and the potential of each to have

different effects on the behaviour of individual components, makes pattern recognition and matching virtually impossible [105].

Variations in the appearance of the analytes relative to technical formulations, which are often used as external standards, have long since plagued reliable environmental measurements. For example, prior to the commercial availability of individual chlorinated biphenyl (CBs) congeners, PCB concentrations were reported as technical equivalents to a particular 'in-house' Aroclor standard, which was thought to closely resemble the profile of the analyte. Much of the ambiguity surrounding reliable environmental measurements for PCB analysis has since been reduced as concentrations can now be reported for individual CB congeners. However, some uncertainty still remains for a number of other environmental contaminants, *viz*, chlorinated bornanes/camphenes (CHBs or toxaphene), polychlorinated terphenyls (PCTs), polybrominated biphenyls (PBBs) and PCAs, for which individual components do not yet exist [36,106,107].

It is difficult, if not impossible, to define a technical mixture with a composition identical to that of any environmental sample [107]. Therefore we attempted to address the extent to which quantitative data would vary with analyte mixtures exhibiting different profiles to that of the external standard. Two approaches were used to assess this aspect of our analytical protocol, the results of which met with mixed success.

In the first approach, a mixture, whose bar graph profile resembles that of the external standard, was selected as the analyte, while in the second instance, an analyte mixture, whose bar graph profile varied significantly from that of the external standard, was selected. Both analytes were quantified using the protocol described above.

The first approach was used to quantify the PCA-70 mixture, now the analyte, using the PCA-60 as the external standard. By the method described above, and assuming that PCA-60 was 100% pure, we determined the response of a known amount of PCA-70, after correction for the presence of ~ 15% of additives that its manufacturer indicated we would not detect, to be  $80 \pm 5\%$  of the theoretical value. This we considered to be an acceptable result.

In the second approach we synthesized an analytical "reference" standard, which was described earlier (*see Section 3.3.3*), the profile of which, we knew would be very different to that of the PCA-60. The bar graph profile for this mixture is shown in Figure 5.9 (a). Included in the figure, for comparison, is the bar graph profile for PCA-60 (Figure 5.9(b)). Despite our best efforts to date, the "purified" products of addition chlorination of 1,5,9-decatriene gave a response of only  $25 \pm 2\%$  of the theoretical value. In addition to purity concerns, there is the possibility that response factors differ significantly between the synthesized material and PCA-60.

These results are important because they illustrate that for samples with profiles differing significantly from that of the standard, because of either environmental *weathering*, or different PCA formulations responsible for the sample site contamination, opportunities for qualitative and quantitative error increase substantially [108]. However, for analytes showing *similar* profiles to the standard, the method becomes remarkably reliable.

The samples investigated in this study, as we will show, were found to closely resemble at least one of the standards we have available in our laboratory. Our levels, therefore, are probably accurate.

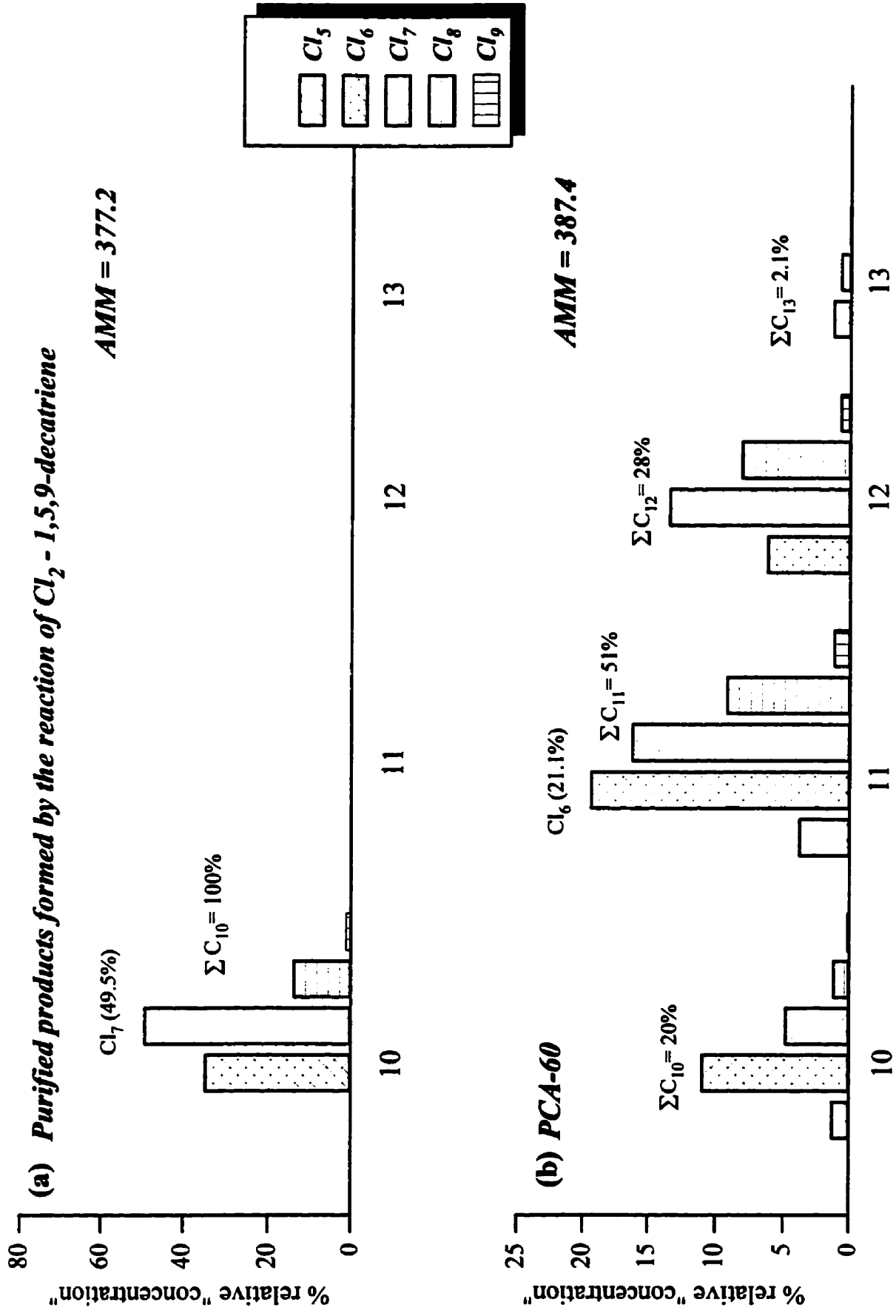


Figure 5.9. (a) Molar compositions of the analytical "reference" standard derived by acid-treating the products formed by chlorination of 1,5,9-decatriene. (b) Molar composition of PCA-60 standard

## **5.6 QUALITY CONTROL-RECOVERY EFFICIENCIES.**

Before applying the analytical protocol to sediment and biotic samples, the analytical recovery efficiencies of PCA-60 and chlordane, from arctic lake trout muscle, known to have low levels of organochlorine residues, and from sodium sulfate (in place of sediment), were first checked. The results are shown in Table 5.3. Consistent percentage recoveries of PCA-60 from multiple samples of fish and sodium sulfate are obtained, with recovery percentages somewhat higher for the lower spiking levels, but acceptably high for both fish and sodium sulfate. A similar observation applies to recoveries of chlordane except that recovery efficiencies from sodium sulfate are nearly the same for both levels of spiking. Recovery efficiencies of PCA-60 and chlordane are comparable.

**Table 5.3. Arithmetic mean  $\pm$  standard deviation % recoveries of PCA-60 and  $^{13}\text{C}_1$ -chlordane from spiked fish muscle (arctic lake trout) and sodium sulfate.**

<b>Sample</b>	<b>PCA-60</b>	<b><math>^{13}\text{C}_1</math>-chlordane</b>
fish <sup>a</sup>	97 $\pm$ 3	97 $\pm$ 2
fish <sup>b</sup>	73 $\pm$ 3	88 $\pm$ 2
ss <sup>a</sup>	90 $\pm$ 3	91 $\pm$ 6
ss <sup>b</sup>	81 $\pm$ 3	87 $\pm$ 2

<sup>a</sup> 1  $\mu\text{g}$  total PCA spiked in 10 g of tissue or sodium sulfate (six samples of each).

<sup>b</sup> 10  $\mu\text{g}$  total PCA spiked in 10 g of tissue or sodium sulfate (six samples of each).

# ***Chapter 6***

## ***ENVIRONMENTAL LEVELS***

### **6.0 INTRODUCTION**

In this section, we present the levels of PCAs detected in a variety of environmental samples from Canada and in the U.S. In an effort to determine if these chemicals are widespread contaminants, we examined samples not only near sites where industrial usage was thought to be high, but also in areas far removed from industrial activity. The primary objective of examining samples from remote locations for PCAs is to ascertain whether these compounds are being dispersed through the environment *via* atmospheric transport.

To the best of our knowledge, the results presented represent the first data on PCA levels in air, arctic marine mammals, sediments and in human breast milk. Apart from the study of Metcalfe-Smith *et al.* (1995), who were unable to detect PCAs in sediment and biota from the St. Lawrence River, this study is also the first to report the concentrations of PCAs in samples from the Great Lakes [24].

### **6.1 DETROIT RIVER AND LAKE ERIE SAMPLES**

The Detroit River connecting Lake St. Clair to the western basin of Lake Erie, is one of many channels joining the Great Lakes [109]. The river, whose length measures 51 km with depths of ~ 7 m, flows southerly, with an average discharge rate of 5200 m<sup>3</sup>/sec [109]. Located in the lower portion of the Detroit

River are several islands that divide the river into a series of channels, one of which is the Trenton Channel, which runs between Grosse Ile and the U.S. mainland (see Figure 6.1).

The Trenton Channel is known to be a major depositional zone; several chemical manufactures discharge waste water effluent directly into the channel [109]. Hamdy and Post (1985) reported PCB and DDT (and its metabolites) levels in sediments (dry wt.) from the Trenton Channel to be 1580 ng/g and 186 ng/g, respectively, while Furlong *et al.* (1988) identified levels (dry wt.) of  $\Sigma$ PCBs ( $\Sigma$  = sum of Cl<sub>3</sub> to Cl<sub>10</sub> congeners) ranging from 9 to 14  $\mu$ g/g,  $\Sigma$ PAHs ( $\Sigma$  = 14 compounds) from 0.35 to 130  $\mu$ g/g and  $\Sigma$ PCTs from n.d. to 2.5  $\mu$ g/g, also in Trenton Channel sediments [109,110]. More recently, Koslowski *et al.* (1994) have reported  $\Sigma$ PCB levels from the western basin of Lake Erie in sediment and silver bass muscle as 47.5 ng/g (dry wt.) and 88 ng/g to 1.2  $\mu$ g/g (wet wt.), respectively [111].

The highly industrialized nature of this region and the occurrence of relatively high levels of other anthropogenic organic contaminants were the reasons for investigating samples collected from this region for PCAs.

Sediment ( $n=3$ ), yellow perch ( $n=3$ ), channel catfish ( $n=2$ ) and zebra mussels ( $n=4$ ) (one from the Detroit River, and three from Middle Sister Isle) were collected at the sampling sites shown in Figure 6.1. The elution profiles for some of the congeners, based on the [M - Cl]<sup>-</sup> ion, found in these samples are shown in Figures 6.2-6.4. The bar graph ion signal profiles for each sample, generated by the procedure outlined earlier, are shown in Figure 6.5(a-d). Also shown in the figure, are the relative abundances of the various formula groups.

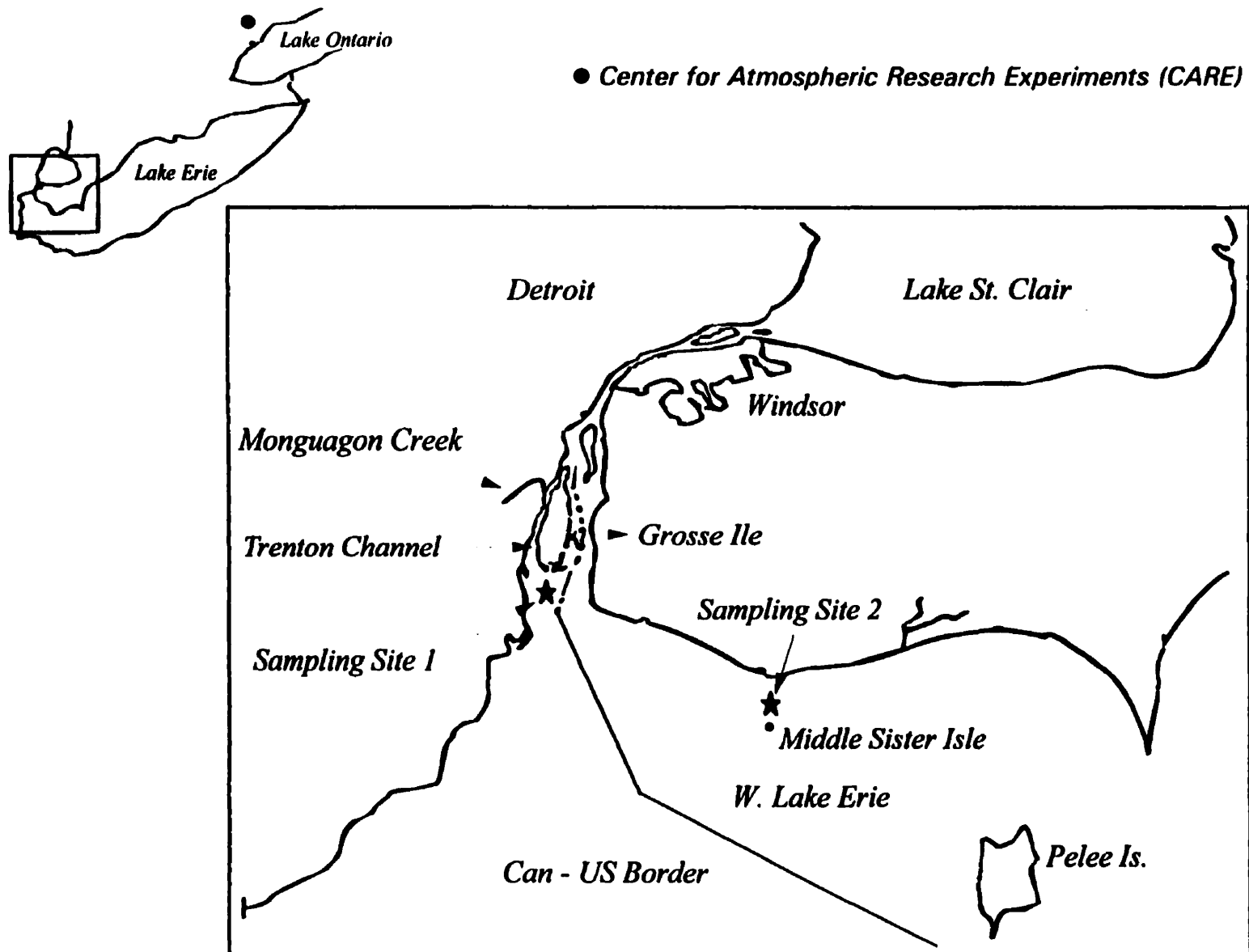


Figure 6.1. Location of sampling sites on the Detroit River and the Western basin of Lake Erie. Sediment, yellow perch, channel catfish and zebra mussels were collected at sampling site #1. Zebra mussels were also collected at sampling site #2. Also shown is the CARE (●) sampling station where air samples were collected.

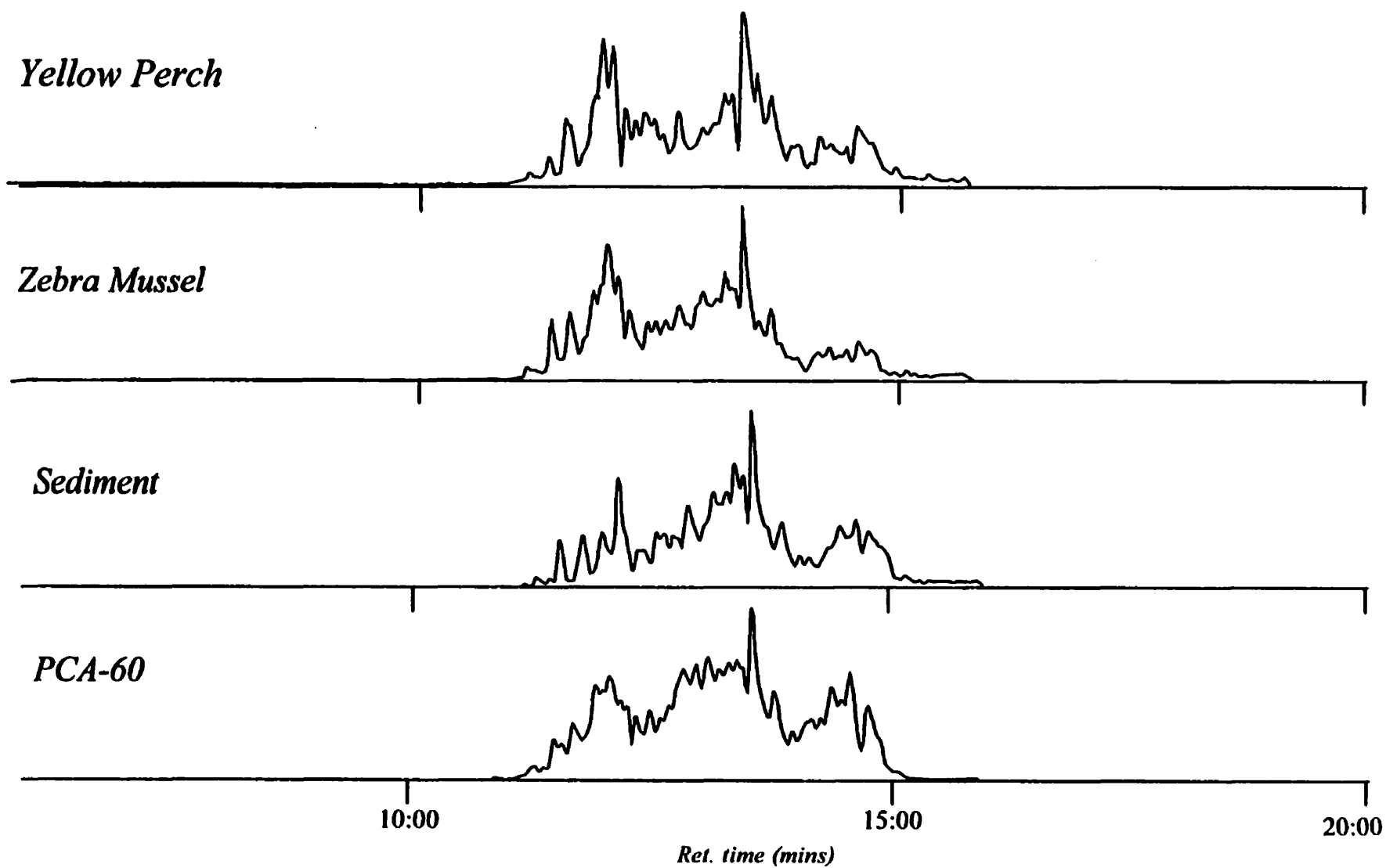


Figure 6.2 ECNI selected ion chromatograms for the heptachlorodecane ( $m/z$  346.92275) congener in various samples from the Detroit River and the PCA-60 external standard.

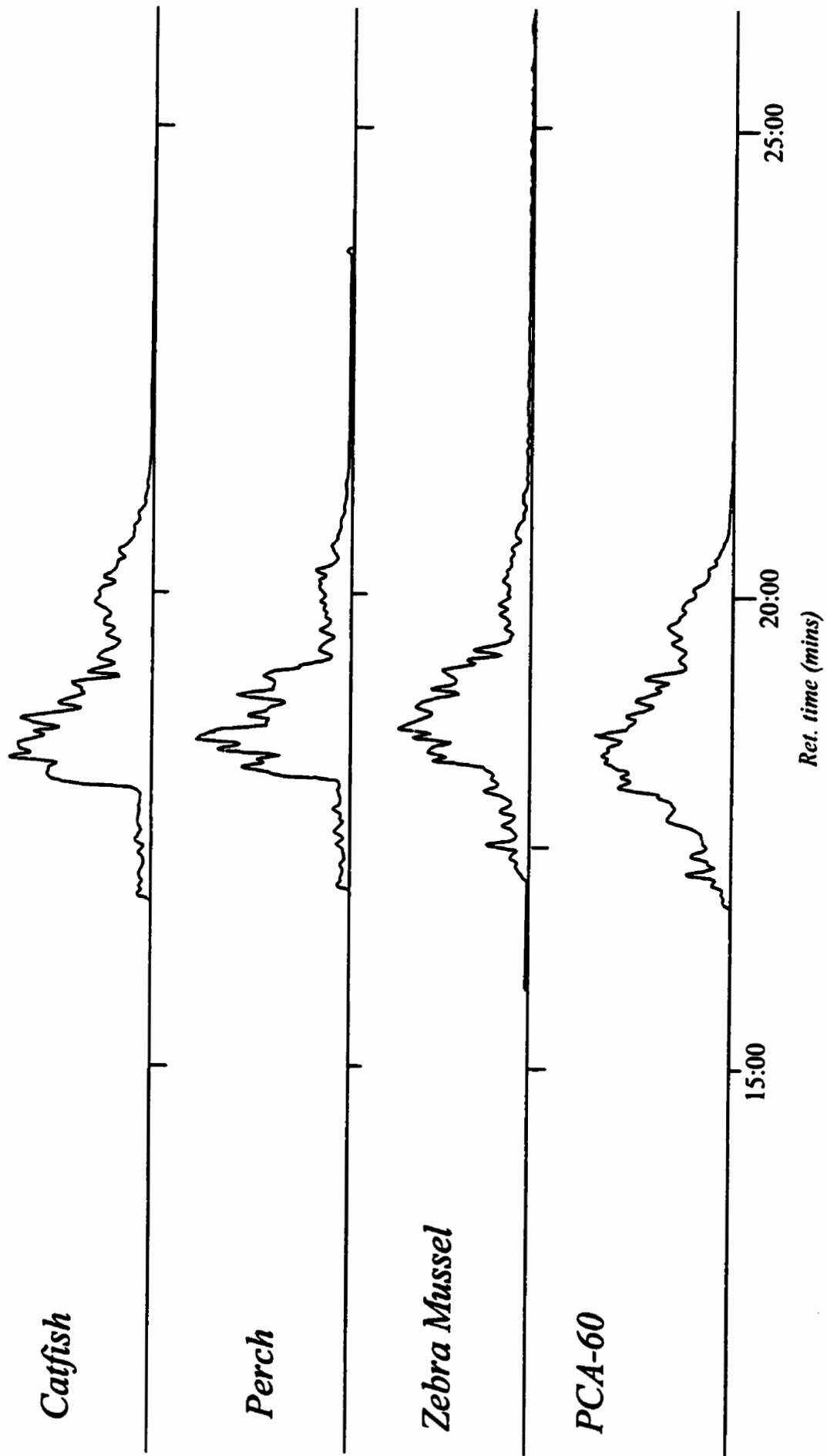


Figure 6.3. ECNI selected ion chromatograms for the nonachloroundecane ( $m/z$  430.8623) congener in various samples from the Detroit River and PCA-60 external standard.

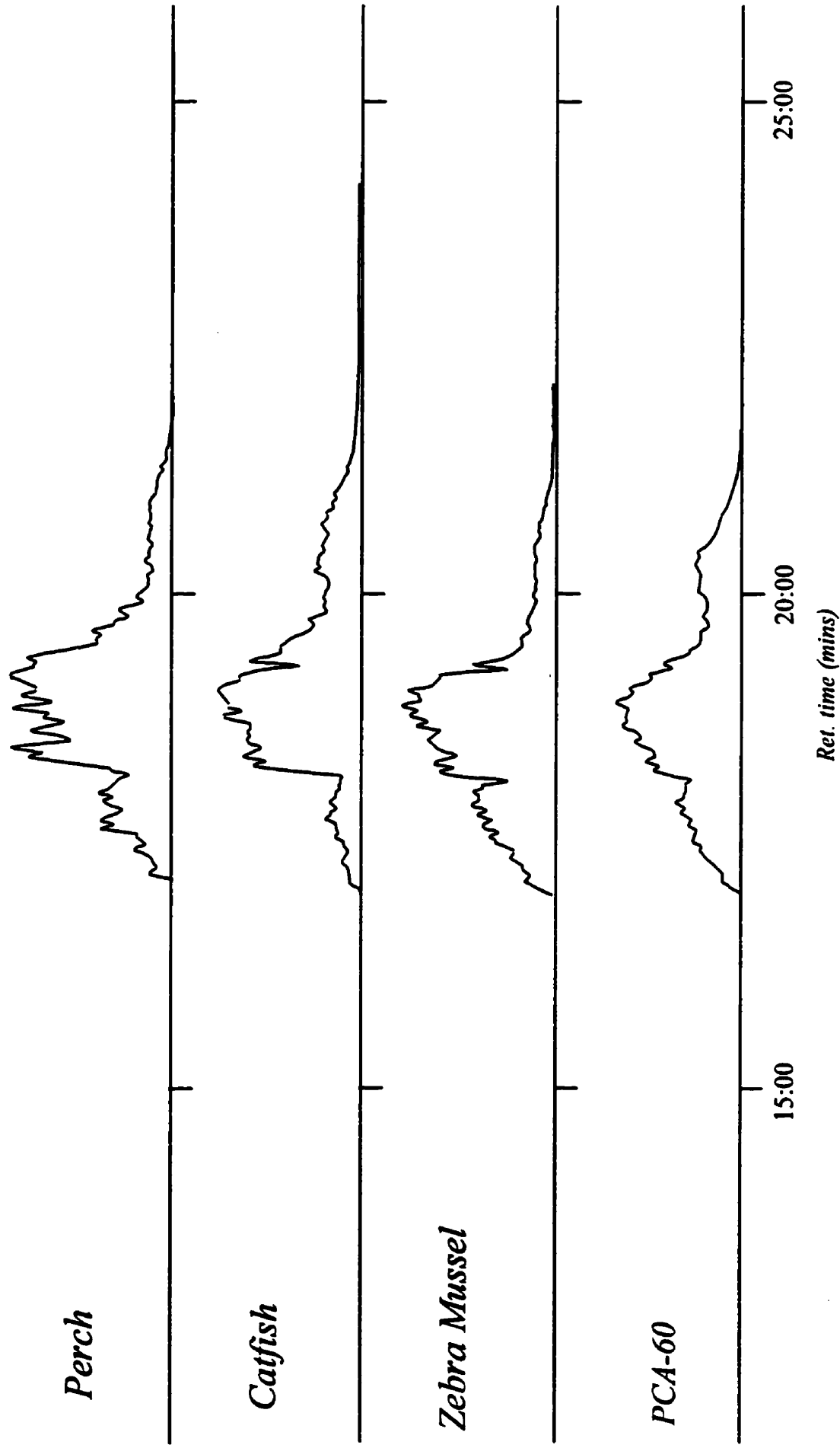


Figure 6.4. ECNI selected ion chromatograms for the octachlorododecane ( $m/z$  408.9199) congener in various samples from the Detroit River and the PCA-60 external standard.

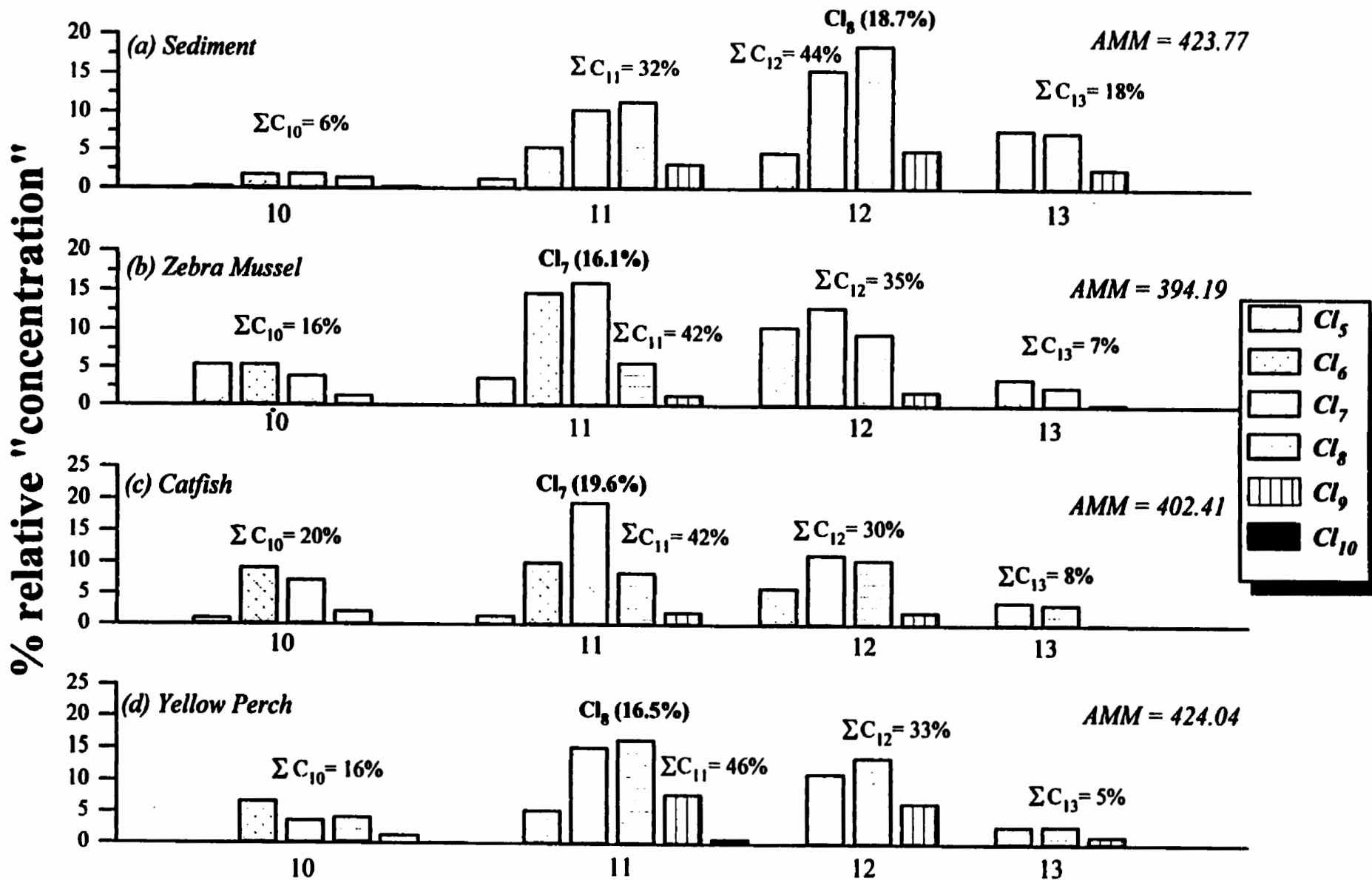


Figure 6.5. Ion signal profiles of samples collected from the Detroit River and western Lake Erie. The most abundant congener (highlighted in bold), whose [M-Cl]<sup>-</sup> ion is used as the quantitation ion, is shown for each sample.

The protocol described in the previous chapter can be illustrated by estimating the mass of PCAs in the perch extract. Because of their similarity, the yellow perch samples were quantified using the PCA-70 mixture as the external standard. *Appendix 5* illustrates the steps in calculating the levels of PCA in the perch sample.

The total concentration of PCAs ( $\Sigma$ PCAs) was calculated to be 1021 ng/g (wet wt.). From Figure 6.5(d), we can express the concentration according to homologue groups, and so the respective concentrations of  $\Sigma C_{10}$ ,  $\Sigma C_{11}$ ,  $\Sigma C_{12}$ ,  $\Sigma C_{13}$  are 163, 470, 337 and 51 ng/g.

These results, although limited, illustrate that PCA concentrations in yellow perch may be higher than other major organochlorine (OCs) contaminants previously reported for samples belonging to the same trophic level from this area [111].

A similar approach is used to quantify the other samples. Table 6.1 shows the PCA levels found in the other sample matrices.

## **6.2 EGBERT AIR SAMPLES**

The atmosphere has long been recognized as a major pathway by which organic contaminants are transported and deposited in areas far removed from their sources [112-116]. The occurrence of PCBs in water, lake trout and snow samples from Siskiwit Lake located on Isle Royale; a remote island in northern Lake Superior located some 50 km from the nearest city (Thunder Bay, Ont.) in 1978, led researchers to suggest that the source of PCBs was *via* the atmosphere [112]. Since that time numerous other studies have established the presence of

Table 6.1. Mean percent recovery of  $^{13}\text{C}_1$ -chlordanes from spiked samples and mean PCA concentrations recovered from biota (ng/g wet wt.) and sediment (ng/g dry wt.) from the Detroit River and Lake Erie (all samples run in duplicate). For  $n = 3$ , the arithmetic mean  $\pm$  standard deviation is shown.

Sample	$^{13}\text{C}_1$ -Chlordane	PCA levels				Total
	% recovery	$\Sigma\text{C}_{10}$	$\Sigma\text{C}_{11}$	$\Sigma\text{C}_{12}$	$\Sigma\text{C}_{13}$	PCA <sup>a</sup>
Perch ( $n=1$ )	88	163	470	337	51	1021
Perch ( $n=2$ )	88	13	38	27	5	83
Catfish ( $n=2$ )	79	46	97	70	19	232
ZM(DR) <sup>b</sup> ( $n=1$ )	54	174	457	381	77	1089
ZM(MS) <sup>c</sup> ( $n=3$ )	54	32 $\pm$ 19	84 $\pm$ 50	70 $\pm$ 42	15 $\pm$ 8	201 $\pm$ 120
Sediment ( $n=3$ )	86	17 $\pm$ 4	93 $\pm$ 21	128 $\pm$ 29	53 $\pm$ 12	291 $\pm$ 66

<sup>a</sup> Estimated by assuming PCA % recoveries are the same as those of  $^{13}\text{C}_1$ -chlordanes.

<sup>b</sup> Zebra mussel from the Detroit River

<sup>c</sup> Zebra mussels from Middle Sister Ile.

OCs in the atmosphere [113-119].

The International Joint Commission (an organization composed of Canadian and U.S. representatives who are responsible for overseeing issues related to cross-border environmental problems) in 1980, concluded that atmospheric deposition of airborne OCs was endangering the *health* of the aquatic organisms indigenous to the Great Lakes. Subsequent workshops on mass balance models of toxic chemicals in the Great Lakes recommended the establishment of a binational network (Integrated Atmospheric Deposition Network, IADN) to monitor the air and precipitation quality within the Great Lakes Basin [118,120,121].

In addition to the air monitoring sites established by Environment Canada as part of the IADN, the Atmospheric Environment Service (AES) has in place the Center for Atmospheric Research Experiments (CARE) in Egbert, Ont., (44° 14' N, 79° 47' W), a rural area located ~ 100 km north of the city of Toronto and some 15 km from industrial sources (*see* Figure 6.1) [72,122]. The location of the research site is subject to impact from air-masses flowing from the west and south, passing the agricultural and industrial heartlands of the U.S. [120].

The bar graph ion signal profiles for air samples collected at the CARE station is shown in Figure 6.6(a). Included in the figure, for comparison, is the bar graph profile for PCA-60 (Figure 6.6(b)), which was used as the external standard.

The appearance of the profiles supports the observations of Drouillard *et al.* (1997), who studied the physicochemical properties of individual PCA congeners, *i.e.*, HLC of congeners appears to decrease with increasing chlorine content for

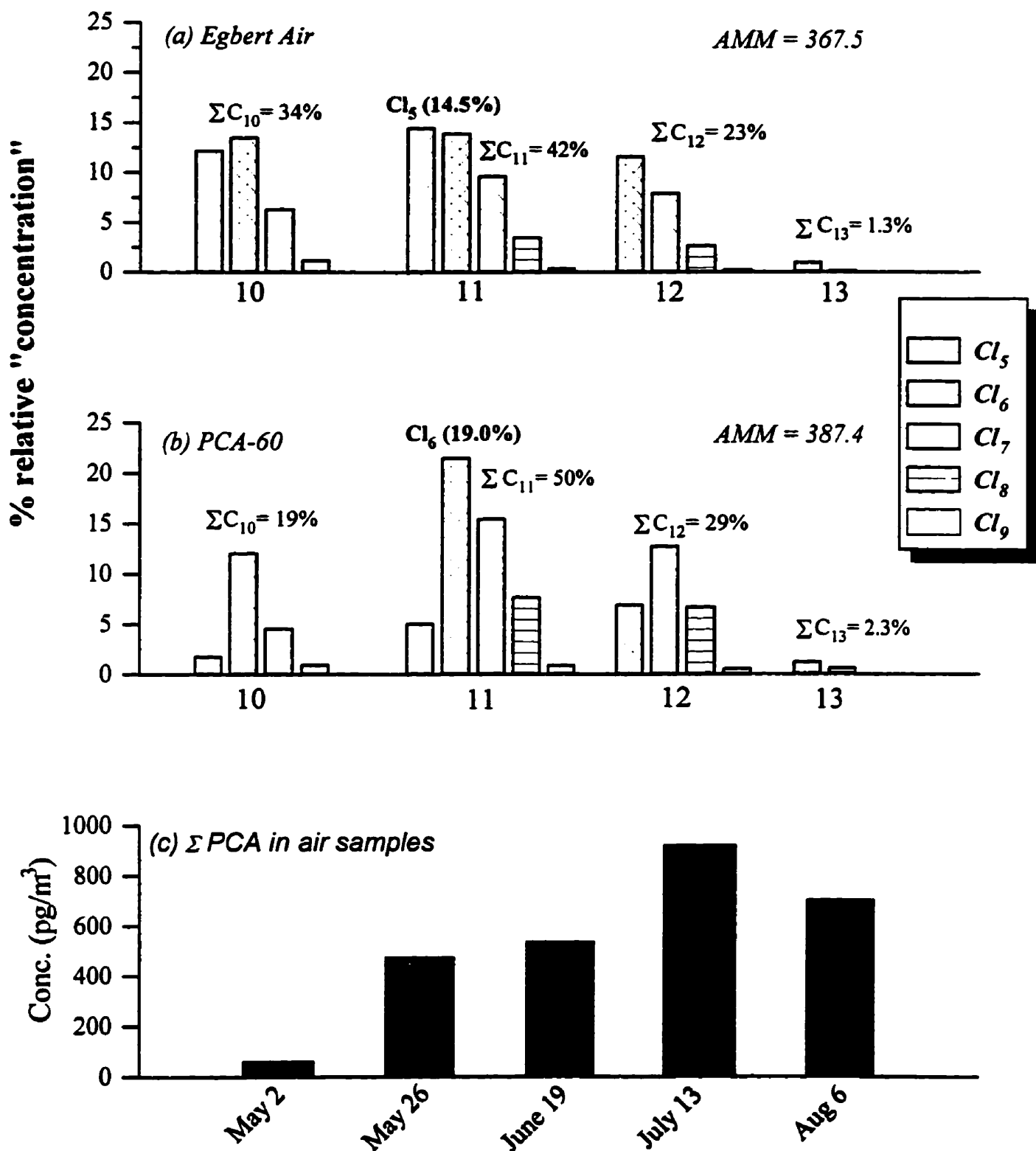


Figure 6.6. Ion signal profiles for components in (a) Egbert, Ont., air samples and (b) PCA-60 standard. The most abundant ion (highlighted in bold) which is used as the quantitation ion, is also shown. (c) ΣPCAs concentrations of air samples collected in 1990.

PCAs containing similar carbon chain lengths, suggesting that lower chlorinated lower carbon chain length PCAs would tend to preferentially volatilize from water bodies and disperse through the environment *via* atmospheric transportation (see Section 1.1.2) [19,20]. In fact, the HLCs calculated by Drouillard *et al.*, suggest that tetrachloro- and pentachloro-*n*-alkanes of chain length C<sub>10</sub> to C<sub>11</sub> exhibit VPs similar to lower chlorinated PCBs [19,20]. The bar graph ion signal profile of the air sample clearly shows that the sum of the C<sub>10</sub> and C<sub>11</sub> congeners correspond to more than 75 % of the total ion signal with the lower Cl containing congeners in each homologue group being the most pronounced.

The concentrations of PCAs in samples collected over a four month sampling period in 1990 are shown in Figure 6.6(c). (Procedural blanks consisted of extracted PUF plugs which were analyzed for PCAs.) We targeted samples that were collected in the middle and late summer months where volatilization, because of the higher temperatures, and atmospheric transport from their source, possibly the industrialized areas of the Detroit River and southern Ontario, to the CARE sampling site would be highest.

The highest  $\Sigma$ PCA concentration (924 pg/m<sup>3</sup>, blank corrected) was observed for the sampling date July 13, while the mean concentration ( $n=5$ ) for the other sampling periods is  $543 \pm 318$  pg/m<sup>3</sup> (arithmetic mean  $\pm$  standard deviation). The maximum  $\Sigma$ PCB ( $\Sigma = 90$  congeners) concentration for the 4 month sampling period was for June 19 (682 pg/m<sup>3</sup>), which is slightly lower than the maximum  $\Sigma$ PCA levels [123]. However, the monthly averages (May 1990 to September 1990, biweekly sampling) of  $\Sigma$ PCBs ranged from 74.3 to 682.3 pg/m<sup>3</sup>, which agrees well with those for  $\Sigma$ PCAs (65 to 924 pg/m<sup>3</sup>) [123].

### **6.3 WATER FROM THE RED RIVER NEAR SELKIRK, MANITOBA**

The Red River flows through the city of Winnipeg and a number of other smaller communities, before emptying into the southern basin of Lake Winnipeg (see Figure 6.7). Selkirk, a small community north of the city Winnipeg, is the last town along the Red River prior to its discharge into Lake Winnipeg.

The bar graph ion signal profiles shown in figure 6.8(b), is for water samples collected from the Red River at Selkirk, MB (see Figure 6.7). The appearance of the ion signal profiles seems to closely resemble that of the technical mixture, PCA-60 (Figure 6.8(a)). This would suggest that input of PCAs into the Red River is from local point sources, possibly from improper disposal of PCAs by industries located near the city of Winnipeg or even as far south as North Dakota.

Concentrations of  $\Sigma$ PCAs and  $\Sigma$ PCBs for water collected over a six month period in 1995 are shown in Table 6.2. (Procedural blanks consisted of extracted 10 000 yr old well water from Rockwood, MB, which were analyzed for PCAs.) Mean concentrations of  $\Sigma$ PCAs ( $30 \pm 14$  ng/L) ( $n=7$ ) were significantly higher than those of  $\Sigma$ PCBs ( $1.1 \pm 1.2$  ng/L) ( $n=5$ ) [124,125]. The highest observed  $\Sigma$ PCA level is observed in early spring (April 11), and may be due in part to the ice melt, because of higher temperatures in the Dakotas, bringing with it PCAs which were once immobile.

### **6.4 MARINE MAMMALS FROM THE ARCTIC AND THE ST. LAWRENCE RIVER**

The presence of OCs in marine mammals of the Canadian Arctic was first reported by Holden (1972), who detected PCBs and DDT in blubber of ringed seals (*Phoca hispida*) from Baffin Island [126]. Since then, numerous other

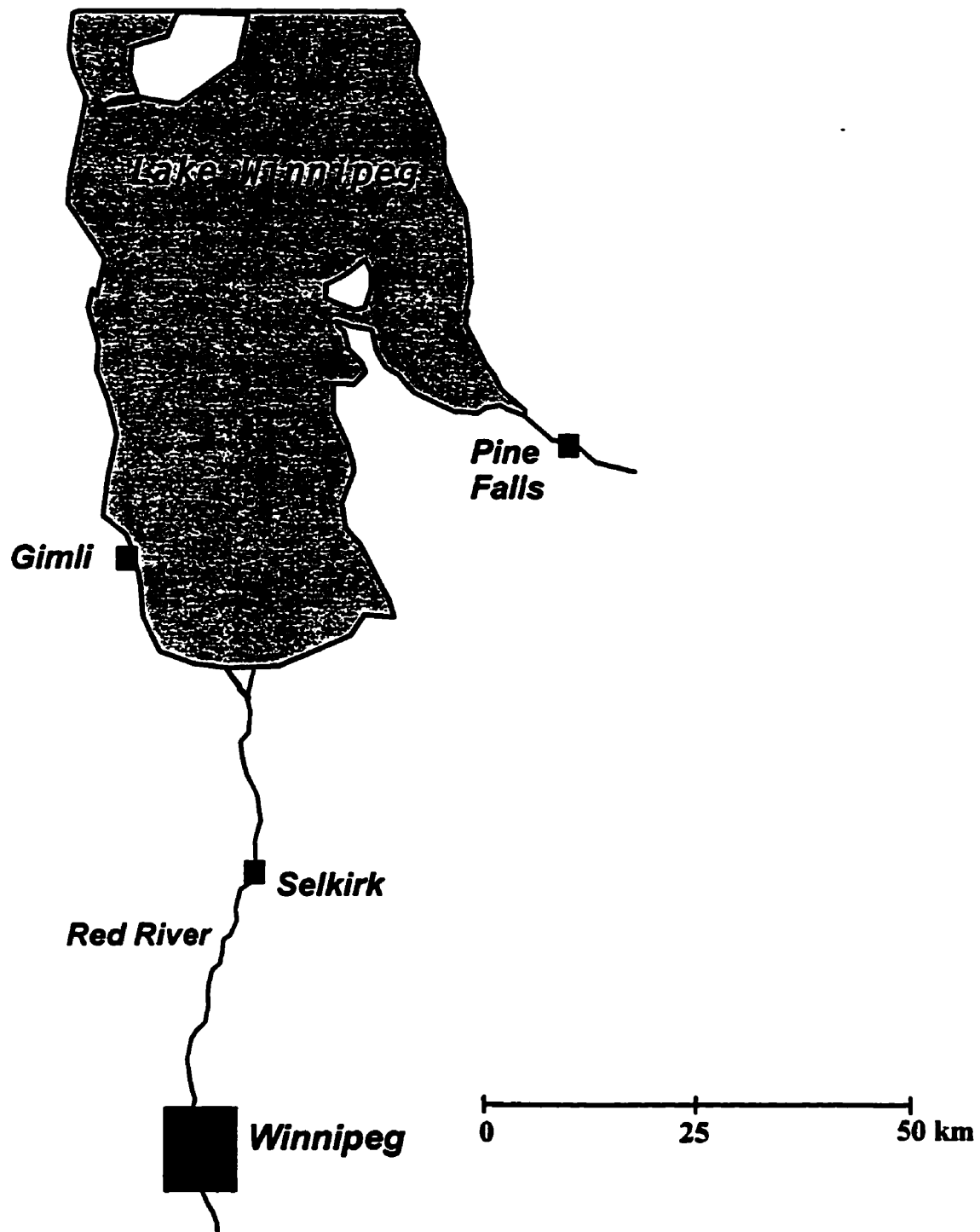


Figure 6.7. Map showing the flow of the Red River into the southern basin of Lake Winnipeg.

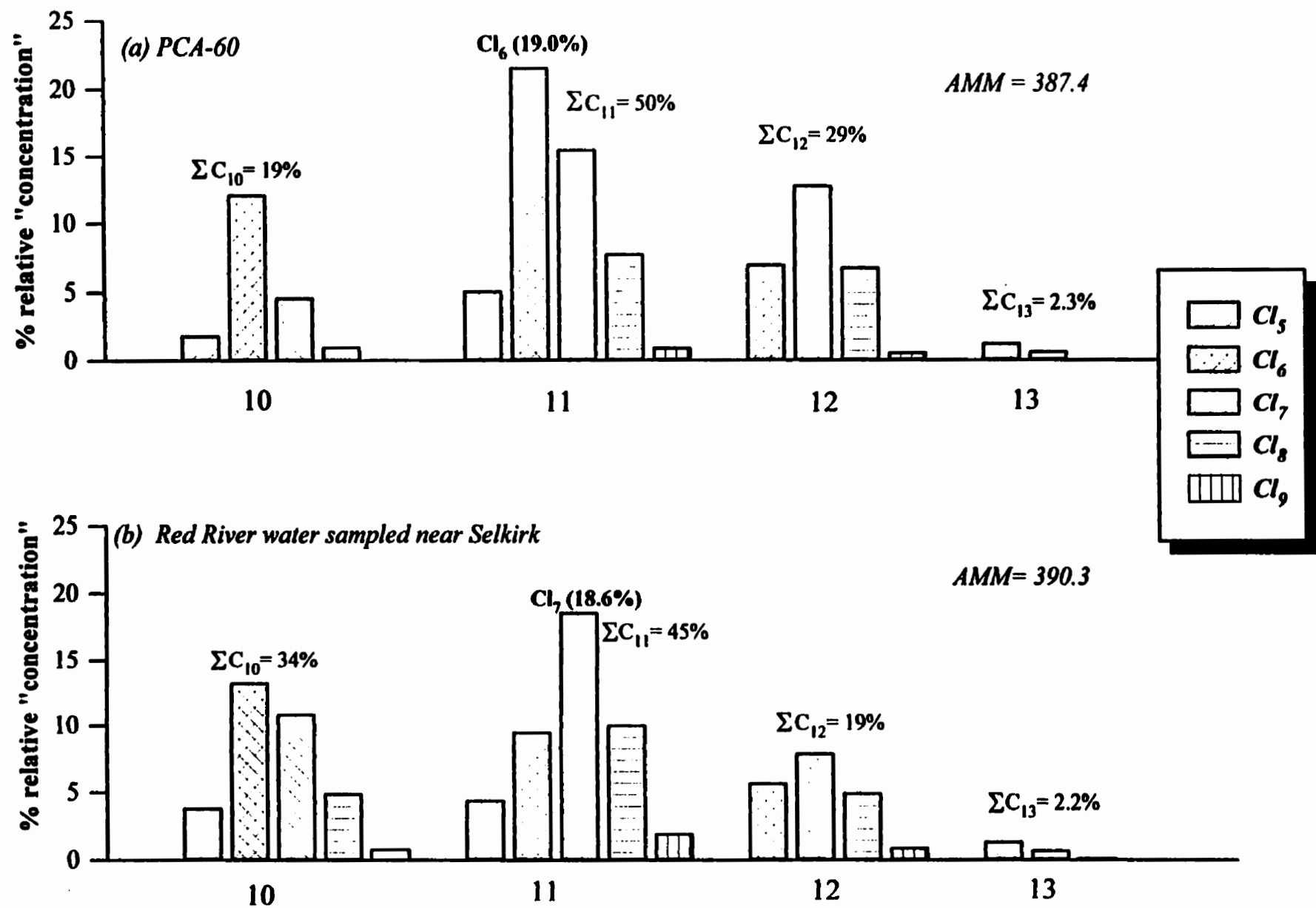


Figure 6.8. Ion signal profiles for components in (a) Red River water samples from Selkirk, MB., and (b) PCA-60 standard. The most abundant congener (highlighted in bold), whose [M-Cl]<sup>-</sup> ion is used as the quantitation ion, is also shown.

Table 6.2. Sampling dates in 1995 and concentrations of  $\Sigma$ PCAs and  $\Sigma$ PCBs in water from the Red River, Selkirk, MB.

Sampling Dates	$\Sigma$ PCAs	$\Sigma$ PCBs <sup>a</sup>
	ng/L	
<i>11 April</i>	54.8	-
<i>25 April</i>	29.3	0.14
<i>24 May</i>	45.6	0.1
<i>20 June</i>	22.9	1.6
<i>5 July</i>	20.5	0.69
<i>22 Aug</i>	25.8	3.03
<i>19 Sept</i>	16.4	-

<sup>a</sup>  $\Sigma$ PCB levels were kindly provided by Thea Rawn, DFO.

measurements of organochlorines in Arctic marine mammals, especially of PCBs and DDT-related compounds, have been reported [127-130].

The pathways of transport of OCs to the Arctic include transport in the troposphere, in the gas phase and on particles, as well as *via* ocean currents [131,132]. Contaminants which become airborne are removed from the atmosphere by absorption, precipitation and dry deposition, while water-borne contaminants enter Arctic ecosystems *via* northward flowing rivers [132].

It is now well accepted that hydrophobic compounds are preferentially accumulated in the lipids of fish and many other marine mammals relative to other 'compartments'. This enrichment of chemicals in the organism relative to the water in which they reside, *i.e.*, bioaccumulation, can occur by three routes: (i) diffusion from the water across the gills, (ii) absorption through the skin, and (iii) transfer from the gastrointestinal tract after ingestion of contaminated food [119,132,133]. For marine mammals, however, the transfer of OCs is predominantly *via* food [132]. Finally, contaminants can be transferred to organisms higher in the food chain, *e.g.*, humans, whales and seals, *via* biomagnification.

Fisk *et al.* (1996), using juvenile rainbow trout, have demonstrated that highly chlorinated short chain PCAs have the greatest *potential* for bioaccumulation or even biomagnification [134]. Our objectives in this study, therefore, were twofold: (i) to investigate whether PCAs were being transported to the Arctic, and if so, (ii) whether they were being accumulated by marine mammals. (Section 6.7 will further illustrate that the transport of PCAs to the Arctic is *via* the atmosphere, as indicated by the presence of PCAs in sediments from remote Arctic lakes).

To do so, we examined a variety of marine mammals from various regions

of the Arctic; these include: (a) NW Greenland and Hendrickson Island beluga whales (*Delphinapterus leucas*), (b) SW Ellesmere Island (Eureka) ringed seal and (c) NW Greenland (Thule) walruses (*Odobenus rosmarus*). For comparison, (d) beluga whales from the St. Lawrence River Estuary were also analyzed for PCAs. The PCA congener profiles from different sampling locations were also compared. We then compared PCA levels to those of other OCs reported in previous studies. Figure 6.9 illustrates the sampling locations of the marine mammals examined in this study.

The bar graph ion signal profiles for each sample, generated by the procedure outlined earlier, are shown in Figure 6.10(a-c) and Figure 6.11(a and b). Except for the St. Lawrence beluga, the ion signal profiles for the Arctic mammals have higher proportions of the shorter chain ( $C_{10}$  and  $C_{11}$ ), lower chlorinated congeners, which suggests contamination *via* long range atmospheric transport. The ion signal profiles for the St. Lawrence beluga, however, closely resembles that of the technical mixture, PCA-60. This suggests that local sources of PCAs, possibly from the Great Lakes and/or the lower industrialized regions of the St. Lawrence river, may be more important inputs of PCAs into the St. Lawrence estuary, and outweigh inputs *via* the atmosphere [128,134].

Concentrations of  $\Sigma$ PCAs in the St. Lawrence beluga were also higher than in any of the Arctic mammals (*see* Tables 6.3-6.5). Mean wet weight  $\Sigma$ PCA levels in St. Lawrence beluga were 4 times higher than in NW Greenland (Sassaq and Nuussuaq) and Hendrickson Island beluga, but only 1.5 times higher than ringed seals from SW Ellesmere Island (Eureka). Walruses from NW Greenland (Thule), also had lower levels,  $\sim 2$  times, of  $\Sigma$ PCAs than St. Lawrence beluga.

The elevated levels of  $\Sigma$ PCAs in beluga from the St. Lawrence river is

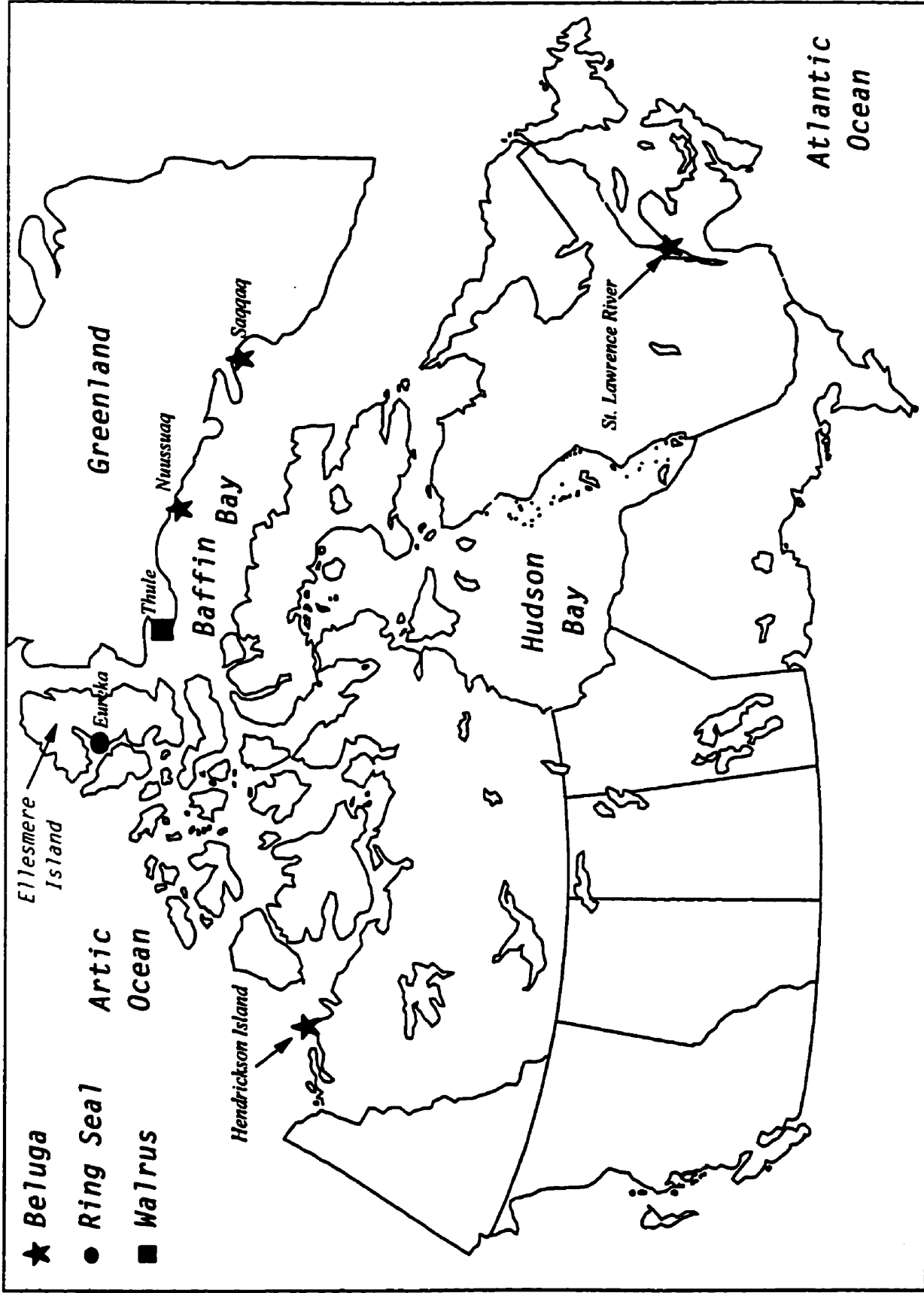


Figure 6.9 Map showing the sampling sites of the marine mammals examined in this study.

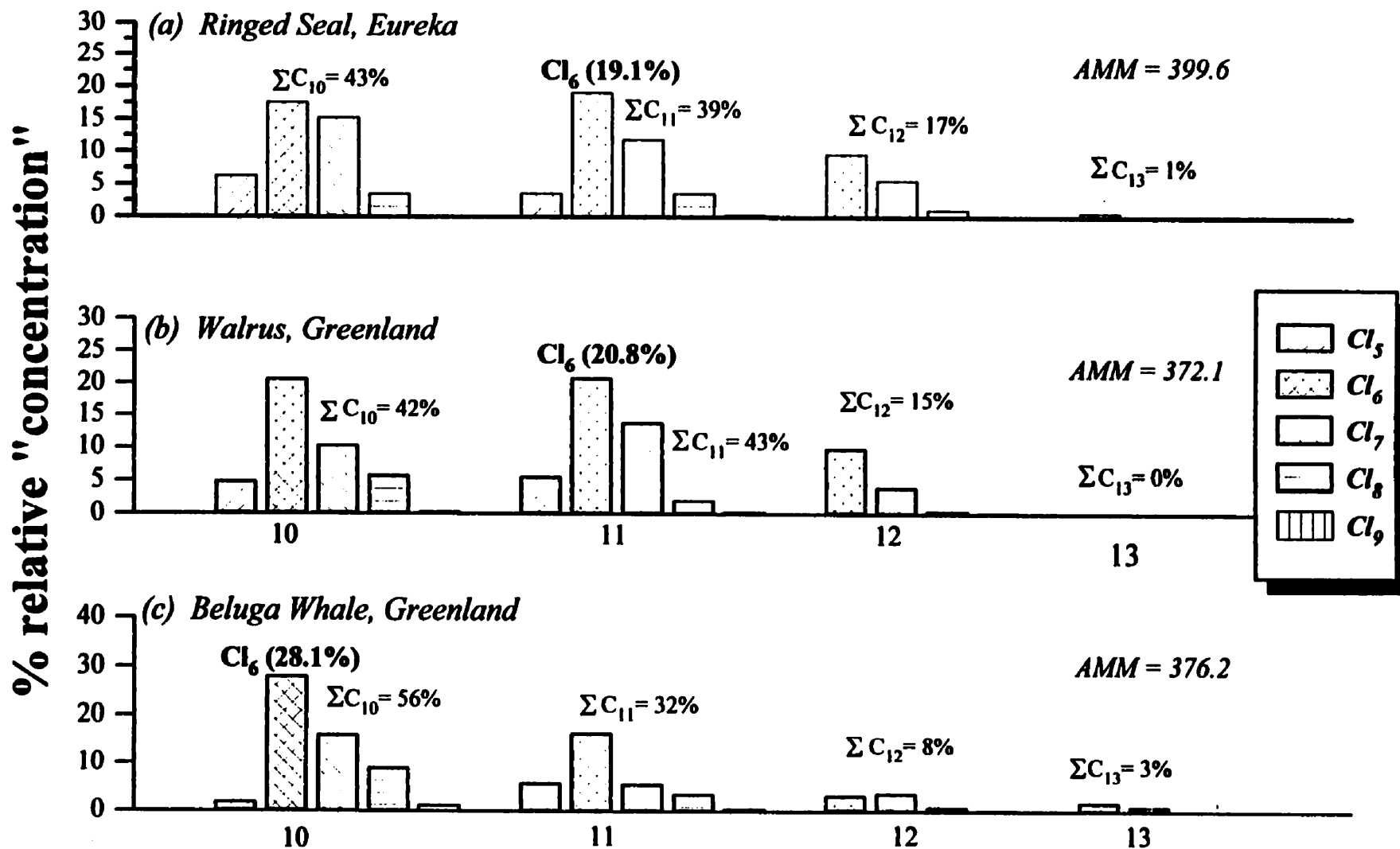


Figure 6.10 Ion signal profiles for components in (a) Ringed Seal, Eureka (b) Walrus, Greenland and (c) Beluga Whale, Greenland. The most abundant congener (highlighted in bold), whose [M-Cl]<sup>-</sup> ion is used as the quantitation ion, is shown for each species.

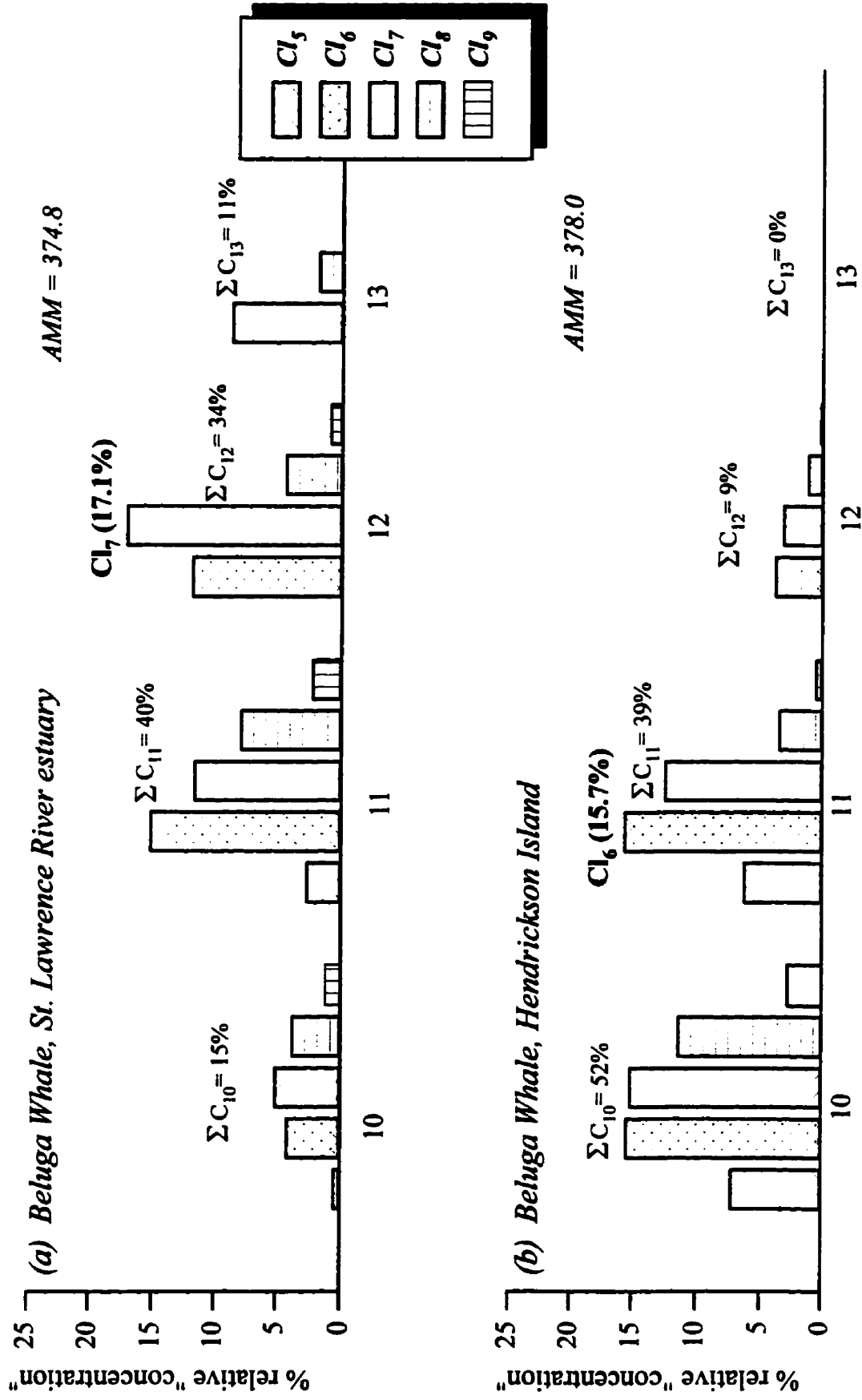


Figure 6.11 Ion signal profiles for components in belugas whales from (a) St. Lawrence River estuary and (b) Hendrickson Island. The most abundant congener (highlighted in bold), whose [M-Cl]<sup>-</sup> ion is used as the quantitation ion, is shown for both species.

**Table 6.3 Collection location, characteristics and concentrations of  $\Sigma$ DDT,  $\Sigma$ PCB and  $\Sigma$ PCAs in beluga sampled from the St. Lawrence River estuary<sup>a</sup>.**

No.	Location	Date	Sex	Lipid (%)	Age <sup>b</sup> (year)	$\Sigma$ DDT	$\Sigma$ PCB	$\Sigma$ PCA
						(ng/g wet wt.)		
1	Baie-des-Sables	May 1988	F	77.8	23+	11 760	22 400	773
2	Baie-des-Sables	Nov. 1988	M	75	20+	95 390	74 700	370
3	Ste Flavie	Aug. 1988	F	93.5	31+	54 790	65 920	655
4	Ste Flavie	Apr. 1989	M	86.3	27+	88 070	72 800	1363
5	Ste Felicits	Dec. 1989	M	83.4	20+	148 900	121 500	764

<sup>a</sup>  $\Sigma$ DDT and  $\Sigma$ PCB levels from Muir *et al.* [128].

<sup>b</sup> Animals maybe older than indicated because dentine layers were difficult to read.

**Table 6.4 Characteristics and concentrations of  $\Sigma$ DDT,  $\Sigma$ PCB,  $\Sigma$ CHB and  $\Sigma$ PCAs in ringed seal blubber from SW Ellesmere Island, Eureka (1994)<sup>a</sup>.**

No.	Sex	Age	Lipid (%)	$\Sigma$ DDT	$\Sigma$ PCB	$\Sigma$ CHB <sup>b</sup>	$\Sigma$ PCA
				(ng/g wet wt.)			
1	F	18	92.7	808	1410	609	376
2	F	16	91.6	516	1101	442	397
3	F	nd <sup>c</sup>	91.4	400	761	380	537
4	F	nd	88.4	492	882	447	767
5	F	33	88.3	696	1264	574	705
6	M	nd	89.5	1046	1606	436	374

<sup>a</sup>  $\Sigma$ DDT,  $\Sigma$ PCB and  $\Sigma$ CHB levels are unpublished results generated by FWI laboratory.

<sup>b</sup>  $\Sigma$ CHB = chlorinated bornanes, *i.e.*, toxaphene.

<sup>c</sup> not determined, some animals are yet to be aged.

Table 6.5 Characteristics and concentrations of  $\Sigma$ DDT,  $\Sigma$ PCB,  $\Sigma$ CHB and  $\Sigma$ PCAs in marine mammal samples from arctic waters.

Species	Region	Location	Sex	Age	Lipid (%)	$\Sigma$ DDT, $\Sigma$ PCB, $\Sigma$ CHB, $\Sigma$ PCA			
						(ng/g wet wt.)			
<i>Beluga</i>	NW Greenland <sup>a</sup> (1989)	Saqqaq	M	12	85.1	2442	4125	2587	253
		Saqqaq	F	6	93.1	2526	3707	2848	215
		Nuussuaq	F	7.5	89.9	2573	4306	3419	222
		Nuussuaq	F	1.5	85	1350	2429	3331	106
	NWT (1995)	Hendrickson Is.	M	nd <sup>b</sup>	94.7	4487	5753	2576	302
		"	M	nd	93.5	3105	4854	4551	178
		"	M	nd	92.6	3092	3829	1923	139
<i>Walrus</i>	NW Greenland (1978)	Thule	M	19	83.5	26	115	327	362
		Thule	M	17	83.2	39	204	223	490

<sup>a</sup>  $\Sigma$ DDT,  $\Sigma$ PCB and  $\Sigma$ CHB levels from Stern *et al.* [130].

<sup>b</sup> not determined, some animals are yet to be aged.

consistent with the findings of elevated levels of organochlorines by Muir *et al.* (1996). They suggested that elevated organochlorine levels in beluga from this region are a consequence of high levels of organochlorines present in the wide variety of species, *viz*, smelt and tomcod, that are lower down in the food chain; local source contamination, undoubtedly, can be attributed to this effect [128].

Concentrations of  $\Sigma$ PCAs relative to other organochlorines, *viz*,  $\Sigma$ PCBs,  $\Sigma$ DDTs (sum of DDT and its metabolites) and  $\Sigma$ CHBs (chlorobornanes or toxaphene) in the marine mammals examined in this study are also shown in Tables 6.3–6.5. Muir *et al.* (1996) reported  $\Sigma$ PCB concentrations ranging from 22 400 to 121 500 ng/g (wet wt.) and for  $\Sigma$ DDT from 11 760 to 148 900 ng/g for belugas from the St. Lawrence River (*see* Table 6.3) [128]. Corresponding  $\Sigma$ PCA concentrations were lower by almost an order of magnitude, with the highest concentration being for the oldest male (1363 ng/g). Although the number of samples is still limited these results seem to support the findings of Addison *et al.* [136]. They suggested that, in males, residue concentration tends to increase with age and occurs because males have no route, other than metabolic degradation, by which to excrete ingested contaminants [136].

Concentration ranges for  $\Sigma$ PCBs,  $\Sigma$ DDTs and  $\Sigma$ CHBs are 761 to 1606 ng/g (wet wt.), 400 to 1046 ng/g and 380 to 609 ng/g, respectively, for ringed seals from SW Ellesmere Island, Eureka (*see* Table 6.4) [123].  $\Sigma$ PCA concentrations ranged from 376 to 767 ng/g. Mean wet weight concentrations for  $\Sigma$ PCAs ( $526 \pm 175$  ng/g) ( $n=6$ ), however, exceeded those of  $\Sigma$ CHBs ( $481 \pm 89$  ng/g), and were only slightly lower than that of  $\Sigma$ DDT ( $660 \pm 240$  ng/g). Mean wet weight concentrations of  $\Sigma$ PCBs ( $1170 \pm 320$  ng/g), however, were higher than  $\Sigma$ PCAs by 2-fold.

$\Sigma$ PCA concentrations in beluga from NW Greenland (Saqqaq and Nuussuaq) and Hendrickson Island, were significantly lower than those of  $\Sigma$ PCBs,  $\Sigma$ DDTs and  $\Sigma$ CHBs (*see* Table 6.5). Stern *et al.* (1992) reported respective mean wet weight concentrations of  $\Sigma$ DDTs,  $\Sigma$ PCBs and  $\Sigma$ CHBs to be  $2222 \pm 580$ ,  $3642 \pm 850$  and  $3046 \pm 390$  ng/g in Greenland beluga, while  $\Sigma$ PCA concentrations in this study were found to be  $199 \pm 64$  ng/g ( $n=4$ ) [130]. Similar differences were observed for Hendrickson Island beluga. Mean wet weight concentrations of  $\Sigma$ DDTs,  $\Sigma$ PCBs and  $\Sigma$ CHBs in these mammals were  $3561 \pm 800$ ,  $4812 \pm 960$  and  $3017 \pm 1370$  ng/g, respectively, while  $\Sigma$ PCA concentrations were found to be  $206 \pm 85$  ng/g [123].

Mean wet weight concentrations of  $\Sigma$ PCAs in walruses from NW Greenland (Thule) were  $427 \pm 64$  ng/g ( $n=2$ ) (*see* Table 6.5). Mean wet weight concentrations of  $\Sigma$ PCBs ( $159 \pm 44$  ng/g) and  $\Sigma$ DDTs ( $32 \pm 6$  ng/g) were significantly lower than those of  $\Sigma$ PCAs; however,  $\Sigma$ CHBs concentrations ( $275 \pm 52$  ng/g) were only 1.5 times lower.

The higher levels of  $\Sigma$ PCAs in walruses from NW Greenland compared to belugas (~2 times) sampled from a similar region is consistent with the findings of Tanabe (1988) and Tanabe *et al.* (1988) [137,138]. These authors have suggested that smaller marine mammals, *i.e.*, cetaceans, may not possess, or have a deficiency of specific drug metabolising enzyme systems, *viz.*, cytochrome P450 isozymes (*e.g.*, CYP1A), which for PCBs, is responsible for arene oxide formation at unsubstituted meta-para positions on the biphenyl ring [139,140]. So that the differences in PCA levels in belugas and pinnipeds may be a result of their varying metabolic capabilities.

## **6.5 HUMAN BREAST MILK**

**Laug *et al.* (1951) were the first to recognize the occurrence of OCs in human breast milk [141]. They reported that milk from healthy women in the U.S. contained elevated levels of DDT (mean  $\Sigma$ DDT = 130 ng/g (lipid wt.)). Since then, numerous other reports have been made, and DDT, together with many other OCs, has been detected [76,142-146].**

**Sea mammals in northern Québec are an important source of food for Aboriginal communities. The undesirable transfer of bioaccumulating anthropogenic contaminants to humans, *via* the consumption of fish and marine mammals, is well documented [76,146,147]. PCAs, like other OCs, therefore, may enter the food chain through the consumption of marine mammals as part of the traditional Inuit diet [76,146,147].**

**Kinloch and Kuhnlein (1986) assessed the levels of PCBs in the Inuit diet in Broughton Island, NWT, Canada, and found that the major contributors of PCB intake were marine mammals such as narwhal, seal and walrus [148]. In fact, the estimated PCB daily intake exceeded the Acceptable Daily Intake (ADI), as defined by Health and Welfare Canada, of 1  $\mu$ g/kg body mass, for 19% of the population studied [76].**

**The bar graph ion signal profile shown in Figure 6.12(a), is for milk samples ( $n=3$ ) collected from women living in settlements along the Hudson Strait of northern Québec (*see* Figure 6.9). Included in the figure, for comparison, is the bar graph profile for PCA-60 (Figure 6.12(b)), which was used as the external standard.**

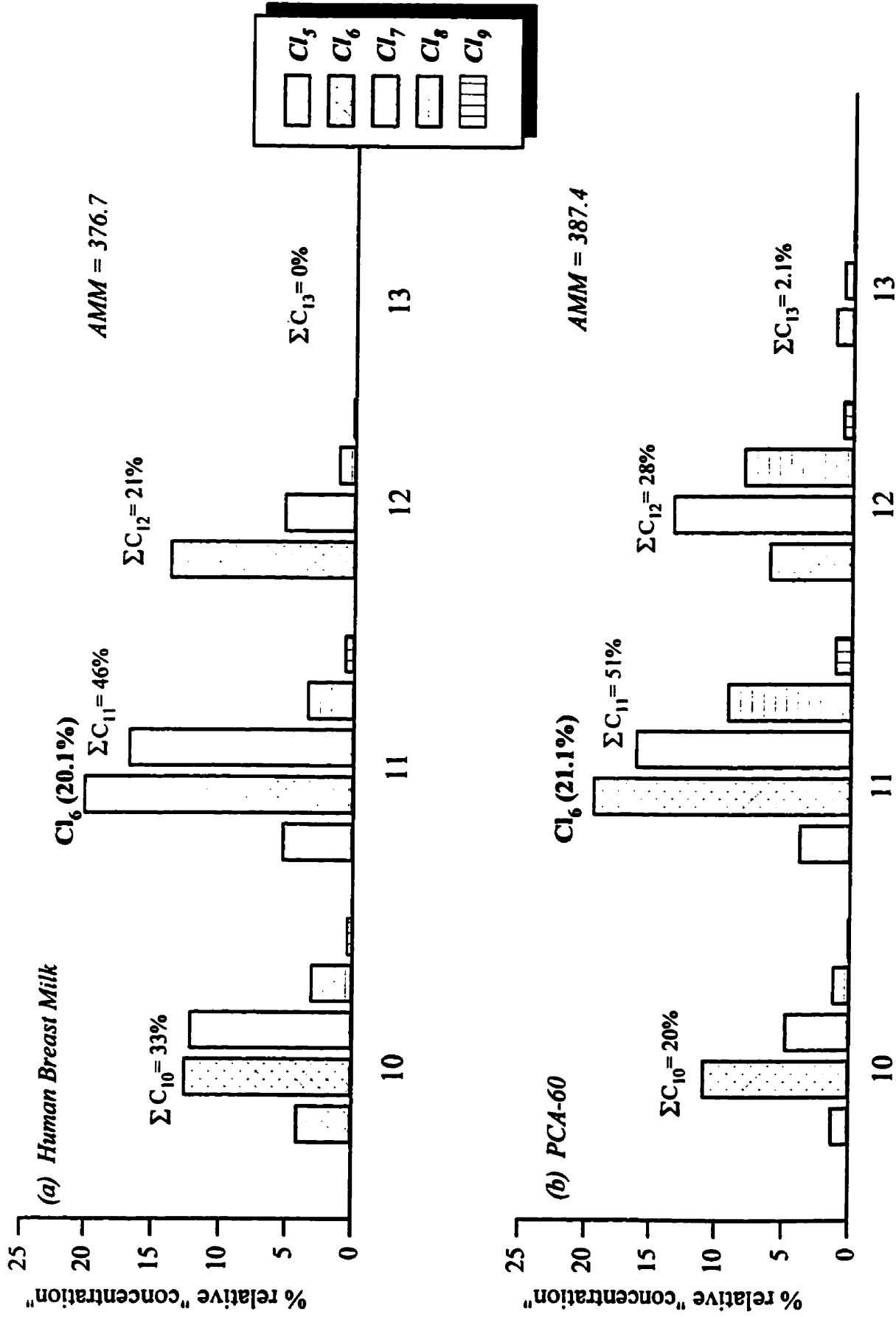


Figure 6.12. Ion signal profiles for components in (a) Human breast milk from an Inuit woman in Northern Quebec and (b) PCA-60 standard. The most abundant congener (highlighted in bold), whose [M-Cl]<sup>-</sup> ion is used as the quantitation ion, is also shown

The  $\Sigma$ PCA concentrations in milk ranged from 10.6 ng/g to 16.5 ng/g (lipid wt., assuming a fat content of 5%), with a mean concentration of  $12.8 \pm 3.2$  ng/g ( $n=3$ ); this is significantly lower than  $\Sigma$ PCB levels of 3.6  $\mu$ g/g (lipid wt.) reported by Dewailly *et al.* [76]. In addition,  $\Sigma$ PCAs were also lower than other organochlorines, *viz.*, 4,4'-DDE ( $185 \pm 150$  ng/g, lipid wt.), 2,2',4,4',5,5'-PCB ( $115 \pm 69$  ng/g, lipid wt.) and  $\Sigma$ CHBs ( $294 \pm 116$  ng/g, lipid wt.), reported by Stern *et al.* (1992) [145].

## 6.6 PCAs IN STANDARD REFERENCE MATERIALS

Since 1980, the Standard Reference Materials (SRM) program of the National Institute of Standards and Technology (NIST) has been providing laboratories that are involved in the analysis of marine mammals and sediments with a source of well-characterized materials for use in the determination of OCs and trace elements [149-152]. These SRMs are available commercially in two forms: (i) as simple calibration solutions containing a number of analytes in a solvent, or (ii) as analytes, whose concentrations have been certified, *i.e.*, two or more independent laboratories that have participated in quantifying the mixture, the results of which are statistically combined, in a natural matrix.

The simple SRM calibration solutions, of which there are 16 (one of which is the SRM 2261 described earlier) are useful for: (i) calibrating chromatographic instruments for retention times and detector response factors, (ii) spiking or fortifying samples, and (iii) analyte recovery studies [153]. Validation of a complete analytical procedure, however, requires the use of materials with matrices similar to those encountered in the analyses of 'real-world' environmental samples. The natural matrix SRMs are, of course, more suitable

materials for this purpose.

Two natural matrix SRMs were analyzed for PCAs. The first, SRM 1588, a cod liver oil that has certified concentrations of 20 PCB congeners and 10 chlorinated pesticides [153]. This material is often used as surrogates for tissue extracts with a high lipid content. This standard has also been fortified with 7 selected polychlorodibenzo-*p*-dioxins (PCDDs) and polychlorodibenzofurans (PCDFs). The other biological matrix, SRM 1945, was prepared from blubber collected from a stranded pilot whale on Cape Cod in 1991, and contains certified concentrations of 27 PCB congeners and 15 chlorinated pesticides [153,154].

The bar graph ion signal profiles shown in Figure 6.13 (a and b) are for SRMs 1588 and 1945, respectively. The appearance of the ion signal profiles seems to closely resemble that of the technical mixture, PCA-60 (Figure 6.12(b)), and so this was used as the external standard.

Concentrations of  $\Sigma$ PCAs relative to  $\Sigma$ PCBs and  $\Sigma$ DDTs are shown in Table 6.6.  $\Sigma$ PCA levels were significantly lower than both  $\Sigma$ PCB and  $\Sigma$ DDT in both SRMs. For SRM 1588,  $\Sigma$ PCAs were 40 times lower than  $\Sigma$ PCBs and 30 times lower than  $\Sigma$ DDTs. Concentration differences for the SRM 1945 were significantly less as respective  $\Sigma$ PCBs and  $\Sigma$ DDTs were only 8 and 5 times higher than  $\Sigma$ PCAs.

These results are important because they are the first that have identified and reported uncertified concentrations of PCAs in SRMs. In the near future, we hope to advise the NIST of these findings so that better characterization, *i.e.*, establishment of certified concentrations of PCAs, of these materials can be made.

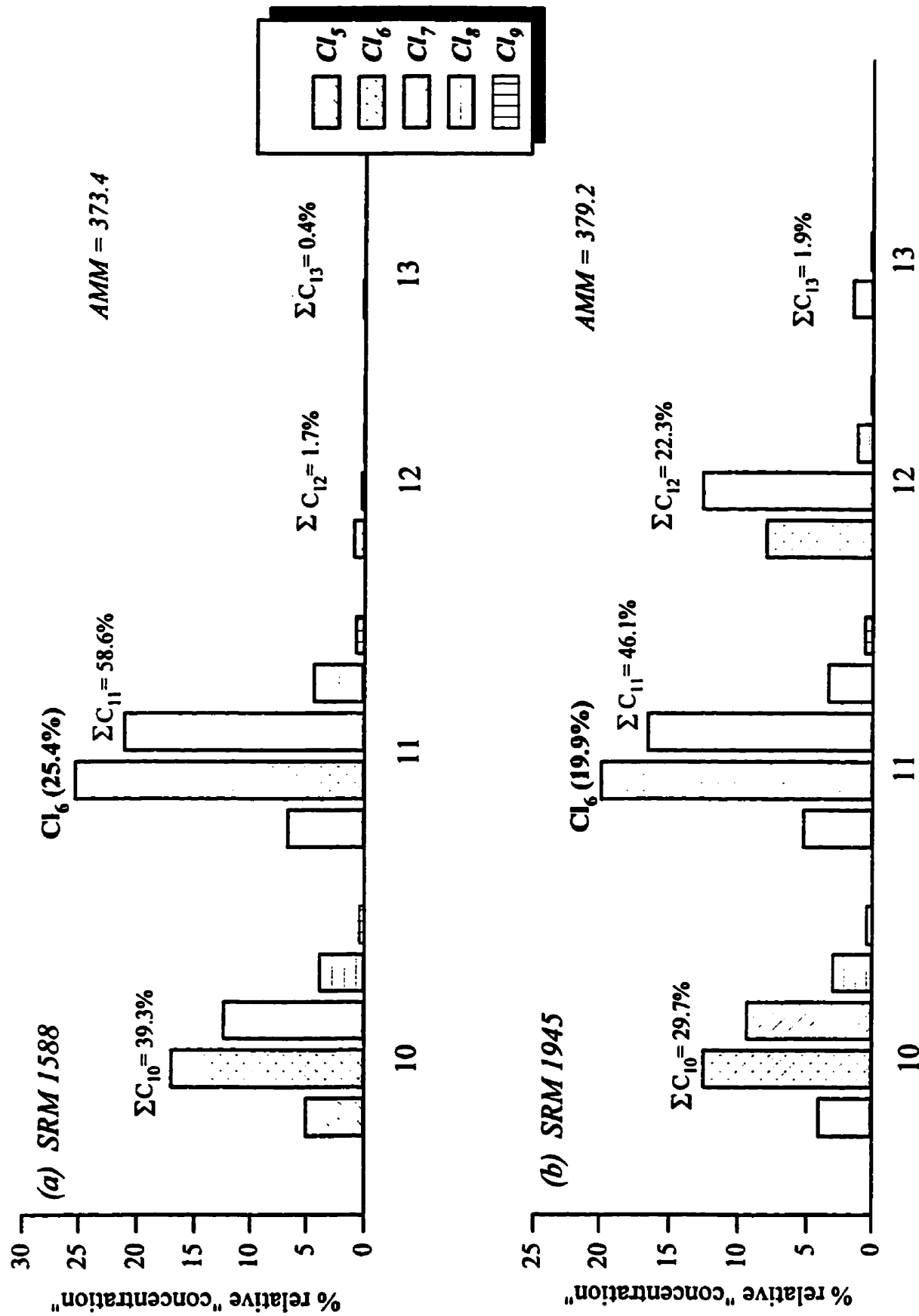


Figure 6.13. Ion signal profiles for components in (a) SRM 1588 and (b) SRM 1945. The most abundant congener (highlighted in bold), whose [M-Cl]<sup>-</sup> ion is used as the quantitation ion, is also shown.

Table 6.6 Mean concentrations of  $\Sigma$ PCBs,  $\Sigma$ DDTs and  $\Sigma$ PCAs in certified natural biological matrices of SRM standards.

SRM standards	Concentration (ng/g)		
	$\Sigma$ PCBs	$\Sigma$ DDTs	$\Sigma$ PCAs <sup>d</sup>
1588	1862 <sup>a</sup>	1661	49
1945 <sup>c</sup>	1312 <sup>b</sup>	959	172

<sup>a</sup>  $\Sigma$  = 20 congeners

<sup>b</sup>  $\Sigma$  = 27 congeners

<sup>c</sup> wet wt. concentrations.

<sup>d</sup> n=2

## 6.7 OCCURRENCE OF PCAS IN CANADIAN MID-LATITUDE AND ARCTIC LAKE SEDIMENTS

Before we examine the levels of PCAs that were found in lake sediments from the Arctic and in other regions of Canada, some of the *terms* which will be used extensively in this section are first defined.

### 6.7.1 INTRODUCTION

The analysis of *dated* sediment cores has the potential for providing chronologies of contaminant input to lakes, *i.e.*, the depositional history, assuming that processes such as bioturbation, molecular diffusion and biotransformation are negligible [70,113,153]. Dating of sediment cores, which are typically sliced into layers (0.5–2cm), as first described by Krishnaswamy *et al.* (1971), is done usually by measuring radionuclides (*e.g.*, lead-210 ( $^{210}\text{Pb}$ ) or cesium-137 ( $^{137}\text{Cs}$ )) [155]. The half-life ( $t_{1/2}$ ) of  $^{210}\text{Pb}$ , 22.26 years, makes the method of  $^{210}\text{Pb}$  dating of sediment cores attractive for retrospective studies of contaminant inputs over the last 150 years [113].

$^{210}\text{Pb}$ , a member of the uranium-238 ( $^{238}\text{U}$ ) decay series, is produced from the decay of radium-226 ( $t_{1/2} = 1622$  years,  $^{226}\text{Ra}$ ) from the earth's crust to radon-222 ( $t_{1/2} = 3.83$  days,  $^{222}\text{Rn}$ ) [113,155,157]. Atmospheric  $^{210}\text{Pb}$  originates because of disintegration of  $^{222}\text{Rn}$  after its diffusion into the air; subsequent removal of  $^{210}\text{Pb}$  from the atmosphere and into the water system then occurs *via* precipitation. The high affinity of  $^{210}\text{Pb}$  for particles ensures a short residence time in the water column, thereby facilitating deposition of  $^{210}\text{Pb}$  to the sediment bed. The decay of this *unsupported*  $^{210}\text{Pb}$  in the sediment column is used for dating. In practice, the 'concentration' of *unsupported*  $^{210}\text{Pb}$  is determined by subtracting the

contribution due to *supported*  $^{210}\text{Pb}$ , which is assumed to be in equilibrium with  $^{226}\text{Ra}$  and is determined by measuring the activity of  $^{226}\text{Ra}$ , from the total observed  $^{210}\text{Pb}$  activity.

Ideally, the activity of the *unsupported*  $^{210}\text{Pb}$  should decrease exponentially with the depth of the sediment slice; thus, a semi-log plot of activity versus depth, often referred to as activity plot, should be linear. The age,  $t$ , in years of a sediment slice, at a mass depth  $m$ , can then be expressed as:

$$t = -\frac{1}{\lambda} \ln \left[ 1 - \frac{A_m}{A_w} \right] \quad [6.1]$$

where  $A_m$  is the *unsupported*  $^{210}\text{Pb}$  activity from the surface to the mass depth  $m$ ,  $A_w$  is the total  $^{210}\text{Pb}$  activity, and  $\lambda$  is the decay constant ( $0.03114 \text{ year}^{-1}$ ) [158].

The *sedimentation rate*, defined as the the rate of settling of suspended sediments because of gravity, can be calculated from the least squares fit for the plot of the activity profile, or by computer modeling [70,157,158]. Sedimentation rates can be expressed as either vertical depth of material deposited per year, or, more commonly, in terms of weight of material deposited per unit area per year [157]. The latter expression can be derived through the multiplication of mm/year by  $(1-\phi)\rho$ , where  $\phi$  represents the porosity (*i.e.*, the volumetric water content of sediments) and  $\rho$  the density of the sedimentary material [157].

The *sediment focusing factor* was first coined by Likens and Davies (1975) to describe the resuspension of sediments from shallower zones by water turbulence, with subsequent transport to, and settling in, the deeper zones of lakes [159- 161]. The factor is determined by taking the ratio of the activity of

*unsupported*  $^{210}\text{Pb}$  stored at a given site to the average activity of *unsupported*  $^{210}\text{Pb}$  in the lake [113].

The *flux* ( $\text{ng}/\text{m}^2 \text{ yr}$ ) is defined as the rate of migration of a chemical, because of a concentration gradient, and is expressed as the mass of chemical passing through unit area per unit time [162]. For our purposes, the flux of contaminants to sediments is calculated by:

$$\text{Flux} = \frac{\text{sedimentation rate} \times \text{concentration}}{\text{sediment focusing factor}} \quad [6.2]$$

Correcting the flux by using the sediment focusing factor normalizes the results for variation in sediment accumulation due to lake size, shape and water column mixing depth, all of which combine to influence the deposition of particulates in deeper zones [161].

For this study, sediments from 4 lakes were examined for the concentration, historical profiles and fluxes of  $\Sigma\text{PCA}$  (see Figure 6.14). Concentrations profiles of  $\Sigma\text{PCA}$  relative to other OCs will be compared (Figures 6.15–6.18). Variation in the congener profiles for sediment slices from a few lakes will also be investigated (Figures 6.19–6.22). The characteristics and focused corrected fluxes of  $\Sigma\text{PCA}$  ( $\text{ng}/\text{m}^2 \text{ yr}$ ) of the lakes studied are shown in Table 6.7.

Ion signal profiles were determined, in most cases, for the surface, middle and bottom slice from each core. Quantitation of individual slices is then achieved by assuming that the profile of the slice to be quantified is similar to the nearest slice for which ion signal profiles have been generated. For example, the second slice of a core would be quantified by using the profiles generated for the top slice.

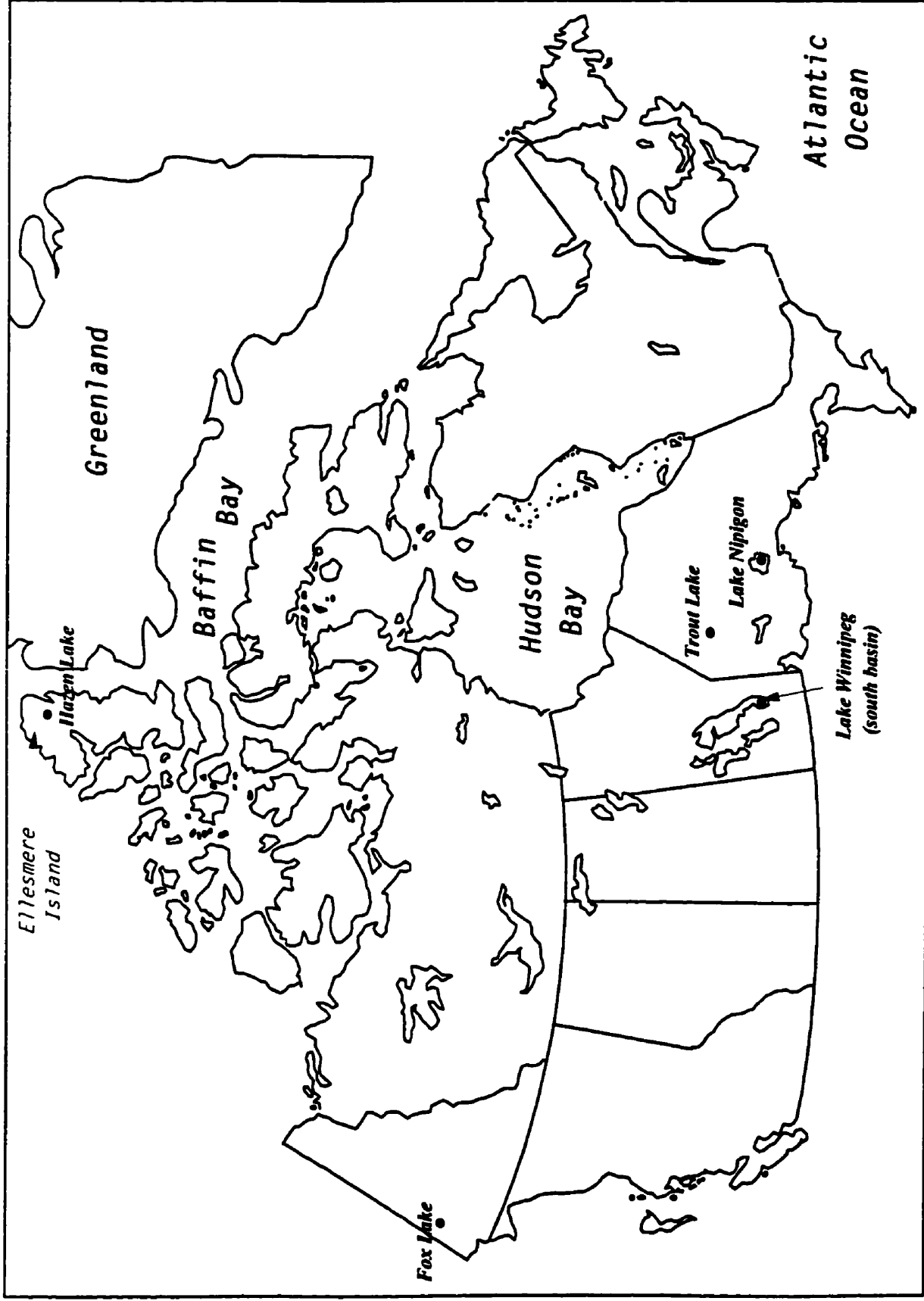


Figure 6.14 Map of Canada and surrounding region showing the locations of the lakes sampled in this study.

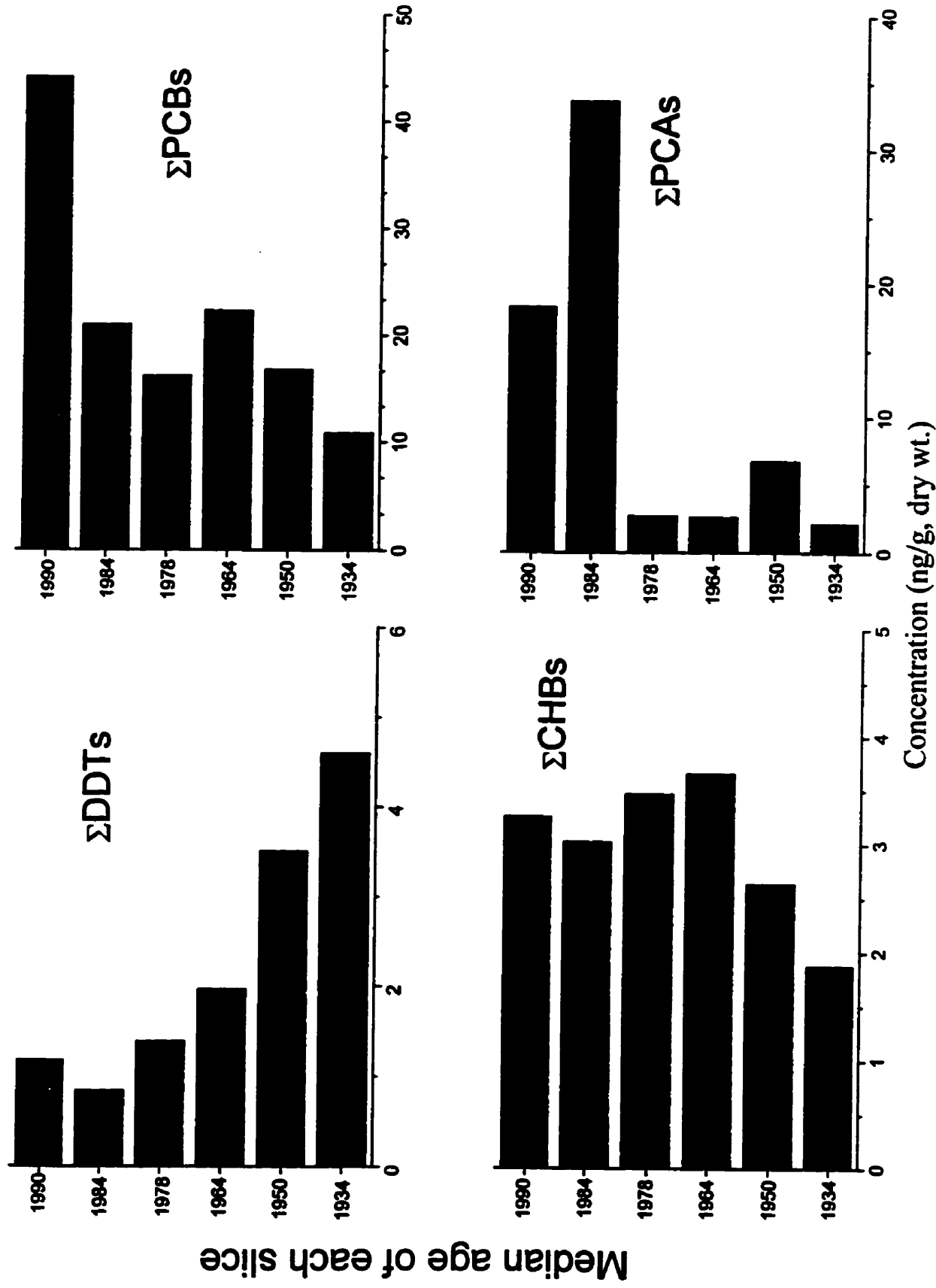


Figure 6.15. Concentration profiles of ΣPCBs, ΣDDTs, ΣCHB and ΣPCAs in a dated sediment core from Lake Nipigon, Ont.

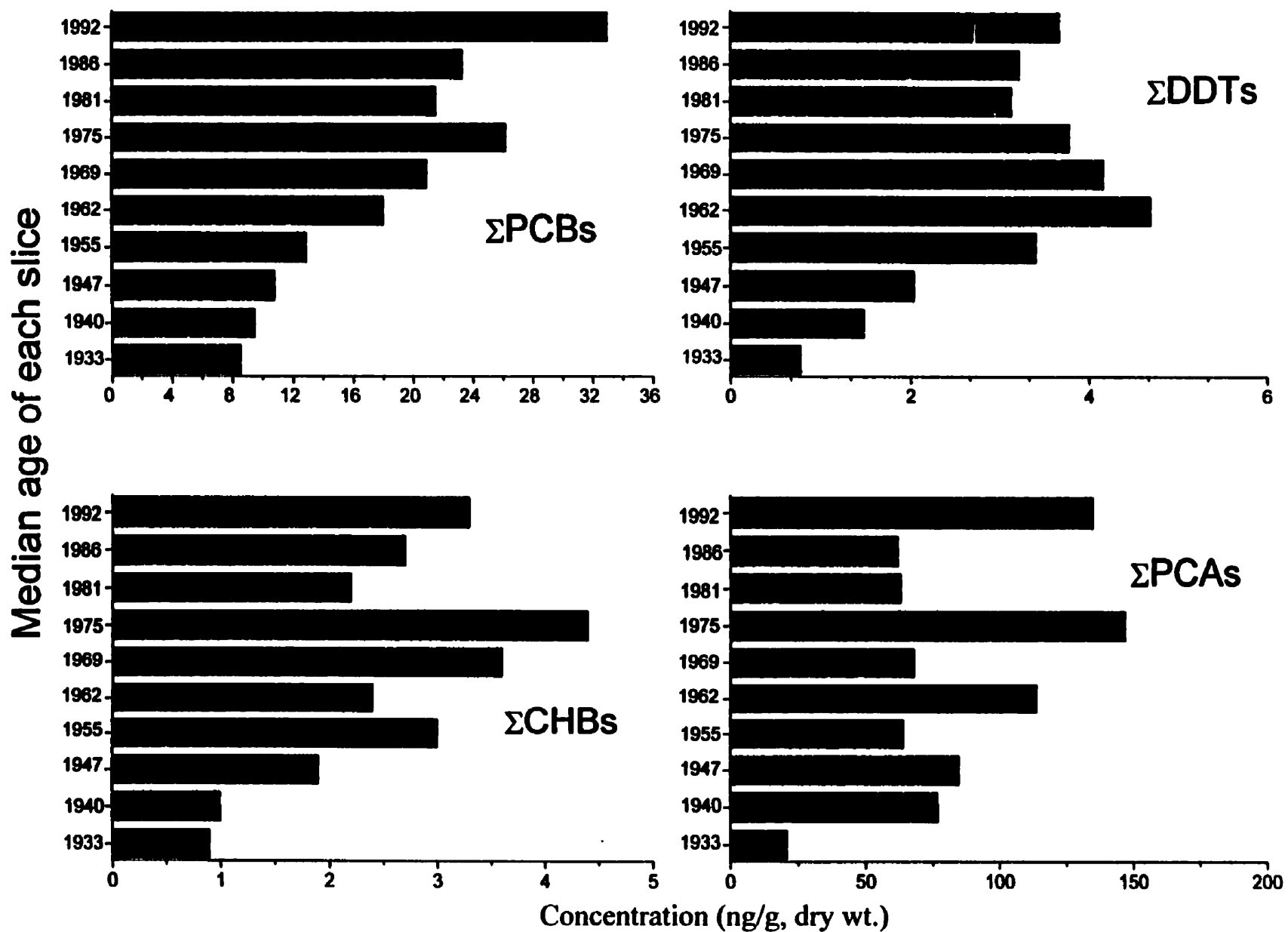


Figure 6.16. Concentration profiles of  $\Sigma$ PCBs,  $\Sigma$ DDTs,  $\Sigma$ CHB and  $\Sigma$ PCAs in a dated sediment core from the southern basin of Lake Winnipeg, MB.

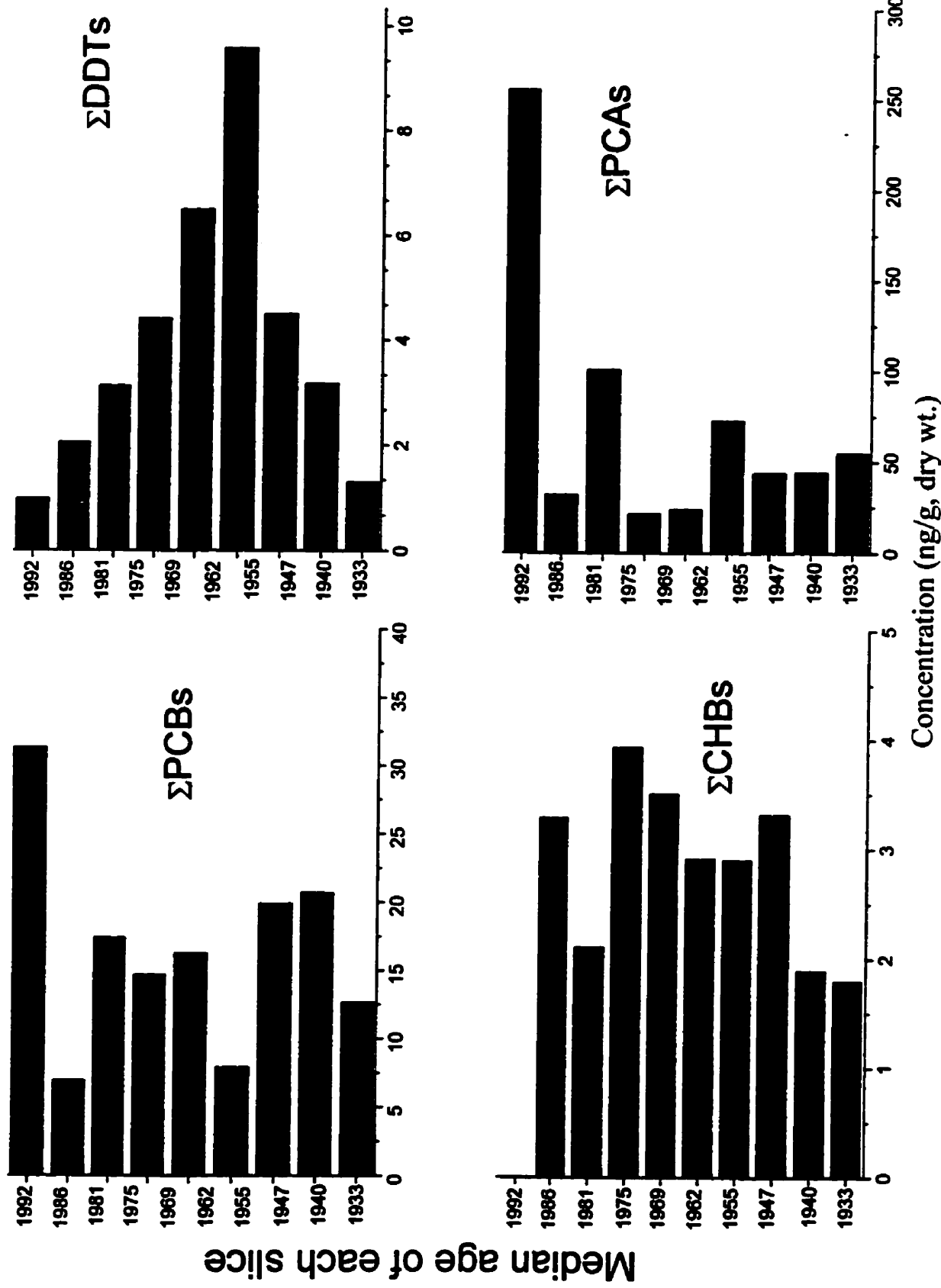


Figure 6.17. Concentration profiles of ΣPCBs, ΣDDTs, ΣCHB and ΣPCAs in a dated sediment core from Fox Lake, Yukon.

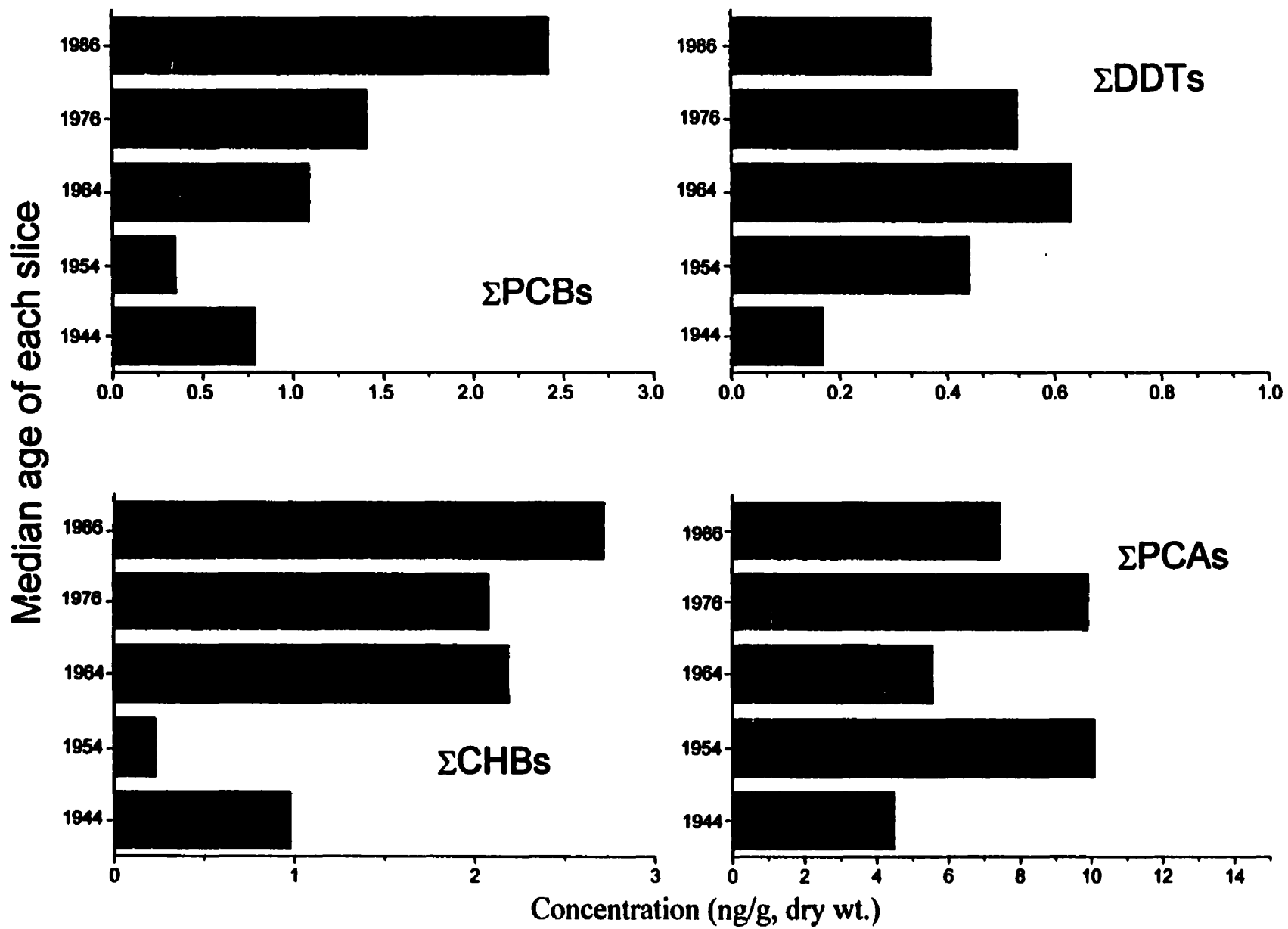


Figure 6.18. Concentration profiles of  $\Sigma$ PCBs,  $\Sigma$ DDTs,  $\Sigma$ CHB and  $\Sigma$ PCAs in a dated sediment core from Hazen Lake, high Arctic

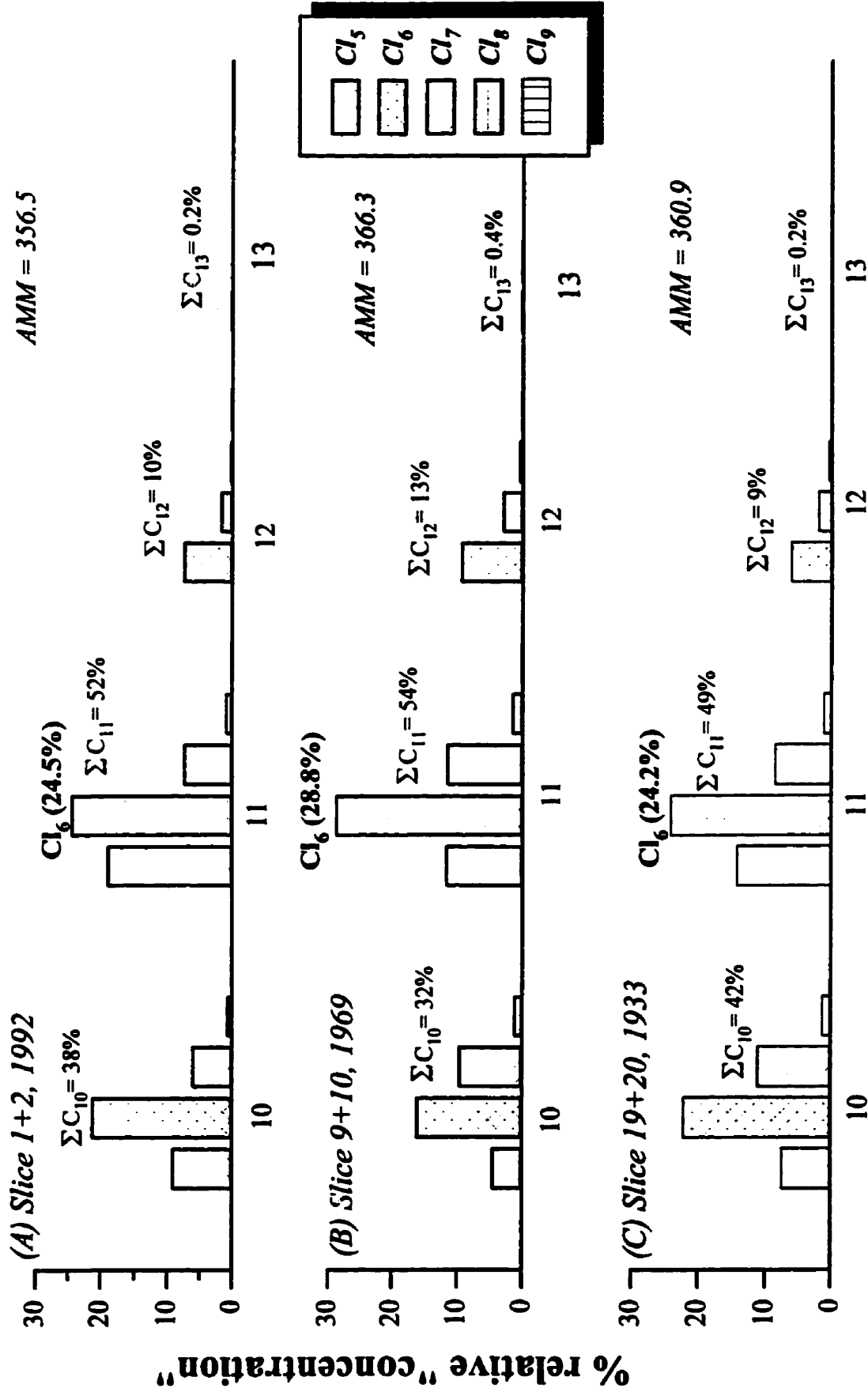


Figure 6.19. Variation in the congener ion signal profiles with sampling depth of dated sediment slices from Lake Winnipeg (MB). The most abundant congener (highlighted in bold), whose [M-Cl]<sup>-</sup> ion is used as the quantitation ion, is shown for each slice.

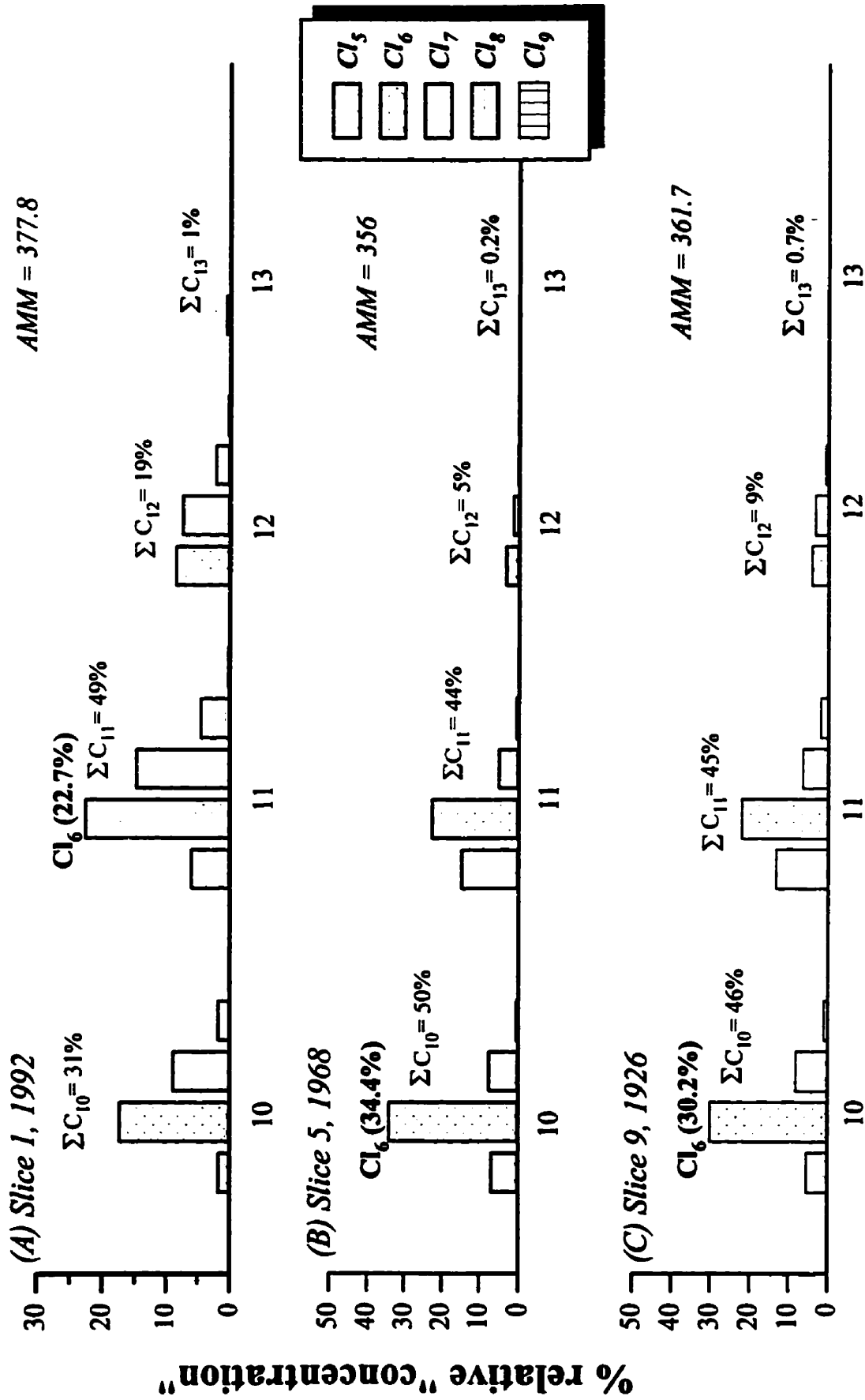


Figure 6.20. Variation in the congener ion signal profiles with sampling depth of dated sediment slices from Fox Lake (Yukon). The most abundant congener (highlighted in bold), whose [M-Cl]<sup>-</sup> ion is used as the quantitation ion, is shown for each slice.

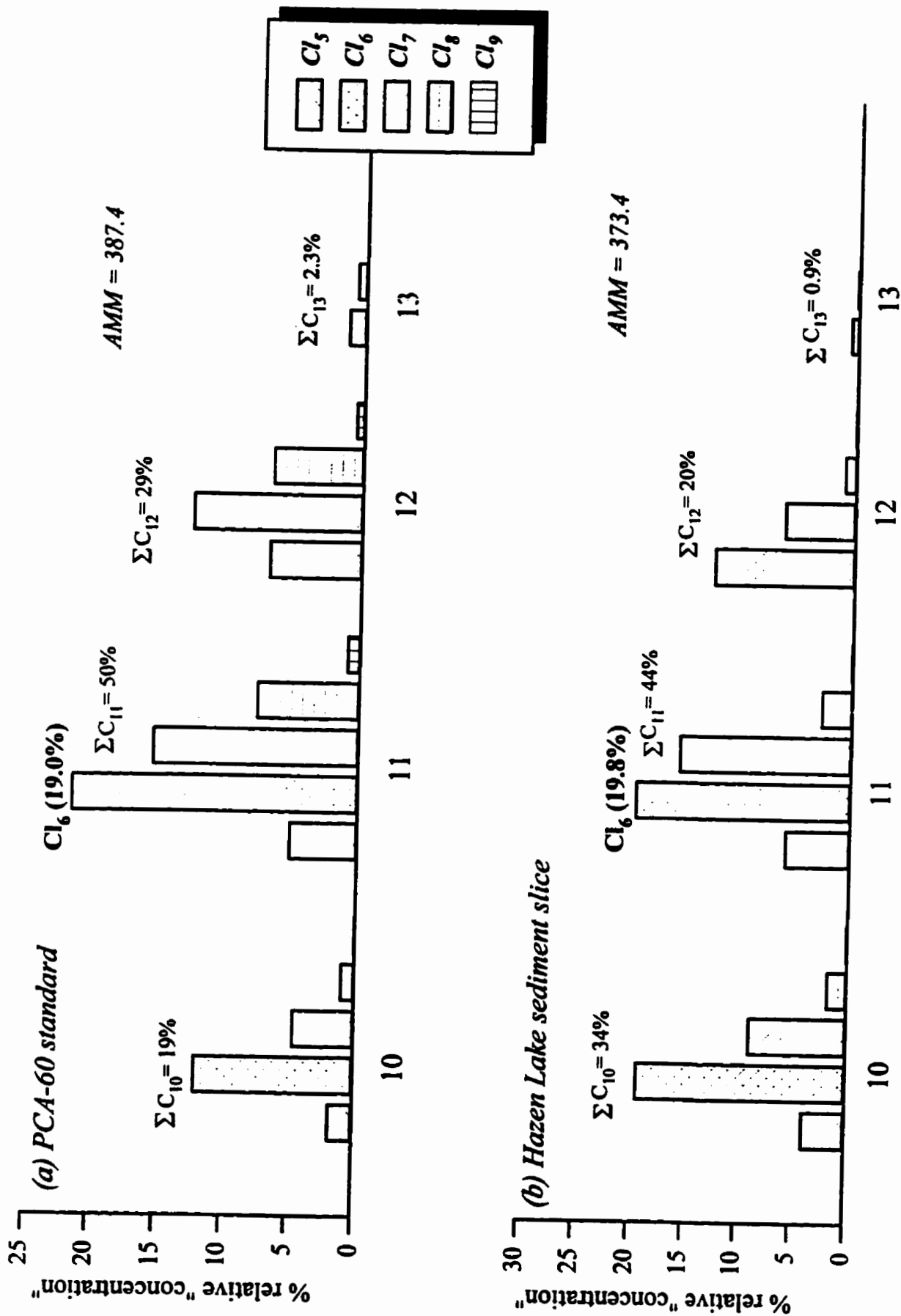


Figure 6.21. Ion signal profiles for (a) PCA-60 standard and (b) sediment from Hazen lake (high Arctic). The most abundant congener (highlighted in bold), whose  $[M-Cl]^-$  ion is used as the quantitation ion, is shown for each.

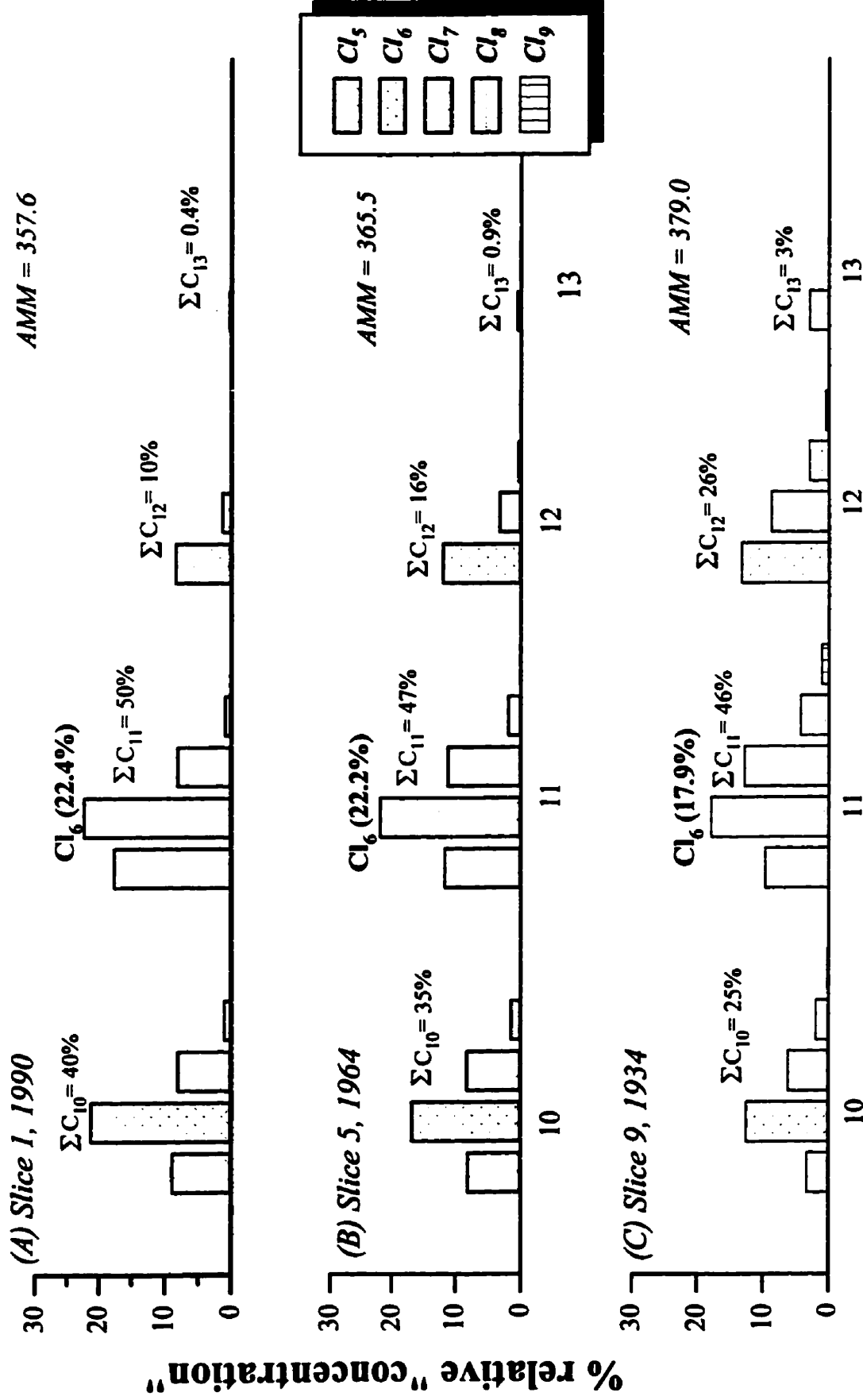


Figure 6.22. Variation in the congener ion signal profiles with sampling depth of dated sediment slices from Lake Nipigon (Ont). The most abundant congener (highlighted in bold), whose  $[M-Cl]^-$  ion is used as the quantitation ion, is shown for each slice.

**Table 6.7. Focused corrected fluxes of  $\Sigma$ PCA ( $\mu\text{g}/\text{m}^2 \text{ yr}$ ) and characteristics of the lakes investigated in this study.**

<b>Lake</b>	<b>Latitude/Longitude</b>	<b>Sedimentation rate (<math>\text{g}/\text{m}^2 \text{ yr}</math>)</b>	<b>Focusing Factor<sup>a</sup></b>	<b>Conc. of <math>\Sigma</math>PCA in surface slice (<math>\text{ng}/\text{g}</math> dry wt.)</b>	<b>Surface flux<sup>b</sup> (<math>\mu\text{g}/\text{m}^2 \text{ yr.}</math>)</b>	<b>Maximum flux (<math>\mu\text{g}/\text{m}^2 \text{ yr.}</math>)</b>
Winnipeg (Man)	50°23'N/96°22'W	1000	1.2	176	147	147
Fox (Yukon)	61°14'N/135°28'W	126	0.95	257	34	34
Nipigon (Ont)	49°25'N/85°30'W	411	2.83	18	3	5
Hazen (Arctic)	81°45'N/71°30'W	278	1.4	4.5	0.9	2

<sup>a</sup> Focusing factor = sediment core  $^{210}\text{Pb}$  / average regional  $^{210}\text{Pb}$ .

<sup>b</sup> Surface flux = sedimentation rate x conc. of  $\Sigma$ PCAs in surface slice / focusing factor.

The most important observation that can be made regarding PCAs in the sediments of the 4 lakes investigated is that they are *present*; even in sediments from the most northerly site, Lake Hazen (the largest lake north of the Arctic Circle (66°30'N), situated at the northern end of Ellesmere Island) (*see* Figure 6.18).

### 6.7.2 PROFILES OF $\Sigma$ PCAs AND OTHER OCs IN SEDIMENT CORES.

In general, the  $\Sigma$ PCA levels in the four lakes examined in this study were highest for sediment slices dated from the 1980s to the 1990s, which is consistent with the usage patterns of PCAs. Concentration profiles of  $\Sigma$ PCA relative to  $\Sigma$ PCB,  $\Sigma$ DDT and  $\Sigma$ CHB for the 4 lakes are shown in Figures 6.15–6.18. The concentration of  $\Sigma$ PCA and the other OCs in dated sediment slices have all been blank corrected, by using the the observed PCA concentration in the oldest slice (usually *pre*-1930s sediment) from each lake as the background.

The highest concentration of  $\Sigma$ PCA in surface slices was observed in Fox lake, a sub-Arctic lake in the Yukon adjacent to the Alaska Highway, (257 ng/g dry wt.). Compared to other OCs,  $\Sigma$ PCAs are 8 times higher than  $\Sigma$ PCBs (31.3 ng/g), 100 times higher than  $\Sigma$ CHBs (2.1 ng/g) and over two orders of magnitude higher than  $\Sigma$ DDTs (0.01 ng/g) (Figure 6.17) [123,163]. The high  $\Sigma$ PCA concentration relative to other OCs would suggest anthropogenic inputs, although actual sources for PCAs are not known.

Concentrations of  $\Sigma$ PCAs in surface slices from the southern basin of Lake Winnipeg (176 ng/g dry wt.) were also higher than  $\Sigma$ PCBs (33 ng/g),  $\Sigma$ DDTs (6 ng/g) and  $\Sigma$ CHBs (3.3 ng/g) (Figure 6.16) [123,163]. Concentration profiles of  $\Sigma$ PCAs in slices from this core closely resembled that of  $\Sigma$ PCB; the highest  $\Sigma$ PCA

and  $\Sigma$ PCB levels were found in slices 1992 and 1975;  $\Sigma$ CHB levels were also elevated for the slice dated 1975.

The elevated levels of  $\Sigma$ PCA relative to  $\Sigma$ PCBs observed in water collected from the Red River in Selkirk ( $30 \pm 14$  ng/L), prior to its entry to the southern basin of Lake Winnipeg, in addition to the elevated levels observed in surface sediments from Lake Winnipeg, suggest that contamination is *via* point sources. The variation in the ion signal profiles for the Red River water sample (*see* Figure 6.8(b)) and the surface slice from Lake Winnipeg (*see* Figure 6.19(a)), also implies additional inputs to Lake Winnipeg, possibly from the Winnipeg River, or that biodegradation is occurring (*see Section 6.7.4*).

$\Sigma$ PCA concentrations in surface slices from Lake Nipigon exceeded those of  $\Sigma$ CHBs (3.26 ng/g) and  $\Sigma$ DDTs (1.18 ng/g), but were lower than  $\Sigma$ PCBs (44.1 ng/g) (Figure 6.15) [163,164]. The highest  $\Sigma$ PCAs for this core is observed for the 1984 dated slice of 33.7 ng/g, prior to which a sharp decline in  $\Sigma$ PCA concentrations is observed.

Concentrations of  $\Sigma$ PCAs in surface sediments from Hazen lake in the high Arctic (4.5 ng/g) were 2 times higher than  $\Sigma$ PCBs (2.42 ng/g), 1.5 times higher than  $\Sigma$ CHBs (2.72 ng/g) and 12 times higher than  $\Sigma$ DDTs (0.37 ng/g) (Figure 6.18) [70,164]. The remote location of this lake and the low levels of  $\Sigma$ PCA, as well as other OCs, imply that long range atmospheric transport is the only mode of input of contaminants to this lake. The decline of  $\Sigma$ PCA in older sediment slices, however, is not apparent, and may be due to diffusion of congeners into the sediment bed because of the low sedimentation rate of this lake [70].

### 6.7.3 FLUX CALCULATIONS

Surficial fluxes of  $\Sigma$ PCA relative to  $\Sigma$ PCB,  $\Sigma$ DDT and  $\Sigma$ CHB to the 4 lakes are shown in Table 6.8. Lake Winnipeg receives inputs of PCAs *via* point sources and so we can expect the flux of  $\Sigma$ PCA to be high. In fact, the fluxes of  $\Sigma$ PCA to Lake Winnipeg were 4 times higher than that of Fox lake and 55 times higher than Lake Nipigon. The flux of  $\Sigma$ PCA to Hazen lake was also lower, 200-fold, than that to Lake Winnipeg.

The flux of  $\Sigma$ PCA to Lake Winnipeg ( $147 \mu\text{g}/\text{m}^2 \text{ yr}$ ) surface sediments was significantly higher than those of  $\Sigma$ CHB ( $2733 \text{ ng}/\text{m}^2 \text{ yr}$ ) and  $\Sigma$ DDT ( $5000 \text{ ng}/\text{m}^2 \text{ yr}$ ), but only 5 times higher than that of  $\Sigma$ PCB [123,163]. Similar observations can be made for contaminant fluxes to Fox lake. The flux of  $\Sigma$ PCA to Fox lake ( $34 \mu\text{g}/\text{m}^2 \text{ yr}$ ) was 100-fold higher than of  $\Sigma$ CHB ( $280 \text{ ng}/\text{m}^2 \text{ yr}$ ) and 2 orders of magnitude higher than of  $\Sigma$ DDT ( $1.3 \text{ ng}/\text{m}^2 \text{ yr}$ ).  $\Sigma$ PCB fluxes, however, were only 8 times lower than that of  $\Sigma$ PCA to Fox lake [123].

The flux of  $\Sigma$ PCA to Lake Nipigon ( $2658 \text{ ng}/\text{m}^2 \text{ yr}$ ) was higher than  $\Sigma$ CHB ( $298 \text{ ng}/\text{m}^2 \text{ yr}$ ) and  $\Sigma$ DDT ( $171 \text{ ng}/\text{m}^2 \text{ yr}$ ), but 2.5 times lower than that of  $\Sigma$ PCB ( $6405 \text{ ng}/\text{m}^2 \text{ yr}$ ) [123]. In Hazen lake, the flux of  $\Sigma$ PCA was also higher than of the other OCs. The fluxes of  $\Sigma$ PCB,  $\Sigma$ DDT and  $\Sigma$ CHB were 480, 73 and 540  $\text{ng}/\text{m}^2\text{yr}$ , respectively, while the  $\Sigma$ PCA flux was 893  $\text{ng}/\text{m}^2 \text{ yr}$ . [70,164].

### 6.7.4 VARIATION OF CONGENER PROFILES WITH SAMPLING DEPTH.

Closer examination of the congener profiles for sediment slices from Lake Winnipeg and Fox lake indicate signs of microbial degradation (*see* Figures 6.19 and 6.20). Inspection of the ion intensities of congeners from sediment slices in

**Table 6.8. Focused corrected fluxes (ng/m<sup>2</sup> yr) of  $\Sigma$ PCAs,  $\Sigma$ CHBs,  $\Sigma$ DDTs and  $\Sigma$ PCBs in surface sediments from lakes in the Yukon, Ontario, the Arctic and in Manitoba.**

<b>Lake</b>	<b><math>\Sigma</math>PCAs</b>	<b><math>\Sigma</math>CHBs</b>	<b><math>\Sigma</math>DDTs</b>	<b><math>\Sigma</math>PCBs</b>
Winnipeg	146666	2733 <sup>a</sup>	5000 <sup>b</sup>	27500 <sup>b</sup>
Fox	34086	280 <sup>a</sup>	1.33 <sup>b</sup>	4155 <sup>b</sup>
Nipigon	2658	298 <sup>b</sup>	171 <sup>b</sup>	6405 <sup>b</sup>
Hazen	893	540 <sup>d</sup>	73 <sup>c</sup>	480 <sup>d</sup>

<sup>a</sup> Stern *et al.* (1996) [163]

<sup>b</sup> Muir *et al.* (1996) [123]

<sup>c</sup> Muir *et al.* (1995) [69]

<sup>d</sup> Muir *et al.* (1996) [164]

Fox lake reveals that  $\Sigma C_{10}$  and  $\Sigma C_{12}$  congeners in the top slice account for 31 and 19% of the ion current, respectively, while further down the sediment bed (slice 9), the  $\Sigma C_{10}$  and  $\Sigma C_{12}$  congeners now account for 46 and 9%, respectively, of the ion current (see Figure 6.20). This variation in abundances of  $\Sigma C_{10}$  and  $\Sigma C_{12}$  congeners can be further illustrated by examining the abundances of individual congeners. The abundance of the predominant congener in the  $C_{12}$  homologue group, viz.,  $C_{12}H_{20}Cl_6$ , accounts for 8.6% of the abundance in slice 1, and decreases by more than 2-fold in slice 9 to 4.4%. Conversely, the predominant congener in the  $C_{10}$  homologue group, viz.,  $C_{10}H_{16}Cl_6$ , increases from 17.5% in slice 1 to 30.2% in slice 9.

In Section 6.7.2 we inferred that the input of PCAs to Fox lake was probably from anthropogenic sources. Therefore, the low abundance of  $\Sigma C_{13}$  congeners observed in slices from this lake could be the result of (i) the PCA formulation initially discharged into the lake did not contain significant amounts of the  $C_{13}$  congeners, or more likely (ii) rapid aerobic degradation of  $C_{13}$  congeners in surficial sediments and much slower degradation in anaerobic subsurface layers to lower congeners. Additional evidence for the latter assumption can be made by inspecting sediment slices from Lake Winnipeg.

The variation of congener abundances in Lake Winnipeg slices (see Figure 6.19), is, admittedly, less pronounced than in Fox lake; differences in the abundances of  $\Sigma C_{10}$ ,  $\Sigma C_{11}$  and  $\Sigma C_{12}$  congeners in the surface and bottom slices are negligible. We have, however, established that one possible source of input of PCAs to Lake Winnipeg is via the Red River with additional inputs likely to be from the Winnipeg River. Nonetheless, the presence of  $C_{13}$  congeners in Red River water samples from Selkirk, MB., as observed in Figure 6.8, and their

absence in Lake Winnipeg sediments, *must* imply that the transformation is a result of microbial degradation. Perhaps the high levels and recent inputs of PCAs to Lake Winnipeg give rise to greater degradative capacity for microorganisms (*i.e.*, acclimation) at the sediment-water interface.

## Summary

The EI mass spectra of individual PCA congeners were useful, to some extent, for characterizing the positional isomers of the compounds investigated in this study. For compounds containing vicinal chlorine atoms located at the terminal positions, we observed an abundant  $m/z$  139 ion,  $C_5H_9Cl_2^+$ , whose structure is that of a five- or six-membered ring, with one of the chlorine atoms as part of the ring. For non-terminal chlorine compounds, this ion was not significant. Other interesting aspects of the EI mass spectra include the occurrence of: (i) five-membered cyclic  $C_4H_8Cl^+$  ( $m/z$  91) and six-membered cyclic  $C_5H_{10}Cl^+$  ( $m/z$  105) ions, (ii) sterically unfavored structures formed, we believe, by the randomization of the double bond, and (iii) many even-electron odd-mass ions of low  $m/z$  belonging to a number of distinct hydrocarbon ion series.

The ECNI mass spectral studies done on the synthesized PCA congeners reveal, as expected, that the temperature of the ion source and the concentration of injected PCAs have profound effects on the appearance on the spectra. By increasing the ion source temperature it was found that there was a decrease in the abundance of both the adduct ion,  $[M+Cl]^-$  and the  $[M-Cl]^-$  ion, while the abundance of structurally non-characteristic ions,  $HCl_2^-$  and  $Cl_2^-$ , increased. By varying the concentration of the injected PCA we showed that the abundance of the  $[M+Cl]^-$  increased, the most notable increase occurring for congeners containing chlorine atoms at terminal positions.

The analytical protocol described for quantifying PCAs in environmental matrices by HRGC/ECNI-HRMS provides significant improvements over existing methods for several reasons: (1) its unparalleled sensitivity, specificity and

selectivity, (2) it is the first that reports PCA levels according to formula groups, (3) it avoids interferences from other PCAs and other persistent organochlorine compounds, and (4) it offers a high degree of accuracy. These features were demonstrated in *Chapters 5 and 6*.

The environmental results illustrated in *Chapter 6* represent the first data on PCAs in lakes and rivers in Canada and the U.S.A, aquatic species in the U.S.A, marine mammals and in humans. Future work in this area would involve the analysis of larger, more representative sample sizes; variations in PCA concentrations with age and sex of the mammals will be further elucidated. Additionally, PCA concentrations will be examined in more lakes to see whether there is a decline in concentration with increasing northern latitude.

In the future, the accuracy of existing and newer methods for PCA analysis will be assessed as we have initiated an International Interlaboratory study consisting of 5 European and 5 North American laboratories. Participating laboratories were supplied with a known amount of the external standard PCA-60 and were asked to quantify PCA-70, the analytical reference standard (PCA-1, *see* Section 3.3.3 and Figure 5.9(a)) and two real world biological samples (RWBS), all of which were supplied in unstated amounts. At the time of writing this thesis, there were still a few participating laboratories that had not submitted their results, and the outcome of the study could not be included in this thesis. A manuscript, however, will be prepared documenting the results once they become available.

Future work will also involve extending the analytical protocol to the analysis of higher chain length PCAs, *viz*, C<sub>14</sub>-C<sub>17</sub>, to see whether these compounds are also widespread contaminants of freshwater environments.

## **LITERATURE CITED**

1. Serrone, D.M.; Birtley, R.D.N.; Wiegand, W.; Millischer, R. 1987. *Food Chem. Toxicol.*, 25, 553-562.
2. Environment Canada, Priority Substances Program, CEPA Assessment Report, Chlorinated Paraffins. 1993. Commercial Chemicals Branch, Hull Quebec.
3. Zitko, V. 1980. In: Handbook of Environmental Chemistry. Springer-Verlag. Vol 3A. 149-156.
4. Chambers, G.; Ubbelohde, A.R. J. 1955. *Chem. Soc.*, 285-295.
5. Fredricks, P.S.; Tedder, J.M. J. 1960. *Chem. Soc.*, 144-150.
6. Colebourne, N.; Stern, E.S. J. 1965. *Chem. Soc.*, 3599-3605.
7. Mukherjee, A.B. 1990. The use of Chlorinated Paraffins and their possible effects in the Environment. National Board of Waters and the Environment, Helsinki, Finland. Series A 66, 53pp.
8. Scheer, W.E. 1944. *Chem. Ind.* 54, 203-205
9. Kirk-Othmer. 1980. Chlorinated Paraffins. Kirk-Othner Encyclopaedia of Chemical Technology. 3rd Edition, John Wiley and Sons, Inc.
10. Willis, B., Crookes, M.J., Diment, J., Dobson, S.D. 1994. Environmental hazard Assessment: Chlorinated Paraffins. Toxic Substances Division. Dept. of the Environment.
11. Swedish National Chemicals Inspectorate. 1991. KEMI Report No. 1.

12. Environmental Protection Agency. 1991. Office of Toxic Substances. Rm1 Decision Package. Chlorinated Paraffins. Environmental risk assessment. Washington DC.

13. Kato, Y., Kenne, K. 1996. *Pharmacol. and Toxicol.*, 79, 23-28.

14. Windrath, O.M and Stevenson, D.R. 1985. Chlorination and bromochlorination paraffins as flame retardants. *Plastics Compounding*. pp 38-52.

15. Morrison, R.T. and Boyd, R.N. 1983. *Organic Chemistry*. 4th Edition, Allyn and Bacon, Inc.

16. Zitko, V. And Arsenault, E. 1977. *Adv. Environ. Sci. Technol.*, 8, 409-418

17. Ostrowski, P.J. 1996. Personal communication, Occidental Chemical Corporation, Basic Chemicals Group. Niagara Falls, NY.

18. Campbell, I.; McConnell, G. 1980. *Environ. Sci. Technol.*, 14; 1209-1214.

19. Drouillard, K.G.; Tomy, G.T.; Muir, D.C.G. and Friesen, K.J. 1997. *Submitted to Environ. Toxicol. Chem.*

20. Drouillard, K.G.; Hiebert, T.; Tran, P.; Tomy, G.T.; Muir, D.C.G and Friesen, K.J. 1997. *Submitted to Environ. Toxicol. Chem.*

21. Hardie, D.W.F. 1964. Chlorinated Paraffins, Kirk-Othmer Encycl. Chem. Technology, 2nd Edition, Vol.5,

22. Svanberg, O. and Linden, E. 1979. *Ambio.*, 8:206-209.

23. Environment Canada, Health and Welfare Canada. 1993. Priority Substances List Assessment Report: Chlorinated Paraffins. Government of Canada, Catalogue No. En 40-215/17E, ISBN 0-662-20515-17E: 32pp.
24. Metcalfe-Smith, J.L.; Maguire, R.J.; Batchelor, S.P.; Bennie, D.T. 1995. Occurrence of Chlorinated Paraffins in the St. Lawrence River near a Manufacturing Plant in Cornwall, Ontario. Aquatic Ecosystem Protection Branch. National Water Research Institute. Dept. of the Environ., Burlington, Ont.
25. Murray, T.M.; Frankenberry, D.H.; Steele, D.H.; Heath, R.G. 1988. Chlorinated Paraffins: A report on the findings from two filed studies, Sugar Creek, Ohio and Tinkers Creek, Ohio., Vol. 1, Technical Report, U.S. Environmental Protection Agency, EPA/560/5-87/012. 150pp.
26. Reiger, R; Ballschmiter, K. 1995. *Fres. J. Anal. Chem.*, 352, 715-724.
27. Tomy, G.T. 1996. *Unpublished results*.
28. Tomy, G.T.; Stern, G.A.; Muir, D.C.G.; Fisk, A.T.; Cymbalisky, C.D. and Westmore, J.B. 1997. *Anal. Chem.*, In press.
29. Tomy, G.T.; Muir, D. C. G.; Westmore, J. B.; Stern, G.A. 1993. Proceedings of the 41st Annual Conference on Mass Spectrometry and Allied Topics, San Francisco, CA. May 30 - June 4.
30. Müller, M.D. and Schmid, P.P. 1984. *J. High Resol. Chromatogr. Chromatogr. Commun.*, 7, 33-37
31. Schmid, P.P. and Muller, M.D. 1985. *J. Assoc. Offic. Anal. Chem.*, 68, 427-430.

32. Kraemer, W. and Ballschmiter, K. 1987. *Fres. J. Anal. Chem.*, 327, 47-48.
33. Hollies, J.I.; Pinnington, D.F.; Handley, A.J.; Baldwin, M.K.; Bennett, D. 1979. *Anal. Chim. Acta.*, 111. 201-213
34. Svanberg, O.; Bengtsson, B.E.; Lindén, E.; Lunde, G.; Baumann-Ofstad. 1978. *Ambio* 7, 64
35. Gjøs, N.; Gustavsen, K.O. 1982. *Anal. Chem.*, 54, 1316-1318.
36. Jansson, B.; Andersson, R.; Asplund, L.; Bergman, Å.; Litzén, K.; Nylund, K.; Reutergårdh, L.; Sellström, U.; Uvemo, U-B.; Wahhlerg, C.; Wideqvist, U. 1991. *Fresenius. J. Anal. Chem.*, 340, 439-445.
37. Stalling, D.L.; Tindle, R.C.; Johnson, J.L. 1972. *J. Assoc. Off. Anal. Chem.*, 55, 32-38.
38. Junk, S.A.; Meisch, H.-U. 1993. *Fres. J. Anal. Chem.*, 347, 361-363.
39. Walter, B.; Ballschmiter, K. 1991. *Fres. J. Anal. Chem.*, 340, 246-249.
40. Mullin, M.D.; Pochini, C.M.; McCrindle, S.; Romkes, M.; Safe, S.H.; Safe, L.M. 1984. *Environ. Sci. Technol.*, 18, 468-476.
41. Alford-Stevens, A. L. 1986. *Environ. Sci. Technol.*, 20, 1194-1199.
42. Rankin, P.C. 1971. *J. Assoc. Off. Anal. Chem.*, 54, 1340-1348.
43. Dougherty, R.C.; Dalton, J.; Biros, F.J. 1972. *Org. Mass Spectrom.*, 6, 1171-1181.
44. Ong, V.S.; Hites, R.A. 1994. *Mass Spectrom. Rev.*, 13, 259-283.

45. Valovoi, V.A.; Polyakova, A.A. 1967. *Zhur. Org. Khim.*, 3, 842-852  
(*English Translation*).
46. NIST Standard Reference Database 1A. 1994. NIST/ EPA/ NIH Mass Spectral Database, Version 4.5, NIST, Gaithersburg, MD 20899.
47. Duckworth, H.E.; Barber, R.C.; Venkatasubramania, V.S. 1988. *Mass Spectroscopy*, 2nd Ed., Cambridge University Press, Cambridge.
48. Chapman, J.R. 1993. *Practical Organic Mass Spectrometry. A Guide for Chemical and Biochemical Analysis*. 2nd Ed., John Wiley & Sons.
49. McDowell, C.A. 1963. *Mass Spectrometry*. McGraw-Hill Book Company, Inc.
50. Cooks, R.G.; Beynon, J.H.; Caprioli, R.M.; Lester, G.R. 1973. *Metastable Ions*, Elsevier, Amsterdam
51. Stern, G.A. Ph.D Thesis. 1990. *Mass Spectrometric and NMR Studies of some Beta-Ketoenolate and Monothio-Beta-Ketoenolate Complexes of Rhodium(III) and Iridium(III)*. University of Manitoba.
52. Rose, M.E.; Johnstone, R.A.W. 1982. *Mass Spectrometry for Chemists and Biochemists*. Cambridge University Press, Cambridge.
53. Lambert, J.B.; Shurvell, H.F.; Lightner, D.; Cooks, R.G. 1987. *Introduction to Organic Spectroscopy*. 1st Ed. Macmillan Publishing Company, New York.
54. Dempster, A.J. 1921. *Phys. Rev.*, 18, 415.
55. Neir, A.O. 1947. *Rev. Sci. Instrum.*, 18, 398.

56. Munson, M.S.B.; Field, F.H. 1966. *J. Amer. Chem. Soc.*, 88, 2621-2630.
57. Harrison, A.G. 1983. *Chemical Ionization Mass Spectrometry*, 1st Ed. CRC Press, Boca Raton, Fla.
58. Ong, V.S.; Hites, R.A. 1993. *J. Amer. Soc. Mass Spectrom.*, 4, 270-277.
59. Hunt, D.F.; Crow, F.W. 1978. *Proceedings of the 9th Materials Research Symposium*, NBS Special Publication 519, National Bureau of Standards, Washington, D.C., pg 601-607.
60. Blakley, C.R.; Carmody, J.J.; Vestal, M.L. 1980. *J. Amer. Chem. Soc.*, 102, 5931.
61. Blakley, C.R.; Vestal, M.L. 1983. *Anal. Chem.*, 55, 750.
62. Schmelzeisen-Redeker, G.; McDowall, M.A.; Giessmann, U.; Levsen, K.; Röllgen, F.W. 1985. *J. Chromatog.*, 323, 127-133.
63. Trio 1000 LC/GC/MS. 1992. Fisons Instruments. VG MassLab., Manchester. England.
64. Mach 3X Training course. 1995. Kratos Analytical. Manchester. England.
65. Boyd, R.K.; Beynon, J.H. 1977. *Org. Mass Spectrom.*, 12, 163-165.
66. Shushan, B.; Boyd, R.K. 1981. *Anal. Chem.*, 53, pp 421-427.
67. Lacey, M.J.; Macdonald, C.G. 1979. *Anal. Chem.*, 51, pp 691-695.
68. Karasek, F.W.; Clement, R.E. 1988. *Basic gas chromatography-mass spectrometry, principles and techniques*. Elsevier Science Publishing Company,

Canada.

69. March, J. 1985. *Advanced Organic Chemistry*. 3rd Ed., John Wiley & Sons., Toronto.
70. Muir, D. C. G.; Grift, N. P.; Lockhart, W. L.; Wilkinson, P.; Billeck, B. N.; Brunskill, G. J. 1995. *Sci. Total Environ.*, 160/161, 447-457.
71. Muir, D. C. G.; Ford, C. A.; Grift, N. P. Metner, D. A.; Lockhart, W. L. 1990. *Arch. Environ. Contam. Toxicol.*, 19, 530-542.
72. Hoff, R.M.; Muir, D.C.G.; Grift, N.P. 1992. *Environ. Sci. Technol.*, 26, 266-275.
73. Rawn, D.F.; Halldorson, T.H.J.; Muir, D.C.G. 1996. *In press*.
74. Robbins, J.A. 1978. Geochemical and geophysical applications of radioactive lead. In: J.O. Nriagu (Ed.), *The Biogeochemistry of Lead in the Environment*, Part A. Elsevier, Amsterdam, pp 285-393.
75. Muir, D.C.G.; Ford, C.G.; Stewart, R.E.A.; Smith, T.G.; Addison, R.F.; Zinck, M.E. and Beland, P. 1990. *Can. Bull. Fish. Aquat. Sci.*, 224, 165-190.
76. Dewailly, E.; Nantel, A.; Weber, J-P. and Meyer, F. 1989. *Bull. Environ. Contam. Toxicol.*, 34, 641-646.
77. Zitko, V. 1973. *J. Chromatogr.*, 81. 152.
78. F. W. McLafferty. 1962. *Anal. Chem.*, 34, 2-15
79. A. M. Duffield, S. D. Sample and C. Djerassi. 1966. *Chem. Commun.*, 193

80. A. Maccoll, and D. Mathur. 1980. *Org. Mass Spectrom.*, 15, 483
81. M. P. Barbalas, F. Turecek and F. W. McLafferty, 1982. *Org. Mass Spectrom.*, 17, 595
82. J. Collin. 1956. *Bull. Soc. Roy. Sci. Liège.*, 25, 520-540.
83. T. Nishishita, F. M. Bockhoff and F. W. McLafferty. 1977. *Org. Mass Spectrom.*, 12, 16-20
84. M. M. Green, R. J. Cook, J. M. Schwab and R. B. Roy. 1970. *J. Amer. Chem. Soc.*, 92, 3076-3083
85. K. C. Kim, J. H. Beynon and R. G. Cooks. 1974. *J. Chem. Phys.*, 61, 1305-1314
86. D. Harnish, J. L. Holmes, F. P. Lossing, A. A. Mommers, A. Maccoll; M. N. Mruzek. 1990. *Org. Mass Spectrom.*, 25, 381-385.
87. S.G. Lias, J.E. Bartmess, J.F. Lebnann, J.L Homes, R.D. Levin and W.G.Mallard. 1988. *J. Phys. Chem. Ref. Data*, 17, Suppl. 1
88. D.J. McAdoo, F.W. McLafferty and P.F Bente III. 1972. *J. Amer. Chem. Soc.*, 94, 2027-2033
89. L.W. Sieck, R. Gordon Jr and P. Ausloos. 1972. *J. Amer. Chem. Soc.*, 94, 7157-7150
90. Stemmler, E.A. and Hites, R.A. 1988. *Biomed. Mass Spectrom.*, 15, 659-667.

91. Stemmler, E.A. and Hites, R.A. 1985. *Anal. Chem.*, 57, 684-692.
92. Miwa, B.J.; Garland, W.A. and Blumenthal, P. 1981. *Anal. Chem.*, 53, 793-797.
93. Crow, F.W.; Bjorseth, A.; Knapp, K.T. and Bennett, R. 1981. *Anal. Chem.*, 53, 619-625.
94. Greaves, J.; Bekesi, J.G. and Roboz, J. 1982. *Biomed. Mass Spectrom.*, 9, 406-410.
95. Stan, H.J. and Kellner, G. 1982. *Biomed. Mass Spectrom.*, 9, 483-492.
96. Busch, K.L.; Norstrom, A.; Bursey, M.M.; Hass, J.R. and Nilsson, C.A. 1979. *Biomed. Mass Spectrom.*, 6, 157-161.
97. McEwen, C.N. and Rudat, M.A. 1981. *J. Am. Chem. Soc.*, 103, 4343.
98. McEwen, C.N. 1986. *Mass Spectrom. Rev.*, 5, 521.
99. Dougherty, R.C.; Roberts, J.D.; Biros, F.J. 1975. *Anal. Chem.*, 47, 54-59.
100. Tannenbaum, H.P.; Roberts, J.D.; Dougherty, R.C. 1975. *Anal. Chem.*, 47, 49-54.
101. Dougherty, R.C.; Dalton, J.; Biros, F.J. 1972. *Org. Mass Spectrom.*, 6, 1171-1181.
102. Glokhovtsev, M.N.; Pross, A. and Radom, L. 1995. *J. Am. Chem. Soc.*, 117, 2024-2032.
103. Long, G.L.; Windefordner, J.D. 1983. *Anal. Chem.*, 55, 712A-724A.

104. Freeman, D.H. 1980. *Anal. Chem.*, 52, 2242-2249.
105. Dunker, J.C.; Hillebrand, M.T.J.; Palmork, K.H.; Wilhelemsen, S. 1980. *Bull. Environ. Contam. Toxicol.*, 25, 956-964.
106. Wester, P.G.; De Boer, J.; Brinkman, U.A.Th. 1996. *Environ. Sci. Technol.*, 30, 473-480.
107. Jansson, B.; Andersson, R.; Asplund, L.; Bergman, Å.; Litzén, K.; Nylund, K.; Reutergårdh, L.; Sellström, U.; Uvemo, U-B.; Wahhlerg, C.; Wideqvist, U.; Odsjö, T.; Olsson, M. 1993. *Environ. Toxicol. Chem.*, 12, 1163-1174.
108. Alford-Stevens, A.L. 1986. *Environ. Sci. Technol.*, 20, 1194-1199.
109. Furlong, E.T.; Carter, D.S.; Hites, R.A. 1988. *J. Great Lakes Res.*, 14(4), 489-501.
110. Hamdy, Y.; Post, L. 1985. *J. Great Lakes Res.*, 11, 353-365.
111. Koslowski, S.E.; Metcalfe, C.D.; Lazar, R.; Haffner, G.D. 1994. *J. Great Lakes Res.*, 20(1), 260-270.
112. Swain, W.R. 1978. *J. Great Lakes Res.*, 4, 398-407.
113. Hites, R.A. and Eisenreich, S.J. 1987. Sources and Fates of Aquatic Pollutants. ACS series. American Chemical Society, Washington, DC.
114. Bidleman, T.F. and Olney, C.E. 1975. *Nature*, 257, 475-477.
115. Czuczwa, J.M.; McVeety, B.D.; Hites, R.A. 1985. *Chemosphere*, 14, 623-626.

116. Eisenreich, S.J. and Hollod, G.J. 1979. *Environ. Sci. Technol.*, 13, 568-573.
117. Chan, C.H. and Perkins, L.H. 1989. *J. Great Lakes Res.*, 15, 465-475.
118. Chan, C.H.; Bruce, G.; Harrison, B. 1994. *J. Great Lakes Res.*, 20, 564-560.
119. Swackhamer, D.L. and Hites, R.A. 1988. *Environ. Sci. Technol.*, 22, 543-548.
120. Chan, C.H. 1996. Environment Canada Web-Page (<http://www.cciw.ca/glimr/data/contaminants-in-precip/intro.html>)
121. International Joint Commission. 1989. A Plan for assessing Atmospheric Deposition to the Great Lakes. Report to the Great Lakes Water Quality Board.
122. Hoff, R.M.; Muir, D.C.G.; Grift, N.P. 1992. *Environ. Sci. Technol.*, 26, 276-283.
123. Muir, D.C.G. *et al.* *Unpublished results.*
124. Muir, D.C.G.; Stern, G.A.; Tomy, G.T.; Rosenberg, B.; Rawn, D.F.; Wilkinson, P. and Lockhart, W.L. 1996. Presented at the Green Plan Toxics Workshop, Jan 28-31, Ottawa.
125. Rawn, D.F. *et al.* 1996. *Unpublished results.*
126. Holden, A.V. 1972. Monitoring organochlorine contamination of the marine environment by the analysis of residues in seals. In: *Marine Pollution and Sea Life*, M. Ruivo, Ed., Fishing News Books Ltd., England. pp. 266-272.

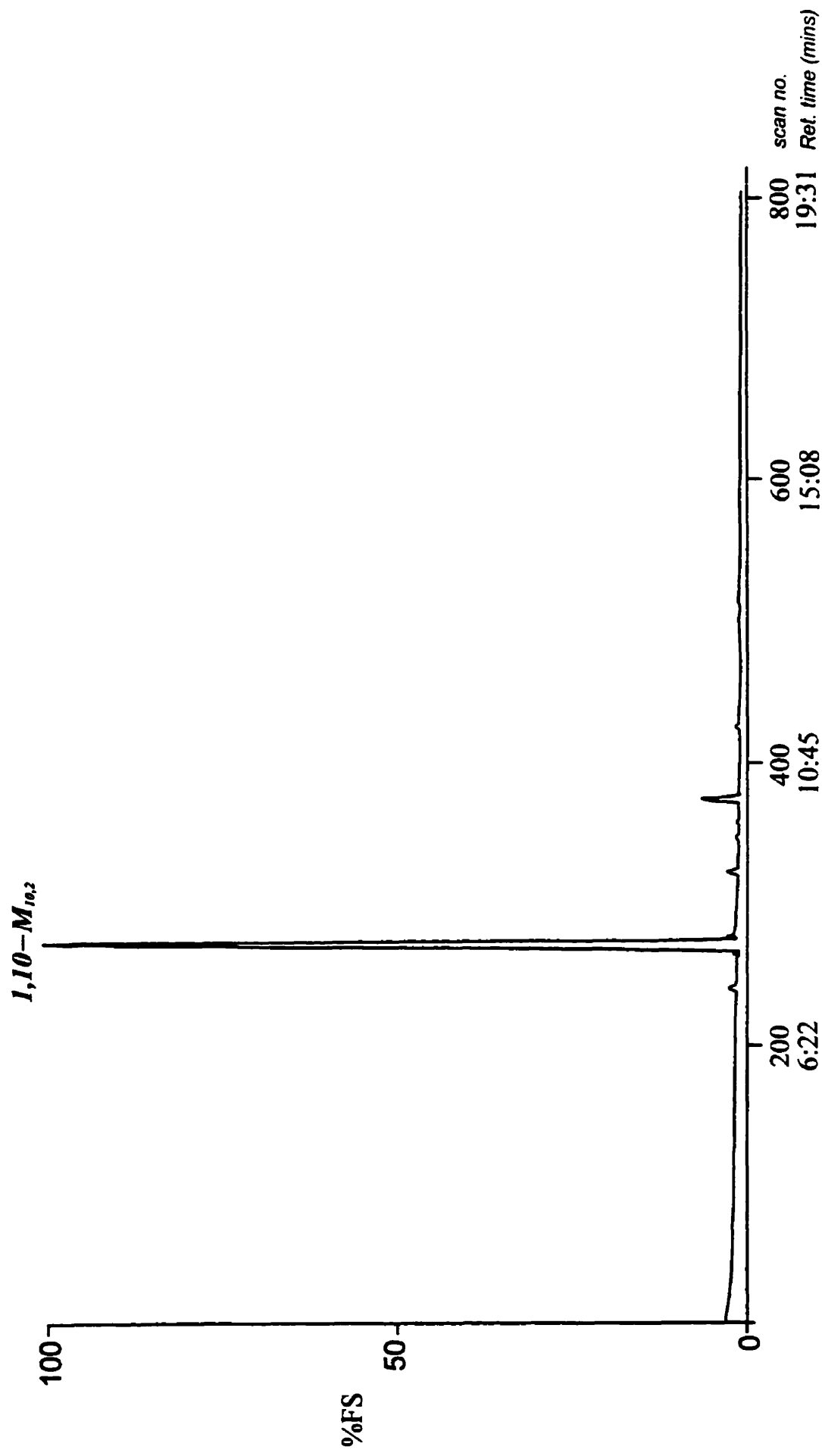
127. Beck, G.G.; Smith, T.G. and Addison, R.F. 1994. *Can. J. Zool.*, 72, 174-182.
128. Muir, D.C.G.; Ford, C.A.; Rosenberg, B.; Norstron, R.J.; Simon, M. and Bèland, P. 1996. *Environ. Pollut.*, 93, 219-234.
129. Cameron, M. and Weis, I.M. 1993. *Arctic*, 46, 42-48.
130. Stern, G.A.; Muir, D.C.G.; Segstro, M.D.; Dietz, R and Heide-Jorgenson, M.P. 1994. *Meddr. Grønland. Biosci.*, 39, 1126-1129.
131. Barrie, L.A.; Gregor, D.; Hargrave, B.; Lake, R.; Muir, D.C.G.; Shearer, R.; Tracey, B. and Bidleman, T. 1992. *Sci. Total Environ.*, 122, 1-74.
132. Muir, D.C.G.; Braune, B.; Norstron, R.; Wagemann, R.; Gamberg, M.; Poole, K.; Addison, R.; Bright, D.; Dodd, M.; Duschenko, W.; Eamer, J.; Evans, M.; Elkin, B.; Grundy, S.; Hargrave, B.; hebert, C.; Johnstone, R.; Kidd, R.; Koenig, B.; Lockhart, L.; Payne, J.; Peddle, J. And Reimer, K. 1996. Chapter 3. Ecosystem Uptake and Effects. In: Shearer, R. (Ed), Canadian Arctic Contaminants Assessment Report, Indian and Northern Affairs Canada, Ottawa.
133. Connell, D.W. 1988. *Rev. Environ. Contam. Toxicol.*, 102, 117-154.
134. Fisk, A.T.; Cymbalisky, C.D.; Bergman, Å. and Muir, D.C.G. 1996. *Environ. Toxicol. Chem.*, 15, 1775-1782.
135. Pham, T.; Lum, K. And Lemieux, C. 1993. *Chemosphere*, 26, 1595-1606.
136. Addison, R.F.; Zinck, M.E. and Smith, T.G. 1986. *Environ. Sci. Technol.*, 1986, 20, 253-256.

137. Tanabe, S. 1988. *Environ. Pollut.*, 50, 5-28.
138. Tanabe, S.; Watanabe, S. and Tatsukawa, R. 1988. *Mar. Mammal Sci.*, 4, 103-124.
139. Muir, D.C.G.; Norstrom, R.J. and Simon, M. 1988. *Environ. Sci. Technol.*, 22, 1071-1079.
140. Matthews, H.B. and Dedrick, R.L. 1984. *Ann. Rev. Pharmacol. Toxicol.*, 24, 85-103.
141. Laug, E.P.; Kunze, F.M. and Prickett, C.S. 1951. *Arch. Industr. Hyg.*, 3, 245.
142. Mes, J. And Davies, D.J. 1978. *Chemosphere*, 9, 699
143. Jensen, A.A. 1984. *Res. Revs.*, 89, 1-128.
144. Westöo, G. and Norèn, K. 1978. *Ambio*, 7, 62-64.
145. Stern, G.A.; Muir, D.C.G.; Ford, C.A.; Grift, N.P.; Dewailly, E.; Bidleman, T.F. and Walla, M.D. 1992. *Environ. Sci. Technol.*, 26, 1838-1840.
146. de Boer, J.; Wester, P.G. 1993. *Chemosphere*, 27, 1879-1890.
147. Kinoch, D.; Kuhnlein, H.V. and Muir, D.C.G. 1992. *Sci. Total Environ.*, 122, 247-278.
148. Kinloch, D. And Kuhnlein, H.V. 1986. Assessment of PCBs in arctic foods and diets. A pilot study in Broughton Island, NWT. Preliminary Report. NWT-Health and Welfare Canada.

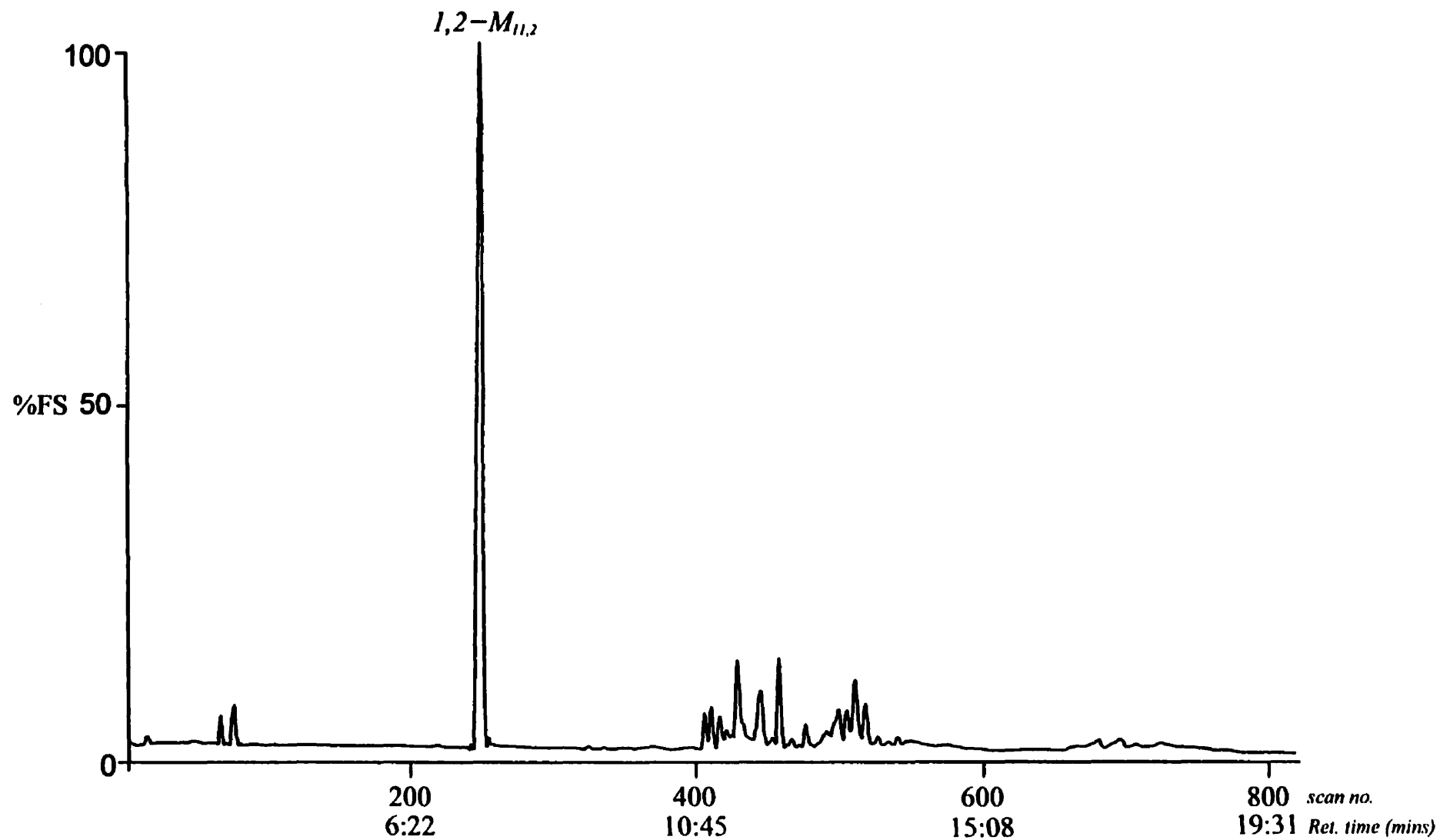
149. Wise, S.A.; Schantz, M.M.; Koster, B.J.; Demiralp, R.; Mackey, E.A.; Greenberg, R.R.; Burow, M.; Ostapczuk, P and Lillestolen, T.I. 1993. *Fres. J. Anal. Chem.*, 345, 270-277.
150. Schantz, M.M.; Parris, R.M.; Kurz, J.; Ballschmiter and Wise, S.A. 1993. *Fres. J. Anal. Chem.*, 346, 766-778.
151. Schantz, M.M.; Koster, B.J.; Wise, S.A. and Becker, P.R. 1993. *Sci. Total Environ.*, 139/140, 323-345.
152. Wise, S.A.; Schantz, M.M.; Parris, R.M.; Rebbert, R.E.; Benner, B.A. and Gills, T.E. 1992. *Analysis*, 20, M57-M61.
153. U.S. Department of Commerce. Technology Administration. National Institute of Standards and Technology. Environmental Organic. 1995. SRM Brochure.
154. Schantz, M.M.; Koster, B.J.; Oakley, L.M.; Schiller, S.B. and Wise, S.A. 1995. *Anal. Chem.*, 67, 901-910.
155. Krishnaswamy, S.; Lal, D.; Martin, J.M. and Meybeck, M. 1971. *Earth Planet. Sci. Lett.*, 11, 407-414.
156. Jones, K.C. 1991. In: Organic contaminants in the environment: environment pathways and effects. Environmental Management Series. Elsevier Science Publishing Co., Inc. New York, NY. USA.
157. Farmer, J.G. 1977. *Can. J. Earth. Sci.*, 15 431-437.
158. Durham, R.W. and Oliver, B.G. 1983. *J. Great Lakes Res.*, 9, 160-168.

159. Likens, G.E. and Davis, M.B. 1975. *Int. Ver. Theor. Angew. Limnol. Verh.*, 19, 982-993.
160. Hilton, J. 1985. *Limnol. Oceanogr.*, 30, 1131-1143.
161. Blais, J.M and Kalff, J. 1995. *Limnol. Oceanogr.*, 40, 582-588.
162. Atkins, P.W. 1994. In: *Physical Chemistry*. 5th Ed., Oxford University Press.
163. Stern, G.A.; Muir, D.C.G.; Billeck, B.; Lockhart, L. and Wilkinson, P. 1996. *Organohalogen Compounds*, 379-384.
164. Muir, D.C.G.; Omelchenko, A.; Grift, N.P.; Savoie, D.A.; Lockhart, W.L.; Wilkinson, P. and Brunskill, G.J. 1996. *Environ. Sci. Technol.*, 30, 3609-3617.
165. Mudroch, A.; Allan, R.J. and Joshi, S.R. 1992. *Arctic*, 45, 10-19.

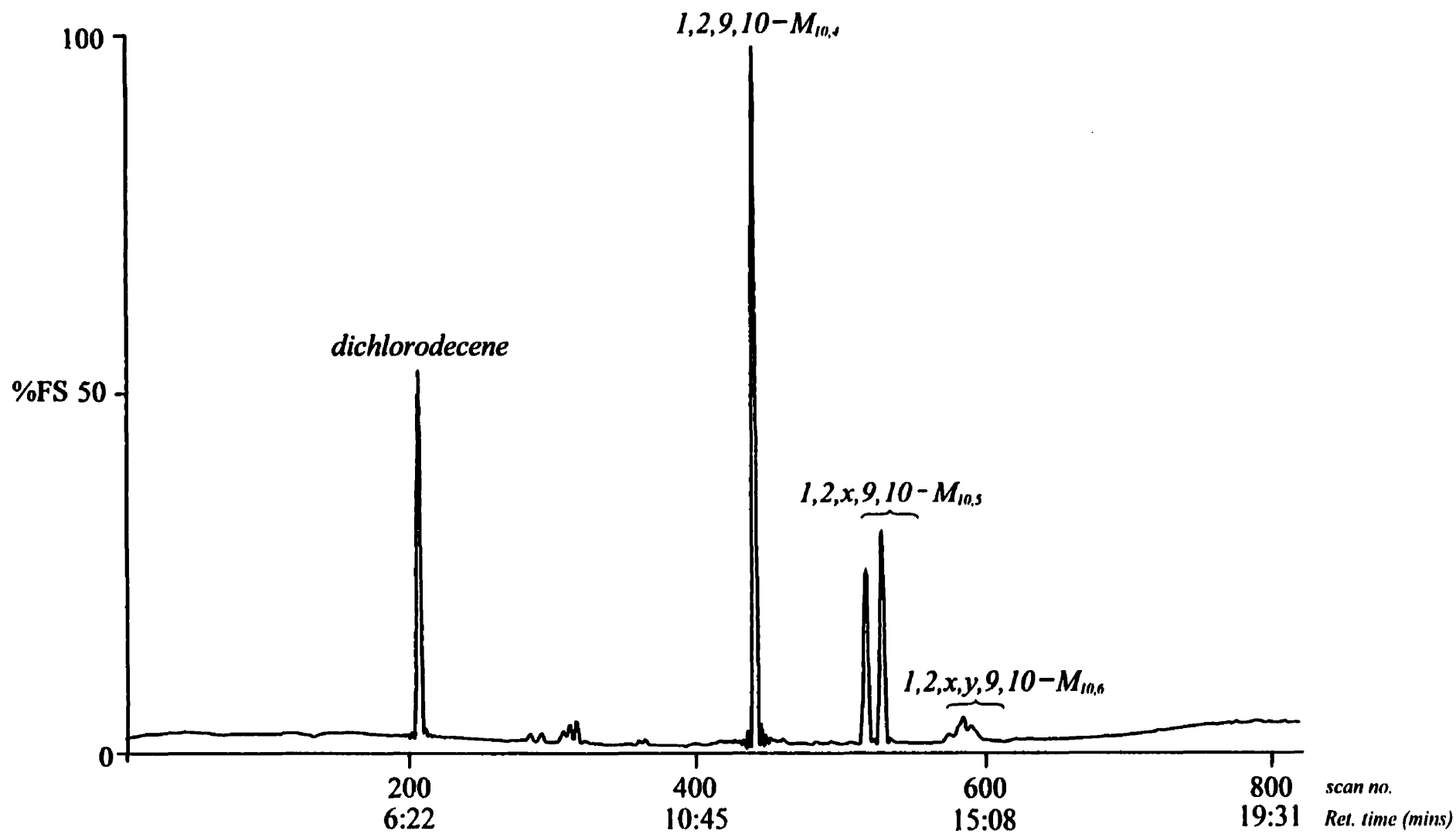
Appendix 1a HRGC-EI/MS total ion chromatogram of 1,10-dichloro-n-decane.



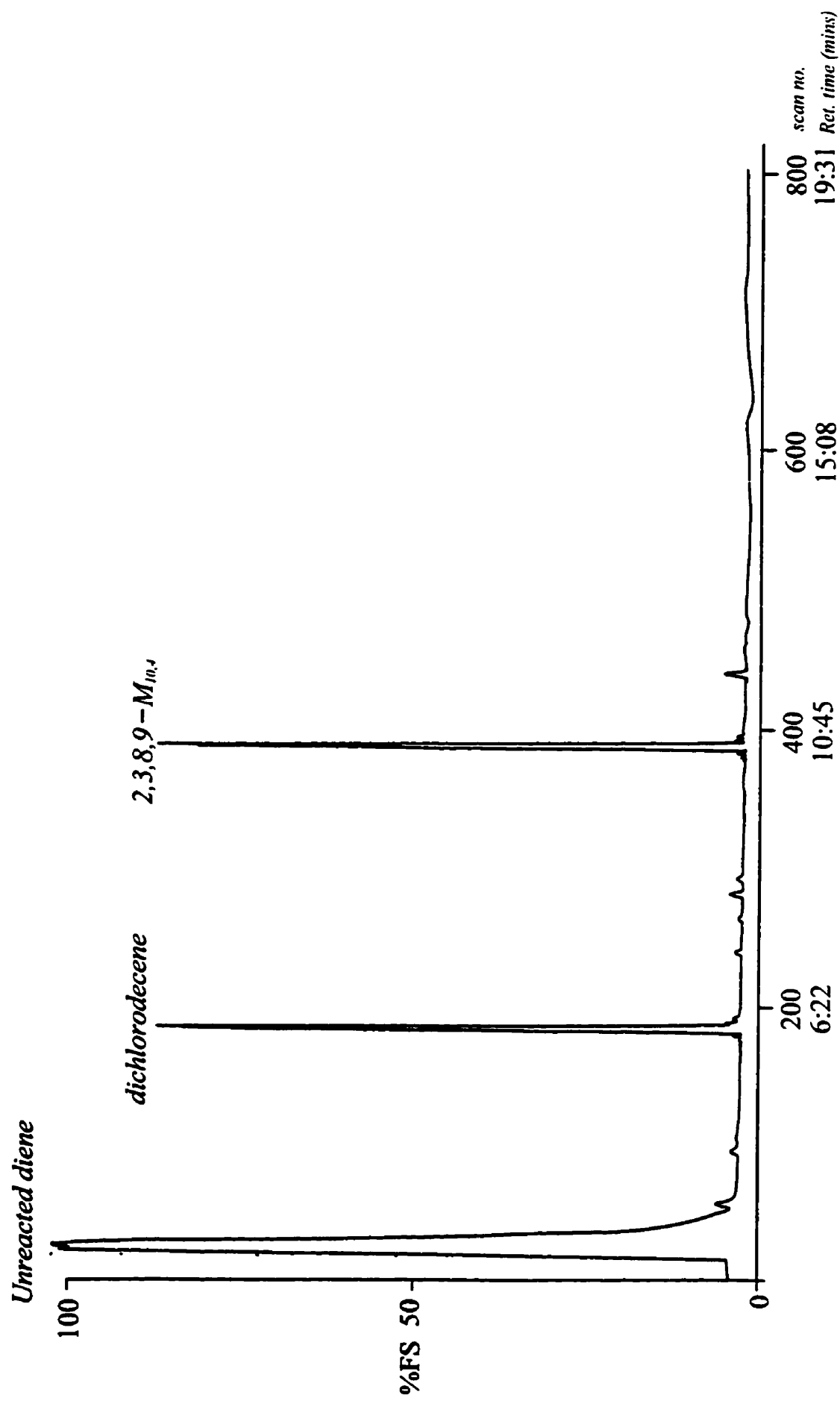
Appendix 1b. HRGC-EI/MS total ion chromatogram of reaction products formed by the reaction of molecular chlorine with 1-undecene.



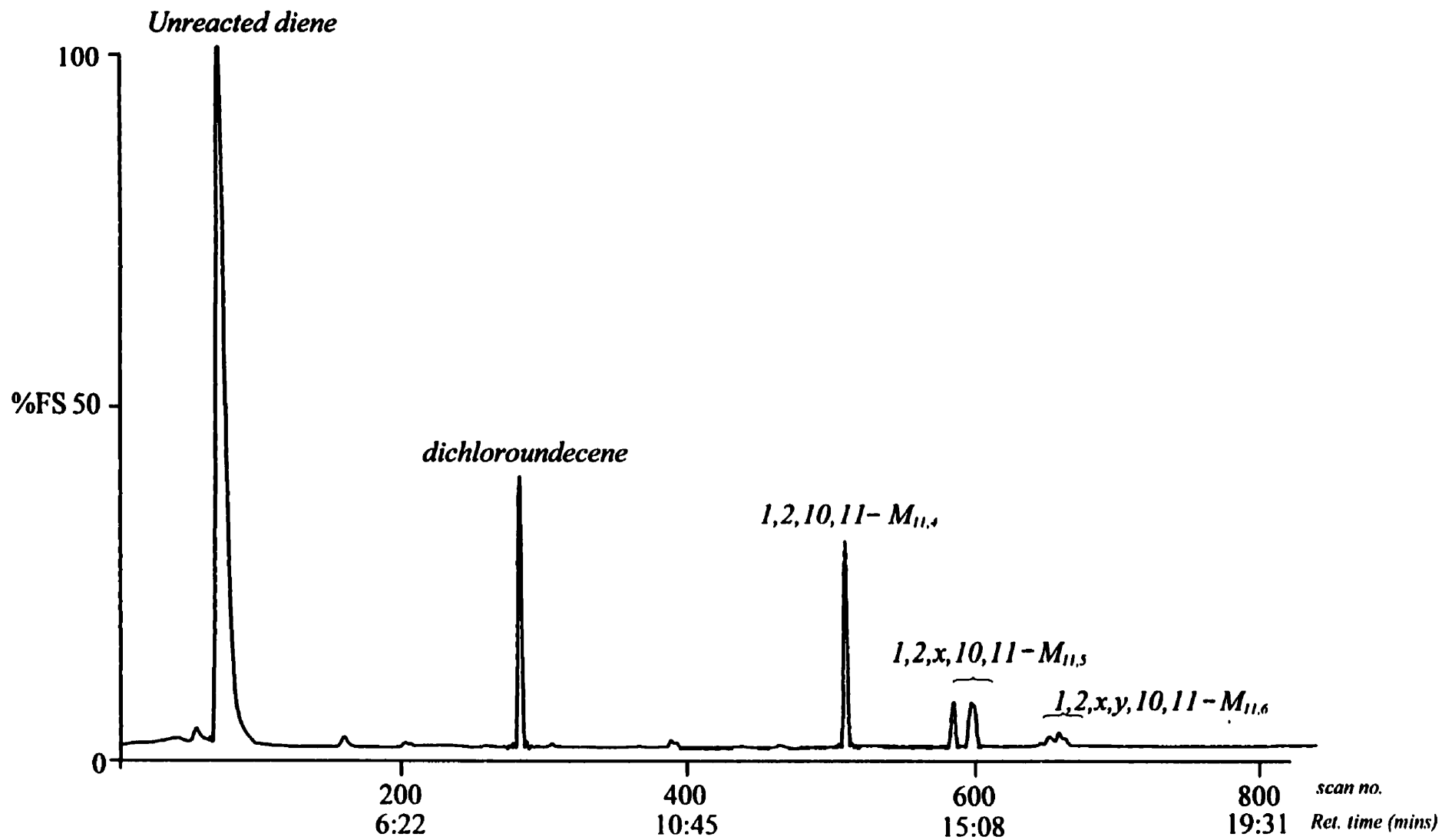
Appendix 1c. HRGC-EI/MS total ion chromatogram of reaction products formed by the reaction of molecular chlorine with 1,9-decadiene.



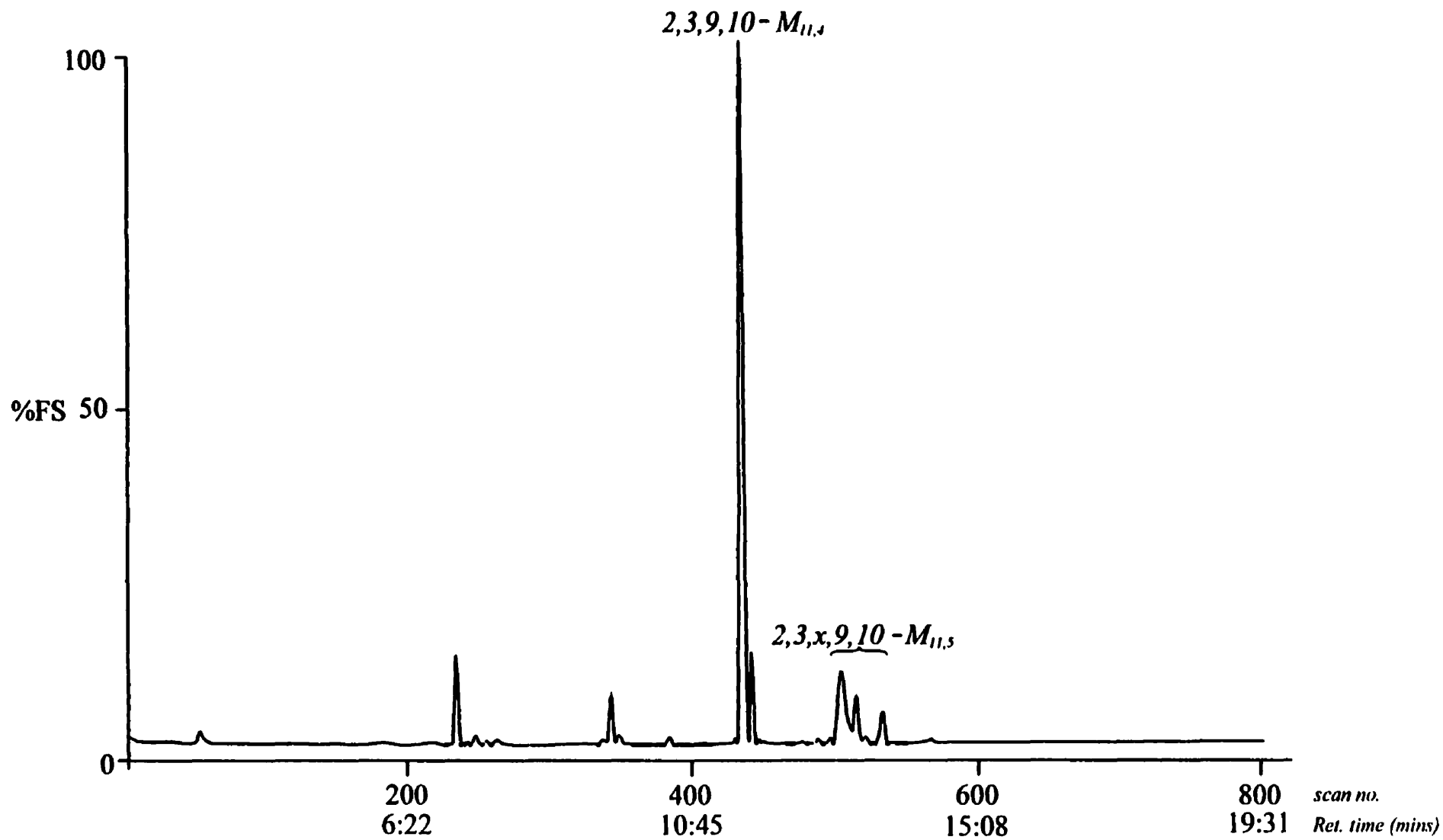
Appendix 1d. HRGC-EI/MS total ion chromatogram of reaction products formed by the reaction of molecular chlorine with 2,8-decadiene.



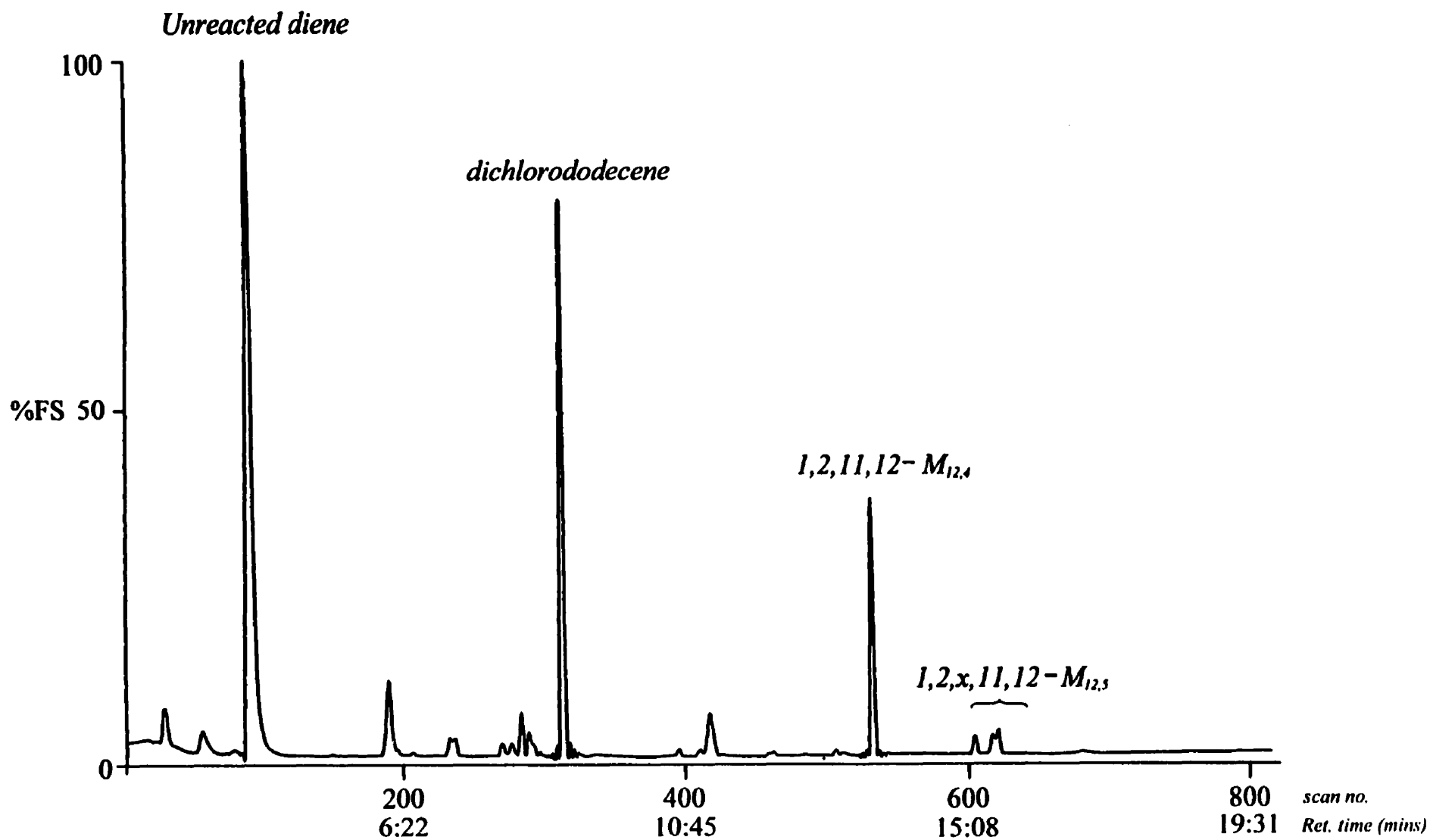
Appendix 1e. HRGC-EI/MS total ion chromatogram of reaction products formed by the reaction of molecular chlorine with 1,10-undecadiene.



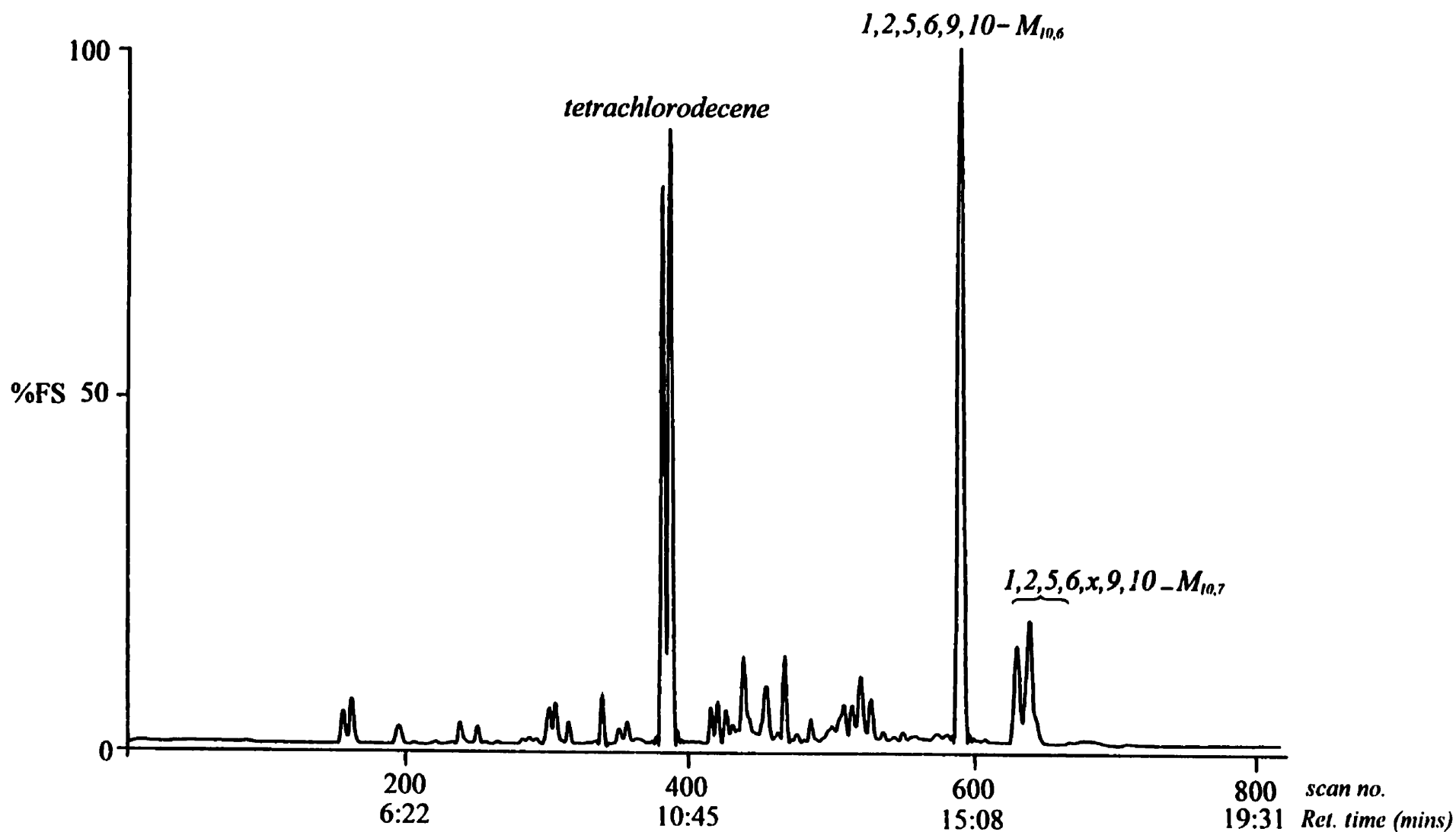
Appendix 1f. HRGC-EI/MS total ion chromatogram of reaction products formed by the reaction of molecular chlorine with 2,9-undecadiene.



Appendix 1g. HRGC-EI/MS total ion chromatogram of reaction products formed by the reaction of molecular chlorine with 1,11-dodecadiene.

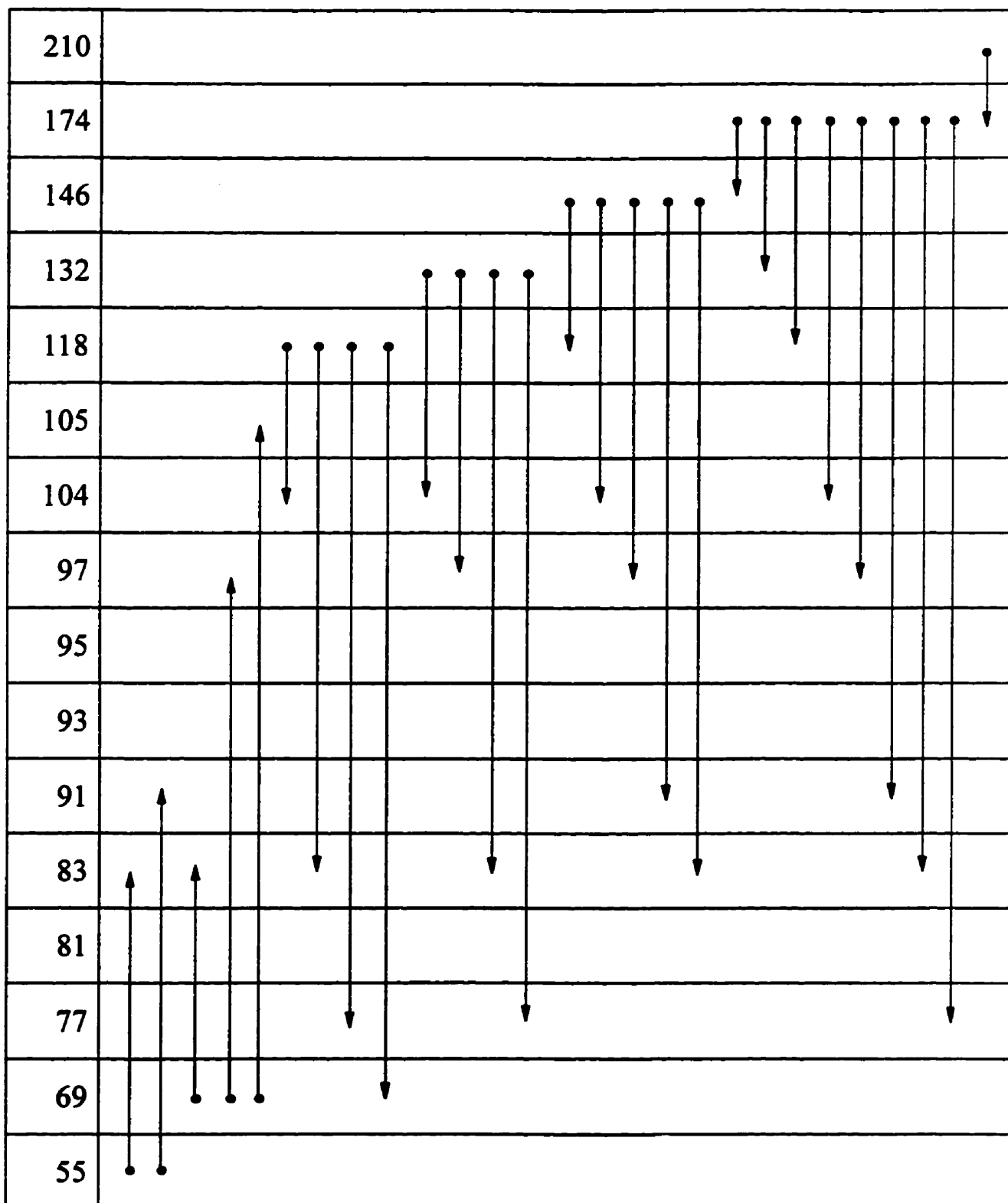


Appendix 1h. HRGC-EI/MS total ion chromatogram of reaction products formed by the reaction of molecular chlorine with 1,5,9-decatriene.



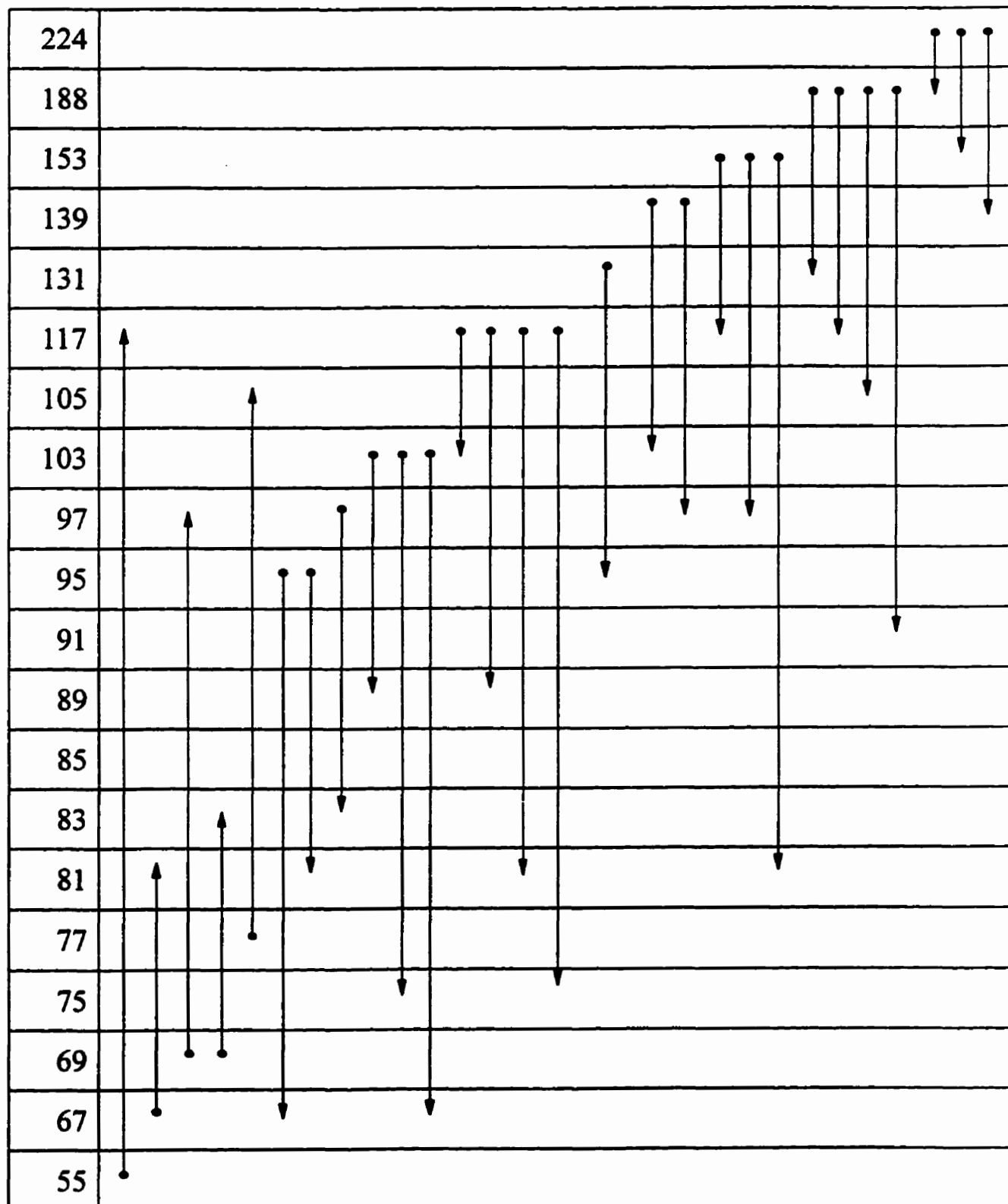
## Appendix 2

(a) Ion fragmentation pathways for 1,10-dichloro-*n*-decane established by linked-field scanning.



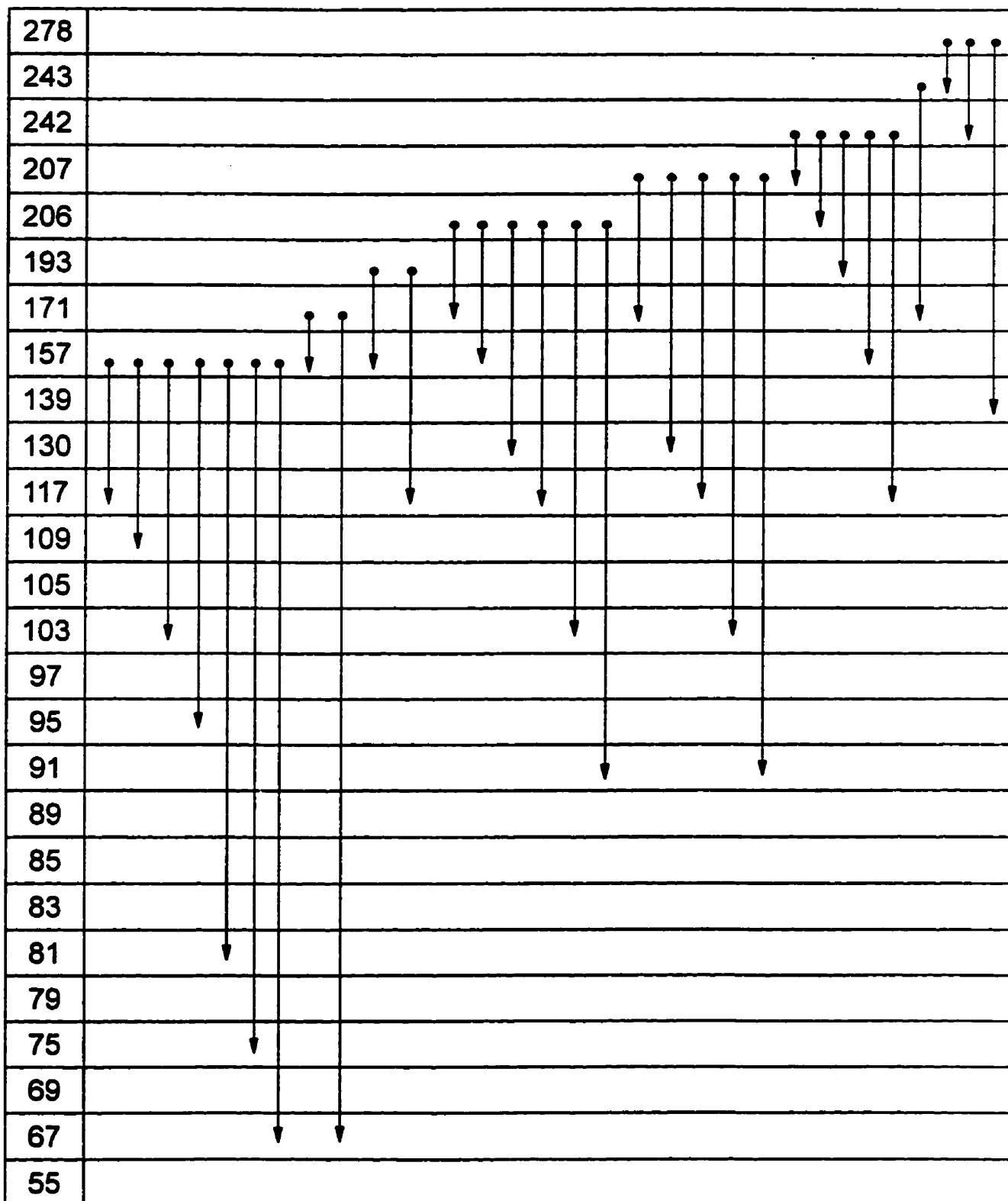
Appendix 2.

(b) Ion fragmentation pathways for 1,2-dichloro-*n*-undecane established by linked-field scanning.



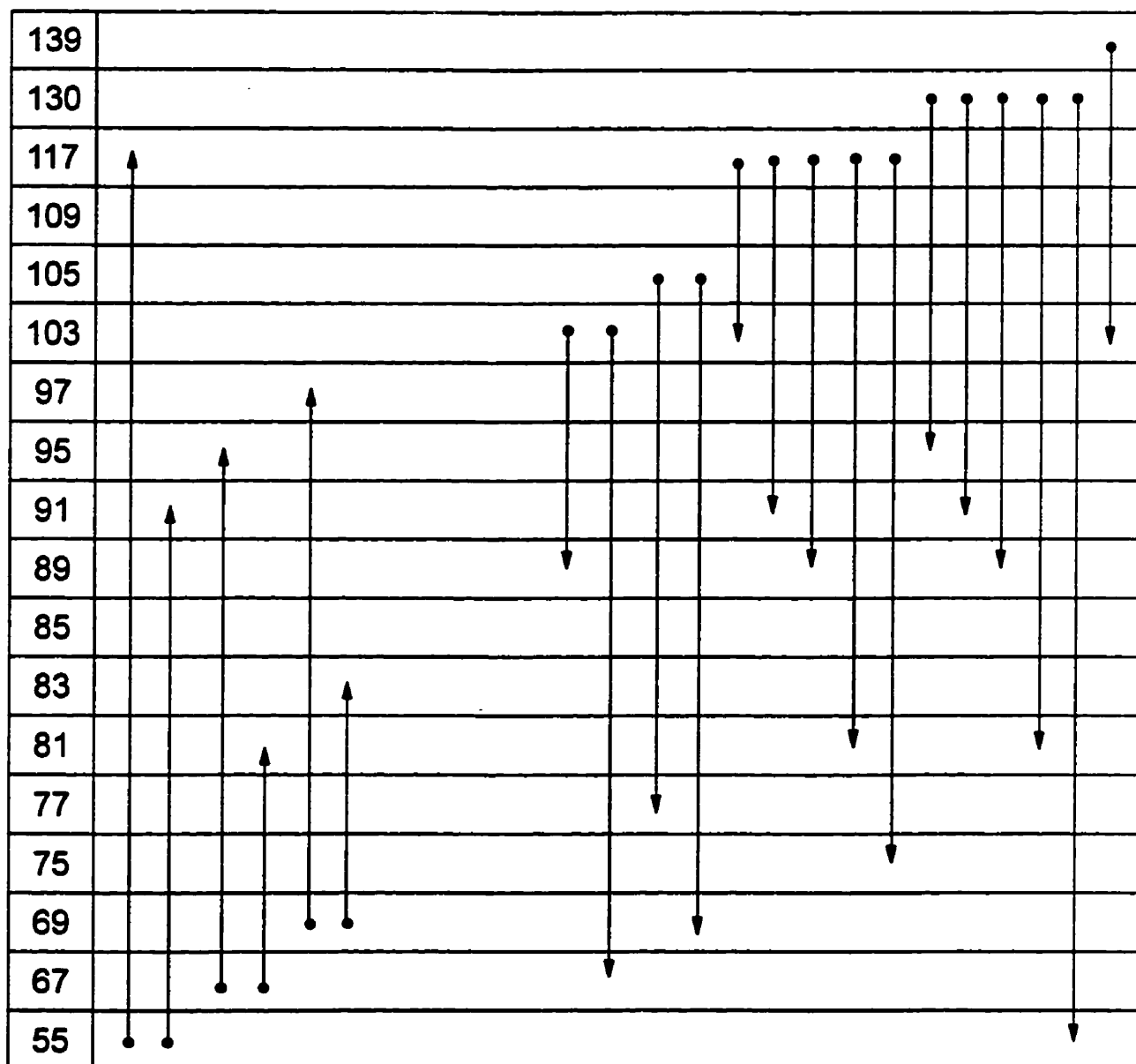
## Appendix 2

(c) Ion fragmentation pathways for 1,2,9,10-tetrachloro-*n*-decane established by linked-field scanning.



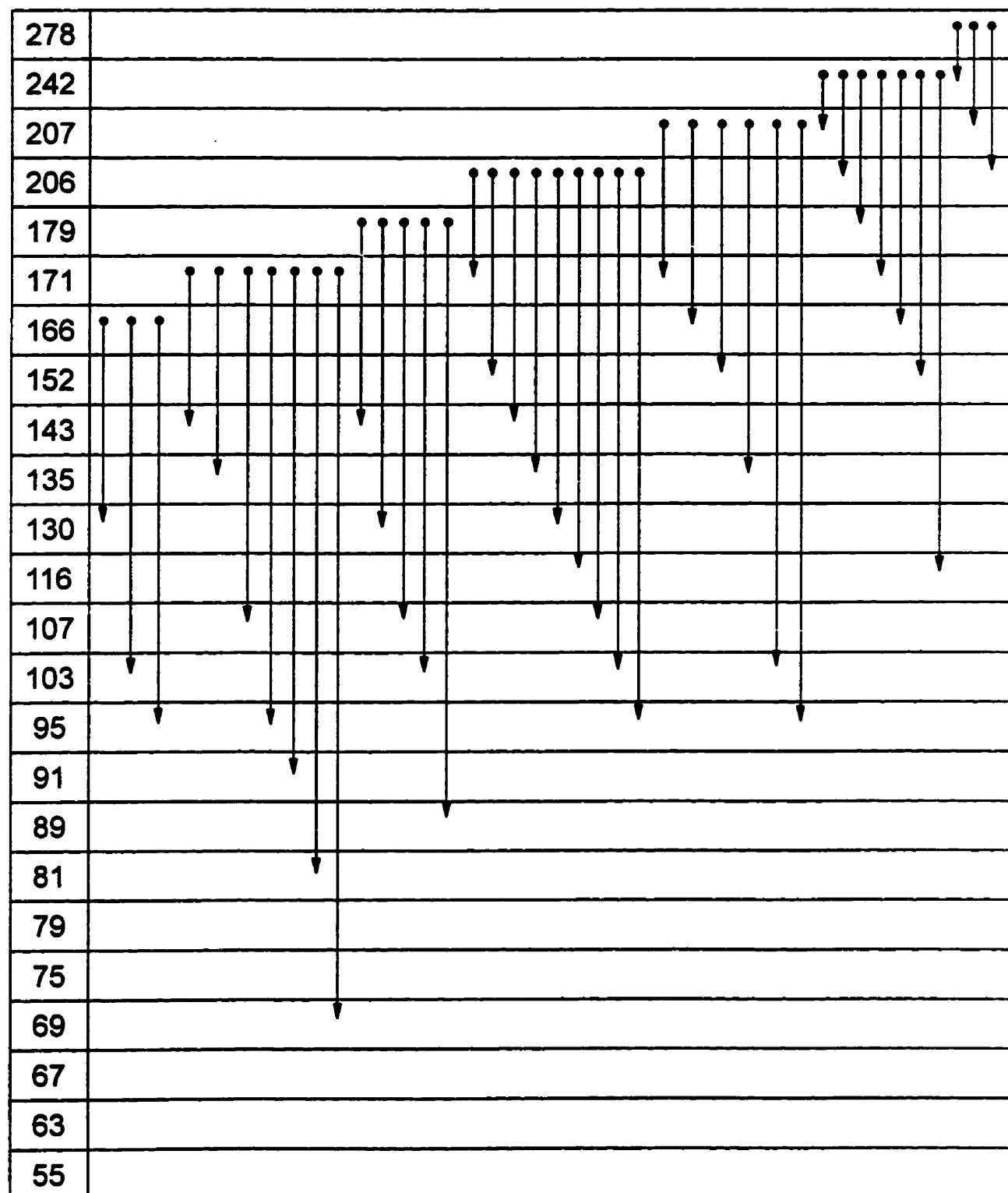
## Appendix 2

(c) (*cont'd*) Ion fragmentation pathways for 1,2,9,10-tetrachloro-*n*-decane established by linked-field scanning.



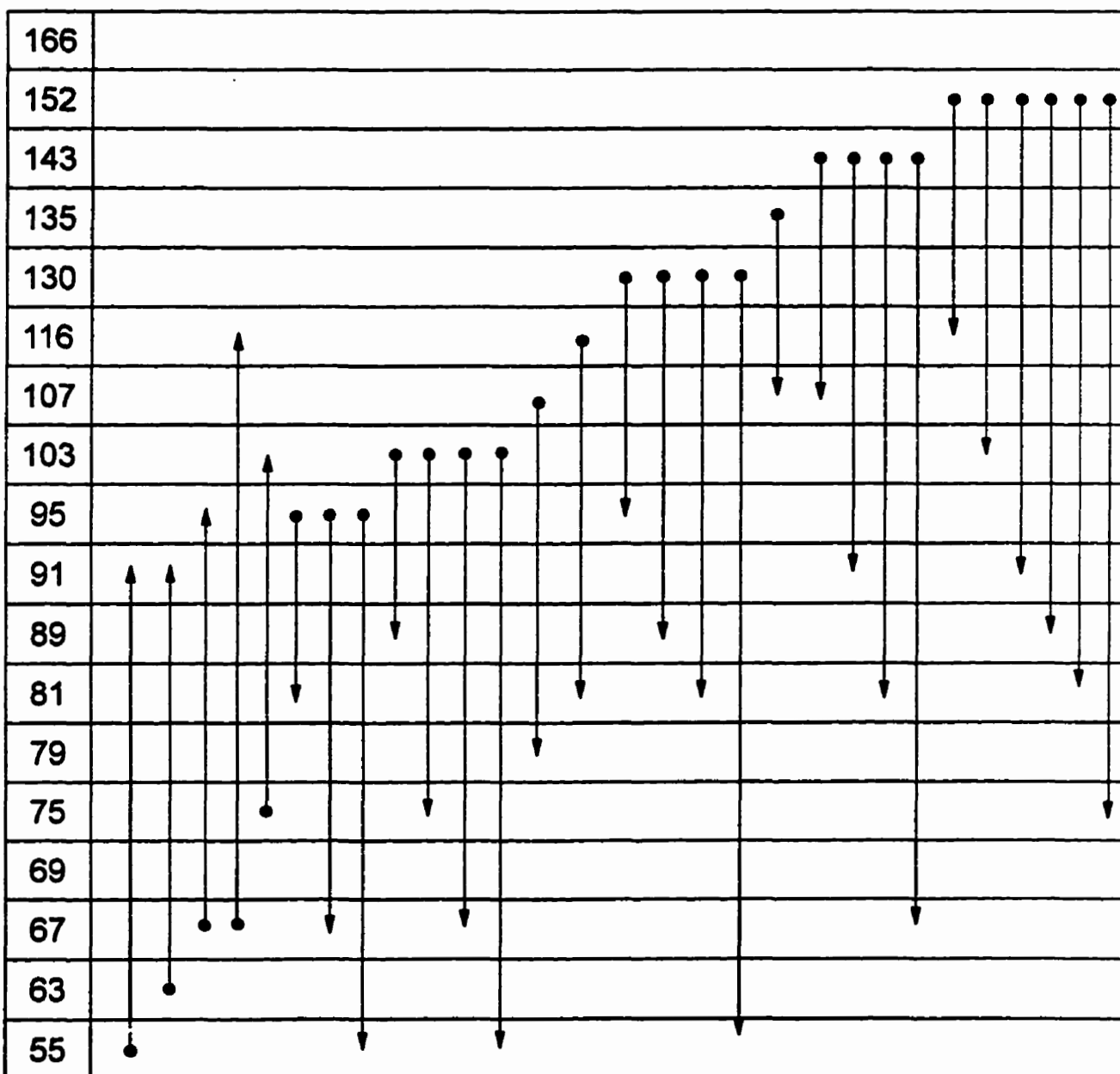
## Appendix 2

(d) Ion fragmentation pathways for 2,3,8,9-tetrachloro-*n*-decane established by linked-field scanning.



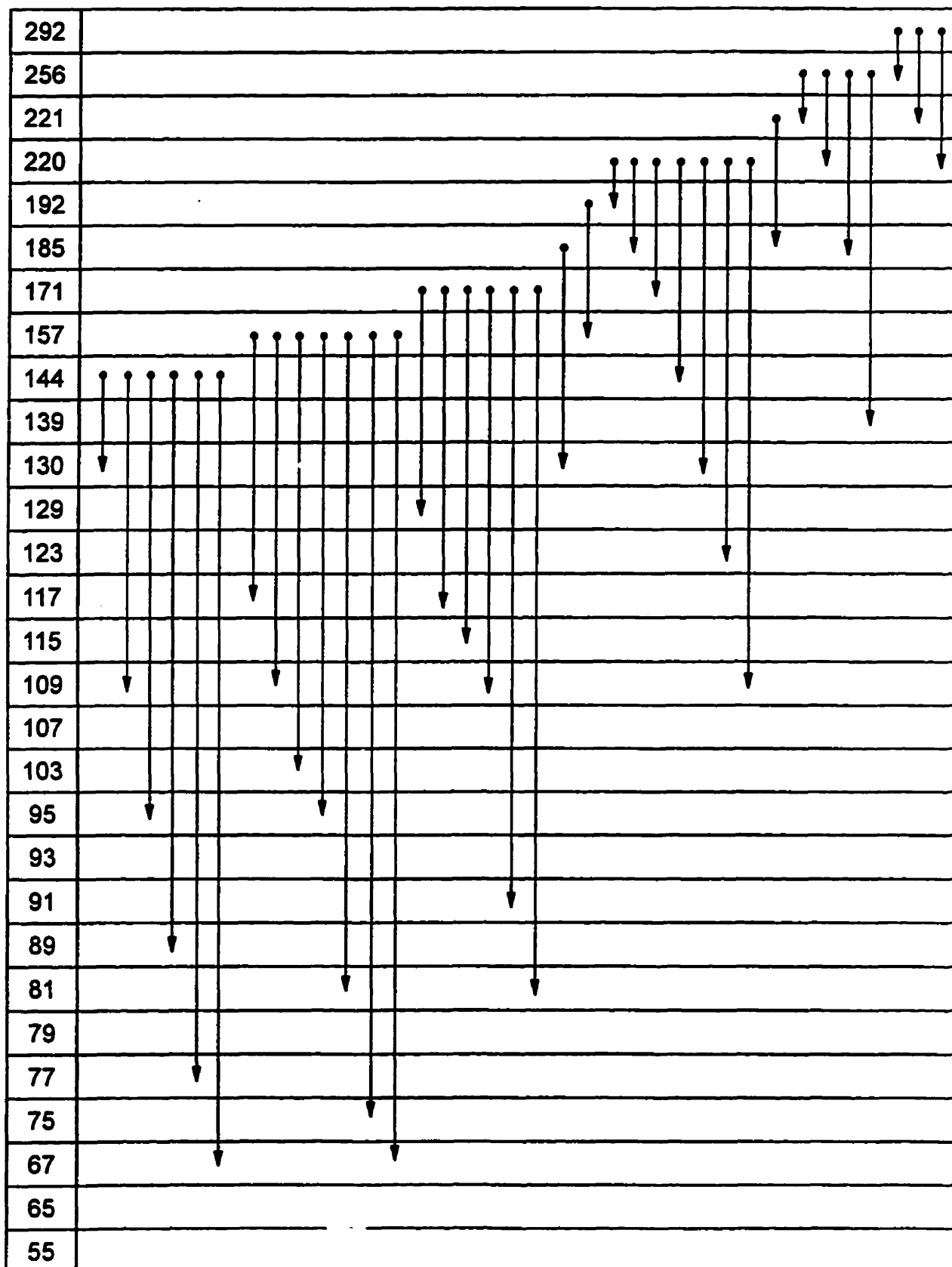
## Appendix 2

(d) (*cont'd*) Ion fragmentation pathways for 2,3,8,9-tetrachloro-*n*-decane established by linked-field scanning.



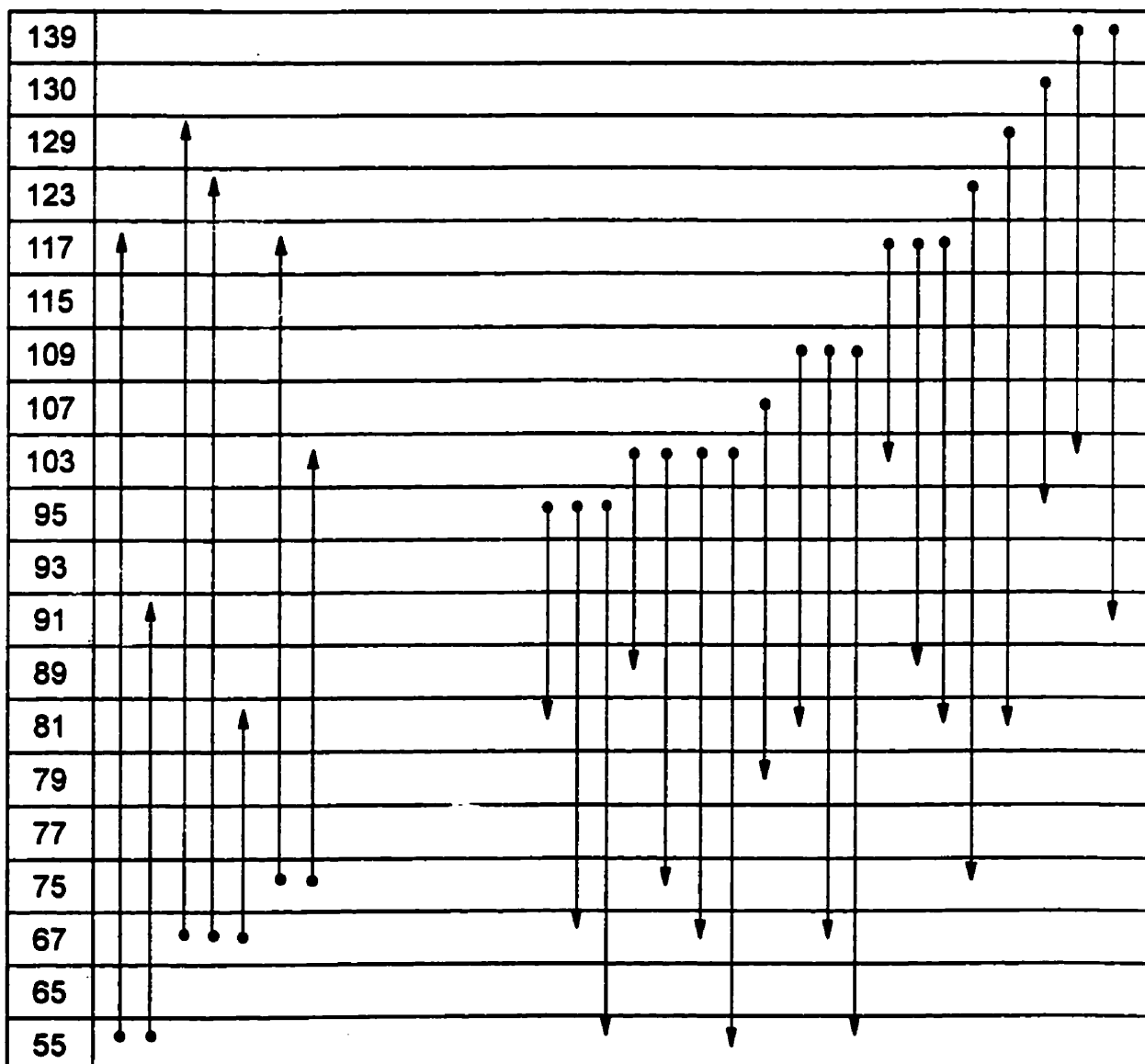
## Appendix 2

(e) Ion fragmentation pathways for 1,2,10,11-tetrachloro-n-undecane established by linked-field scanning



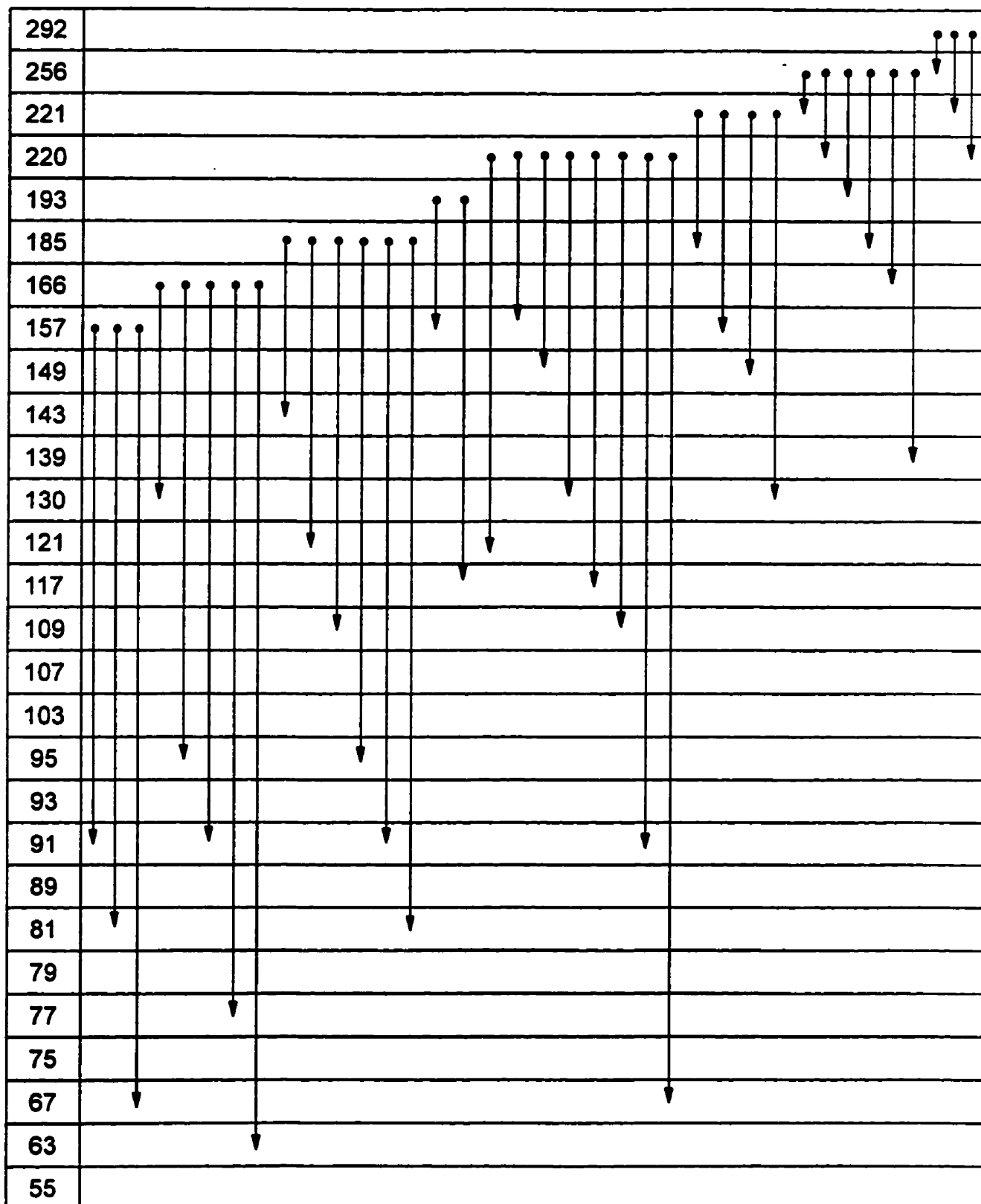
## Appendix 2

(e) (*cont'd*) Ion fragmentation pathways for 1,2,10,11-tetrachloro-n-undecane established by linked-field scanning.



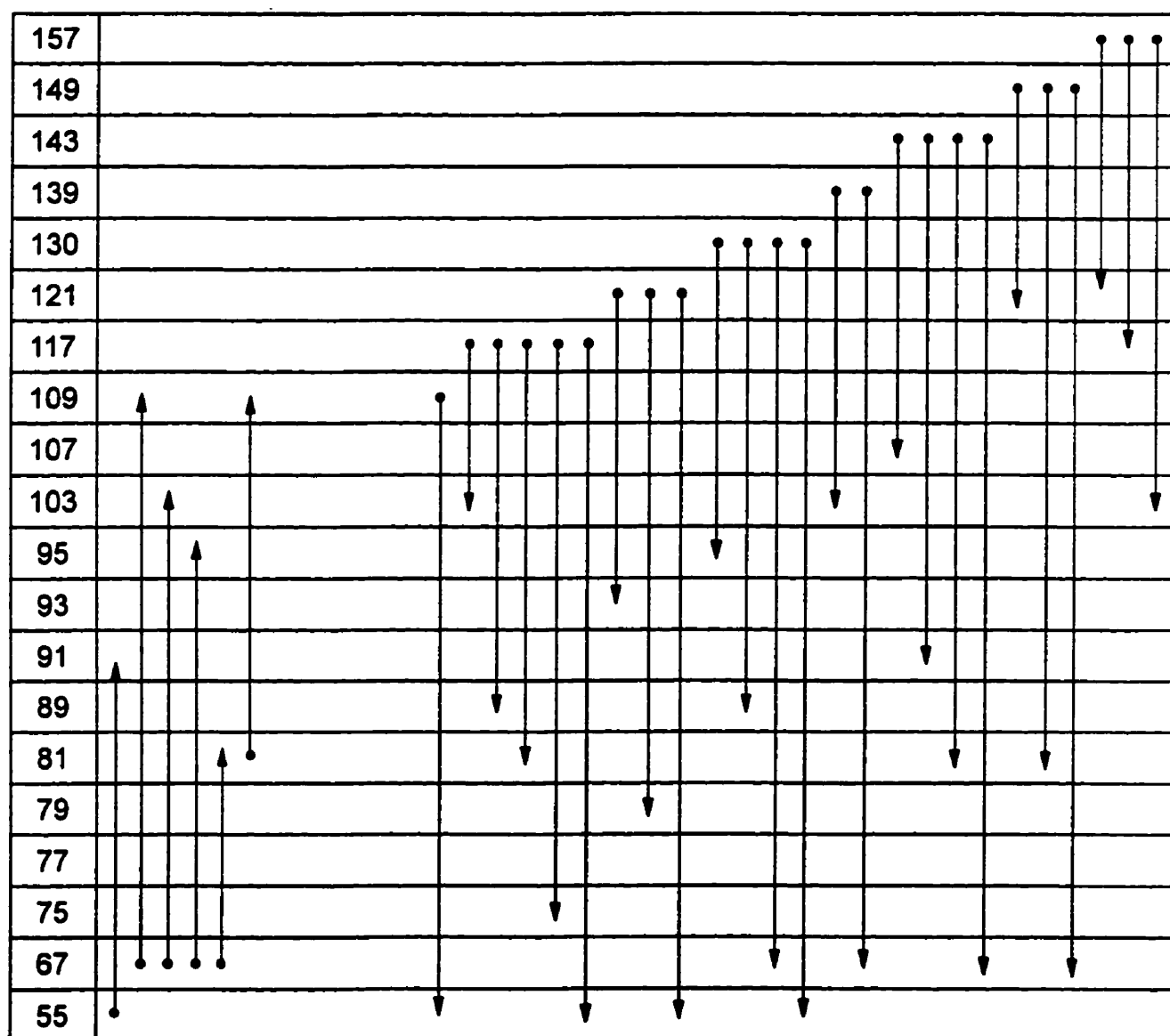
## Appendix 2

(f) Ion fragmentation pathways for 2,3,9,10-tetrachloro-*n*-undecane established by linked-field scanning



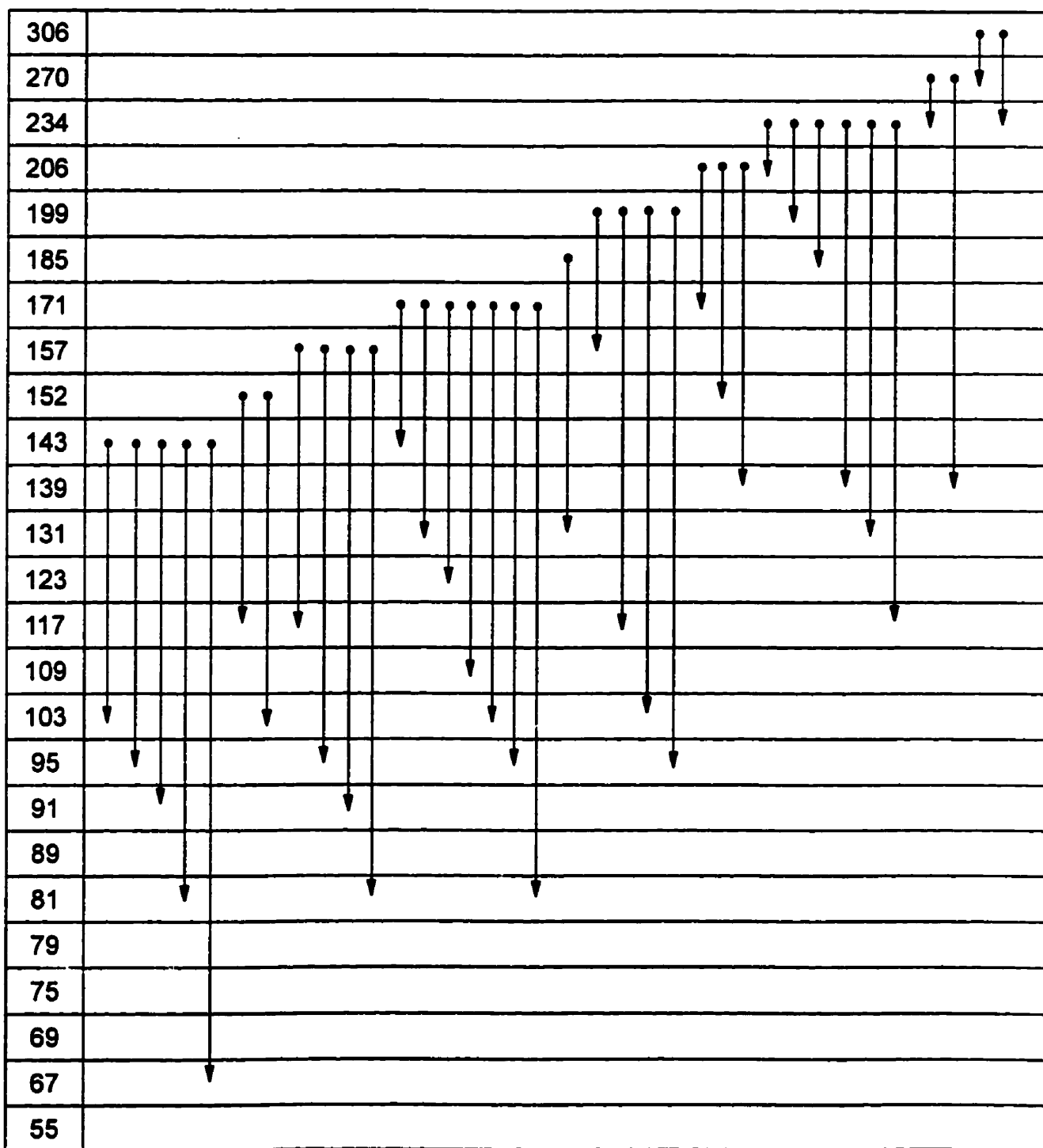
## Appendix 2

(f) (*cont'd*) Ion fragmentation pathways for 2,3,9,10-tetrachloro-*n*-undecane established by linked-field scanning.



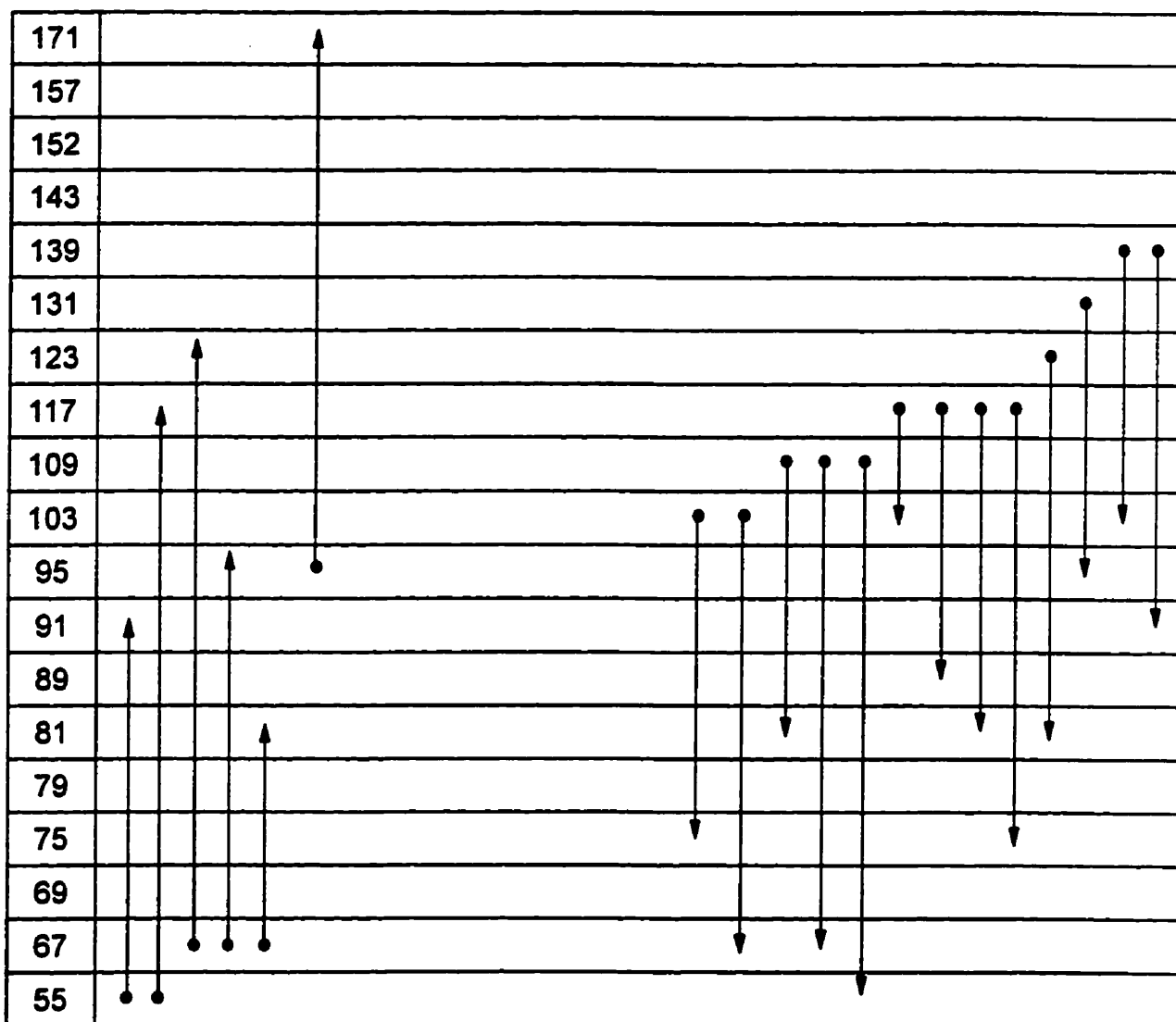
## Appendix 2

(g) Ion fragmentation pathways for 1,2,11,12-tetrachloro-*n*-dodecane established by linked-field scanning



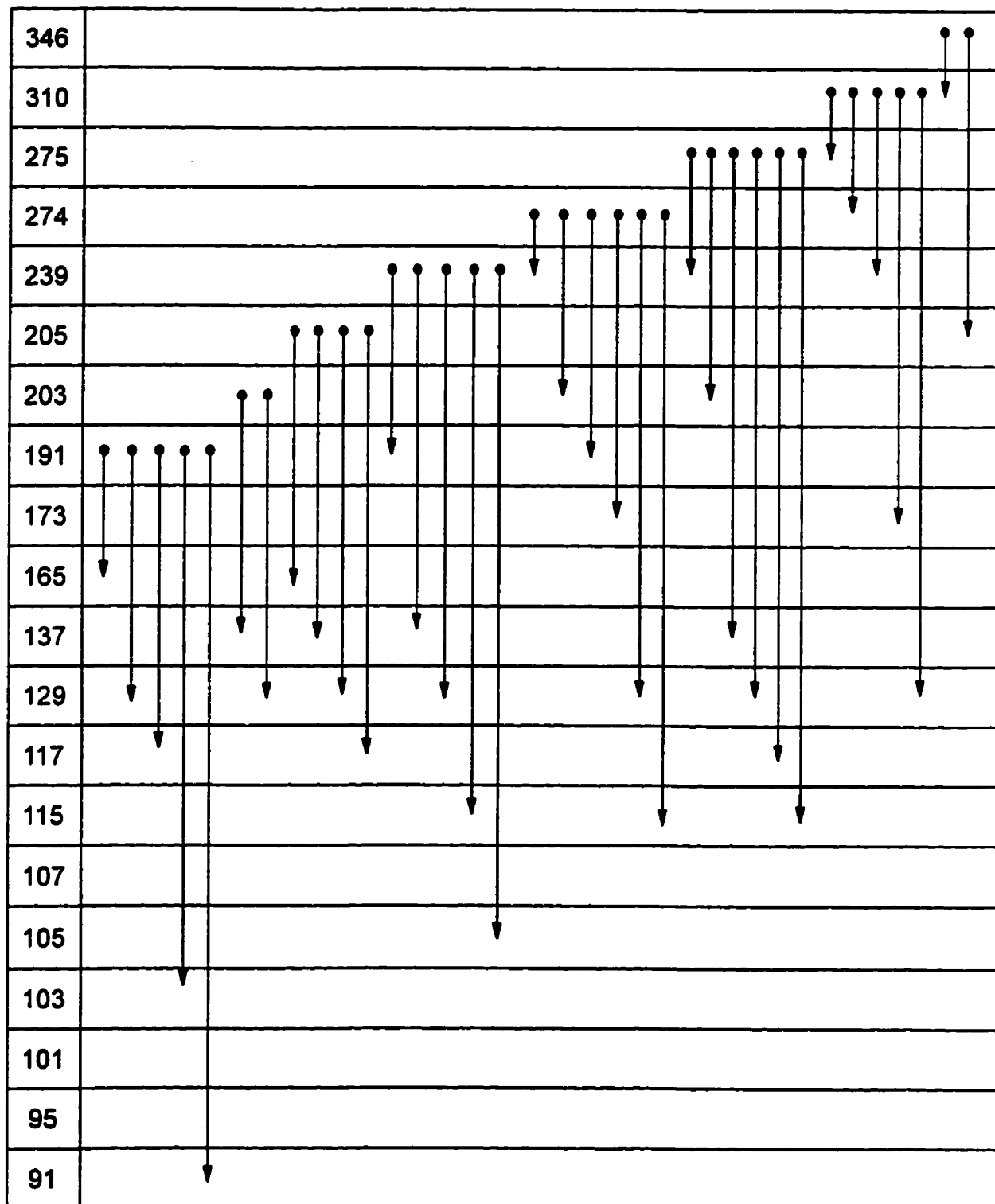
## Appendix 2

(g) (*cont'd*) Ion fragmentation pathways for 1,2,11,12-tetrachloro-*n*-dodecane established by linked-field scanning.



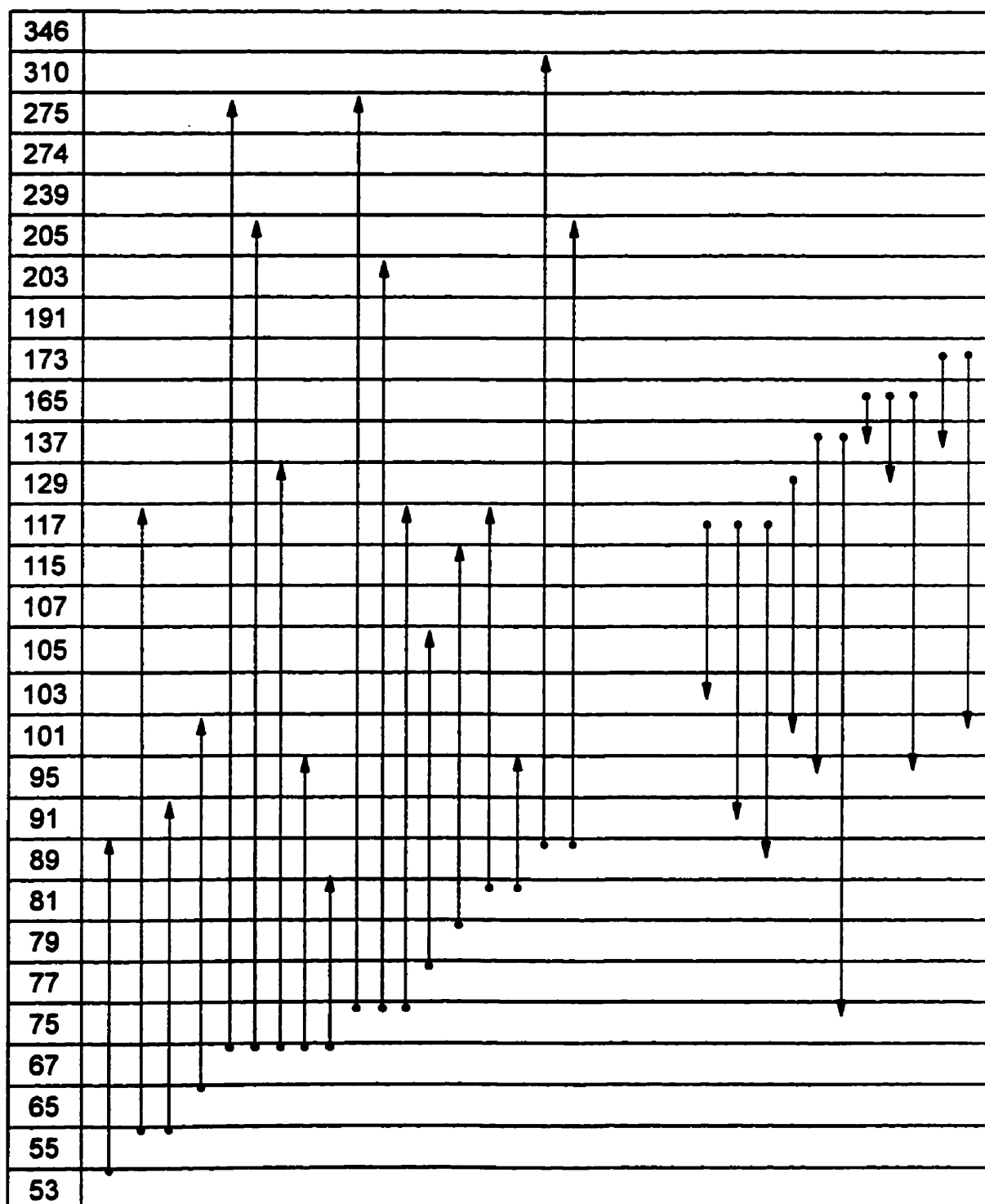
## Appendix 2

(h) Ion fragmentation pathways for 1,2,5,6,9,10-Hexachloro-*n*-decane established by linked-field scanning.



## Appendix 2

(h) (*cont'd*) Ion fragmentation pathways for 1,2,5,6,9,10-hexachloro-*n*-decane established by linked-field scanning.



**Appendix 3a. Effect of ion source temperature and concentration of injected PCA on the ECNI mass spectrum of 1,2,9,10-M<sub>104</sub>**

Source temp-- Injection Vol.(uL)-	120°C		150°C		175°C		200°C		220°C				
	0.1	0.5	1.0	0.1	0.5	1.0	0.1	0.5	1.0	0.1	0.5	1.0	
<b>Ion†</b>	<b>% corrected relative abundance</b>												
Cl <sub>2</sub> <sup>•-</sup> (m/z 70)	87.3	76.6	92.7	88.8	91.6	97.2	93.2	97.1	95.6	93.3	100	100	100
HCl <sub>2</sub> <sup>-</sup> (m/z 71)	100	100	100	100	100	100	100	100	100	100	94.7	88.0	95.0
[M - HCl] <sup>•-</sup> (m/z 242)	16.8	15.4	14.5	3.9	3.0	2.9	0.9	0.9	1.0	0.2	0.3	0.2	0.0
[M - Cl] <sup>-</sup> (m/z 243)	73.2	70.5	57.2	21.8	18.2	19.5	10.9	8.1	9.4	2.0	2.6	2.7	0.5
[M + Cl] <sup>-</sup> (m/z 313)	11.6	14.3	12.5	4.5	5.3	5.0	4.4	4.3	3.0	0.5	0.8	0.8	0.1

**NB. All abundances are for the most intense ion in the group**

**Appendix 3b. Effect of ion source temperature and concentration of injected PCA on the ECNI mass spectrum of 1,2,x,9,10-M<sub>10.5</sub>**

Source temp-	120°C		150°C		175°C		200°C		220°C						
	0.1	0.5	1.0	0.1	0.5	1.0	0.1	0.5	1.0	0.1	0.5	1.0			
Injection Vol.(uL)-	0.1	0.5	1.0	0.1	0.5	1.0	0.1	0.5	1.0	0.1	0.5	1.0			
Ion↓	% corrected relative abundance														
Cl <sub>2</sub> <sup>-•</sup> (m/z 70)	65.0	57.2	58.8	100	100	100	100	100	100	100	100	100			
HCl <sub>2</sub> <sup>-</sup> (m/z 71)	41.0	37.5	35.3	61.1	59.5	52.7	60.7	55.0	58.5	60.5	59.0	53.7	57.8	53.4	
[M- 2HCl] <sup>-•</sup> (m/z 240)	2.6	2.2	2.5	1.9	1.3	1.1	0.0	0.0	0.6	0.0	0.0	0.3	0.0	0.0	
[M- HCl] <sup>-•</sup> (m/z 276)	26.4	23.3	27.6	11.5	10.9	10.7	3.8	3.9	5.1	0.7	0.8	1.2	0.0	0.4	
[M- Cl] <sup>-</sup> (m/z 277)	100	100	100	66.1	61.0	60.4	23.1	28.6	31.2	8.5	7.3	9.9	1.2	2.3	4.1
[M+Cl] <sup>-</sup> (m/z 347)	0.2	0.0	1.8	0.0	0.4	0.9	0.2	0.5	0.2	0.0	0.0	0.0	0.0	0.0	0.0

NB. All abundances are for the most intense ion in the group

**Appendix 3c. Effect of ion source temperature and concentration of injected PCA on the ECNI mass spectrum of 1,2,5,6,9,10-M<sub>10,6</sub>.**

Source temp--	120°C		150°C		175°C		200°C		220°C						
	0.1	0.5	1.0	0.1	0.5	1.0	0.1	0.5	1.0	0.1	0.5	1.0			
Injection Vol.(uL)--	0.1	0.5	1.0	0.1	0.5	1.0	0.1	0.5	1.0	0.1	0.5	1.0			
Ion I	% corrected relative abundance														
Cl <sub>2</sub> <sup>-•</sup> (m/z 70)	35.3	38.3	28.8	54.6	72.0	79.6	96.0	100	96.5	100	96.8	97.1	100	100	100
HCl <sub>2</sub> <sup>-</sup> (m/z 71)	42.3	37.6	25.3	60.7	74.0	80.4	100	98.7	100.0	99.9	100	100	90.9	89.2	77.3
[M - HCl - Cl <sub>2</sub> ] <sup>-•</sup> (m/z 240)	2.2	2.2	2.6	1.5	1.1	1.3	0.0	0.2	0.3	0.0	0.0	0.0	0.0	0.0	0.2
[M - 3Cl] <sup>-</sup> (m/z 241)	7.3	5.8	6.4	4.9	4.9	4.9	1.0	1.1	1.5	0.7	1.0	1.0	0.3	1.0	1.0
[M - 2HCl] <sup>-•</sup> (m/z 274)	9.0	8.3	9.5	4.9	5.2	5.1	1.1	1.2	1.6	0.4	0.8	0.8	0.0	0.7	0.8
[M - HCl - Cl] <sup>-</sup> (m/z 275)	5.8	5.2	5.5	2.8	3.0	2.8	0.8	0.8	1.2	0.7	0.7	0.7	0.3	0.9	1.2

**Appendix 3c. (cont'd) Effect of ion source temperature and concentration of injected PCA on the ECNI mass spectrum of 1,2,5,6,9,10-M<sub>106</sub>**

<b>[M - HCl]<sup>-•</sup> m/z 310</b>	65.6	67.3	81.9	44.0	44.7	46.2	10.7	11.6	16.6	5.0	6.7	7.1	2.2	4.7	6.1
<b>[M + Cl]<sup>-</sup> m/z 381</b>	0.0	0.9	2.3	0.8	1.4	2.1	0.7	1.3	2.8	0.6	1.3	1.7	0.3	0.6	1.1
<b>[M - Cl]<sup>-</sup> m/z 311</b>	100	100	100	100	100	100	36.2	39.8	53.2	26.1	35.2	34.7	13.7	29.6	35.4

**NB. All abundances are for the most intense ion in the group**

**Appendix 3d. Effect of ion source temperature and concentration of injected PCA on the ECNI mass spectrum of 1,2,5,x,6,9,10-M<sub>107</sub>**

Source temp~ Injection Vol.(uL)~	120°C		150°C		175°C		200°C		220°C				
	0.1	0.5	1.0	0.1	0.5	1.0	0.1	0.5	1.0	0.1	0.5	1.0	
<b>Ion↓</b>	<b>% corrected relative abundance</b>												
Cl <sub>2</sub> <sup>•-</sup> (m/z 70)	31.6	33.3	24.8	54.0	51.1	78.0	100	100	100	100	100	100	
HCl <sub>2</sub> <sup>-</sup> (m/z 71)	10.7	12.1	9.1	18.0	18.3	28.8	31	36.6	38.6	36.8	409	37.9	35.0
[M - HCl - Cl <sub>2</sub> ] <sup>•-</sup> (m/z 274)	3.4	4.6	4.6	3.3	2.1	2.4	0.6	0.5	0.6	0.0	0.0	0.0	0.1
[M - 3Cl] <sup>-</sup> (m/z 275)	10.4	9.5	9.8	9.9	8.0	8.1	2.1	2.4	2.0	1.2	1.4	0.7	2.2
[M - 2HCl] <sup>•-</sup> (m/z 308)	5.2	6.3	7.8	5.7	5.2	6.2	2.1	1.6	1.6	0.5	0.9	0.0	0.6
[M - HCl] <sup>•-</sup> m/z 344	40.4	40.9	45.0	25.8	27.3	30.0	10.7	8.2	8.1	4.9	6.4	1.7	4.3
[M - Cl] <sup>-</sup> m/z 345	100	100	100	100	100	100	48.4	41.9	39.4	36.7	48.7	21.3	42.7

NB. All abundances are for the most intense ion in the group

**Appendix 3e. Effect of ion source temperature and concentration of injected PCA on the ECNI mass spectrum of 1,2,10,11-M<sub>114</sub>**

Source temp-	120°C		150°C		175°C		200°C		220°C				
	0.1	0.5	1.0	0.1	0.5	1.0	0.1	0.5	1.0	0.1	0.5	1.0	
Injection Vol.( $\mu$ L)-	0.1	0.5	1.0	0.1	0.5	1.0	0.1	0.5	1.0	0.1	0.5	1.0	
Ion1	% corrected relative abundance												
Cl <sub>2</sub> <sup>•-</sup> (m/z 70)	81.4	89.8	94.0	79.9	82.7	92.8	85	93	93	93	96	100	100
HCl <sub>2</sub> <sup>-</sup> (m/z 71)	100	100	100	100	100	100	100	100	100	100	100	85.6	94.4
[M - HCl] <sup>•-</sup> (m/z 256)	4.8	2.4	2.9	1.4	2.0	1.2	0.0	0.3	0.2	0.1	0.0	0.2	0.1
[M - Cl] <sup>-</sup> (m/z 257)	11.9	6.6	3.9	6.5	8.1	5.7	1.4	1.3	1.5	0.8	0.5	1.2	0.8
[M + Cl] <sup>-</sup> (m/z 327)	3.2	2.6	4.1	4.0	6.3	4.9	0.6	1.8	1.7	0.3	0.7	0.4	0.8

NB. All abundances are for the most intense ion in the group

**Appendix 3f. Effect of ion source temperature and concentration of injected PCA on the ECNI mass spectrum of 1,2,x,10,11-M<sub>11,5</sub>**

Source temp-	120°C		150°C		175°C		200°C		220°C					
	0.1	0.5	1.0	0.1	0.5	1.0	0.1	0.5	1.0	0.1	0.5	1.0		
Injection Vol.(uL)-	0.1	0.5	1.0	0.1	0.5	1.0	0.1	0.5	1.0	0.1	0.5	1.0		
Ion I	% corrected relative abundance													
Cl <sub>2</sub> <sup>-•</sup> (m/z 70)	100	100	100	100	100	100	100	100	100	100	100	100		
HCl <sub>2</sub> <sup>-</sup> (m/z 71)	69.3	65.6	60.1	66.9	62.7	65.4	66.7	63.6	65.4	62.9	66.3	65.5	53.8	56.8
[M - 2Cl] <sup>-•</sup> (m/z 256)	0.7	0.4	0.3	0.0	0.3	0.3	0.0	0.0	0.0	0.2	0.0	0.0	0.0	0.0
[M - HCl] <sup>-•</sup> (m/z 292)	9.7	6.2	4.8	3.3	3.8	4.0	0.2	0.8	0.9	0.1	0.2	0.1	0.6	0.2
[M - Cl] <sup>-</sup> (m/z 293)	26.4	17.3	13.3	16.6	14.5	17.1	2.9	4.6	4.5	1.7	1.4	1.7	3.9	1.5

NB. All abundances are for the most intense ion in the group

**Appendix 3g. Effect of ion source temperature and concentration of injected PCA on the ECNI mass spectrum of 1,2-x,y,10,11-M<sub>116</sub>**

Source temp--	120°C		150°C		175°C		200°C		220°C						
	0.1	0.5	1.0	0.1	0.5	1.0	0.1	0.5	1.0	0.1	0.5	1.0			
Injection Vol.(uL)-	%														
Ion†	corrected relative abundance														
Cl <sub>2</sub> <sup>-•</sup> (m/z 70)	100	100	100	100	100	100	100	100	100	100	100	100			
HCl <sub>2</sub> <sup>-</sup> (m/z 71)	39.7	37.3	36.8	39.8	38.3	35.7	41.5	38.2	37.1	39.7	41.1	39.8	35.5	38.4	
[M - 2HCl] <sup>-•</sup> (m/z 288)	0.4	0.4	1.8	0.0	0.2	0.3	0.0	0.0	0.0	0.1	0.2	0.0	0.0	0.0	
[M - HCl] <sup>-•</sup> (m/z 324)	15.1	9.7	8.4	7.4	8.1	7.7	1.0	1.8	2.3	0.0	0.0	0.0	0.2	0.2	
[M - Cl] <sup>-</sup> (m/z 325)	32.5	20.7	18.5	26.3	27.2	25.9	8.2	9.8	11.1	4.4	4.0	3.2	10.9	4.4	2.7

NB. All abundances are for the most intense ion in the group

**Appendix 3h. Effect of ion source temperature and concentration of injected PCA on the ECNI mass spectrum of 1,2,x,y,z,10,11-M<sub>1,7</sub>**

Source temp→	120°C			150°C			175°C			200°C			220°C		
Injection Vol.(uL)→	0.1	0.5	1.0	0.1	0.5	1.0	0.1	0.5	1.0	0.1	0.5	1.0	0.1	0.5	1.0
Ion!	% corrected relative abundance														
Cl <sub>2</sub> <sup>-•</sup> (m/z 70)	100	100	100	100	100	100	100	100	100	100	100	100	100	100	100
HCl <sub>2</sub> <sup>-</sup> (m/z 71)	19.0	13.0	11.1	17.3	15.4	9.3	17.0	15.3	10.5	16.2	5.7	16.9	27.6	0.4	19.2
[M - 2HCl] <sup>-•</sup> (m/z 322)	0.8	0.5	0.1	0.2	0.2	0.8	0.2	0.0	0.2	0.0	0.0	0.0	1.4	0.0	0.0
[M - HCl] <sup>-•</sup> (m/z 358)	13.7	9.5	7.1	7.2	9.1	8.8	0.3	1.5	2.3	0.0	0.0	0.0	2.9	0.0	0.0
[M - Cl] <sup>-</sup> (m/z 359)	29.0	21.1	17.0	30.6	30.3	32.9	11.2	14.2	15.7	7.2	5.8	1.9	15.4	6.7	4.8

**NB. All abundances are for the most intense ion in the group**

## Appendix 4 Derivation of the equation used for estimating analyte PCA concentration

The number of moles of injected PCA is determined by normalizing the integrated area of the ion signal (SIM) with the fractional relative abundances of the monitored  $m/z$  species in the ion formula ( $m/z$  ab) and also with the fractional relative abundance of the molecular formula in the PCA ( $form$  ab). Normalizing the SIM in this manner provides us with the true integrated ion signals:

$$moles(anal) = \frac{SIM(anal)}{m/z\ ab(anal)\ form\ ab(anal)}$$

Now the number of moles of the analyte can be related to the number of moles of the standard by:

$$\frac{moles(anal)}{moles(std)} = \frac{SIM(anal)}{m/z\ ab(anal)\ form\ ab(anal)} \times \frac{m/z\ ab(std)\ form\ ab(std)}{SIM(std)}$$

Converting from moles to mass by using the AMM we derive the relation :

$$\frac{g(anal)}{g(std)} = \frac{SIM(anal)}{SIM(std)} \times \frac{m/z\ ab(std)}{m/z\ ab(anal)} \times \frac{form\ ab(std)}{form\ ab(anal)} \times \frac{AMM(anal)}{AMM(std)}$$

## Appendix 5 An example calculation of analyte PCA concentration

Based on monitoring the most abundant peak in the analyte and PCA-70 primary standard we therefore use  $m/z$   $ab(std) = 0.281$  (for  $m/z$  394.9042) and  $m/z$   $ab(anal) = 0.281$  (for  $m/z$  394.9042) (see Table 5.2). From Figures 5.7(b) and Figures 6.5(d) we obtain  $form\ ab(std) = 0.255$  and  $form\ ab(anal) = 0.165$ , while the respective AMM of standard and analyte are 433.4 and 424.1. Thus, from equations 5.7 and 5.8 we get:

$$\begin{aligned}\frac{PCA(anal)(ng/\mu L)}{PCA(std)(ng/\mu L)} &= \frac{SIM(anal)}{SIM(std)} \times \frac{0.281}{0.281} \times \frac{0.255}{0.165} \times \frac{424.1}{433.4} \times R \\ &= \frac{240908640}{197236336} \times 1.51 \times \frac{313864}{67887} \\ &= 8.53\end{aligned}$$

The concentration of the standard solution used was 4.7 ng/ $\mu$ L, the final volume of the analyte solution was 125  $\mu$ L; thus the mass of PCAs in the analyte is

$$\begin{aligned}PCA(anal)\ ng &= 8.53 \times 4.7\ ng/\mu L \times 125\ \mu L \\ &= 5011.4\ ng\end{aligned}$$

The weight of the fish tissue used in the analysis was 5.579 g, the percent recovery of  $^{13}C_1$ -chlordane was 88%, and assuming that the PCA percentage recoveries are the same as those of  $^{13}C_1$ -chlordane, the total concentration of PCAs is 1021 ng/g (wet wt.).